The Impact of Voltage Unbalance and Regulation on the Life Expectancy of LV Induction Machines

Prepared by:
Samuel Mponwana
MPNSAM002

Department of Electrical Engineering
University of Cape Town

Prepared for:
Prof Paul Barendse

December 2019

Submitted to the Department of Electrical Engineering at the University of Cape Town in full fulfilment of the academic requirements for the Degree of Master of Science in Electrical Engineering.

DECLARATION

I, **Samuel Seemole Mponwana**, declare that this dissertation is my own work. All information that is not my own has been clearly referenced. I declare that this thesis has not been presented and will not be presented to any other University or institution for any similar or other degree.

I know the meaning of plagiarism and declare that all the work in the document, save for that which is properly acknowledged, is my own. This thesis/dissertation has been submitted to the Turnitin module (or equivalent similarity and originality checking software) and I confirm that my supervisor has seen my report and any concerns revealed by such have been resolved with my supervisor

Signed: Samuel Seemole Mponwana Date: 2019/02/05

I, Samuel Seemole Mponwana, declare that this dissertation is my own work. All information that is not my own has been clearly referenced. I declare that this thesis has not been presented and will not be presented to any other University or institution for any similar or other degree.

I know the meaning of plagiarism and declare that all the work in the document, save for that which is properly acknowledged, is my own. This thesis/dissertation has been submitted to the Turnitin module (or equivalent similarity and originality checking software) and I confirm that my supervisor has seen my report and any concerns revealed by such have been resolved with my supervisor

Signed: Date: 2019/02/05

Signed by candidate

To mother, Mokgadi Mponwana, my father Matsobane Mponwana, my brother William Mponwana, my sister Phuti Mponwana and all my friends and colleagues, thank you for the support throughout this journey.

ACKNOWLEDGEMENTS

I would like to thank the following people:

- My parents Mokgadi and Matsobane Mponwana for the support and motivation throughout this journey.
- My siblings Phuti Mponwana and William Mponwana for their continual moral support.
- My supervisor Professor Paul Barendse and co-supervisor Professor Azeem Khan for their guidance throughout the duration of this research report.
- AMES Group administrator, Mrs Shireen Sabodien for all the help in administrative issues.
- My friends and colleagues and members of the AMES research group both past and present who have supported and assisted me greatly;
- The machines lab chief technical supervisor Mr Chris Wozniak for his support, guidance and patience throughout the duration of his research project.
- Mr Philip Titus and the CPUT in-service training students for their assistance and support.
- And to the National Research Foundation, the Advanced Machinery and Energy System Group and the University of Cape Town Department of Electrical Engineering for providing funding and research facilities during the duration of this research project.

EXECUTIVE SUMMARY

The induction machine is the most widely used electrical machine in the world, they are used for industrial, commercial and industrial applications. When manufactured they have nameplate ratings that stipulate the voltages and currents at which they may be operated. The quality of supply from power utilities can lead to them being operated under unbalanced voltage conditions. Power utilities experience voltage unbalances and voltage dips when they provide services to end users. In South Africa ESKOM is the primary power utility, it has a license agreement with NERSA stipulating the allowable voltage levels. In most cases the operating levels are within the agreed limits however many consumers are exposed to voltage levels at the fringe of these specified limits. This can be detrimental to electrical equipment if operated under these conditions for considerable lengths of time.

For ESKOM, the maximum deviation from standard or declared voltages should be $\pm 15\%$ for voltages less than $500V$. An induction machine with a rated voltage of $380V$ or $480V$ will experience over and under voltages and the severity of the condition will depend on how far it is from the source of supply. In South Africa the tolerable voltage unbalance is 2% on three phase networks and can be as high as 3% in rural areas. During its lifespan an induction machine will experience a combination of over and under voltages combined with voltage unbalance. This combination will reduce the lifespan of the induction machine. The rate at which life is lost will depend on the severity of these three extremes.

The purpose of this research project is to investigate and quantify the impact of voltage regulation (over and under) and unbalance conditions on a typical rural feeder on the lifespan of induction machines. There are various definitions of voltage unbalance by NEMA, the IEC and the IEEE. The IEC definition is used in this research report, it is known as the true definition and incorporates both magnitude and phase information. To estimate the loss of life in induction machines operating under unbalanced conditions, the positive and negative sequence per phase equivalent circuits must be determined and the thermal model needs to be obtained and quantified as well. The losses obtained from the per phase sequence circuits are inputs to thermal model which in turn is used to predict the induction machine stator windings temperatures. Factors that are considered when analysing the impact of voltage unbalance and regulation on the life expectancy of machines include, the induction machine manufacturer, the size of the induction machine, the voltage rating of the induction machine and the efficiency class of the induction machine.

Approach

Four induction machines were procured for this research report. This list of machines includes two machines (7.5kW and 11kW) from Manufacturer A and two machines (7.5kW and 11kW) from Manufacturer B. All four machines were low voltage (400V), 4-pole, 50Hz machines.

The IEEE and IEC do not have standards for determining induction machine losses and efficiencies for voltage unbalances exceeding 0.5%. Symmetrical components can be

implemented using the positive and negative sequence circuits to determine the stator copper losses of the machine under unbalanced voltage conditions. The parameters of the sequence circuits are obtained using the IEEE 112-B standard no load and locked rotor tests. The negative sequence rotor impedance is different to that of the positive sequence because the frequencies of the rotor currents are higher. The no load test as outlined by IEEE 112-B was used in obtaining the core losses of the four machines under the different voltage unbalance conditions. Unlike IEC 34-2-1, IEEE 112-B does not compensate for the voltage drop across the stator winding resistance and the core losses are obtained directly using the machine operating terminal voltage. Similar to induction machine losses, there is no defined procedure to determine the efficiency of induction machines under unbalanced supply conditions. Multiple complications can arise when determining the individual loss components. The direct method as outlined in IEEE 112-B was used in determining the efficiencies of the four machines under unbalanced voltage conditions.

The losses obtained from the sequence circuits and IEEE-112-B no load tests were inputs to the thermal model. The thermal model parameters are obtained through a series of DC tests performed on the induction machines [1]. The thermal model used in this research report assumes that no heat flows from the rotor to the stator but rather that the heat flows from the rotor to the shaft and eventually to the ambient. The thermal model is validated through a series of simulations where measured temperatures are compared with predicted ones. Fourth order Runge-Kutta methods were applied in solving the differential equations defining the temperature rise in the induction machines. The loss of life due to operation under unbalanced conditions combined with over/undervoltage is analysed and discussed.

Voltage unbalance minimization techniques based on symmetrical components are discussed and analysis is conducted on one of the considered voltage unbalance condition. The sensitivity of each parameter on the induction machine voltage unbalance is also analysed. Two analytical methods are discussed and implemented, voltage minimization by variation of one parameter and voltage minimization by variation of three magnitudes simultaneously. Knowledge of the sensitivity of the voltage unbalance to each parameter helps in selecting which parameter to change to reduce the voltage unbalance, this helps reduce potential harm to equipment.

Results

The core loss results for the two 7.5kW machines under unbalanced voltage conditions are almost equal. Manufacturer B 7.5kW machine's core losses are 3.24% (9.05W) greater than the Manufacturer A machine. This trend is observed for all the other voltage unbalance combined with over-and undervoltage conditions. Similar observations were found for the 11kW machines, it was found that Manufacturer B machine yielded greater core losses than its Manufacturer A counterpart. This is observed for all the test conditions. The test conditions that this research report is limited to includes 0-3% voltage unbalance combined with 90-110% voltage regulation. The core loss results indicated that the 3% voltage unbalance combined with 110% voltage regulation results in the highest core losses. The core losses are dependent on the voltage, since the voltage unbalance and regulation were achieved by altering each of the three phases, some phases were greater than others resulting in additional core losses from phases with voltages above the rated voltage. The results showed that the core losses increased with increasing voltage and unbalance. The core losses also decrease with an increase in machine temperature.

The stator copper losses of the four machines were obtained using the positive and negative sequence per phase equivalent circuits. The sequence circuits were validated by comparing the stator copper losses obtained using IEEE 112-B with the ones obtained using the sequence circuits (under balanced operating conditions). The sequence circuits accuracy levels were within 0.19% of the IEEE 112-B standard under balanced operating conditions. Both Manufacturer A machines have greater stator copper losses than their Manufacturer B equivalents (at rated operating conditions). It was found that the worst operating condition for all the machine arises when there is a combination of 3% voltage unbalance with 90% voltage regulation at full load. The opposite was true for loads less than 75% of the rated load, voltage unbalance combined with overvoltage results in greater stator copper losses. The operation of induction machines at higher voltages tends to push the magnetic portion of the machine into saturation resulting in the machine drawing excessive currents to magnetize the iron core beyond the point to which it can easily be magnetized. Whenever the voltage is increased beyond the machine's saturation point additional flux is only possible with a disproportionally large increase in current.

Machine efficiencies were obtained for nominal (0%) and 3% voltage unbalance conditions combined with over/under voltage. For operation under voltage unbalance the efficiencies decreased with an increase in voltage unbalance. This is largely attributed to the increase of the machine losses. Under undervoltage operating conditions the peak efficiency is shifted towards the partial load region. The constant losses are less significant under this condition and more current is drawn to compensate for the reduced magnetisation of the machine core. The maximum efficiency is shifted towards the higher loading region when the machine is operating under overvoltage conditions. Magnetization of the core is increased, and lower currents are required to develop the required load torque. The resultant thermal models had accuracy ranges of 5.73°C and -5.34°C for the individual phases temperature prediction and accuracy range of 2.313°C and -1.7°C for the average stator winding steady state temperature.

Industry Perspective

The research presented in this report is primarily focused on the impact of voltage unbalance and regulation on the life expectancy of low voltage induction machines. The operating conditions considered in this report are prevalent on a typical rural feeder. Most customers connected to rural 11/22kV networks are farmers and a large portion of load pumps are driven by low voltage induction machines. This report presents the effect of these operating conditions on the life expectancy of the machines. The thermal model presented is suitable for continuously operated machines (S1). Since the operating conditions considered are primarily prevalent on typical rural feeders, the machines considered were also the machines primarily used in those regions. This has consequence that relates to the way in which the network voltages are managed, and claims lodged against power utilities resulting from damage to end user's induction machines. The thermal model presented in this report can be incorporated as an algorithm and be implemented in microprocessor devices which enhance the level of accuracy and flexibility. As a practical application of the thermal model real time data can be processed according to the firmware thermal algorithm program and results are compared with the expected values and stored in memory. If a machine protection device is used, it computes an analog value which is then compared with the output of the thermal model algorithm. In practice the MPD usually triggers the digital outputs if the compared analog values exceed the set thermal threshold.

TABLE OF CONTENTS

LIST OF FIGURES

LIST OF TABLES

LIST OF SYMBOLS

f_1	Power supply frequency (in Hertz)
n_s	Synchronous speed (in revolutions per minute)
n_r	Rotational speed (in revolutions per minute)
p	Number of pole pairs.
s	Per unit slips
f_2	Frequency at which the voltage and current are induced in the rotor circuit
L	Life of the winding insulation (in hours)
P_{lt}	Flicker severity
U_{NL}	No load voltage
U_L	Terminal load voltage
U_{avg}	Average line voltage
VUF	Voltage Unbalance Factor
Z_p	Positive sequence impedance
Z_n	Negative sequence impedance
U_p	Positive sequence voltage
U_n	Negative sequence voltage
$CVUF$	Complex Voltage Unbalance Factor
ω	Frequency (in radians)
U_z	Zero sequence voltage
ζ	Dynamic response of system
$S_{\alpha_j}^{\zeta_i}$	Sensitivity of system
I_n	Negative Sequence Current
I_p	Positive Sequence Current
K	Thermal conductivity
q	Conductive/Convection heat transfer
q_r	Radiative heat transfer
C	Thermal Capacitance
G	Thermal Conductance
T	Temperature
T_x	Percent lifetime at rated temperature
T_c	Total allowable temperature for insulation class

T_{rated}	Rated Torque
δ	Boltzmann constant
ρ	Density of the material
c_p	Specific heat of material
$\propto$	Coefficient of heat transfer
g	Gravitational force for Cape Town
k_{hyst}	Hysteresis current loss
k_{eddy}	Eddy current loss
B	Magnetic flux density
k_{Cu}	Temperature coefficient of copper
k_{Al}	Temperature coefficient of aluminium
P_{FE}	Core losses
P_{FW}	Friction and Windage Losses
P_{Cu}	Stator Copper Losses
η	Motor Efficiency

NOMENCLATURE

AC	Alternating current
AIEE	American Institute of Electrical Engineers
AMES	Advanced Machinery and Energy Systems Group
ANSI	American National Standards Institute
CUF	Current Unbalance Factor
CVUF	Complex Voltage Unbalance Factor
DAQ	Data acquisition
DC	Direct current
DSM	Demand Side Management
DSP	Digital Signal Processing
EPRI	Electric Power Research Institute
ERC	Energy Research Centre
ESKOM	Electricity Supply Commission
FEM	Finite Element Method
HIC	Half Interval Index
HV	High Voltage
HVF	Harmonic Voltage Unbalance
ICs	Integrated Circuits
IEA	International Energy Agency
IEC	International Electrotechnical Commission
IEEE	Institute of Electrical and Electronic Engineers
IFM	Insulation Failure Mechanisms
IR	Insulation Resistance
KCL	Kirchhoff's Current Law
LV	Low Voltage
LVUR	Line Voltage Unbalance Factor
MGI	Motor and Generator Institute
MMF	Magneto Motive Force
MPD	Machine Protection Device
MTBF	Mean Time Between Failures
MUVU	Mixed Undervoltage Unbalance Factor
MV	Medium Voltage
NDE	Non-drive end

NEMA	National Electrical Manufacturers Association
NERSA	National Energy Regulator South Africa
NI	National Instrument
NRS	National Regulatory Standards
OEM	Original Equipment Manufacturer
ORNL	Oak Ridge National Laboratory
OVU	Overvoltage Unbalance
PI	Polarization Index
PVUR	Phase Voltage Unbalance Factor
PWM	Pulse Width Modulation
RK	Runge-Kutta
RMS	Root Mean Square
RPM	Revolutions per Minute
RTD	Resistance Temperature Detectors
RTI	Relative temperature index
SANS	South African National Standards
SF	Service Factor
SLL	Stray Load Losses
TEFC	Totally Enclosed Fan Cooled
THD	Total Harmonic Distortion
TI	Temperature Index
TNM	Thermal Network Model
TNM	Thermal Network Models
UBEV	Unbalanced Equal Voltage
UVU	Undervoltage Unbalance
VFD	Variable frequency Drives
VR	Voltage Regulation
VSD	Variable Speed Drive
VUF	Voltage Unbalance Factor

1. INTRODUCTION

1.1 Background

The induction machine is commonly known as the workhorse of industry. It can convert electrical energy to mechanical energy. Induction machines are the main driving force to equipment such as pumps and conveyors and they are necessary for numerous processes in production and manufacturing plants [2]. The main advantages of induction machines are that they are highly reliable, require low maintenance and have a relatively high efficiency. The wide range of power rating of the induction motor which is from hundreds of watts to megawatts satisfies the production needs of most industrial processes [2].

A report by the international energy Agency (IEA) indicates that electric motors account for 43-46% of the global energy consumption [3]. Since they consume such a large percentage of the global energy consumption it is of huge importance that they are always running at their optimal capability. Every effort should be made to ensure the machine's operating state is optimal to avoid unwanted machine failure leading to unnecessary out of service situations and production downtime.

In ideal operating conditions, induction machines have an overall lifecycle duration in the range of 12-20 years, and they can be rewound 2 to 4 times during this period (in developed countries) depending on their rated power and operating conditions [4]. Recent studies undertaken in [4] found that in modern industries there are many machines much older than their operating life expectancy, with ages largely higher than 20 years.

Induction machines are designed to perform best when supplied by balanced sinusoidal waveforms. In practice, the ideal supply conditions are not easy to realise. The power system experiences voltage unbalance, over- and undervoltages, voltage dips and harmonic distortions. These disturbances in the power system quality results in a reduction in the efficiency and life span of the machine.

Thermal protection is one of the main aspects to consider in the condition monitoring and extension of induction machine insulation lifespan. According to [5], approximately 30-35% of machine failures are related to the stator winding insulation. Various surveys on large induction machines conducted by the IEEE-IAS, the EPRI and Allianz are compared in Table 1-1 and Table 1-2. The survey conducted by the *Motor Reliability Working Group of the IEEE-IAS and EPRI* focuses on medium sized induction machines while the Allianz survey focuses on medium to high voltage large induction machines.

Table 1-1: Percentage Failure by Component [6]

Failed Component	Percentages of Failures (%)		
	IEEE-IAS	EPRI	Allianz
Bearing related	44	41	13
Stator related	26	36	66
Rotor related	8	9	13
Others	22	14	8

Table 1-2 : The primary root causes of failures in squirrel cage induction machines and their respective effects and possible resulting damages [6] [7] [8] [9] [10]

Primary Causes	Effects	Damages
Cooling & Ambient	Winding Overtemperature	Burnt stator windings
Humidity/moisture	Shortened Insulation lifetime	Winding short circuit
Contamination	Shortened lubrication lifetime	Shorted turns
Poor Frame/Fins cleaning	Increased losses	Winding earth faults
Damaged Cooling Fan		Bearing damages
Restricted/Obstructed Cooling/Ventilation		
Excessive Ambient Temperature		
Electrical/Magnetic	**Line-Fed SCIMs**	Winding parts burnt
General:	Unbalanced stator currents	Winding short circuit
Poor/Old Insulation	Winding overtemperatures	Shorted turns
Damaged Core	Unbalanced winding temperatures	Shorts phases
Load electric charge build up	Motor vibrations	Winding-Earth Faults
Electromagnetic Asymmetries	Unbalanced rotor radial forces	Bearing damages
Line-Fed SCIMs	Bearing discharge currents	
Unbalanced Voltages	Additional losses	
Single-phase/Phase loss conditions		
Voltage surges/transients	**VSD-Fed SCIMs**	
Lightning strikes	Winding overtemperature	
Poor motor protection	Additional losses	
VSD-Fed SCIMs		
PWM low/high order harm. Losses		
High voltage pulses/surges		
Lack of VSD output filters		
Poor grounding		
Mechanical & Duty Cycle	Uneven wear of bearings	Bearing and rotor cage damage
Rotor Dynamic imbalance	Additional losses	Winding parts burnt
Airgap dynamic/static eccentricities	Winding overcurrents	Winding short circuit

Motor load shaft misalignment	Winding overtemperatures
Extreme starting conditions	Accelerated Insulation wear
Shock loads	Increased shaft stress
Excessive start/stop cycles	
Excessive reversal cycles	
Vibrating loads	

Operation of an induction machine under unbalanced, over- and undervoltages results in thermal overloading of the machine. It is therefore of great importance to have precise and reliable monitoring of the stator winding temperature to minimize the financial losses due to unexpected process downtime. There are generally two approaches for monitoring induction machine temperatures:

Invasive techniques: Invasive techniques involve using sensors and probes to give precise but localised temperature information.

Non-Invasive techniques: These techniques involve using induction machine thermal models for indirect estimation of machine temperature without any physical connection to the machine. This approach allows you to track both transient and steady state temperature rise.

1.2 Problem Statement

Numerous research has been focused towards the operation of induction machines under unbalanced voltages. Work from as early as the 1950s can be found in AIEE Transactions now known as the Institute of Electrical and Electronics Engineers (IEEE). It is very important to know the effects of operation under unbalanced and over- and undervoltage conditions for modern induction machines since they are designed more efficiently as opposed to older machines which were often overdesigned with the emphasis more on the minimization of the cost of production. Consequently, their ability to operate under abnormal conditions is reduced from the older machines. Most of the three phase induction machines in South African industries are designed to operate from 380/400V supplies. ESKOM supplies the commercial and industrial systems with a line voltage range of 400V$\pm$ 10%. The major reason for this higher voltage is to allow for the line voltage drop so that the correct voltage at the terminals of the machines can be achieved.

NRS-048 provides limits for voltage regulation and voltage unbalance which exist on the network at various voltage levels. It is the responsibility of each utility to ensure that the quality of power supplied to each consumer complies with the minimum standards specified in NRS-048. As per ESKOM's license agreement with NERSA, the voltage unbalance on a three-phase system is limited to 2%, and 3% for single phase systems [11]. Utilities have standards and operating procedures in place to run the networks optimally within these limits. Although these operating levels are within specified limits a large portion of the customer's plant can be exposed to voltage levels well above or below the rated value of the equipment. Operation under these conditions can eventually lead to failure of the customer's equipment. The impact of operating AC machines with voltage levels above or below the rated levels has not been fully determined on rural networks in South Africa. Research is therefore required to assess the impact of these operating conditions on customer equipment in rural areas and whether utility operating procedures need to be revised to take into consideration customer equipment. This has consequence for Eskom Distribution that relates to:

a) the way in which the network voltages are managed and

b) claims lodged against the distribution business resulting from damage to customer's motors.

1.3 Research Questions

The research presented in this report focuses on the impact of voltage unbalance and regulation on the life expectancy of low voltage induction machines. In this regard, several questions have been formulated

- Can the impact on motor life expectancy be assessed based on real network and operational conditions which induction machines are exposed to?
- What is the impact of a combination of loading, voltage regulation and voltage unbalance on the life expectancy of induction machines?
- How can the modelling of induction machines be integrated with the operational conditions to determine the impact on machine life expectancy?
- What impact does the following factors:
  (i) Manufacturer
  (ii) Size
  (iii) Voltage rating
  (iv) Efficiency
  (v) Insulation class
  have on the life expectancy of induction machines?
- Can a predictive tool be developed to assess the impact of operational conditions on the life expectancy of induction machines?

1.4 Objectives of Research Work

The primary objectives of this research are to determine the impact of voltage unbalance and regulation prevalent on a typical rural feeder, on the life expectancy of induction machines up to 11kW. Most customers connected to rural 11/22kV networks are farmers, where a large portion of the load pumps are driven by low voltage induction machines. These feeders are typically subjected to power quality issues due to the long distance of the feeders. The second objective of this research is to refine a thermal model to predict the temperature rises for combinations of unbalance, over- and undervoltage conditions and validate experimentally. The temperature results are used to estimate the lifespan of induction machines under various supply and operating conditions for the selected range and class of induction machines. The third objective is to develop a modelling tool for estimating the life expectancy of induction machines under various supply and loading conditions.

1.5 Scope and Limitations of Report

This study investigates the power quality issues with low voltage induction machines. These power quality issues are limited to voltage unbalance combined with over- and undervoltages. The report focuses only on four induction machines, two machines (7.5kW and 11kW) from Manufacturer A and two machines (7.5kW and 11kW) from Manufacturer B. Tests performed on these motors are based on IEEE 112-B: *IEEE Standard Test Procedure for Polyphase Induction Motors and Generators.* Thermal model parameters are obtained for the four induction machines in question, the measured temperatures under the different operating conditions are compared with the outputs of the thermal model.

1.6 Organization of the Research Project

The remainder of this research report is structured as follows:

Chapter 2 provides a literature review on the operational principles of the induction machine under unbalanced voltage conditions. The current testing and temperature monitoring methods for insulation systems are discussed in detail. The main causes of stator winding insulation failures are classified and discussed. A brief description of Arrhenius equations used for life estimation is given. The latest thermal modelling literature associated with temperature approximation of electrical machines is presented and discussed.

Chapter 3 outlines the power quality issues experienced by induction machines during operation. Harmonics, flicker, dips and swells and voltage regulation are discussed in detail. The different definitions of voltage unbalance from the different institutions are described and the one used in this research report is discussed. A summary of the types of voltage unbalances is discussed and the impact of voltage unbalance of the induction machine is summarised.

Chapter 4 uses the theory and development described in chapters 2 and 3 to help describe the electrical and thermal modelling of the induction machine. The positive, negative and zero sequence equivalent circuits are discussed, and the Fortescue transformations used in the calculation of the positive and negative currents are summarised. The developed power and torque from the sequence circuits are also formulated. Basic thermal modelling theory is discussed, and the proposed thermal model is described.

Chapter 5 reviews the experimental equipment used to obtain the test data from the induction machines and the apparatus used to analyse the data. The IEEE/IEC standards requirements are discussed, and the laboratory setup is compared to these requirements. All the test procedures followed in this research report are discussed in this chapter.

Chapter 6 presents the results and analysis of the results. The results in this chapter are focused on the electrical models. The core losses, stator copper losses, friction and windage losses as well as the machine efficiencies are discussed in detail. The impact of voltage unbalance and regulation on the machine losses and efficiencies is discussed.

Chapter 7 discusses the thermal model results. The measured temperatures are compared to the thermal model temperatures.

Chapter 8 involves the loss of life calculations for the four induction machines.

Chapter 9 presents the research reports' conclusions and recommendations.

2. LITERATURE REVIEW ON INDUCTION MACHINES AND FACTORS AFFECTING LOSS OF LIFE

2.1 Introduction

This chapter provides a summary of the operating principles of induction machines under unbalanced, over- and undervoltage conditions. Testing and monitoring methods for insulation systems used in electrical machines are discussed. Insulation Failure Mechanisms (IFMs) that are most prominent in electrical machines are classified and the most prevalent ones are discussed. Arrhenius equations associated with loss of life estimation in insulation materials are presented and described. Finally, the latest thermal modelling literature associated with temperature approximation in induction machines is presented and discussed.

2.2 The Induction Motor

2.2.1 Construction of Induction Motors

The induction machine is the most widely used electric motor in industry due to its favourable characteristics. It can operate both as a generator and as a motor. The induction machine can fundamentally be divided into three basics parts, the stator, the rotor and an airgap [12]. The stator makes up the induction machine magnetic core and is made up of laminations manufactured from high grade sheet steel. These laminations are stacked together to form the induction machine metal frame. In the conventional three phase induction machine, evenly distributed stator windings are inserted in the inner perimeter of the steel laminations. These windings are distributed at an even 120 electrical degrees around the stator core. The distributed winding configuration offers a better usage of the iron and results in a high quality MMF waveform. Connection to the required three phase supply can either be in star or delta configuration [13].

Induction motors have uniform airgaps unlike the DC motors. In most designs the airgap is designed to be minimal to ensure a minimal reluctance path, hence maximising the flux densities in the core of the machine [12]. The uniform airgap separates the rotor from the stator. This rotor is made from ferromagnetic material and has a cylindrical form with slots for the rotor windings or bars to be inserted. Like the stator windings, there are various rotor winding configurations. This research report is limited to squirrel cage configured rotor which consists of shorted copper bars. This configuration is more rigid and cost efficient than the wound configuration [12].

2.2.2 Principle of Operation

The stator windings of the induction machine are connected to a three-phase supply from which an alternating current (AC) is supplied [12]. A sinusoidal magnetomotive force is produced by each of the three phase currents. The sum of these magnetomotive forces produce a rotating

magnetic field in the machine air gap [14]. The magnetic field produced is dependent on the instantaneous value of the current flowing in the phase coil and rotates at synchronous speed. The synchronous speed is defined by the number of poles the machine has and the supply frequency [14] [12]:

$$n_s = \frac{120}{p} f_s \tag{2-1}$$

Where:

n_s is the synchronous speed in RPM

f_s is the fundamental supply frequency

p is the number of poles pairs in the induction machine

Faraday's law states that the rotating magnetic field induces voltages in both the stator and rotor windings at the same frequency f_s, the voltage induced across the rotor bars produces rotor currents that interact with the air gap magnetic field. _ The machine slip is defined by equation (2-2).

$$s = \frac{n_s - n_r}{n_s} \tag{2-2}$$

The voltage and current in the rotor circuit are induced at frequency f_2

$$f_2 = sf_1 \tag{2-3}$$

For the squirrel cage machine, the slip and the current are low at full load and the efficiency and power factor are high. For direct-online start-up situations the power factor and the torque are low whilst the current is very high. If the induction machine is connected to a load that requires a large starting torque, the induction machine will accelerate slowly, this will result in the starting currents flowing for longer periods of time. These higher starting currents flowing for longer periods of time will result in overheating and will lead to degradation of the stator winding insulation.

2.2.3 Modes of Operation of the Induction Machine

The induction machine's mode of operation is determined by the relationship between the rotor's and airgap's MMF direction and speed [12]. The three modes of operation are generating, motoring and plugging. Operation under motoring mode occurs when the rotor's speed is less than that of the rotating magnetic field in the airgap. This is the primary mode of operation of the induction machine [14]. The generating mode of operation occurs when the rotor speed is greater than that of the rotating airgap [12]. The induction machine will produce a torque that is acting in the opposite direction of the airgap rotating field, where the kinetic energy of the rotor is fed back into the stator supply [14]. Plugging mode of operation occurs when the direction of the rotor is in the opposite direction of the rotating airgap magnetic field. In this mode of operation, the resultant torque is said to be a breaking torque [12]. In most cases this mode of operation is used in drive applications to control the machine speeds [14].

2.3 Literature Review on Testing and Monitoring Methods for Insulation Systems

Induction machines convert electrical energy to mechanical energy or vice versa. This is achievable because of the interaction between the magnetic and electric circuits across the machine airgap. The two circuits are separated by adequate insulation material with the required thermal properties. Whenever there is a transfer of energy across the machine airgap, ohmic losses are dissipated as heat in the electric circuit. In the magnetic circuits, the eddy and hysteresis losses are dissipated as heat. There is correlation between the performance of the insulation materials used in the machine windings and the temperature the machine operates at. This insulating material deteriorates rapidly as the temperature of the windings increases. Unfortunately, temperature is not the only factor that contributes towards insulation failure, other factors commonly known as Insulation Failure Mechanisms (IFMs) contribute to the deterioration of the insulation of the machine. According to most literature and interviews with industry experts, induction machines used for industrial and utility applications have an expected life expectancy of 20-40 years before rewinding is required. In earlier years, the required life of an insulation system was achieved by a trial and error method [15]. If the stator windings of a machine never reached its expected life, extra insulation would be added in the next design of the machine. The most common practice to avoid this premature failure was to add safety margins to the design, the outcome of this practice would be stator winding insulation systems that greatly outperformed the specified life. Present day Manufacturers utilise an accelerated ageing test during the design phase of the induction machine insulation system. The basic principle is to develop a model of the stator winding insulation system and apply above nominal stresses to the model. These stresses include voltage, mechanical forces, radiation, temperature, etc. The model under consideration would than fail prematurely and results from these stress tests can then be extrapolated and service life estimated [15].

Recent developments in technology particularly in ICs, DSP, and communications has helped researchers develop new procedures in the testing and monitoring of induction machines [16].
Developments in online monitoring of electrical signatures (current, voltage), allows the monitoring algorithm to reside in the machine control centres or in some instances the machine control devices. Early fault detection techniques and early deterioration detection of the primary and secondary insulation systems have been tested and implemented. These testing and monitoring methods are classified into two groups. The first of these groups is offline testing, this method requires the induction machine to be removed from service. The second method is online monitoring, this can be done without removing the machine from service [16].

2.3.1 Offline Testing

The status of the induction machine stator winding is a critical factor in the overall wellness of an induction machine [16]. This wellness can be ensured by performing various offline tests on the machine. The testing allows the operator to an adequate assessment of the condition of the machine. Offline testing is more direct and more accurate than online testing [16].The IEEE, IEC, MGI and NEMA all specify the tests that can be performed on induction machines to diagnose the turn insulation conditions. The tests are summarised in Table 2-1.

Table 2-1: Various parameters used to detect the status of the insulation in induction motors [15]

Method	Standards	Insulation Tested & Diagnostic Value
Winding resistance/DC Conductivity Test		Detect short turns, has no predictive value
Insulation Resistance (IR)	IEEE 43, NEMA MGI	Obtain contaminations and defects in phase to ground insulation
Polarization Index (PI)	IEEE 43	Obtain contaminations and faults in phase to ground insulation
DC High Potential Test (DC High Pot)	IEEE 95, IEC 34.1, NEMA MGI	Obtain contaminations and faults in phase to ground insulation
AC High Potential Test (AC High Pot)	IEC 60034, NEMA MGI	Obtain contaminations and faults in phase to ground insulation
Signature Analysis of Terminal Voltage after Switch-Off		Can detect turn to turn faults
Surge Test	IEEE 522, NEMA MGI	Can detect deterioration of the turn-to-turn insulation
Offline Partial Discharge	IEEE 1431	Can detect deterioration of the phase –to-ground and turn-to-turn insulation
Dissipation Factor	IEEE 286, IEC 60894	Detects deterioration of the phase to ground insulation
Inductive Impedance		Can detect shorted turns and has no predictive value.

2.3.2 Online Testing

There are multiple monitoring techniques that been developed that allows the use of measured quantities to diagnose the condition of the machine insulation system [16]. A number of these techniques use different machine parameters to perform these diagnostics. The most common parameters used are the magnetic flux, the temperature, the stator current and in some instances the input power. Online monitoring is favourable for continuous applications such as petroleum/chemical plants or water treatment systems [16]. Its main advantage is that the machine is not taken out of service. By constantly monitoring the machine, predictive maintenance is made easier, this means that failures can easily be detected and actions set in motion to prevent further downtime. The prime disadvantage of online monitoring is the addition of additional equipment on each induction machine. When compared to the offline solution it is

strenuous to detect some failure processes. More recent techniques include non-intrusive methods which use electrical signatures (machine currents and voltages) [16].

This report is focused on the temperature rise and lifespan of induction machines through monitoring of machine temperatures. In most induction machines temperature sensors are inserted in the windings, the stator core and the frame. Thermocouples are the most popular amongst the sensors used. The use of these sensors allows operators to measure the smallest of temperature changes allowing early detection of problems in the insulation system [16]. This knowledge allows maintenance to be scheduled before a breakdown occurs. The monitoring of stator winding insulation over time can be utilised by maintenance personnel to analyse the condition of the stator insulation [16].

2.4 Insulation Failure Mechanisms

The induction machine stator insulation may fail from more than one failure process. Each failure process is driven by one or more stresses like temperature, pollution, voltage and mechanical force. In most instances one stress does not define the life of insulation winding. As briefly described in the preceding section there are multiple stresses affecting the deterioration rate of the stator winding insulation. These stresses are commonly known as Insulation Failure Mechanisms (IFMs). Depending on the operation of the induction machine the IFMs can occur at a constant rate or they can be transient [15]. Further classification of IFMs can be those that occur constantly such as the operating temperature of the machine, the operating voltage of the machine and induced mechanical stresses. In [15] it is assumed that for failures due to constant IFMs, the time to failure is proportional to the number of operating hours for the induction machine. Stresses that take place for brief periods of time are known as transient stresses, these stresses include motor starting and out of phase synchronization. Similarly, [15] stipulates that the time to failure is proportional to the number of transients the machine experiences.

2.4.1 Thermal Stresses

Thermal stresses have the most effect on the deterioration rate of the induction machine stator windings insulation system. This stress is caused by the operating temperature of the induction machine. The operating temperature is a function of machine losses, this includes copper losses, eddy and stray load losses and the heating due to the core losses. Modern insulation systems fitted in induction machines experience a chemical reaction when operated above the recommended temperature. Oxidation results in the insulation material becoming brittle and delamination occurring. The delamination occurs because of the separation of the ground wall tape layers, this occurs because of the loss of bonding strength and impregnating compound [15]. This process can be modelled using a first order chemical reaction which is governed by the Arrhenius rate of flow. This was first proposed by Dakin [17], the life of the winding insulation (L, in hours) is related to operating temperature $(T, in\ °K)$ by (2-4)

$$L = Ae^{\frac{B}{T}} \tag{2-4}$$

Where parameters A and B are constants. This equation approximates the general notion that the life of the winding will decrease by 50% for every 10°C rise in temperature. Several variations of

this equations are used in [1] where the average winding life is calculated under various operating conditions. Figure 2-1 shows the primary causes of insulation failure in an induction machine.

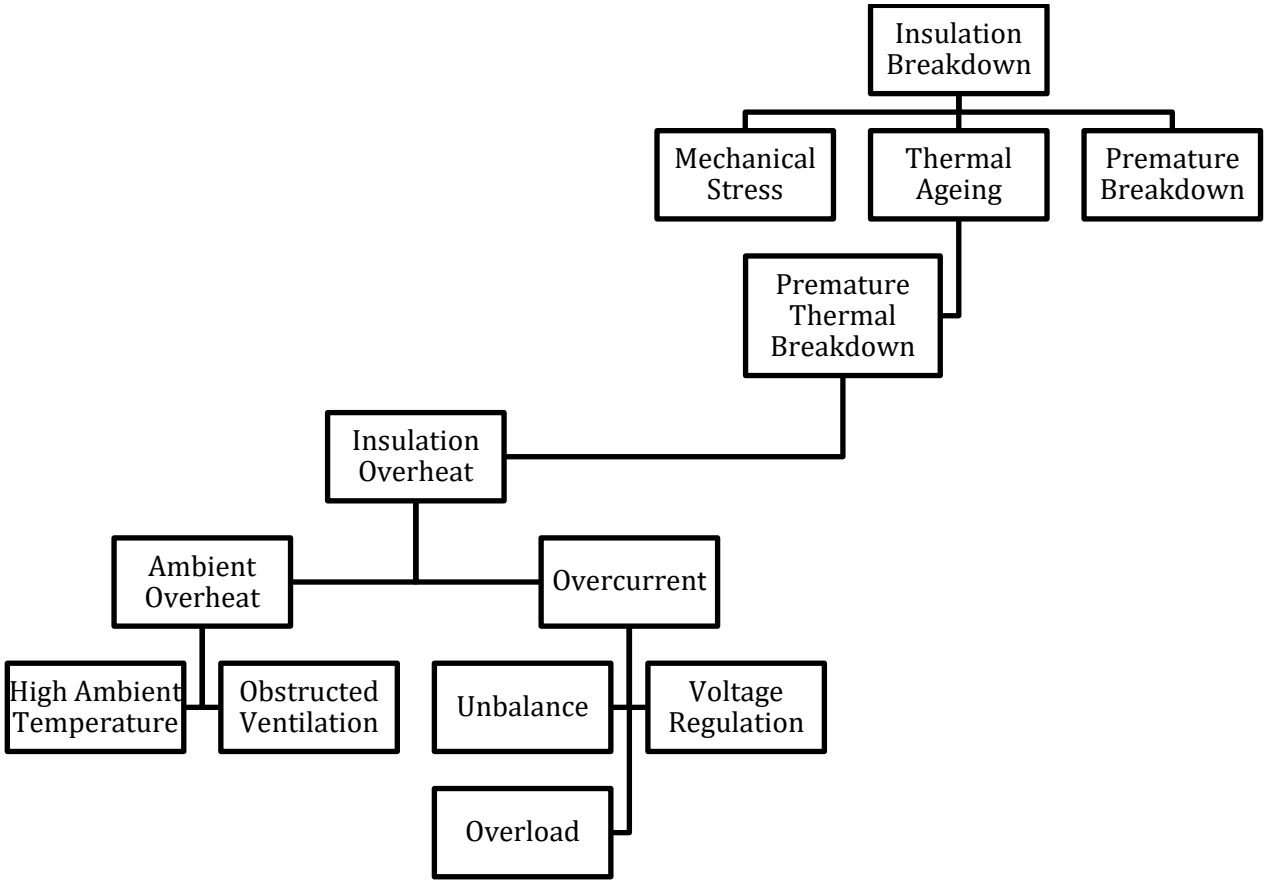

Figure 2-1 : Insulation Failure Flow Diagram

Insulation systems are classified according to the temperature they can operate at. The IEEE and IEC thermal classifications and definitions are similar. In most instances the IEC classification system is used, this system classifies both insulation systems and electrical equipment [15]. This system developed a thermal endurance graph which shows the relationship between the time to failure and the reciprocal of the absolute test temperature. Table 2-2 illustrates the accepted temperature indices of materials in accordance with IEC 60085.

Table 2-2 : Thermal classification of rotating machine insulation materials (IEC 60085) [18]

Numerical Classification	Letter Classification	Temperature (°C)
105	A	105
130	B	130
155	F	155
180	H	180

The older classification system (IEEE Standard 275-1985 and NEMA M&G) was according to a letter designation (A, B, F…) [16]. A numerical designation is preferred. Expected lifespan is based on a 20 000 hour (about 3 years) continual operation. This means that this average life approximation is based on the machine operating continually without any downtime. IEEE 275-1981 classification system is based on an ambient temperature of 40°C and the allowable

temperature rise for each insulation class is given. The IEEE 275-1981 classification system is summarised in Table 2-3.

Table 2-3 : Thermal classification of rotating machine insulation materials (IEEE 275-1981) [18]

Insulation Class	Maximum Allowable Temperature (℃)	Allowable Temperature Rise (℃)
A	105	65
B	130	90
F	155	115
H	180	140
H'	220	180

The ambient temperature directly impacts the machine operating temperature. An induction machine operating under a certain load condition will operate at a level of temperature increase known as the temperature rise. The operating temperature of the machine will then be this rise plus the ambient temperature. All machines have the maximum allowable ambient temperature on their nameplates. IEC machines are limited to 40 ℃ (104 F) ambient as per IEC 6003-1. The design temperature rise at rated load conditions plus the maximum ambient should not exceed the temperature class rating [19].

Thermal stresses can be divided into three groups: ageing, cycling and overloading. A general rule of thumb stipulates that for every 10℃ increase in temperature the insulation life is halved because of thermal ageing [20]. It is true that winding failure will occur irrespective of the degree of thermal ageing if the other stresses occur. The impact of temperature on the ageing of stator insulation can be reduced to prolong the thermal life by reducing the operating temperature or increasing the insulation class of the winding material used. Variation of the applied voltage, unbalanced phase voltages, obstructed ventilation and higher ambient temperature all cause thermal overloading.

2.4.5 Electrical Stresses

Electrical stress on the machine insulation usually occurs during start-up when there is a surge in current. Most machines now use star-delta start-up to avoid inrush currents at start-up. The electrical stresses that result in winding faults can be classified into dielectric, tracking, corona and voltage transients. The transient voltage conditions caused by line-to-line, repetitive re-striking, open and closing of breakers, lightning and capacitor switching reduce the stator winding insulation life. Tracking takes place in machines operating above 600V resulting in ground faults since the stator winding insulation system is not completely protected from the environment. Transient gaseous ionisation in the insulation system where the voltage exceeds the critical levels on motors operating above 5kV range results in corona [21].

2.4.6 Mechanical Stresses

These are stresses that accelerate the degradation of motor insulations; they include coil movement, rotor striking the stator and mechanical vibrations [23]. The current in the machine stator windings produce a force on the coils that is proportional to the square of the current. The force in context is maximum under starting cycle or transient overloads, this causes the coils to

vibrate at twice the line frequency in both the radial and tangential directions [23]. This movement leads to stator insulation damage/failure. The induction machine rotor can strike the stator due to multiple reasons such as shaft deflection, air gap eccentricities and broken rotor bars. If the strike takes place during the starting cycle the force of the rotor causes the stator laminations to puncture the insulation [20], if the strike occurs during full speed steady operation it can cause premature grounding in the coil in the stator slots [21].

2.4.7 Environmental Stresses

Environmental stresses cover contamination of foreign material and condensation/moisture. The introduction of foreign material can result in reduced heat dissipation causing adverse implications on the stator winding insulation. It is therefore of great value to restrict foreign particles from interacting with the surface of the machine. Condensation/moisture development leads to grounding in the slot. Condensation can be prevented by drying out the windings using space heaters during the off cycle [21].

The factors mentioned above mean that the temperature of the windings must be monitored and proper care should be taken to ensure they are within the specified limit. These limits must reflect the mechanical, electrical and environmental conditions in which the machine will operate [24]. To predict the temperature in induction machines thermal models are used. Thermal models of induction machines vary in the degree of complexities depending on areas of applications and the level of accuracy required [24]. Thermal models are used to determine the allowable short time overloads of a machine and hence form a key element for motor protection and condition monitoring. It should be noted that the altitude also influences the temperature of the induction machine, as the altitude increases, the air gets thinner and its ability to carry heat away from the machine is reduced. If a machine is operated at altitudes greater than 1000 m, its design should be adjusted to accommodate the less efficient cooling that results [19].

2.5 Insulating Material Thermal Ageing Test Standards

There are standardized tests that are available which Manufacturers use when testing the average life of insulating materials. In IEEE practice, the standard used for all insulating materials and insulation is the latest version of ANSI/IEEE Standard *No.1- "The Recommended Practice for Temperature Limits in the Rating of Electrical Equipment and for the Evaluation of Electrical Insulations*" [15]. Other standards for material evaluation are IEEE *No.98 – "Standards for the Preparation of Test Procedures for the Thermal Evaluation of Solid Electrical Insulating Materials" and IEEE No.101- "Statistical Analysis of Thermal Life Test Data".* There are several IEC standards that are comparable to the above-mentioned IEEE standards.

IEEE 275 is used during the design process of insulation systems to obtain the thermal ageing of a form wound stator coil [15]. An accelerated test is used to obtain the thermal ageing, this standard stipulates that at least four unidentical temperatures be used with heating done in an oven. Following each thermal cycle, the insulation under testing is then exposed to mechanical stress followed by moisture exposure and finally voltage exposure at a level derived from the rated line to line voltage [15]. If an insulation system is classified as Class F, its thermal endurance graph must result in failure times that are equal to or longer than a reference insulation system already shown to have a satisfactory life in service [15].

In the case of random-wound stator windings, IEEE 117 uses motorettes which consists of model coils installed in a simulated slot. This standard determines approximate life using at least ten or more thermal ageing cycles [15]. These cycles are then followed by exposure to vibrations and then exposure to humidity with condensation in a special chamber. It is evident that both these procedures (IEEE 275 & 117) require specialised equipment and personnel. This research report intends to investigate the impact of unbalance, over-and undervoltage conditions on the life of induction machines for various types of motors.

2.6 Induction Motor Thermal Models

The primary purpose of thermal protection of induction machines is to protect the machine from damage and to quickly isolate the machine from the rest of the power system when its operating above set thresholds. Thermocouples, resistance thermal detectors (RTDs) and infrared thermal sensors can be used for direct measurement of the stator winding temperatures. Applications of these devices is limited due to economic reasons more especially for small and medium sized machines, installation of these devices is difficult and costly. The most commonly used thermal protection devices include the dual element time delay fuses and overload relays. These devices are designed based on thermal limit curves which are only rough and conservative representation of the thermal characteristics of machines. The devices only use input current as a function of time to determine the thermal properties of the system. The thermal limit curves ignore the effects of the ambient temperature, voltage unbalance and the changes of the cooling capabilities of the machine.

Based on its insulation class, the thermal limit of an induction motor is the point at which it is operating above its rated temperature. Whenever this happens the following undesirable effects take place:

- Vibration and wearing of bearings
- Deterioration of bearing lubricants
- Loss of dielectrical property of the insulating material
- Thermal bending of the rotor and loss of eccentricity
- Thermal stresses and changes in the geometry of the induction machine elements due to thermal expansion.

To prevent any of these effects from occurring the temperature of the induction machine must be kept within the specified limits [24]. The temperature of the induction machine can be monitored using sensors (thermocouples) to ensure operation within the confined limits. Thermal models are tools used to predict the temperature of electric machines. Induction machine thermal models vary in the degree of complexity and machine type. These differences are brought about by the level of accuracy and applications, most models are based on the similarity between Ohm's law of electrical conduction and Fourier's law of heat conduction [24]. Thermal models can be used to determine the allowable short-time overloads of an induction machine and they form a key element for monitoring and protection of machines.

Lumped parameter models [25] [26] [27] [28] [29] are the most frequently used thermal models, Finite Element Method (FEM) methods are also used in the prediction of machine temperature [30]. Lumped parameter models have been used for a long period of time for temperature estimation in induction machines and turbine generators. Lumped parameter models also known

as thermal network models (TNM) usually comprise of thermal capacities and thermal conductances interconnected to form a network. The parameters of these thermal network models can be determined using a set of predetermined tests depending on the model or alternatively dimensional information can be used. This makes it easier to adapt the model to a range of machine sizes. The biggest drawback of using dimensional information to obtain the thermal parameters is that the calculations involved in determining these parameters are complex. Using dimensional information requires vast knowledge of thermal heat flow paths and distribution of heat energy within the machine. In [31] and [1], tests are defined which can be used to determine the parameters of the induction machine thermal model. These tests reduce the complexities of using dimensional information. Once the parameters of the thermal model are obtained the resulting set of differential equations which describe the machine steady state and transient states thermal performances can be computed. The thermal network model approximates average temperatures accurately, but the method fails in predicting hot spot temperatures [27]. The thermal temperature procedure is summarised in ***Error! Reference source not found.***

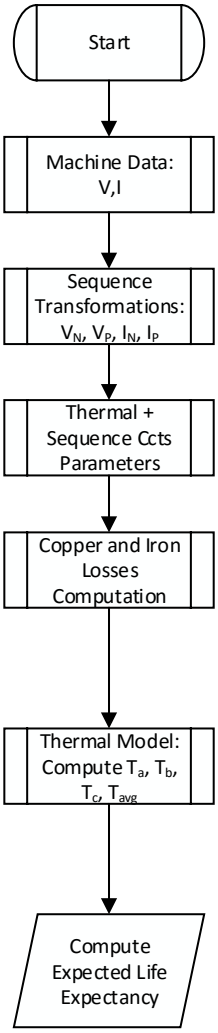

Figure 2-2: Thermal Model Development Process

The thermal model implemented in [31] assumes the thermal conductances are constant. It has however, been experimentally verified in [30] that the contribution of convection to the conductance improves the temperature approximation. This contribution has been assumed to vary linearly with the induction machine speed. This improvement of the model in [31] is discussed further in section 4.4.2 of this report. The results of this addition to the thermal model is summarised in Chapter 7.

The Finite Element Method (FEM) is commonly used for large machines where thermal asymmetries are common [24]. The three dimensional and time dependent problems associated with FEM models are related to both software and hardware implementation. For small and medium sized electrical machines FEM is less suited because the temperature gradients are small [27]. In this research report, thermal network models for several motors are developed. The temperatures predicted by thermal models are then used for life estimation of the induction machine.

2.7 Concluding Remarks

This chapter summarized the basic operating principles of the squirrel cage induction machine. The structure of the machine and its operating principles are discussed. The chapter continues with a literature survey of the latest testing and monitoring methods for insulation systems used in induction machines. The online and offline testing techniques and the standards from which they were adopted are discussed in further detail. It was realized that most of the available insulation testing methods are directed at detecting stator winding faults. The IEEE, IEC, MGI and NEMA all specify tests that can be undertaken on three phase induction machines to diagnose the turn insulation conditions.

The stresses that contribute to the loss of life in induction machines are also discussed and the thermal life equation is presented. Insulation materials are classified in accordance to the temperature rise they can withstand, the two classification systems (IEC 60085 and IEEE 275-1981). The chapter is concluded with the HICs discussion and a literature review of the lumped parameter thermal models and finite element methods (FEM). The lumped parameter thermal model will be used in the estimation of stator windings temperature. Since the induction machine will be operated under unbalanced, over- and undervoltage conditions, the model should allow analysis of each phase individually.

3. QUALITY OF SUPPLY

3.1 Introduction

This chapter introduces the power quality issues experienced by induction machines during operation. It also underlines the operation and performance of induction machines under non-nominal conditions. The performance and temperature of the induction machine is compromised due to issues associated with the quality of supply. There are specified tolerances which motors can be subjected to. In most instances, these tolerances are specified on the nameplate or Manufacturer s data sheets. These conditions are easier to obtain in laboratory conditions but are harder to achieve in the field [2]. **Error! Reference source not found.** illustrates some of the common conditions experienced by end users related to the voltage supply [2]. Voltage unbalance and voltage regulation are discussed in depth in the next section.

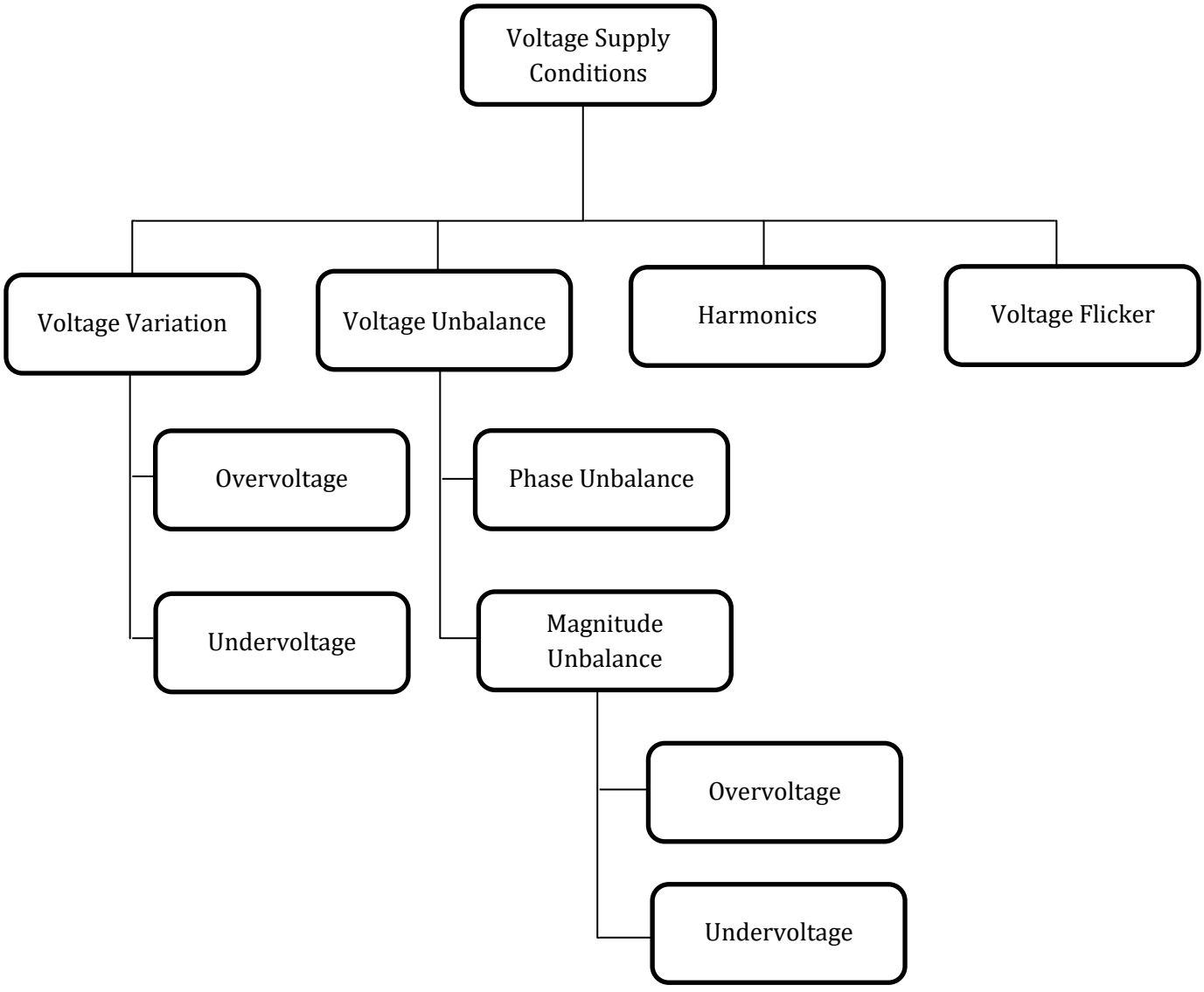

Figure 3-1: Overview of quality of supply problems [2]

3.2 Voltage Regulation

Voltage regulation is the change in voltage magnitude that will occur at a specified power factor when the load is reduced from the rated value to zero. This usually occurs when there is no internal adjustment of voltage control. It is expressed as a percentage of the nominal rated value. Voltage regulation is a convenient way to determine the sensitivity of the device due to load variations. Voltage load regulation is the ability of the utility to maintain constant voltage at generation, transmission as well as at the customer end of the distribution network [32]. All modern power systems are governed by specific standards, whereby machines and equipment supplied by these networks are therefore supplied at agreed nominal values. These values are within a specified tolerance limit.

In some cases, operation of the induction machine at the fringe of these specified tolerance limits may lead to an increased rate of deterioration. There are two voltage regulation definitions (regulation up and regulation down). The difference between the two is due to the reference voltage. Voltage regulation is defined as:

$$Regulation\ (\%) = \frac{|U_{NL}| - |U_L|}{|U_{NL}|} \times 100 \qquad (3\text{-}1)$$

Where U_{NL} is the no load voltage and U_L is the terminal load voltage.

3.3 Harmonics

Modern induction machines are driven by variable frequency drives which in many cases inject harmonics which appear at the motor's terminals. In their paper, De Abreu and Emanuel concluded that sub-harmonics have a remarkable effect on the thermal ageing and loss of life of the induction machine [33]. The harmonic currents produce rotating magnetic fields in the motor airgap. These rotating magnetic fields produced by the harmonic currents rotate at higher speeds than those produced by the fundamental current [2]. The result of the rotating magnetic fields is parasitic torques. Parasitic torques are present under balanced operating conditions but they are more harmful to the machine when the machine is operating under unbalanced conditions. An induction motor which has large harmonics will have a reduced fundamental torque and large asynchronous torques. These parasitic torques affect the induction machine efficiency and contribute to the total losses in the machine.

3.4 Flicker

Power line flicker is defined as the rapid changes in voltage magnitude which leads to what is known as fluctuations in a power system. In transmission systems, flicker is mainly caused by switching of large loads repeatedly such as the starting of machines. There are standards that are currently available that stipulate the various methods that can be used to determine the severity and type of flicker that occur in distribution systems.

IEC 61000-4-12:2010 standard contains the various methods for determining the severity of flicker in a distribution system. The NRS 048-2 standards show that a short-term flicker severity

(P_{st}) measurement will be carried out when it exceeds a ten-minute period. NRS 048-2 also shows that long flicker severity calculations will be when it exceeds over a two-hour period. This flicker severity can be calculated using (3-2):

$$P_{lt} = \sqrt[3]{\frac{\sum_{k=1}^{12} P^3{}_{st.k}}{12}} \tag{3-2}$$

3.5 Dips and Swells

Voltage dips are the temporary reduction of the RMS voltage. In most instances this is caused by a short circuit, overloading or in some cases starting of an electric machine connected to the system. IEEE 1159 defines a sag as a decrease in rms voltage between 0.1 pu to 0.9 pu for a duration of 0.5 cycles to 1 minute. Voltage dips occur when the voltage drop is more than 90% for a period longer than one or two cycles. Even though voltage dips are not as adverse as the interruptions, the total number of voltage dips is far more threatening than interruptions. Voltage sags are assessed according to their duration and magnitude [34].The magnitude is the percentage residual voltage during the sag and the duration is defined as time duration from onset (when the voltage drops below the agreed threshold) of sag till it clears out.

According to IEEE 1159 standards a "*voltage swell is the momentarily increase in RMS voltage level to 110%-180% of the nominal at the power frequency durations of half cycle to one minute".* These swells can be categorised as instantaneous (1.1-1.8pu), momentary (1.1-1.4pu) and temporary (1.1-1.2pu) [35]. NRS048-2:2003 stipulates that the phase to phase voltage swells in the South African network do not go beyond 1.15 of the declared voltages. It also states that the voltage swell in the South African network is due to events involving switching out of large loads or issues with the voltage control devices, these swells are not as common dips/sags.

According to the NRS 048, the standard low voltage supplied to customers shall be 400 volts phase to phase and 230 volts phase to neutral [36]. The deviation from these voltages shall not be greater than 10% above and below the standard voltage. Therefore, the maximum values to which the phase to phase voltage can vary is between 440 volts and 360 volts, and the phase to neutral voltage between 253 volts and 207 volts. Voltage regulation as a power quality disturbance is measured over a 10-minute averaging interval. A condition whereby the supply voltage exceeds the 10% threshold above the standard voltage of 400-volt phase to phase for a period longer than 10 consecutive minutes is called an overvoltage condition. In the event where the supply voltage exceeds the lower 10% threshold of the standard voltage of 400 volts for a period greater than 10 consecutive minutes then the condition will be called an under-voltage condition. A further 5%-voltage drop is allowed between the point of supply and the load according to SAN 10142, therefore it is possible to experience under-voltages of up to 85%.

3.6 Standards and Definitions

3.6.1 Energy Efficiency Standards

There are several standards that offer guidance in the measurement of induction machine efficiency. The IEEE 112-B (2004) and IEC 34-2 international standards are the most commonly used references when determining the efficiency of induction machines. There are minor differences between these two techniques. Different measurement procedures and calculation techniques are used by these standards. The major focus of the two standards is in the determination of stray load losses, the reference temperature and the correction of the stator winding resistance for calculating the stator and rotor copper losses. For the IEEE 112-B methodology, the temperature obtained during the rated load thermal test is used as the reference temperature. For the considered load conditions, the stator and rotor copper losses are corrected to the temperature measured at that load condition. The stray load losses are part of the total machine losses [37].

IEC 34-2 uses the insulation class temperature as the reference temperature. No thermal correction of the stator and rotor copper losses is required. The stray load losses are approximated to be equal to 0.5% of the input power under rated/nominal operating conditions. These different approaches lead to SLL values that vary slightly and the efficiency values obtained from these two procedures being different. IEC 34-2 is less accurate when compared to IEEE 112-B and is currently under review [37].

3.6.2 Voltage Unbalance Standards

Different countries have different qualities of supply; this means that the voltage unbalance standards from different countries will differ. The *American National Standards Institute (ANSI) standard C84.1-1995 'For Electric Power Systems and Equipment'* states that electrical supply systems should be designed and operated to limit the maximum voltage unbalance to 3% when measured at the electric-utility revenue meter under no load conditions [37].

The European voltage characteristics standard (EN50160) recommends that:
"*under normal operating conditions during each period of one week 95% of the 10-minute rms values of the negative phase component of supply shall be within the range of 0 to 2% of the positive phase sequence component. In some areas with partly single phase or two phase connected customers 'installations, unbalances up to about 3% at three phase terminals occur"* [37].

NEMA MGI-1993 "Motors and Generators" recommends that induction machines should be derated for voltage unbalance greater than 1%. This standard also recommends not operating an induction motor at all when the voltage unbalance exceeds five percent. IEC 60034-26 standard also recommends derating machine if the voltage unbalance is greater than 1% [38]. The IEC 1000-2-1 recommends a maximum limit of 2% of voltage unbalance. This voltage unbalance is defined using symmetrical components [39].

The South African Electricity Supply Utility (ESKOM)'s license agreement with NERSA (National Energy Regulator of South Africa) stipulates that the maximum deviation from the standard/declared voltages should be $\pm 10\%$ for voltages less than 500V and $\pm 5\%$ for voltages greater than or equal to 500V [36]. NERSA's NRS 048-2:2003 report states that the compatibility

level for unbalance on LV, MV and HV three phase networks should be 2%. On networks where there is predominance of single phase or two-phase customers a compatibility level of 3% may be applied [36]. Table 3-1 summarises them maximum allowable voltage unbalance as per the different standards.

Table 3-1: Overview of the maximum allowable voltage unbalance on motor terminals

Standard	Maximum Allowable VUB on Motor Terminals	Minimum derating VUB
NEMA MGI-1993	5%	1%
IEC 60034-26	2%	1%
EN50160	3%	-
ANSI	3%	-
SANS	3%	-

The American National Standard Institute (ANSI) deals with nominal and acceptable operating levels for voltages at 60Hz and between 100V and 230kV. In terms of voltage unbalance, the NEMA definition is utilised and it should not exceed 3% under nominal operating conditions [39].

3.7 Voltage Unbalance

Voltage unbalance is a critical power issue that cannot be totally removed. This power quality issue is present in most electric networks. There are currently three voltage unbalance definitions accepted and used in electrical engineering. Voltage unbalance is mainly found in individual customer loads because of the phase unbalance. This is most prevalent where large single-phase power loads are utilised [40]. Voltage unbalance is still considered a power issue even though in the most cases the voltages at the power utility are balanced. The unbalance at the receiver end comes because of unequal system impedance and unequal distribution of single phase loads [41]. Symmetrical component theory is used when computing voltage unbalances. The voltages are decomposed into positive, negative and zero sequence components. The level of voltage unbalance in a system can be evaluated as the percentage unbalance as defined by the National Electrical Manufacturer's Association (NEMA), the International Electro-Technical Commission (IEC) or the Institute of Electrical and Electronics Engineers (IEEE) definition.

3.7.1 NEMA Definition

The National Equipment Manufacturer's Association defines voltage unbalance as the ratio of maximum voltage deviation from the average line voltage divided by the average line voltage this is referred to as the line voltage unbalance rate (LVUR) [42].

$$LUVR(\%) = \frac{Max\left[\left|U_{ab} - U_{avg}\right| \cdot \left|U_{bc} - U_{avg}\right| \cdot \left|U_{ca} - U_{avg}\right|\right]}{U_{avg}} \qquad (3\text{-}3)$$

Where the average line voltage is given by:

$$U_{avg} = \frac{U_{ab} + U_{bc} + U_{ca}}{3} \qquad (3\text{-}4)$$

Phase information is ignored in this definition.

3.7.2 IEEE Definition

The IEEE uses the same definition of voltage unbalance as NEMA, the only difference is that the IEEE uses phase voltages rather than line to line voltages. Like the NEMA definition, the phase angle information is lost since only magnitudes are considered. This definition is known as the phase voltage unbalance rate (PVUR)

$$PVUR(\%) = \frac{Max\left[\left|U_a - U_{avg}\right| \cdot \left|U_b - U_{avg}\right| \cdot \left|U_c - U_{avg}\right|\right]}{U_{avg}} \tag{3-5}$$

Where the average phase voltage is given by:

$$U_{avg} = \frac{U_a + U_b + U_c}{3} \tag{3-6}$$

3.7.3 IEC Definition

The IEC definition also known as the true definition is defined as the ratio of the negative sequence voltage component to the positive sequence voltage component. It is known as the percentage voltage unbalance factor VUF (%), it is given by:

$$VUF(\%) = \frac{Negative\ Sequence\ Voltage\ Component}{Positive\ Sequence\ Voltage\ Component} \tag{3-7}$$

The voltage sequence components are obtained by resolving the three-phase unbalanced line/phase voltages into two symmetrical components of the line/phase voltages. The positive and negative sequence components are obtained using the following

$$U_p = \frac{U_{ab} + a \cdot U_{bc} + a^2 \cdot U_{ca}}{3} \tag{3-8}$$

$$U_n = \frac{U_{ab} + a^2 \cdot U_b + a \cdot U_{ca}}{3} \tag{3-9}$$

Where the operator $a = -0.5 + j0.866$ and $a^2 = -0.5 - j0.866$.
In most applications, the zero sequence currents cannot flow in the three-phase wire system as used by induction motors. The zero-sequence phase voltage is therefore of little to no importance, the negative sequence component is of high significance as it shows the voltage level that attempts to turn a three-phase induction motor in the opposite direction to the direction established by the positive sequence voltages [43]. This definition contains both magnitude and phase information. In his paper Wang [44], showed that two sets of three phase voltages of the same magnitudes of the complex voltage unbalance factor may affect the operation of an induction motor differently because of the different angles of the complex voltage unbalance factor, this has proven that the angle of the complex voltage unbalance has to be taken into account in order to determine the possible worst-case scenarios.

Another formula is given in [45] to compute the percentage voltage unbalance by avoiding the use of complex algebra:

$$VU\ (\%) = \sqrt{\frac{1-\sqrt{3-6\beta}}{1+\sqrt{3-6\beta}}} \times 100 \tag{3-10}$$

Where:

$$\beta = \frac{U_{ab}^4 + U_{bc}^4 + U_{ca}^4}{U_{ab}^2 + U_{bc}^2 + U_{ca}^2} \tag{3-11}$$

This formula is known as the "Beta" formula. A second formula that gives a good approximation of the true definition with minimal complex numbers is given by:

$$VU(\%) = \frac{82 \cdot \sqrt{U_{abe}^2 + U_{bce}^2 + U_{cae}^2}}{U_{average\ line}} \tag{3-12}$$

Where U_{abe} is the difference between line voltage U_{ab} and the average line voltage.

The LVUR as defined by NEMA and the VUF as defined by the IEC are both positive and real quantities that represent the level of unbalance. NEMA's definition is more convenient for field measurements since it only involves the magnitude of the three phase voltages. Computation of the VUF requires both the magnitude and phases of the three voltages to be known, which is more difficult to compute in the field. The IEC definition provides better physical interpretation of the cause of voltage unbalance and is more useful in prediction and the analysis of the effects of voltage unbalance on the induction machine. In this research project, the true definition of voltage unbalance is used when determining the losses, efficiency and temperature rise of the stator windings.

3.8 Types of Voltage Unbalance

A supply system can experience various kinds of voltage unbalance conditions for definite periods of time, these unbalance conditions can be combined with variations below and above the rated voltage [46]. This variation below and above the rated voltage has allowed us to classify voltage unbalance into undervoltage unbalance (UVU), rated voltage unbalance (RVU) and overvoltage unbalance (OVU). The undervoltage unbalance condition is prevalent whenever there is a voltage unbalance and the positive sequence component is less than the rated voltage. Conversely the overvoltage condition occurs when there is an unbalance and the positive sequence component is larger than the rated voltage value.

3.8.1 Voltage Unbalance Interpretation Ambiguities

As previously described in the preceding section, voltage unbalance as described by the IEC is

$$VUF(\%) = \frac{U_n}{U_p} \times 100 \tag{3-13}$$

Where U_n and U_p are the magnitudes of the negative and the positive sequence voltage components. If only magnitude is considered, the total number of combinations that can give us a certain voltage unbalance is infinite [47]. The total number of possible combinations can be restricted to a particular case if the complex voltage unbalance factor is used (CVUF). The complex voltage unbalance factor is defined as the ratio of the negative sequence voltage to the positive sequence voltage, it is expressed mathematically in the expression below:

$$CVUF(\%) = \frac{U_n}{U_p}\angle\theta_N - \theta_P \tag{3-14}$$

This definition is case specific whenever a voltage unbalance condition is considered. If the NEMA derating curve was considered for a particular voltage unbalance case, the question that will generally arise will be, "what voltage combination corresponds to a particular voltage unbalance?". Clarity is required because by applying different voltage sets to the induction machine terminals the operating behaviour changes. To be able to separate the various voltage combinations that constitute the same voltage unbalance, the positive sequence is used as the reference quantity. Several definitions can be used to specifically describe the type of voltage unbalance. The first is known as overvoltage unbalance VUF_{OVU}(OVU). This occurs when the positive sequence voltage component is greater than the rated voltage of the machine. All the line voltages as well as the positive sequence voltage should be greater than the rated machine voltage [48] [49].

$$VUF_{OVU}(\%) = \frac{U_{PL}}{U_{RL}} \times 100 \tag{3-15}$$

Where U_{PL} and U_{RL} are the positive sequence voltage component and the rated line voltage respectively. The second case is known as the mixed overvoltage unbalance factor VUF_{MOVU}(MOVU). This occurs when the positive sequence unbalance is greater than the rated line voltage, but the individual line voltages can be greater or less than the rated line voltage [47].

$$VUF_{MOVU}(\%) = \frac{U_{PL}}{U_{RL}} \times 100 \tag{3-16}$$

These two definitions give a clearer interpretation of overvoltage unbalance. This assists in analysing the impact of voltage unbalance on induction machines, instead of generalizing a voltage unbalance condition only a certain specified condition can be considered [47]. The third condition occurs when all individual voltage magnitudes and the positive sequence voltage component are all less than the rated line voltage. This is generally known as undervoltage unbalance VUF_{UVU}(UVU) expressed as:

$$VUF_{UVU}(\%) = \frac{U_{PL}}{U_{RL}} \times 100 \tag{3-17}$$

The fourth case occurs when all the individual line voltage magnitudes can be larger or less than the rated line voltage, but the positive sequence component must be less than the rated line voltage. This is referred to as the mixed undervoltage unbalance VUF_{MUVU}(MUVU) [47]. The final case is the IEC definition of voltage unbalance factor. The VUF can be defined as the ratio of the

negative sequence voltage to the positive sequence voltage with the major exception being that the positive voltage equals the rated voltage. This case is known as the unbalanced equal voltage (UBEV) an is expressed as

$$VUF(\%) = \frac{U_n}{U_p} \times 100 \qquad (3\text{-}18)$$

3.9 The Impact of Voltage Unbalance and Regulation on Induction Machines

3.9.1 Effects of Voltage Regulation on Motor Life

Over- and undervoltage takes place when the positive line/phase sequence is lower than or higher than the rated or nominal values respectively. When the voltage unbalance is expressed as a per unit quantity, the positive sequence voltage is usually (in realistic situations) very close to 1.0pu. while the negative sequence voltage is close to the voltage unbalance factor (VUF). Under heavy loads, when the supply voltage drops, the low voltage causes the torque developed to decrease. This causes a reduction in speed or an increase in slip, the motor will then have to draw above nominal current to maintain the power required to drive the load. At low load conditions, the motor draws below nominal currents when an undervoltage condition occurs. When an overvoltage occurs during heavy load conditions, less current is drawn because the motor can attain higher torque due to the increase in voltage. The opposite applies at light loads; high current is drawn due to the reduction in the motor torque [45]. The increase in currents drawn by the induction machines leads to an increase in stator winding temperatures and possibly insulation wear and motor damage [50]. It is important to note the region and range of cross-over of the undervoltage, overvoltage and rated voltage efficiency characteristics occurring in induction motors.

3.9.2 Effects of Voltage Unbalance on Motor Life

Operation of the induction motor under unbalanced voltage conditions leads to multiple complications within the motor. Increased stator currents and rotor losses are some of the more important results. Induction machines connected to unbalanced three phase voltage supplies will result in the machine drawing unbalanced currents [51]. These currents are known to be multiple times the voltage unbalance. There is a rule of thumb that stipulates that for every one percent of voltage unbalance a standard motor experiences, it will draw about five to six times as much current unbalance. This value fluctuates depending on the design and manufacturing techniques of induction motors. The induction machine can be viewed as two machines operating in opposite directions, this is represented by the positive and negative sequence circuits [43]. When operating under rated conditions the positive slip is typically close to zero and the negative slip close to 2. It therefore means that the rotor impedance of the negative sequence circuit is considerably smaller than the positive sequence impedance. This is the main reason low levels of voltage unbalance can lead to large negative sequence currents. This rapid increase in stator currents will eventually lead to an increase in resistive losses. Resistive losses are dissipated as heat and this causes overheating leading to damage of the induction machine windings. For the induction motor to maintain the same operational life as a motor operating at nominal conditions, the motor would have to be derated, i.e. the motor load reduced to limit the temperature rise to its rated value. The basic principles of derating involve determining the allowable power for a

machine operating under unbalanced voltage conditions. NEMA developed a generalised curve that is widely used in the industry because of its simplicity (shown in Figure 3-2) [52] [45]. The information developed by NEMA and various researchers shows that when voltages are unbalanced the percent increase in temperature rise equals about twice the square of the percent voltage unbalance. This is defined by the following relation [53] [52]:

$$1 + \frac{2(percent\ unbalance)^2}{100} = \left(\frac{percent\ load}{100}\right)^2 \qquad (3\text{-}19)$$

This is used to determine the appropriate load for operation for each voltage unbalance condition.

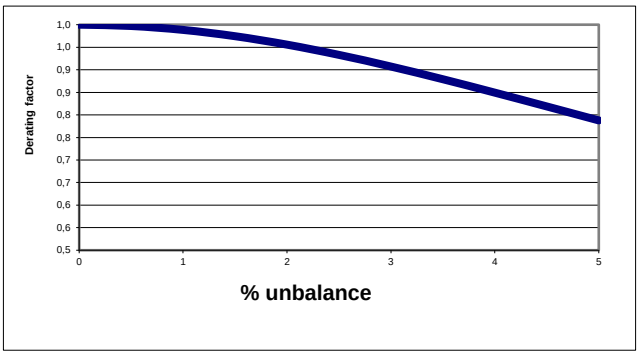

Figure 3-2: NEMA derating curve

Operation under increased voltage unbalance also leads to an increase in rotor losses. These losses occur more rapidly than stator copper losses [54]. As with stator losses the rotor losses are dissipated as heat and this heat causes damage to the rotor and its bearings. The induction motor fan cannot easily reduce the heat in the rotor.

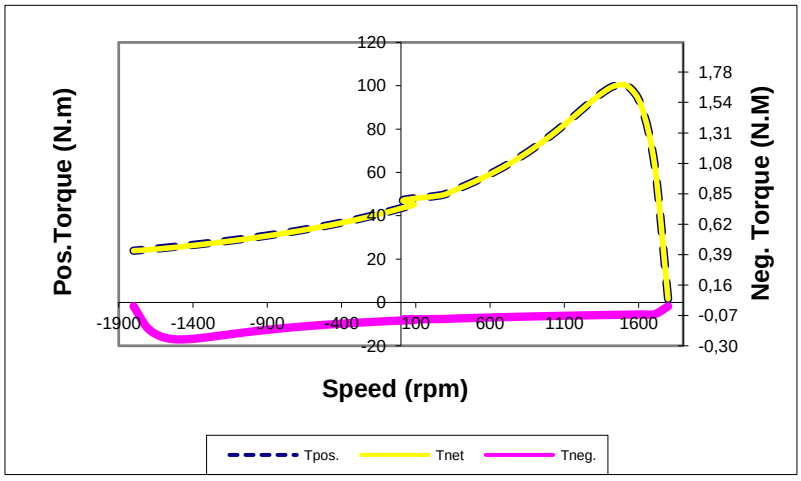

Figure 3-3: Positive, negative and resultant developed torque if an induction motor is supplied with voltage unbalance

As shown in Figure 3-3, the current produced by the negative sequence impedance, produces a torque in the opposite direction to the torque developed by the positive sequence current [51]. The resultant torque delivered by the induction machine is the summation of the two which is less than the positive torque. The reduction of effective torque and power means that the machine will have to operate above nominal conditions and this will lead to a rapid rise in temperature. In [45] it is shown that a lower positive sequence voltage with unbalance leads to a higher temperature rise when compared to a higher positive sequence voltage with unbalance. This is due to that the fact that a machine operating below rated voltage will have to do more work to deliver the same amount of power as one operating at rated values.

The induction machine rotor is affected by its impedance which depends on its frequency. This phenomenon is known as the "skin effect". Operation of the machine under unbalanced voltages leads to higher frequencies which causes the rotor current to concentrate on the surface of the rotor conductors [55]. The result will be an increase in effective rotor resistance and a decrease in the effective rotor leakage reactance. This decrease and increase in reactance and resistance depends on the type of rotor that the induction machine has, and this has a considerable impact on the negative sequence impedance. Literature by Williams has shown that single cage rotors have a lower resistance than double-cage rotors used for high starting torque [56]. It was also shown that additional rotor losses due to voltage unbalance are larger for motors with multiple cage rotors.

3.10 Voltage Unbalance Numerical Evaluation and Minimization

It is important to know the relationship between the individual line voltages, the phase angles and the voltage unbalance. By understanding these relationships, we can obtain the variations required to reduce the voltage unbalance. In a recently published paper (2009) "*voltage unbalance numerical evaluation and minimization*" Garcia [57] presents methods that use sensitivity analysis to determine the influence on the voltage on each parameter of the system (voltage magnitudes and phase angles) and how to mitigate/change the voltage unbalance using analytical solutions [57]. As previously described, the symmetrical components can be expressed as:

$$\begin{aligned} U_z &= \frac{1}{3}(U_A + U_B + U_C) \\ U_p &= \frac{1}{3}(U_A + aU_B + a^2U_C) \\ U_n &= \frac{1}{3}(U_A + a^2U_B + aU_C) \end{aligned} \tag{3-20}$$

Using these initial equations as references, several equations can be derived for simplification of the sensitivity method. By expressing each phasor in terms of its magnitude and angle, the following equations are obtained:

$$U_p = \frac{U_A\angle\theta_A + U_A\angle(\theta_A - 120°) + U_A\angle(\theta_A - 120°)}{3} \tag{3-21}$$

$$U_n = \frac{U_A\angle\theta_A + U_A\angle(\theta_A - 120°) + U_A\angle(\theta_A + 120°)}{3} \tag{3-22}$$

After obtaining the magnitude of the sequence components, the square root and the multiplying term $\frac{1}{3}$ can be eliminated resulting in the following equations

$$U_p^2 = \{U_A \cos\theta_A + U_A cos(\theta_B + 120°) + U_C cos(\theta_C - 120°)\}^2 + \{U_A \sin\theta_A + U_B sin(\theta_B + 120°) + U_C sin(\theta_C - 120°)\}^2 \quad (3\text{-}23)$$

$$U_n^2 = \{U_A \cos\theta_A + U_B cos(\theta_B - 120°) + U_C cos(\theta_C + 120°)\}^2 + \{U_A \sin\theta_A + U_B sin(\theta_B - 120°) + U_C sin(\theta_C + 120°)\}^2 \quad (3\text{-}24)$$

The terms on the right side of the equations above can be further simplified resulting in the following

$$U_p^2 = U_A^2 + U_B^2 + U_C^2 + 2U_A V_B cos(\theta_{AB} - 120°) + 2U_B U_C cos(\theta_{BC} - 120°) + 2U_A U_C cos(\theta_{CA} - 120°) \quad (3\text{-}25)$$

$$U_p^2 = U_A^2 + U_B^2 + U_C^2 + 2U_A U_B cos(\theta_{AB} + 120°) + 2U_B U_C cos(\theta_{BC} + 120°) + 2U_A U_C cos(\theta_{CA} + 120°) \quad (3\text{-}26)$$

Where $\theta_{AB} = \theta_A - \theta_B$; $\theta_{BC} = \theta_B - \theta_C$; $\theta_{CA} = \theta_C - \theta_A$

The resultant expression can be obtained by multiplying the right side of the equations by three and taking the square root

$$K = \sqrt{\frac{9V_2^2}{9V_1^2}} \quad (3\text{-}27)$$

3.10.1 Voltage Unbalance Sensitivity

The primary goal of sensitivity studies is to determine the response of a system when its parameters are varied [57]. Mathematically it is described as the relation between a parameter vector $\propto = \{\propto_1 \propto_2 \ldots \propto_r\}^T$ and a vector $\zeta = \{\zeta_1 \zeta_2 \ldots \zeta_n\}^T$ which represents the dynamic response of the system [57]. The two vectors can be defined as the summation of two vectors, the first being the nominal values ($\alpha_0 and\ \zeta_0$) and the other vector being the variations around the nominal values($\Delta\alpha\ and\ \Delta\zeta$) [57]. Mathematically this can be expressed as

$$\alpha = \alpha_0 + \Delta\alpha \quad (3\text{-}28)$$

$$\zeta = \zeta_0 + \Delta\zeta \quad (3\text{-}29)$$

The definition given above is a first-degree approximation and only valid under particular conditions and for minor parameter changes ($\|\alpha_0\| \ll \|\Delta\alpha\|$).

$$\Delta\zeta \approx S(\alpha_0)\Delta\alpha \tag{3-30}$$

The absolute and relative sensitivity functions that are used in determining the change in the system are defined by the following equations

$$S_{\alpha_j}^{\zeta_i} = \frac{\partial\zeta_i}{\partial\alpha_j} \tag{3-31}$$

$$\bar{S}_{\alpha_j}^{\zeta_i} = \frac{\partial\zeta_i/\zeta_i}{\partial\alpha_i/\alpha_i} = S_{\alpha_j}^{\zeta_i}\frac{\alpha_{j0}}{\zeta_{i0}} \tag{3-32}$$

The relative and absolute sensitivity functions that affect each parameter on the overall voltage unbalance can be determined [57]. The influence of each system parameter on the overall system voltage is done by initially setting α_0 as the magnitude and angle values of the three phases in an unbalanced system and ζ_0 as the corresponding unbalance factor for these values. The rate of change of voltage unbalance in response to the change in each parameter can be obtained. To ensure that only terms with the same dimensions are compared, only the relative sensitivity function will be utilized. The relative sensitivity function can be directly applied where α_j is equal to $U_A, U_B, U_C, \theta_A, \theta_B$ or θ_C. Derivatives that are very complex are the result when directly applying the function and it requires a few simplifications. The derivative of the square root is developed and then the quotient rule for the derivative is applied. The resultant sensitivity function is expressed in equation (3-36).

$$S_{\alpha_j}^{-K} = \alpha_j\sqrt{\frac{9U_p^2}{9U_n^2}}\frac{\partial}{\partial\alpha_j}\left(\sqrt{\frac{9U_n^2}{9U_p^2}}\right) \tag{3-33}$$

$$S_{\alpha_j}^{-K} = \frac{\alpha_j}{2}\frac{9U_p^2}{9U_n^2}\frac{\partial}{\partial\alpha_j}\left(\frac{9U_n^2}{9U_p^2}\right) \tag{3-34}$$

$$S_{\alpha_j}^{-K} = \frac{1}{2}\left(\frac{\alpha_j}{9U_n^2}\frac{\partial(9U_n^2)}{\partial\alpha_j} - \frac{\alpha_j}{9U_n^2}\frac{\partial\left(9U_p^2\right)}{\partial\alpha_j}\right) \tag{3-35}$$

$$\bar{S}_{\alpha_j}^{K} = \frac{1}{2}\left(\bar{S}_{\alpha_j}^{9U_n^2} - \bar{S}_{\alpha_j}^{9U_p^2}\right) \tag{3-36}$$

Equation (3-36) represents the relative sensitivity function of $K(\bar{S}_{U_A}^K, \bar{S}_{U_B}^K, \bar{S}_{U_C}^K, \bar{S}_{\theta_A}^K, \bar{S}_{\theta_B}^K)$ and $\bar{S}_{V_C}^K$ since α_j can be $(U_A, U_B, U_C, \theta_A, \theta_B)$ or θ_B can be developed through differentiation of equations. The sensitivity function shows the influence of each system parameter on the corresponding voltage unbalance, it does not tell us the changes in magnitude or angle required to reduce the voltage unbalance to a desired value [57]. The next sub-section 3.10.2 describes how analytical solutions can be used to reduce the voltage unbalance to a desired value. There are three ways one can possibly reduce the voltage unbalance

3.10.2 Voltage Unbalance Minimization

Three possible ways are considered when trying to find an analytical solution to voltage unbalance reduction: changing of one parameter separately (magnitudes and angles of each phase), changing of two magnitudes concurrently and changing of three magnitudes simultaneously

Variation of one parameter (magnitudes and angles of each phase)

For voltage unbalance reduction by variation of one parameter separately, the initial equation must be manipulated so that one variable can be isolated, the following equation is obtained (full derivation given in [57])

$$\begin{aligned} K^2\{U_A^2 + U_B^2 + U_C^2 + 2U_AU_Bcos(\theta_{AB} - 120°) + 2U_BU_Ccos(\theta_{BC} - 120°) \\ + 2U_AU_Ccos(\theta_{CA} - 120°)\} \\ = U_A^2 + U_B^2 + U_C^2 + 2U_AU_Bcos(\theta_{AB} + 120°) \\ + 2U_BU_Ccos(\theta_{BC} + 120°) + 2U_AU_Ccos(\theta_{CA} + 120°) \end{aligned} \quad (3\text{-}37)$$

For this equation to be true, one of the parameters has to be changed for us to obtain a new value for the voltage unbalance K, this new desired voltage unbalance can be called K_{new}. If we choose to isolate the parameter U_A from the previous equation, a quadratic polynomial will be the result. New terms A_{U_A} , B_{U_A} and C_{U_A} these new terms are defined in the equations that follow

$$A_{VA}V_A^2 + B_{VA}V_A + C_{VA} = 0 \quad (3\text{-}38)$$

$$A_{VA} = 1 - K_{new}^2 \quad (3\text{-}39)$$

$$\begin{aligned} B_{VA} = 2V_B[cos(\theta_{AB} + 120°) - K_{new}^2 cos(\theta_{AB} - 120°)] \\ + 2V_C[cos(\theta_{CA} + 120°) - K_{new}^2 cos(\theta_{CA} - 120°)] \end{aligned} \quad (3\text{-}40)$$

$$\begin{aligned} C_{VA} = 2V_BV_c[cos(\theta_{AB} + 120°) - K_{new}^2 cos(\theta_{AB} - 120°)] \\ + (1 - K_{new}^2)(V_B^2 + V_C^2) \end{aligned} \quad (3\text{-}41)$$

$$\begin{aligned} C_{VA} = 2V_BV_c[cos(\theta_{AB} + 120°) - K_{new}^2 cos(\theta_{AB} - 120°)] \\ + (1 - K_{new}^2)(V_B^2 + V_C^2) \end{aligned} \quad (3\text{-}42)$$

Equations given above show that if you are given the values of the voltage magnitudes and angles, a different value of voltage unbalance factor K can be chosen K_{new} and two values of U_A can satisfy

the selected new voltage unbalance factor. These two new values will only make sense for positive real values, so the following condition holds

$$B_{VA}^2 - 4A_{VA}C_{VA} \geq 0 \tag{3-43}$$

For the equation that satisfies the above condition and isolates K_{new} limit values can be determined for the correction of the voltage unbalance. The following equations present the required formulas.

$$\begin{gathered} A_{VAK}K_{new}^4 + B_{VAK}K_{new}^2 + C_{VAK} = 0 \\ A_{VAK} = \alpha_{VAK}^2 + 4\gamma_{VAK} \\ B_{VAK} = 2\alpha_{VAK}\beta_{VAK} + 4(\delta_{VAK} - \gamma_{VAK}) \\ C_{VAK} = \beta_{VAK}^2 - 4\delta_{VAK} \\ \alpha_{VAK} = -2V_B\cos(\theta_{AB} - 120°) - 2V_C\cos(\theta_{CA} - 120°) \\ \beta_{VAK} = 2V_B\cos(\theta_{AB} + 120°) + 2V_C\cos(\theta_{CA} + 120°) \\ \gamma_{VAK} = -2V_BV_C\cos(\theta_{BC} - 120°) - V_B^2 - V_C^2 \\ \delta_{VAK} = 2V_BV_C\cos(\theta_{BC} + 120°) + V_B^2 + V_C^2 \end{gathered} \tag{3-44}$$

The newly defined parameters are the parameters that indicate that by satisfying equation (3-44) (i)) and the condition $K_{new} \geq 0$ the minimum value of K_{new} can be obtained by varying U_A given the initial values for $U_B, U_C, \theta_A, \theta_B$ and, θ_C. A similar approach is used for the other two phases which will result in similar equations. The procedure for the angles is similar but the final equations are different, the derivation is shown in [39].

Variation of three magnitudes simultaneously

Like varying one magnitude, the initial equation is used for derivation. Since there are three variables and one equation the solutions are infinite. If we consider the Euclidean distance, the minimization problem is described as: obtain $min((U_A - U_{A0})^2 + (U_B - U_{B0})^2 + (U_C - U_{C0})^2)$ in terms of equation (3-37) where U_{B0}, U_{C0} and U_{A0} are the initial values of the phases B, C and A. By applying Laplace's method, we can introduce a new variable (λ) to include in equation (3-37) [57]. This helps us create a new function that needs to minimize, this is given below.

$$\begin{aligned} min\{&(V_A - V_{A0})^2 + (V_B - V_{B0})^2 \\ &+ \lambda\{(V_A^2 + V_B^2 + V_C^2)(1 - K_{new}^2) \\ &+ 2V_AV_B[cos(\theta_{AB} - 120°) - K_{new}^2 cos(\theta_{AB} + 120°)] \\ &+ 2V_BV_C[cos(\theta_{BC} - 120°) - K_{new}^2 cos(\theta_{BC} + 120°)] \\ &+ 2V_BV_C[cos(\theta_{BC} - 120°) - K_{new}^2 cos(\theta_{BC} + 120°)]]\} \end{aligned} \tag{3-45}$$

By obtaining the derivatives of the equation given above with respect to U_{B0}, U_{C0} , U_{A0} and λ, and equating them to zero results in a system of equations with four variables. The solutions to these equations are solved using MATLAB. Similarly, the procedure for two magnitudes the function to be minimized is $(U_A - U_{A0})^2 + (U_B - U_{B0})^2$ which subject to equation (3-37). The voltage unbalance factor conditions considered in this research report are tabulated in Table 3-2.

Table 3-2: Considered Voltage Unbalance Conditions and Identification

VR	VUF (%)	U_{AB}	U_{BC}	U_{CA}	U_{AVG}	VUF_{ID}
100	0	400	400	400	400	VUF_{UBEV}
	1	400	392	405	399	VUF_{MUVU}
	2	416	396	388	400	VUF_{MUVU}
	3	400	379	420	399.67	VUF_{MUVU}
90	0	360	360	360	360	VUF_{UVU}
	1	360	352	365	359	VUF_{UVU}
	2	376	356	352	361.33	VUF_{UVU}
	3	360	342	380	360.67	VUF_{UVU}
110	0	440	440	440	440	VUF_{OVU}
	1	440	432	448	440	VUF_{OVU}
	2	456	436	426	439.33	VUF_{OVU}
	3	440	418	462	440	VUF_{OVU}

Since only magnitude conditions are considered, the methods described in this chapter are validated using the VUF_{OVU} overvoltage unbalance condition using the 3% voltage unbalance condition.

$$\begin{aligned} U_A &= 440\angle 0° \\ U_B &= 418\angle -120° \\ U_C &= 462\angle 120° \end{aligned} \tag{3-46}$$

The relative positive and negative sensitivity values of the three voltage magnitudes is given in Table 3-3. The negative sign is to define the growth direction of the derivative of the VUF (K) as per each parameter.

Table 3-3: The relative sensitivity of the VUF and minimum values for correction through each parameter for a system with two unbalanced magnitudes

	U_A	U_B	U_C	θ_B	θ_C
Relative Sensitivity (Dimensionless)	-0.33	-9.82	10.15	-11.49	12.70
Minimum K (%) (Individual Parameter Δ)	2.89	1.41	1.49	2.54	2.47
Corresponding values for minimum K	438.98V	450.26V	427.10	122.79	117.31°
Minimum K (%) (Simultaneous Parameter Δ)	0	0	0	0	0
Corresponding values for minimum K	440V	440V	440V	-120°	120°
Desired K (%) value					
K = 0% (Individual Parameter Δ)	-	-	-	-	-
K = 0% (Simultaneous Parameter Δ)	440V	440V	440V	-120°	120°
K = 1% (Individual Parameter Δ)	-	-	-	-	-
K = 1% (Simultaneous Parameter Δ)	440.17V	432.54V	447.79V	-120°	120°
K = 2% (Individual Parameter Δ)	-	432.31V	412.20V	-	-
K = 2% (Simultaneous Parameter Δ)	440.16V	424.91V	455.40V	-120°	120°

Similarly, by disregarding the negative signs it can be observed that for this voltage unbalance condition, K is more sensitive to the angles than to the voltage magnitudes. The two voltage minimizing techniques (minimization by variation of one parameter and minimization by variation of three magnitudes simultaneously) are considered.

For the voltage unbalance case under consideration, the maximum achievable voltage unbalance minimization by variation of one parameter and the corresponding values that yield this minimization are given in Table 3-3. It is shown that the minimum voltage unbalance that can be obtained using the variation of one parameter is 1.4%. This is achieved by increasing $U_B = 418\angle -120°$ to $U_B = 450.26\angle -120°$. It should be noted that for this method all the parameters are considered separately, meaning all the other parameters are kept constant whilst changing one. It is not possible to minimize the voltage unbalance to zero using this method.

Voltage unbalance minimization by variation of three magnitudes simultaneously was considered. As expected, minimization by variation of three magnitudes is possible for all voltage unbalance conditions. Several voltage unbalance cases were selected to validate the results in Table 3-3.

3.11 Loss of Life in Induction Machines

The lifespan of any equipment is defined as the time from when it was manufactured to the time when it can no longer do what it is required to do at the rate at which it was rated to do [18]. If operated within its specified temperature limits and not exposed to electrical overloading or mechanical stresses the insulation system of a modern induction machine will have a lifespan of approximately 20000 operating hours [6]. In practice it is difficult to achieve these ideal operating conditions and the stator insulation is exposed to different IFMs that result in accelerated deterioration. In the case for the totally enclosed fan cooled induction motor ageing due to thermal stresses is the dominant factor in the deterioration of the stator winding insulation. It was mentioned in Table 2-3 that the thermal class of any insulation system determines the maximum temperature that insulation system can operate at. This is the temperature at full load operating conditions at an ambient temperature of 40℃ [6].

The insulation winding deterioration is a chemical process which is largely dependent on temperature. *Arrhenius law* describes the relationship between the induction machine operating temperature and the expected lifespan of a specific insulation material. Every 10-K increase in the temperature doubles the degradation rate of the insulation material [6]. As shown in in Figure 3-4, it decreases the useful lifetime by over 50%. Excessive high temperatures for short durations do not have a large impact on the lifespan of the machine insulation. It is only when these high temperatures are continuous that they become a major problem. In an induction machine the average stator winding temperature rise depends on the inner losses, the thermal resistance (or conductance), the thermal capacity and the ambient temperature. Short term voltage peaks or surges can be caused by variable speed drive (VSDs) or when the machine is line fed by atmospheric discharges and manoeuvres in the electric power network [6]. At the point where the maximum voltage impressed equals the breakdown voltage of the insulation system, motor failure becomes imminent [4]. If the motor insulation has deteriorated to level that is affected by surges, arcs may result leading to greater deterioration of the insulation breakdown up to a level close to the operating voltage of conductors which will weld together causing failure due to the level of current induced [6].

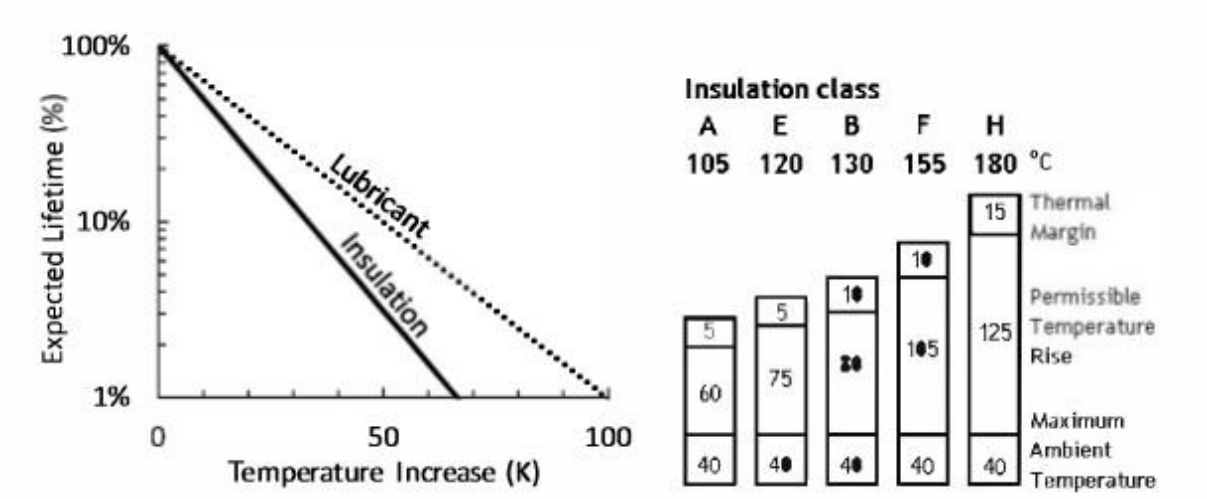

Figure 3-4: Expected useful lifetime of insulation materials and lubricants as a function of operating temperature [6] [58]

An equation was developed using Arrhenius' law to estimate insulation lifespan under certain conditions. The initial equation assumes that the induction machine is operating continuously at the same temperature throughout its lifespan [53].

$$L_x = L_{100} \cdot 2e^{\frac{T_c - T_x}{HIC}} \tag{3-47}$$

Where:

L_x is the percent lifetime at temperature T_x(℃)
L_{100} is the percent lifetime at the rated the temperature T_c(℃)
T_x is the hotspot temperature for insulation class (℃)
T_c is the total allowable temperature for insulation class (℃)
HIC is the halving interval for the insulation class (℃)

The halving intervals for the various insulation classes are given in Table 3-4. The values are given in degrees centigrade.

Table 3-4: Halving intervals of various insulation classes [53] [1]

Insulation Class	Halving Interval
A	14
B	11
F	9.3
H	8
H'	10

Arrhenius equations make it easier to model acceleration of the ageing process when the induction machine is operating at temperatures that are above the rated temperatures. Unfortunately, these ideal conditions are never met, and it is unrealistic to assume that the machine will operate at the same temperature throughout its life at the same temperature. A

different version of the equation has also been derived to make provisions for the variation of temperature over time:

$$ln\left(\frac{t_r}{t_i}\right) = \frac{\varphi}{k}\left(\frac{1}{T_r} - \frac{1}{T_i}\right) \quad (3\text{-}48)$$

Where:

t_r is the time at temperature T_r
t_i is the time at temperature T_i
k is $0.8617 \times 10^{-4}\ eV/K$
φ is $1.05eV$

Both these equations can be applied in the estimation of induction machine life.

3.11.1 VSD fed Machines

Literature shows that for VSD-fed induction machines the extra losses due to harmonics can result in up to 10% increase in the machine operating temperature [7] [59]. The coils near the machine terminal leads are exposed to PWM voltage pulses that are very high in amplitude. The reflection of the PWM voltage pulse in the power cable between the induction machine and the VSD, in the worst-case scenario, causes the voltage peaks imposed on the machine windings to reach double the VSD DC-bus voltage [6]. This results in an accelerated deterioration rate and partial discharge may occur which eventually leads to premature failure of the insulation system [6]. The voltage peaks that occur are directly related to the PWM switching frequency, the reduction of the PWM switching frequency can lead to an increase in the stator winding insulation life from a thermal perspective. The opposite also holds that machine harmonic losses may increase leading to increased operating temperatures [6].

3.11.2 Efficiency Classes

When considering thermal ageing of machines, higher efficiency machines offer a clear advantage. Due to the small difference in the pricing between the class F/H insulation and the class B insulation materials, most Manufacturers tend to use class F/H insulation. This is done regardless of the actual temperature rise which in this case is much lower in Premium/IE3 and Super-Premium/IE4 machines because of both lower losses and improved heat dissipation by conduction and convection. These machines offer an extended winding insulation lifetime or a higher service factor (SF). In [6] it was concluded that induction machines with higher efficiency and same insulation class:

(a) offer a longer winding MTBF (mean time between failures) for the same ambient temperature;
(b) can withstand higher ambient temperatures for the same MTBF;
(c) can withstand higher additional losses due to power quality for the same ambient temperatures and winding MTBF;
(d) can withstand higher output power for the same ambient temperatures and winding MTBF [6].

The combination of the previously mentioned conditions results in a gain in lifetime. High efficiency induction machines have a lower rotor impedance and starting torque, therefore they

are more sensitive to operation under voltage unbalance conditions from a starting performance point of view [6].

3.12 Concluding remarks

Chapter 3 gives a conclusive overview of the power quality issues experienced by induction machines, primarily in the South African context. Power quality issues discussed include voltage unbalance, voltage regulation, harmonics, flicker and dips and swells. Since this report is focused on the impact of voltage unbalance and regulation on the life expectancy of induction machines, the voltage unbalance standards from different countries are compared. It was found that the European voltage standard (EN50160) stipulates that for normal operating conditions, for each period of one week, 95% of the 10-minute rms values of the negative sequence phase component supply must be within 0 to 2% range of the positive sequence phase component. The European standard allows a maximum voltage unbalance of 3% in areas with single phase or two phase connected customers. The concept of derating is introduced by NEMA MGI-1993 and IEC 60034-26, both recommend derating of machines operating for voltage unbalances greater than 1%.

ANSI recommends a maximum voltage unbalance of 3%, this voltage unbalance is defined in terms of the NEMA definition. For South African networks the NRS 048 stipulates that the compatibility level for unbalance on LV, MV and HV three phase networks should be 2%. On networks where there is predominance of single phase or two-phase customers a compatibility level of 3% may be applied. The NEMA, IEEE and IEC voltage unbalance definitions are discussed. NEMA's voltage unbalance definition is more convenient for field/on-site measurements because it only requires magnitudes of the three phase voltages. Like the NEMA definition, the IEEE definition only requires the magnitudes of the voltage. The IEC (VUF) definition of voltage unbalance requires both the magnitude and phases of the three voltages to be known, this can become cumbersome when taking measurements in the field. The IEC definition provides a better physical interpretation of the cause of voltage unbalance and is much more useful in the prediction of and analysis of the effects of voltage unbalance in induction machines. The IEC definition of voltage unbalance will be used throughout this report. This definition includes phase information which should be considered when voltage unbalance is analyzed. The measurement devices used in this research report allowed for precise measurement of phase angles allowing for accurate voltage unbalance measurements. As mentioned in the preceding sections, by using the complex voltage unbalance factor analysis becomes case specific.

Methods used to minimize voltage unbalance based on symmetrical components theory were discussed. This focused on the sensitivity of each parameter on the overall voltage unbalance as well as the mathematical solutions to minimize the voltage unbalance. One voltage unbalance condition was considered where two phases were unbalanced. Angle unbalance was not considered because none of the considered unbalance conditions in this research project involve any angle unbalance. These methods can serve as a valuable tool for analyzing and minimizing voltage unbalance in power systems.

4. ELECTRICAL AND THERMAL MODELLING OF INDUCTION MACHINES

The purpose of this research project is to estimate the loss of life in induction machines due to voltage unbalance and regulation. The thermal model attempts to predict the stator windings temperatures of the machine, this temperature is used in the life prediction model. Inputs to the thermal model includes, the machine losses and the ambient temperature. The losses are obtained using the electrical model and the ambient temperature is measured using a thermometer.

The induction machine per phase equivalent circuit is used to analyse machine performance under balanced operating conditions. When voltage unbalance is introduced, symmetrical components can be used to analyse the machine on a per phase basis. Under balanced operating conditions it is assumed that the currents in the three phases are equal, with the introduction of voltage unbalance, the three-phase unbalanced system is decoupled into three networks, two balanced systems (positive and negative sequence components) and a zero-sequence component. The three networks can be analysed separately, and the overall effect can be found by superposition [53]. In most applications, induction machines usually use a delta or ungrounded star configuration. This eliminates the currents from the zero sequence components in the absence of any fault condition. All the zero components have the same magnitude and zero phase displacement between them [51]. By using the Fortescue transformation matrix, the two balanced systems can be used to analyse each of the three phases. Under balanced operating conditions, single phase thermal models are used to predict the three-phase temperature rise. Analysis of each phase and its interaction with the other phases, the core and the ambient temperature is required when voltage unbalance is introduced. The analysis using the electrical model and sequence components allows us to determine the stator copper losses associated with each phase, these are inputs to each of the phases of the thermal model. The core losses are determined using the standardized no load test in accordance with IEEE 112-B standard.

The lumped parameter thermal network allows us to divide the induction machine into basic thermal elements. These elements are interconnected forming a network of nodes. The primary assumption in these networks is that all the heat generation in each component is concentrated in one point, this point is referred to as a node. This node represents the average temperature of the component. There are several ways of subdividing the machine and the choice of subdivision results from the compromise between simplicity of the thermal model and the quality of information sought. For this application the machine subdivision is based on physical factors that contribute significantly to the temperature rise of the phase windings. The accurate prediction of an induction machine temperature does not only depend on the thermal model network but also on the correct allocation of losses to the nodes in the network. The correct allocation of the stator copper and core losses is discussed in section 4.3.2. Thermal models can be incorporated as algorithms and be implemented in microprocessor devices which enhance the level of accuracy

and flexibility. As a practical application most, thermal model algorithms operate as per the following sequence:

- Real-time machine data is supplied to the microprocessor device
- The supplied real-time data is processed according to the firmware thermal algorithm program and the results are compared with the expected values and stored in memory.
- If a machine protection device (MPD) is being used, it computes an analog value which is then compared with the output of the thermal model algorithm.
- The MPD triggers the digital outputs if the compared analog value exceeds the threshold.

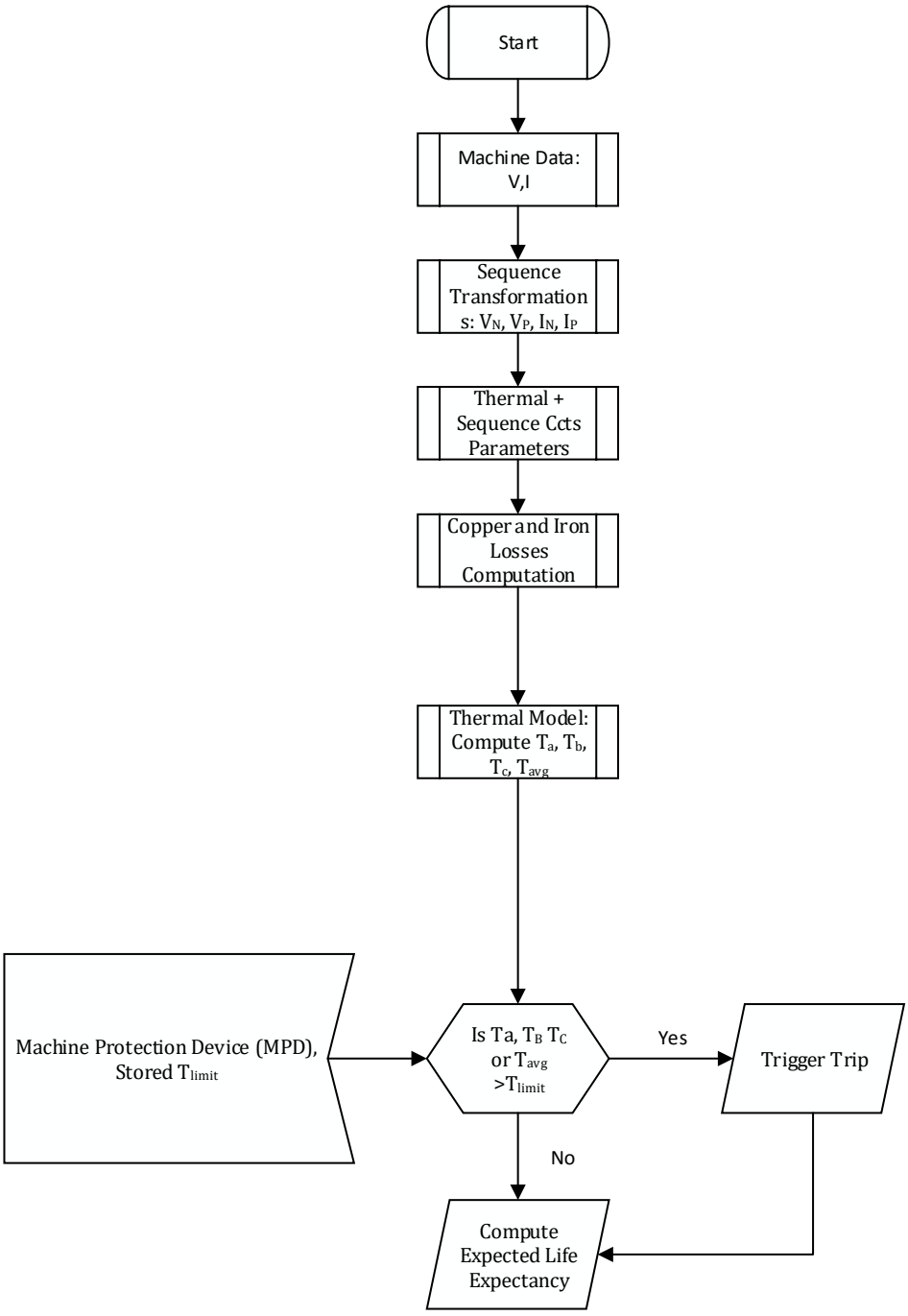

Figure 4-1: Incorporation of the proposed thermal model with MPDs

Thermocouples and Resistance Temperature Detectors (RTDs) offer realistic results in monitoring machine temperatures under balanced operating conditions but they do not offer the best monitoring of fast thermal transients. They are also not economical especially for low and medium sized machines where installation is difficult and costly. Other conventional machine thermal protection devices include time delay fuses and overload relays this are discussed in more detail in section 7.2 of this report. Modern thermal models form part of machine protection devices that primarily consists of the following:

- A voltage unbalance measuring/diagnostic circuit which is configured to detect and evaluate a supply line voltage unbalance and to produce a fault indication signal when the supply line voltage unbalance is above a certain threshold (current unbalance diagnostic circuit can also form part of the machine controller)
- Current relays that based on thermal limit curves which define the safe operating time for different magnitudes of input currents under both transients and running overload conditions. /microprocessor based thermal overload protective circuits which calculate machine temperatures using thermal models of ac machines.

The proposed thermal model can use real time inputs to compute the machine steady state windings temperature. The machine windings temperature is a function of current and time, this and pre-determined parameters such as iron losses, per-phase equivalent circuit parameters and thermal model parameters are employed to develop and employ a real time steady state thermal model. Knowledge of the thermal limit of the machine stored in the MPD can be used as thermal limits which can be triggered if outputs of the thermal model are above these limits. The thermal model considered in this research project can be incorporated with MPDs as illustrated in Figure 4-1. The machine losses can be determined and fed into the thermal model, the predicted/calculated temperatures from the thermal model are then compared with the thermal thresholds stored in the MPDs. If the predicted temperatures of the machine are greater than the thermal limits stored in the MPDs the machine can be isolated from the power system to prevent further damage to the machine. Under both operating conditions (temperatures lower or greater than the thermal limit) the expected life of the induction machine can still be computed.

The transfer of heat from the machine windings to the housing and from the housing to the ambient is briefly discussed and parameters are carefully allocated to each machine node. As with most modern thermal models the requirements of the thermal model presented in this report can be summarized as follows:

- Accuracy: the thermal model should be able to predict temperature under balanced and unbalanced operating condition
- Simplicity: the model is easy to implement and understand, the parameters for the electrical and thermal model are obtained from specified tests. Real-time current, temperatures and voltage values are used in the predict of windings temperatures.
- Flexibility: the thermal model can be extended to monitor rotor temperatures and machine core temperatures.

The focus of this research study is loss of life due to the degradation of the machine stator windings. There is also a thermal risk associated with the machine rotor, the rotor conductor may

deform or melt when operated at extremely high temperatures. The squirrel cage induction machine rotor has no insulation and can therefore be operated at higher temperatures than the stator conductors, this by default means that thermal limits set to protect the stator conductor also protect the rotor conductors. It has been difficult and impractical to set a numerical temperature value defining the rotor thermal limit. Most Manufacturers stipulate the maximum allowable rotor temperatures under stall, acceleration or any other fast transient conditions by stating the stall time thermal limits for a hot or cold machine. The general rule of thumb states that "*when the voltage rating of the machine is equal to or greater than 10 times the horsepower rating, the machine is stator limited*". This means that all the machines considered in this research report are stator limited (7.5kW/400V and 11kW/400V) and hence thermal analysis and protection of the stator windings is adequate.

4.1 Symmetrical Components Theory

The transformation matrix used to obtain the sequence components from a three-phase supply is shown below [51].

$$\begin{aligned} U_z &= \frac{1}{3}(U_a + U_b + U_c) \\ U_p &= \frac{1}{3}(U_a + aU_b + a^2U_c) \\ U_n &= \frac{1}{3}(U_a + a^2U_b + aU_c) \end{aligned} \tag{4-1}$$

$$\begin{aligned} U_a &= U_z + U_p + U_n \\ U_b &= U_z + a^2U_p + aU_n \\ U_c &= U_z + aU_p + a^2U_n \end{aligned} \tag{4-2}$$

Where the operator $a = -0.5 + j0.866$ and $a^2 = -0.5 - j0.866$. This research report focuses on the operation of the induction machine under steady state conditions. The frequency of the machine will be kept constant and the amplitudes of the phase voltages varied. It has already been established that the voltage unbalance varies between 0 and 1, this means that the positive sequence component will never be less than the negative sequence component.

$$U_p \geq U_n \tag{4-3}$$

A similar transformation can be used to obtain the stator line currents

$$\begin{aligned} I_a &= I_z + I_p + I_n \\ I_b &= I_z + a^2I_p + aI_n \\ I_c &= I_z + aI_p + a^2I_n \end{aligned} \tag{4-4}$$

Where the three phase rotor currents are given by:

$$\begin{aligned} I_{ra} &= I_{rz} + I_{rp} + I_{rn} \\ I_{rb} &= I_{rz} + a^2I_{rp} + aI_{rn} \\ I_{rc} &= I_{rz} + aI_{rp} + a^2I_{rn} \end{aligned} \tag{4-5}$$

4.1.1 Positive Sequence Network

The positive sequence network comprises of the three phasors in the normal a-b-c sequence with equal magnitudes and 120° phase displacement.

4.1.2 Negative Sequence Network

The negative sequence network comprises of three phasors in the reversed a-c-b sequence with equal magnitudes and 120° phase displacement [51].

4.1.3 Zero Sequence Network

The zero-sequence network comprises of three phasors of equal magnitudes and with a zero-phase displacement. Induction machines are generally connected in delta or ungrounded star and as a result the line currents have zero sequence component unless a fault occurs. In addition, the sum of the line voltage is zero because these voltages form a close triangle in the absence of a fault. Since the zero-sequence component is eliminated the line voltages are resolved into the positive (U_p) and negative sequence component (U_n).

4.2 Per-Phase Equivalent Circuit Models

The induction machine can be viewed as behaving as two machines operating in opposite directions, represented by the positive and the negative circuits [43]. One of the machines can be viewed as operating at a voltage U_p and slip s whilst the other operates at voltage U_n and slip $2 - s$. An equivalent sequence circuit exists for each sequence component as shown in Figure 4-2 and Figure 4-3. The machine equivalent circuits are based on the IEEE and IEC standards, their parameters are based on the results obtained from the locked rotor and no-load tests. The circuits are on a per phase basis meaning that each one of them characterises one of the three phases of an induction machine connected in star or delta. The equivalent circuit for the four machines considered were obtained for a delta configuration and all the parameters were referred to the stator (primary) side. Correction of the resistance was performed to compensate for the temperature rise.

4.2.1 Positive Sequence Equivalent Circuit

The per phase steady state equivalent circuit for the positive sequence is illustrated in Figure 4-2. This circuit represents the normal operating condition of the induction machine when no unbalance is present in the supply.

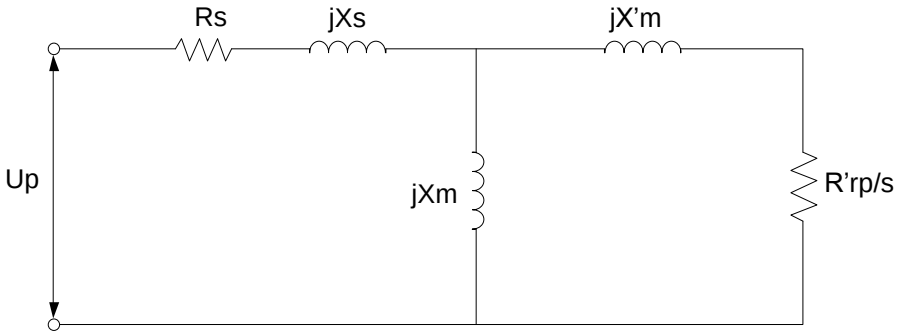

Figure 4-2: Positive Sequence per Phase Equivalent Circuit.

Where

R_s is the stator resistance

R'_{rp} is the positive sequence rotor resistance
X_s is the stator reactance
X'_{rp} is the positive sequence rotor reactance
X_m is the magnetizing reactance

4.2.2 Negative Sequence Equivalent Circuit

The negative sequence operates in the opposite direction of the positive sequence circuit and the result is a reduced torque and power output.

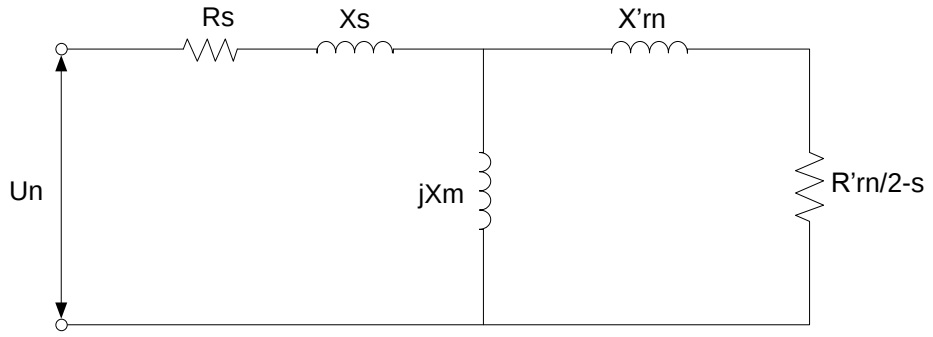

Figure 4-3: Negative Sequence per Phase Equivalent Circuit.

Where

R_s is the stator resistance
R'_{rn} is the negative sequence rotor resistance
X_s is the stator reactance
X'_{rn} is the negative sequence rotor reactance
X_m is the magnetizing reactance

Given that a small amount of voltage unbalance will result in a comparatively large current unbalance [60], it is important to consider the current unbalance factor (CUF). An unbalance in the stator voltage will result in an unbalance of the stator currents. The current unbalance factor is defined by:

$$CUF(\%) = \frac{I_n}{I_p} \times 100\% \qquad (4\text{-}6)$$

It is highly desirable to correlate the VUF to the CUF through the appropriate sequence impedances. The CUF can be defined as a function of the VUF and the negative and positive sequence impedance as shown in equation (4-7).

$$CUF = \frac{|I_n|}{|I_p|} = \frac{U_n/Z_n}{U_p/Z_p} = \left(\frac{Z_p}{Z_n}\right) \cdot VUF \qquad (4\text{-}7)$$

The impedance ratio given above defines the sensitivity of the CUF to the voltage unbalance. For normal operating conditions the positive sequence impedance is much larger than the negative sequence impedance [61].

$$\frac{CUF}{VUF} = \frac{Z_p}{Z_n} \tag{4-8}$$

The ratio of the current unbalance factor to the voltage unbalance factor in terms of sequence impedances is given above. This ratio is a nonlinear function of slip, only assuming the machine parameters stay constant. A low voltage unbalance will result in a considerable level of machine line current unbalance [61]. The general rule of thumb for standard efficiency machines is that for every 1% of voltage unbalance, the resulting current unbalance will be about 5-6 times as much.

Energy efficient machines have a reduced negative sequence impedance; this has led to an increase in their negative sequence currents when operating under unbalanced voltages. The result of higher negative sequence currents is additional heating of the rotor and vibration of twice the supply frequency [51]. Energy efficient machines operate at higher speeds and may result in increased power delivered to the load causing further heating of the machine. Current unbalance can be expressed as

$$CUF(\%) = \frac{I_n}{I_p} \times 100\% \tag{4-9}$$

Where

I_n is the negative sequence current

I_p is the positive sequence current

From the positive and negative sequence equivalent circuits, the following proportionalities can be attained:

$$I_p \propto \frac{s}{R'_{rp}} \tag{4-10}$$

$$I_n \propto \frac{2-s}{R'_{rn}} \tag{4-11}$$

Combining the two equations into the current unbalance factor equation, the following proportionality is obtained

$$CUF \propto \frac{2-s}{s} \tag{4-12}$$

The lower operational slip of the energy efficient machines means that they have a higher current unbalance for a voltage unbalance and it is in most cases higher than the standard machines.

Parameters of the negative sequence per phase equivalent circuit

The stator winding resistance and reactance are equal for the positive and negative sequence per phase equivalent circuits. The parameters on the rotor side of the negative sequence per phase equivalent circuit are different to those of the positive sequence per phase equivalent circuit. This

is because the frequencies of the rotor currents are higher, since it is assumed the field rotates in the opposite direction to the field for the positive case.

$$f_n = f_1 \cdot (2 - s) \approx 2f_1 \gg s \cdot f_1 \tag{4-13}$$

Ideally the values of the negative sequence resistance $R_{r,n}$ and reactance $X_{r,n}$ are determined from the parameters of the short circuit tests, $R_{r,SC}$ and $X_{r,SC}$. It has been shown that these parameters are dependent on the ratio of the conductor height and the field penetration depth. The negative sequence parameters can also be obtained by using the measured values of the voltage and current under a supply condition. From first principles, the negative sequence impedance can be expressed approximately by

$$Z_n = Z_s + \frac{Z_r Z_m}{Z_r + Z_m} \tag{4-14}$$

Where

$$Z_s = R_s + jX_s \tag{4-15}$$

$$Z_r = \frac{R'_{rn}}{2 - s} \tag{4-16}$$

$$Z_m = jX_m \tag{4-17}$$

The original negative sequence impedance equation can therefore be to the following:

$$Z_n = Z_s + Z_r \tag{4-18}$$

$$Z_n = R_s + \frac{R'_{rn}}{2 - s} + j(X_s + X'_{rn}) = R_n + jX_n \tag{4-19}$$

Where the magnetising reactance has been omitted since $\frac{R'_{rn}}{2-s} \ll jX_m$. The negative sequence resistance can therefore be computed using:

$$R'_{rn} = \left(R_{n,measured} - R_s\right)(2 - s) \tag{4-20}$$

4.2.3 Developed Torque and Power

The rotor, stator and magnetizing branches conductance can be expressed as:

$$\begin{gathered} \vec{Z}_{s,i} = R_s + jX_s \\ \vec{Z}_{r,i} = R_{r,i} + jX_s \\ \vec{Y}_m = \frac{1}{jX_m} \end{gathered} \tag{4-21}$$

$$\vec{Y}_{stator,i} = \frac{1}{\vec{Z}_{stator,i}} \tag{4-22}$$

$$\vec{Y}_{rotor,i} = \frac{1}{\vec{Z}_{rotor,i}} \tag{4-23}$$

$$\vec{Z}_m = \frac{1}{\vec{Y}_m} \tag{4-24}$$

The stator, rotor and magnetizing currents can be computed using the derived equations

$$\vec{I}_{s,i} = \frac{\vec{U}_{s,i} \cdot \vec{Y}_{stator,i}\left(\vec{Y}_{rotor,i} + \vec{Y}_m\right)}{\vec{Y}_{stator,i} + \vec{Y}_{rotor,i} + \vec{Y}_m} \tag{4-25}$$

Where the positive and negative sequence currents are given by

$$I_p = \frac{U_p \cdot \left(Z_{rp} + Z_m\right)}{Z_s \cdot \left(Z_{rp} + Z_m\right) + Z_m Z_{rp}} \tag{4-26}$$

$$I_n = \frac{U_n \cdot (Z_{rn} + Z_m)}{Z_s \cdot (Z_{rn} + Z_m) + Z_m Z_{rp}} \tag{4-27}$$

The magnetizing current is attained using the following

$$\vec{I}_{m,i} = \frac{\vec{U}_{s,i} \cdot \vec{Y}_{stator,i} \cdot \vec{Y}_m}{\vec{Y}_{stator,i} + \vec{Y}_{rotor,i} + \vec{Y}_m} \tag{4-28}$$

$$\vec{I}_{r,i} = \frac{\vec{U}_{s,i} \cdot \vec{Y}_{stator,i} \cdot \vec{Y}_{rotor}}{\vec{Y}_{stator,i} + \vec{Y}_{rotor,i} + \vec{Y}_m} \tag{4-29}$$

Where the positive and the negative sequence rotor currents are given respectively by:

$$I'_{rp} = \frac{U_p}{\sqrt{\left(R_s + \frac{R_{rp}}{s}\right)^2 + \left(X_s + X'_{rp}\right)^2}} \tag{4-30}$$

$$I'_{rn} = \frac{U_n}{\sqrt{\left(R_s + \frac{R_{rn}}{s}\right)^2 + (X_s + X'_{rn})^2}} \tag{4-31}$$

The magnetizing current is defined by the magnetizing leakage reactance and the stator and rotor resistances. The negative sequence currents result in negative power and torque components that reduce the resultant torque and power. The total mechanical power due to the negative and positive currents is given by:

$$P_m = I'^2_{rp} \times R'_{rp} \times \left(\frac{1-s}{s}\right) - I'^2_{rn} \times R'_{rn} \times \left(\frac{1-s}{(2-s)}\right) \tag{4-32}$$

The total torque can be expressed as:

$$T_m = I'^2_{rp} \times R'_{rp} \times \left(\frac{1}{s\omega_0}\right) - I'^2_{rn} \times R'_{rn} \times \left(\frac{1}{(2-s)\omega_0}\right) \quad (4\text{-}33)$$

Where

ω_0 Is the synchronous speed in radians per second.

The input power of the machine is obtained using the following equation

$$P_{in} = 3\left(\frac{U_p^2}{|Z_{eq,p}|}\cos(\varphi_p) + \frac{U_n^2}{|Z_{eq,n}|}\cos(\varphi_n) + \right) \quad (4\text{-}34)$$

Where φ_p, is the angle between the positive sequence voltage (U_p) and current (I_p) and similarly, φ_n is the angle between the negative sequence voltage (U_n) and current(I_n).

4.3 Thermal Modelling of Induction Machines

The maximum rating of an induction machine of a given size is limited by the maximum temperature rise the machine can withstand. There are two dominant factors that influence the temperature rise of an induction machine, the losses and the efficiency of heat dissipation [62]. The complexity in the thermal modelling of induction machines has led to research in this field lagging other aspects of machine design. The complexity is due to the study involving the interaction of heat transfer and electrical behaviour of induction machines [62]. This is made more strenuous by the fact that the induction machine is itself a complex system, it is made from different materials and there are multiple sources of heat. Initially researchers proposed empirical formulae that could predict the temperature rise of the induction machine, the formulae were derived using temperatures obtained from tests. Several assumptions were made when applying this formula, the formulae neglected the effects of airflow and insulation on the induction machine and hence the temperature prediction was unsuccessful [63].

The two major categories that thermal models can fall under are broadly discussed in chapter one. The first category includes models that use numerical method techniques such as finite difference methods. The second is the previously discussed lumped parameter models. The numerical method techniques divide the induction machine into 2-D and 3-D regions [62]. The smaller regions are interconnected at nodes which are normally arranged along grid lines. Basic functions are selected to approximate the temperature over each region. An iteration process is then undertaken until the temperature distribution corresponds with the governing partial differential equations. The lumped parameter thermal model is simpler than the finite element procedures. The induction machine is modelled as a series of equivalent networks representing each part of the machine [62]. The parameters of this network can be obtained through a series of tests or in some instances using the dimensional information of the machine. Some of the lumped parameter thermal networks make drastic assumptions to reduce the complexity of the model. A lot of these equivalent networks have been developed for different machine sizes, different applications and for different operating conditions [62].

4.3.1 Heat Transfer Theory

Electrical machines have three heat transfer mechanisms, namely conduction, convection and radiation. The are several prerequisites for heat to be transferred from one body to another, the first is that a temperature difference must exist between the two bodies. The second being that heat is transferred from the body with the higher temperature (the heat source) to the body with the lower temperature (heat sink). In real conditions the transfer of heat is a combined method [64]. Totally enclosed fan cooled induction machines remove heat by convection through the air, for flange mounted machines some of the heat is removed by conduction through the flange to the device connected to the machine. Very little heat is transferred through radiation and can be ignored without introducing any significant errors.

4.3.1.1 Conduction

Whenever there is temperature gradient in a system, energy is transferred from a heat source to a heat sink. This type of heat transfer is known as conduction. The heat transferred per unit is directly proportional to the normal temperature gradient. The basic equation governing heat conduction in rectangular coordinate system (x, y, z) is defined

$$\frac{1}{\propto}\frac{\partial\theta}{\partial t} = \frac{\partial^2\theta}{\partial x^2} + \frac{\partial^2\theta}{\partial y^2} + \frac{\partial^2\theta}{\partial z^2} + \frac{1}{k}Q \tag{4-35}$$

$$\alpha = \frac{k}{\rho c_p}\frac{1}{\propto}\frac{\partial\theta}{\partial t} \tag{4-36}$$

Where

c_p = Specific heat of material (J/Kg.°C)
Q = Heat generation rate (W/m^3)
ρ = Density of the material (kg/m^3)
K = Thermal conductivity (W/m. °C)
θ = Temperature (°C)

In this research project, the focus will only be on one dimensional analysis and the general expression for the conductive heat transfer and is described by Fourier's law

$$q = -k\frac{\partial\theta}{\partial x} \tag{4-37}$$

Where

q = heat flux (W/m^2)
x = distance (m)

Using machine dimensions, the thermal resistance between two points can be expressed as

$$R_{th} = \frac{x_2 - x_1}{kA} \tag{4-38}$$

Where

A = cross sectional area (m^2)

The equation above is known as Fourier's law of heat conduction and is the primary definition for thermal conductivity. In most of cases the thermal conductivity of most solids varies very little with temperature. Heat transfer in solid bodies can take one of two processes: the first is transfer of thermal energy via lattice vibration, the second is thermal energy transfer by free electrons. Solids that are conductors have an enormous number of free electrons moving around in the conductor, these electrons transfer thermal energy from a high temperature region to a low temperature region, they also transfer electric charge. For one dimensional analysis of electrical machines the thermal conductance can be taken as constant. The Table 4-1 shows the thermal conductivity values of some of the materials used in the induction machines considered in this research project.

Table 4-1: Thermal Conductivities of Various Induction Machine Parts [25]

Material	Part	$K(W/m.K)$
Al-Si 20	Frame	161
Steel (0.5% C)	Shaft	54
Aluminum	Rotor Cage	240
Carbon Steel (0.5% C)	Stator core and rotor core	36
Copper	Stator winding	386
Unsaturated polyester	Stator winding impregnation and slot insulation	0.2
Air at 300K	Air gap, ambient air	0.02624

4.3.1.2 Convection

The transfer of thermal energy between a solid surface and a cooling fluid is known as convection. This transfer of thermal energy comes because of the motion of the cooling fluid relative to the solid surface. The general governing equation for heat transfer through convection is given by

$$q = \propto (\theta_w - \theta_f) \tag{4-39}$$

Where

θ_w = temperature of the surface

θ_f = temperature at a distant point from the surface

$\propto$ = coefficient of heat transfer

The coefficient of heat transfer is dependent on the geometry of the body under consideration, the nature of the heat transfer (natural or forced) and the average temperature and physical characteristics of the fluid. In the induction machine the convective heat transfer is divided into internal and external transfer. The internal convectional heat transfer is across the air gap and from the windings to end caps and housing. The external convective heat transfer is between the frame of the machine and the ambient. The thermal resistance due to convection can be approximated using

$$R_{th} = \frac{1}{\propto A} \tag{4-40}$$

4.3.1.3 Radiation

The resultant radiation that leaves the surface of an object depends on the area, the material characteristics, the temperature and the surroundings. The emissivity and absorptivity of a compact body are usually put equal and there is no transmission. The net heat transfer by radiation between two bodies is derived from Stefan-Boltzmann's law

$$q_r = A_1 \varepsilon_1 \delta \left({\theta_w}^4 - {\theta_f}^4 \right) \tag{4-41}$$

Where

A_1 = the area of surface one

ε_1 = the emissivity of surface one ($0 \leq \varepsilon \leq 1$). for iron $\varepsilon = 0.96$ for aluminium $\varepsilon = 0.08$

δ = Stefan-Boltzmann constant ($5.6697 \times 10^{-8}\, W/(m^2.K^4)$)

To properly analyse heat transfer mechanisms in an induction machine, the machine is divided into basic elements. These basic elements are identified as nodes in the proposed thermal model. There are several ways of subdividing the machine and the choice of subdivision results from the compromise between simplicity of the thermal model and the quality of information sought. For this application the machine subdivision is based on the physical factors that contribute significantly to temperature rise.

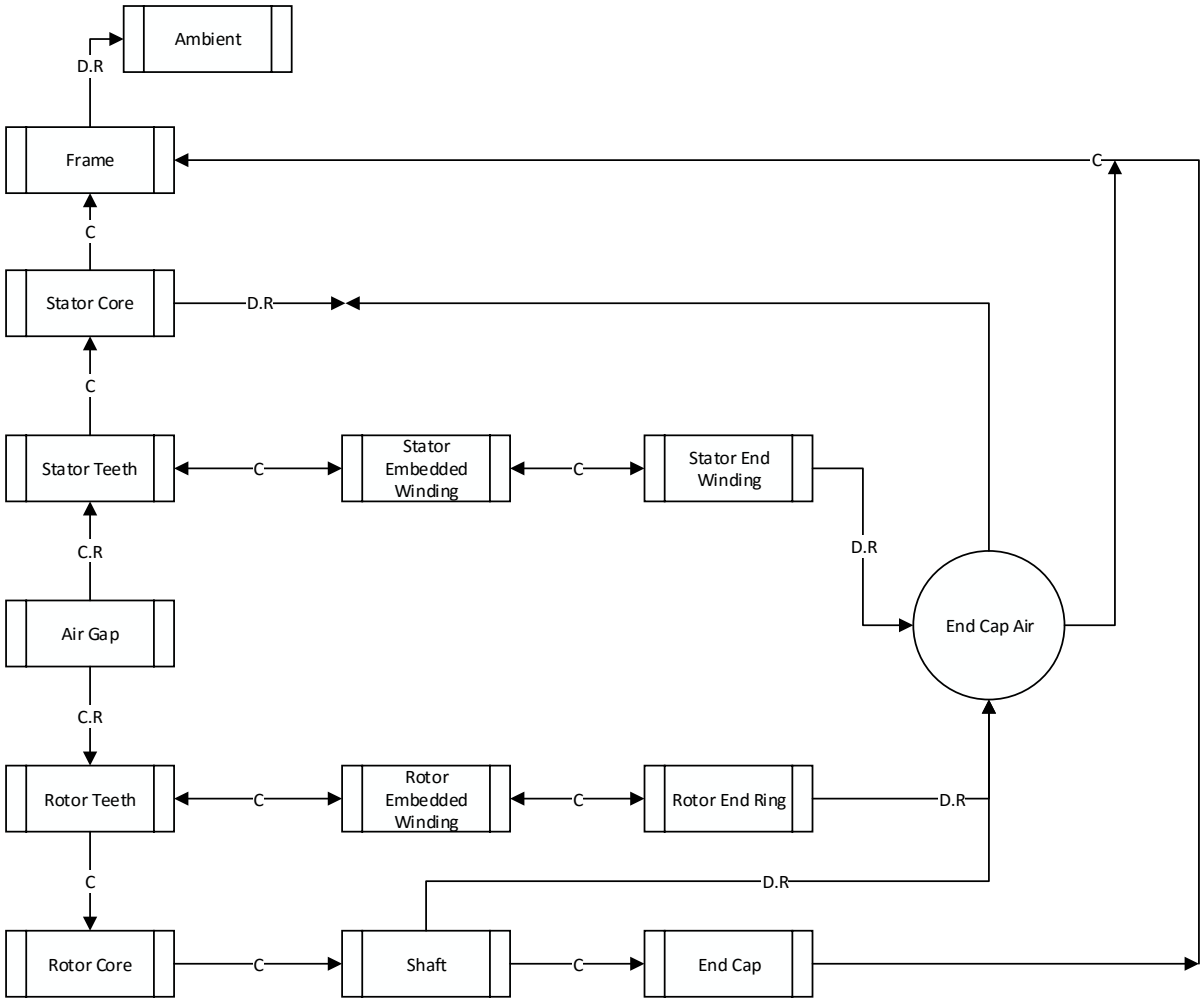

Figure 4-4: Basic heat exchange map of an induction machine [65]

C: Conduction, D: Convection, R: Radiation

The basic heat exchange map and the associated heat transfer methods in an induction machine are illustrated in Figure 4-4. Most of the heat transfer between the machine elements is through conduction. Very little heat is transferred through radiation and this type of heat transfer will be ignored in the considered thermal model. Convective heat transfer takes place between the machine frame and the ambient, this transfer is a function of the total surface area and the efficiency of the cooling fins. The transfer of heat in the machine airgap is not well documented, although experimental data for heat transfer across a gap between concentric cylinders exists, the results are not consistent and cannot be rationalised so that they can be extended to other situations/applications [66]. Ideally for a TEFC machine, there is minimum axial heat flow from the airgap into the surrounding end cap air.

4.3.2 Induction Machine Ventilation

The design of induction machines usually includes a system designed to carry heat away that is produced by the winding and bearings. This system is known as the cooling circuit of the induction machine. The effectiveness of this system depends on things such as the fan diameter,

shaft speed, air duct, altitude and the deflector presence and location [19]. The amount of air provided by the fan varies as the cube of the diameter and is directly proportional to the speed. In many instances, the fan is greatest contributor of noise in TEFC machines. Open and enclosed machines use air deflectors to direct air to locations that need it and to reduce turbulence, turbulent air is not an efficient method of cooling. The efficiency of the machine cooling circuit depends on the location of the air deflectors. If the machine ducts ever become clogged or the air deflectors are missing or incorrectly located, the machine may overheat [19]. All the machines tested in this research are TEFC machines, these machines are provided with an external forced cooling fan mounted on the non-drive end (NDE) of the shaft, they also have cooling ribs running axially along the outer surface of the motor frame. The cooling ribs are designed to keep air flow close to the surface of the machine along its entire length, this helps improve the cooling and self-cleaning of the ribs. The systems used to describe the method currently used by IEC is being changed, the current designation system is given in Figure 4-5. The designation method consists of the following [67]:

- A prefix comprising of the IC (index of cooling)
- A letter designating the cooling medium, this is left out if only air is used
- Two numerals representing:
    - The cooling circuit layout
    - The way in which the power is supplied to the circulation of the cooling fluid, fan, no fan, separate forced ventilation.

Code	Description	Drawing
IC 01	- Open machine - Fan mounted on shaft - Often called 'drip-proof' motor	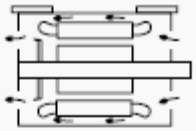
IC 40 (New : IC 410)	- Enclosed machine - Surface cooled by natural convection and radiation - No external fan	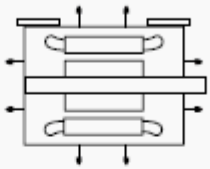
IC 41 (New : IC 411)	- Enclosed machine - Smooth or finned casing - External shaft-mounted fan - Often called TEFC motor	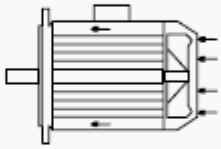
IC 43 A (New : IC 416A)	- Enclosed machine - Smooth or finned casing - External motorized Axial fan supplied with machine	
IC 43 R (New : IC 416R)	- Enclosed machine - Smooth or finned casing - External motorized Radial fan supplied with machine	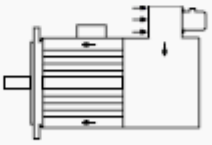
IC 61 (New : IC 610)	- Enclosed machine - Heat Exchanger fitted - Two separate air circuits - Shaft-mounted Fans - Often called CacA motor	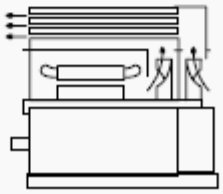

Figure 4-5: Designation of the most common methods of cooling [67]

4.3.3 Thermal Network Theory

When using the lumped parameter thermal network, the induction machine is divided into basic thermal elements which are represented by a specific nodal configuration (in most cases a thermal resistance and a thermal capacitance). The various elements are interconnected forming a network of nodes, thermal resistance and thermal capacities. The main assumption in lumped parameter thermal networks is that all the heat generation in the component (machine part) is concentrated in one point, this point is referred to as the node. A node represents the mean temperature of the component, each of the nodes is assigned a thermal capacitance C_i and heat flowing between the nodes which is represented as a current source P_i which is passed through a thermal resistance R_i.

Lumped parameter thermal networks that are applicable to induction machines range from one dimensional to three dimensional. A two or three-dimensional thermal network model is assembled by connecting several one-dimensional models together in one point of the mean temperature. Thermal networks offer both the steady and transient state solutions for temperature difference between the elements and the ambient temperature. By assuming that there are n nodes and each of the nodes is linked to a thermal capacitance C_{ij} and thermal resistance R_{ij} where i and j are the indices of the linked nodes. The basic transient equation for the basic one-dimensional thermal model with n nodes and each linked to others via thermal resistances R_{ij} can be described by the differential equation

$$C_i \frac{\partial \theta_i}{\partial t} = P_i - \sum_{j=1}^{n} \frac{\theta_i - \theta_j}{R_{ij}} \tag{4-42}$$

Where

i = $1 \ldots . n$
C_i = the nodal thermal capacitance
θ_i = nodal temperature rise
R_{ij} = the thermal resistance between adjoining nodes i and j
P_i = the heat generation at node i

In matrix form the equation above can be represented by

$$\frac{\partial \theta_t}{\partial t} = [C_t]^{-1}[P_t] - [C_t]^{-1}[G_t][\theta_t] \tag{4-43}$$

Where

C_t = the thermal capacitance matrix
P_t = the losses matrix
θ_t = the temperature rise matrix
G_t = the conductance matrix

These matrices are defined in equations (4-44)-(4-47)

$$C_t = \begin{bmatrix} C_1 & 0 & 0 & - & - & - & 0 \\ 0 & C_2 & 0 & - & - & - & 0 \\ 0 & 0 & C_3 & - & - & - & 0 \\ - & - & - & - & - & - & - \\ - & - & - & - & - & - & - \\ - & - & - & - & - & - & - \\ 0 & 0 & 0 & 0 & 0 & 0 & C_n \end{bmatrix} \tag{4-44}$$

$$P_t = \begin{bmatrix} P_1 \\ P_2 \\ P_3 \\ - \\ - \\ - \\ P_n \end{bmatrix} \tag{4-45}$$

$$\theta_t = \begin{bmatrix} \theta_1 \\ \theta_2 \\ \theta_3 \\ - \\ - \\ - \\ \theta_n \end{bmatrix} \tag{4-46}$$

$$G_t = \begin{bmatrix} \sum_{i=1}^{n} G_{1,i} & -G_{1,2} & -G_{1,3} & - & - & - & -G_{1,n} \\ -G_{2,1} & \sum_{i=1}^{n} G_{2,i} & -G_{2,3} & - & - & - & -G_{2,n} \\ -G_{3,1} & -G_{3,2} & \sum_{i=1}^{n} G_{3,i} & - & - & - & -G_{3,n} \\ - & - & - & - & - & - & - \\ - & - & - & - & - & - & - \\ - & - & - & - & - & - & - \\ -G_{n,1} & -G_{n,2} & -G_{n,3} & - & - & - & \sum_{i=1}^{n} G_{n,i} \end{bmatrix} \tag{4-47}$$

Several observations can be made from the conductance matrix [68]:

- All the diagonal terms are positive
- Non-diagonal terms are all negative, therefore satisfying Kirchhoff's law
- The matrix is symmetrical $(G_{ij} = G_{ji})$ unless there is a fluid transport conductance.
- In general, most of the non-diagonal terms are null, this is due the fact that each node has its energy balance only linked to its direct neighbourhood. The matrix is therefore sparse, and the interactions are local ones [68].

From the equation given above the thermal conductance is as

$$G_{1,i} = \frac{1}{R_{1,i}}, etc \tag{4-48}$$

The steady state nodal temperature rises are related by

$$P_i = \sum_{j=1}^{n} \frac{\theta_i - \theta_j}{R_{ij}} \tag{4-49}$$

The stationary solution of the temperature rise in an induction machine can be obtained directly from the equation given above. The following electrical/thermal analogies are useful when analysing the thermal circuit

Table 4-2: Electrical Thermal Analogies

Electrical Circuit	Thermal Circuit
Voltage (V)	Temperature (T)
Current (I)	Heat Flow (P)
Electrical Conductance (G)	Thermal Conductance (G)
Electrical Capacitance (C)	Thermal Capacitance (C)

4.3.4 Uncoupled Thermal Networks

Uncoupled thermal networks are networks where the rotor and the stator are uncoupled from each other. The uncoupling assumes that the rotor heat does not flow through the stator to the ambient but via the shaft to the ambient [53] [1]. The thermal heat flow process for uncoupled thermal models was initially proposed by Zocholl in [69]. When the machine starts up, very little to no heat transfer occurs between the machine and the environment because the heat lost is very little compared to the input heat [69]. As the machine is running the stator copper heat is dissipated through the stator insulation and finally into the ambient helped by the machine ventilation. The thermal equivalent circuit of an induction machine can be taken as symmetrical about its radial plane through the centre of the machine [65]. The influence of asymmetrical temperature distribution which exists because of the fan being mounted at one end will be assumed to be minimal. The following assumptions are made when considering the lumped parameter thermal model:

- Independent Heat Flow: the heat flowing in the axial and radial directions are independent of each other.
- Single Mean Temperature: the mean temperatures in the axial and radial directions are the same.
- No circumferential Heat Flow: the circumferential variation of temperature is assumed to be negligible, the heat transfer in this direction is ignored and conduction is only in the radial and axial planes.
- Uniform Thermal Capacitance: elements which have isotropic material will have a constant specific heat capacity and density resulting in a uniform thermal capacitance
- Uniform Heat Generation: It is assumed that the heat generation is uniform throughout each component, this is generally for stator windings and induction rotor bars where Joulean heat generation occurs due to current flow.

The iron core is heated by the eddy and hysteresis losses and the heat due to the rotor conductor losses flows into the rotor iron. This heat is then guided out via the ventilation and shaft [69]. The uncoupling of the stator and the rotor allows us to study the stator winding temperatures independently from the rotor. By separately studying the stator, focus can be placed on the individual phases under non-ideal supply conditions. Souto [70] and Manyage [53] both

implemented uncoupled thermal models to investigate the impact of unbalanced supplies on the life expectancy of three phase induction machines.

4.3.5 Coupled Thermal Networks

Coupled thermal networks couple the stator and the rotor circuits of the induction machine. The stator, rotor and core losses are all considered as heat sources when computing the machine temperature rise. The major drawback of the coupled thermal model is the inability to analyse each phase winding independently, all three windings are considered at a single node.

4.4 Proposed Thermal Model of Induction Machine

As discussed in the literature review, most thermal models are complex and require the machine's physical dimensions when determining the model parameters. Finite element methods are time consuming as too many parameters must be obtained. The coupled and uncoupled thermal models discussed in 4.3.4 and 4.3.5 require simple tests to determine the thermal parameters and do not require knowledge of the machine's dimensional information. A simple thermal model that predicts both the transient and steady state temperatures of a three-phase squirrel cage induction machine was adapted from Manyage [53]. The thermal model in Figure 4-6 allows the analysis of the stator temperature in each phasor winding. This is vital because during operation under unbalanced voltage conditions the temperatures in the different windings are differ

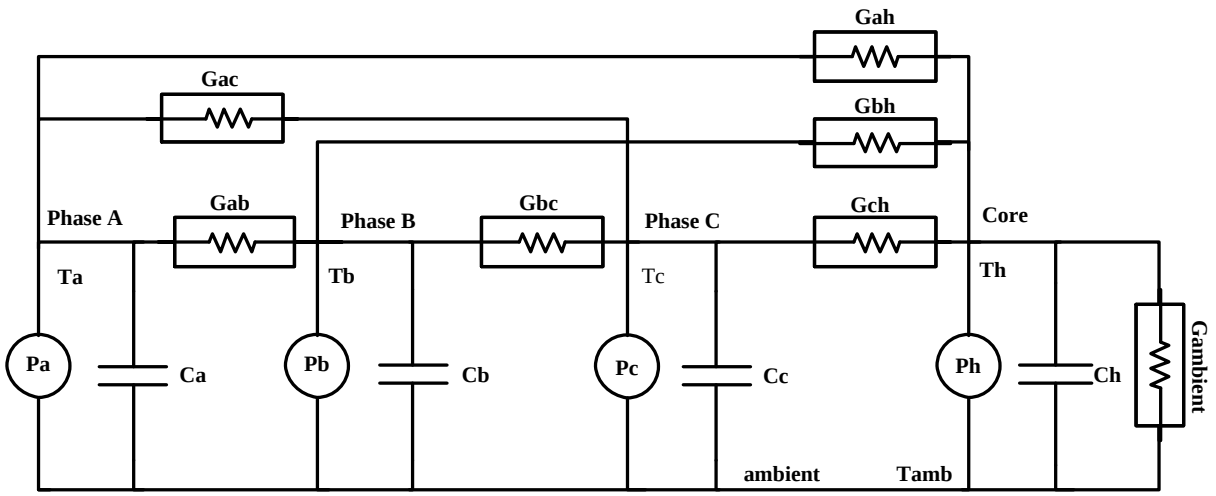

Figure 4-6: Stator Thermal Model

All three phases are considered because of the different currents and temperatures under unbalanced supply conditions. Each phase is represented by a heat source and three conductances; one linking it to the other phases and the other one to the core.

Where:

Table 4-3: Stator Thermal Model Parameters

$T_a, T_b, T_c,$	Temperature at each phase (°C)
T_{amb}	Ambient temperature (°C)
T_h	Core temperature (°C)
C_a, C_b, C_c, C_h	Thermal capacitance ($Ws/$°C)
G_{ab}, G_{bc}, G_{ac}	Phase to phase thermal conductances ($W/$°C)
G_{ah}, G_{bh}, G_{ch}	Phase to phase thermal conductances ($W/$°C)
G_{amb}	Core to ambient thermal conductance($W/$°C)
$P_a, P_{b,}P_{b,}$	Stator copper loss of each phase (W)

P_h	Stator core loss (W)

Even though it is not considered in this project, the rotor thermal model illustrated in Figure 4-7 comprises of a heat source from the bars, thermal conductance to the core and a heat source as result of core losses.

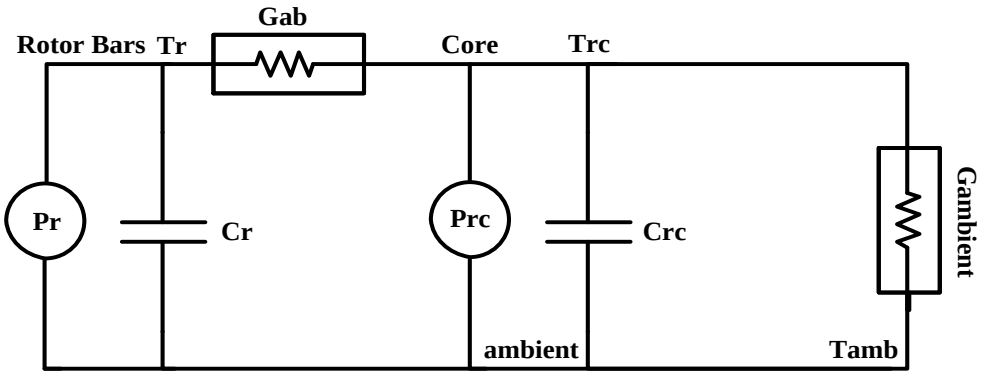

Figure 4-7: Rotor Thermal model

Table 4-4: Rotor Thermal Model Parameters

P_r	Rotor copper loss (W)
P_h	Rotor core loss (W);
G_{rc}	Thermal conductance between rotor bars and core ($W/$°C);
C_r, C_{rc}	Rotor thermal capacitance ($Ws/$°C);
T_r, T_{rc}	Rotor temperature (°C)

4.4.1 Thermal Model Circuit Analysis

The stator thermal model is treated like an electrical circuit. The thermal model can be analysed by applying Kirchhoff's' current law (KCL) on the respective circuit nodes. Applying KCL at the phase A node in the stator thermal model yields [53] [1]

$$P_a - (T_a - T_b) \cdot G_{ab} + (T_a - T_c) \cdot G_{ac} - (T_a - T_h) \cdot G_{ah} - C_a \frac{\partial T_a}{\partial t} = 0 \qquad (4\text{-}50)$$

This can be rearranged into the following

$$\frac{\partial T_a}{\partial t} = \frac{P_a - (T_a - T_b) \cdot G_{ab} + (T_a - T_c) \cdot G_{ac} - (T_a - T_h) \cdot G_{ah}}{C_a} \qquad (4\text{-}51)$$

Applying KCL at all the other nodes and rearranging the equations results in the following

$$\frac{\partial T_b}{\partial t} = \frac{P_b - (T_b - T_a) \cdot G_{ab} + (T_b - T_c) \cdot G_{bc} - (T_b - T_h) \cdot G_{bh}}{C_b} \qquad (4\text{-}52)$$

$$\frac{\partial T_c}{\partial t} = \frac{P_c - (T_c - T_a) \cdot G_{ac} + (T_c - T_b) \cdot G_{bc} - (T_c - T_h) \cdot G_{ch}}{C_c} \quad (4\text{-}53)$$

$$\frac{\partial T_h}{\partial t} = \frac{(T_a - T_h) \cdot G_{ah} + (T_b - T_h) \cdot G_{bh} - (T_c - T_h) \cdot G_{ch} - (T_h - T_{amb}) \cdot G_{amb}}{C_h} \quad (4\text{-}54)$$

The general mathematical expression that is used to represent the relationship between stator heating and the temperature rise is given by

$$\frac{\partial [T]}{\partial t} = [C]^{-1}([P] - [G][\Delta T]) \quad (4\text{-}55)$$

Where:

C = the thermal capacitance matrix
P = the losses matrix
T = the temperature rise matrix
G = the conductance matrix

4.4.2 Thermal Model Parameters

Thermal Conductance

As described earlier in this chapter, conduction refers to the transfer of thermal energy from a body with a higher temperature (heat source) to a lower temperature body (heat sink). The ability of the bodies to perform this transfer of thermal energy is known as thermal conductance [1]. The capacity to transfer heat between two different temperatures is usually defined by an equivalent thermal resistance or its inverse thermal conductance. A low thermal conductance between two points will result in a high temperature differential between the two points in context because of the high thermal resistance. In this body of work, it will be considered that the heat transfers between each of the parts into which the system is divided is carried out by the combination mechanism of conduction and convection. The heat exchange ΔQ is outlined as

$$\Delta Q = G\Delta\theta \quad (4\text{-}56)$$

Where the thermal conductance between any two surfaces is by G and the temperature difference between them is by $\Delta\theta$. The contribution of convection (especially by the machine fan) is represented by the coefficient b which affects the value of the thermal conductance and has been assumed to vary linearly with the induction machine motor speed ω [31]. If we let the thermal conductance at zero speed be G_0, the relationship between the heat exchange, thermal conductance and speed can be represented as

$$\Delta Q = G_o(1 + b \times \omega)\Delta\theta \quad (4\text{-}57)$$

The following heat transfer mechanism is considered: the power losses generated in the induction machine stator, core and rotor are transformed into heat. Part of this heat contributes to the modification of the part temperatures with their heat storage capacities (thermal capacitances). The rest of the heat is transferred to the environment via the core to ambient conductance and the conductances between the phases. Considering the previous equation, the general equation for the conductances (phase to phase, phase to core and core to ambient) can be written as

$$G_{ab} = G_{ab0}(1 + b_{ab} \times \omega) \quad (4\text{-}58)$$

$$G_{ah} = G_{ah0}(1 + b_{ah} \times \omega) \quad (4\text{-}59)$$

$$G_{amb} = G_{amb0}(1 + b_{amb} \times \omega) \quad (4\text{-}60)$$

Where G_{ab0},G_{ah0} and G_{amb0} are the values of the thermal conductances at zero speed. The stator thermal circuit shown in Figure 4-6 shows seven thermal conductances. The phase to phase conductances are equal ($G_{ab} = G_{bc} = G_{ac}$) and the phase to core conductances are also equal to each other ($G_{ah} = G_{bh} = G_{ah}$) [1]. This reduces the number of unknown thermal conductances to three hence fewer tests are required to find their values. The thermal conductances of the thermal model are determined under steady state conditions so that the capacitances can be assumed to be charged to their steady state values.

Thermal Capacitance

The thermal capacitance represents the materials ability to store heat. [1] The value of the capacitance is related to the physical configuration, size and the mass of the material. The thermal capacitances allow us to analyse the transient temperature rise of induction machines. Tests detailing how the thermal capacitances were obtained are described in Chapter 5.

4.5 Concluding remarks

The positive, negative and zero sequence components are explained in detail in this chapter. Since unbalanced voltage conditions are the focus of this research project, the relevant per phase equivalent circuit models are identified. The IEEE and the IEC standards both have specified methods for determining the parameters of the equivalent circuits. For both standards the positive and negative per phase stator impedances are equal. The positive and negative sequence rotor resistance and reactance are different, which is attributed to the difference in rotor currents representing the backward and forward rotating magnetic fields.

There are two methods one can use to determine the negative sequence resistance and reactance; the first method uses the normal parameters of the short circuit test. Literature has shown that these parameters are dependent on the ratio of the conductor height and the field penetration depth. The second method described in this chapter involves using measured voltage and current for a supply condition.

The fundamentals of heat transfer theory are discussed in this chapter. Thermal models can basically take one of two forms, the lumped parameter thermal models or ones that utilise numerical techniques such as finite element and finite element difference methods. Numerical methods divide the machine into 2-D or 3-D regions, simple functions are then chosen to

approximate the variation of temperature over each region. Iteration is applied until the distribution satisfies the governing partial differential equations.

Lumped parameter thermal networks are used to represent the induction machine, in some instances drastic assumptions are introduced to alleviate the complexities of modelling the actual convection and conduction heat processes. Two approaches can be used to determine parameters of the lumped parameters. Dimensional data of the induction machine can be used or a simpler method which has proven to yield appropriate results uses tests on the induction machine to attain the parameters. A one-dimensional lumped parameter thermal model is used in the research report to estimate the temperature rise of induction machines under the various operating conditions. The next chapter gives an in-depth description of the tests undertaken to attain the thermal model parameters.

5. EXPERIMENTAL SETUP AND PROCEDURES

This chapter describes the experimental setup used to obtain test data from the induction machine and the apparatus used to analyse the data to produce temperature, efficiency and loss estimations from the methods described in the previous chapters.

5.1 Specifications of Induction Machines Considered

The IEEE 112-B standards are followed in obtaining the steady state temperature of the machine as well as the core losses. Machines and motorised systems globally account approximately for 40% of global electric energy consumption [71]. In South Africa induction machines account for up to 60% of the total industrial (mining included) energy used and about 57% of the peak demand [71]. Data gathered by Eskom DSM in a machine survey conducted in 2007 is shown in Table 5-1, this shows the distribution of machines according to size, with machines ranging from 0.18kW to 90kW being the most commonly used. A survey conducted by the Energy Research Centre (ERC) at the University of Cape Town, found that the application of the machines is distributed as follows:

Table 5-1: Estimated motor applications

Application	Percentage (%)
Pumps	40
Miscellaneous	25
Fans	20
Conveyors	10
Compressors	5

After surveying various suppliers of irrigation equipment to the South African agricultural market (sourced from: http://www.irrigation4africa.co.za and http://www.agrico.co.za), the type and range of motors were identified. The machine most commonly used in this sector are: 0.9-22kW, 4-pole, IE1 squirrel cage induction motors. This concurs with the findings of [72], and guided the selection of motors for this project, as indicated by

Table 5-2. The four new motors are selected from two Manufacturers, with sizes 7.5kW and 11kW. They are totally enclosed fan cooled (TEFC) motors with protection class IP55. One 7.5kW and one 11kW induction motor were purchased from each of the Manufacturers with a voltage rating of 400V, to compare results across the different Manufacturers. The primary purpose of this project is to explore the impact of power quality issues on the lifespan of induction machines from different Manufacturer s with different power ratings. The project also explores the use of models to predict machine temperatures under the different power quality conditions. The temperatures predicted using these models are compared with the measured temperatures and used for loss of life calculations.

Table 5-2: Estimated market demand for electric machines in SA [73]

Motor Rating (kW)	Estimated Market Demand in SA
0.18 - 2.2	40600
3	5200
4	5400
5.5	4800
7.5	6000
9.2	300
11	3700
15	3000
18	5 1500
22	2400
30	1700
37	1300
45	1100
55	1000
75	1100
90	500
110	700
132	300
160	400
185	200
200	200
Total Units	**81400**

The machines that were tested are from two Manufacturers, Manufacturer A and Manufacturer B. Two machines from each Manufacturer were tested, two 7.5kW and two 11kW machines were considered. All the considered machines are totally enclosed fan cooled (TEFC), four pole, 400V, 50Hz type. The machine specifications are summarised in the
Table 5-3. Manufacturer A is a larger Manufacturer than Manufacturer B. Manufacturer A is a global leader in the production of electrical motors, transformers and drives while Manufacturer B is much smaller OEM.

Table 5-3: Nameplate ratings of induction machines under consideration

	Manufacturer B		Manufacturer A	
Rated Output *(kW)*	7.5	11	7.5	11
Rated Frequency (Hz)	50 Hz	50 Hz	50 Hz	50 Hz
Poles	4	4	4	4

Rated Line Voltage *(V)*	400	400	400	400
Rated Line Current *(A)*	15	21.6	15.2	22.0
Rated Speed *(rpm)*	1450	1460	1455	1460
Rated P.F.	0.84	0.84	0.82	0.82
Efficiency Class	IE1	IE1	IE1	IE1
Insulation Class	F	F	F	F

5.2 Test Rig

The test rig used for this research project is capable of testing induction machines up to and including 22kW. It consists of the dynamometer mechanically coupled to an induction machine via an inline torque transducer [51]. The test bed setup is illustrated in Figure 5-1 and Figure 5-2 respectively.

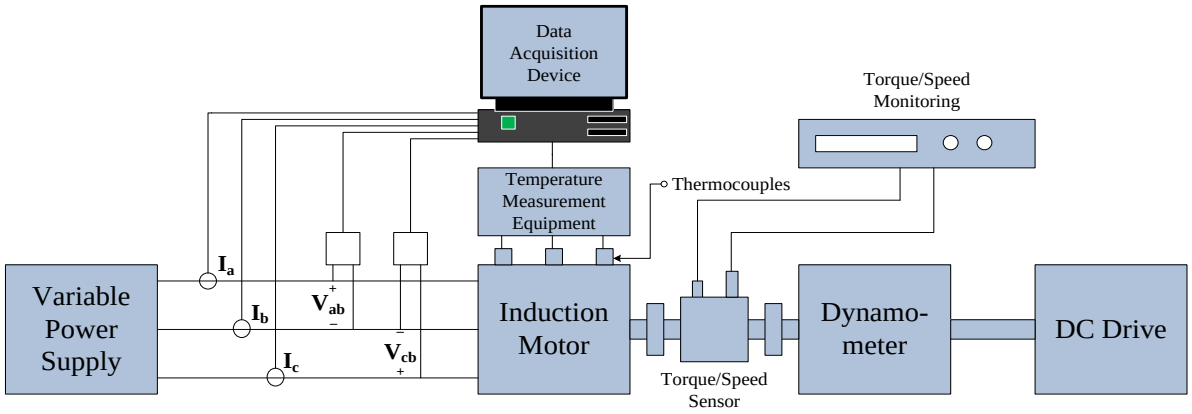

Figure 5-1: Schematic of the test rig

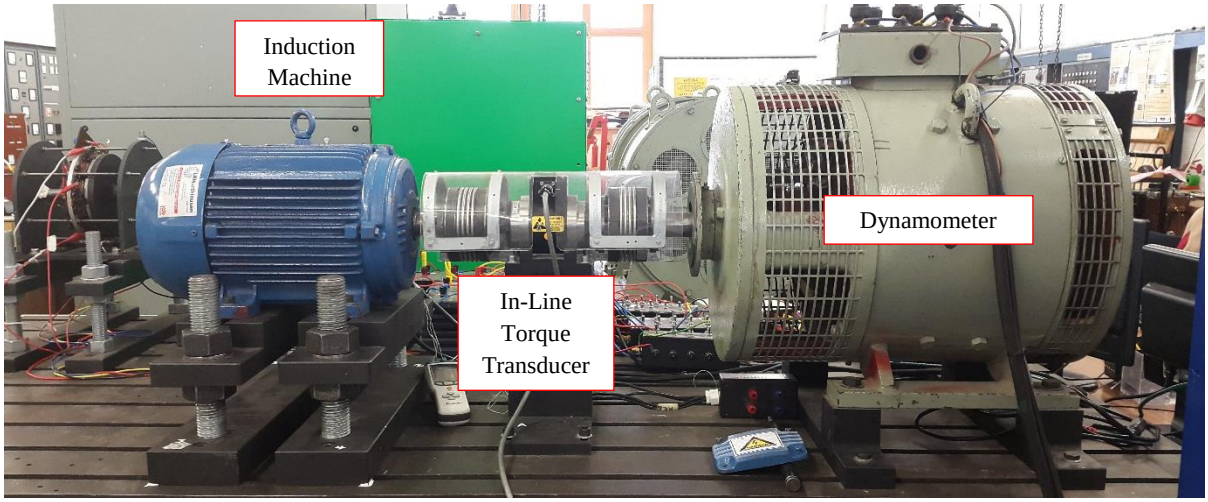

Figure 5-2: Physical setup of the test rig

The dynamometer is a separately excited DC machine whereby the torque is controlled by adjusting the armature current. The three-phase, four quadrant rectifier/inverter is responsible for controlling the armature current, which provides a return path for the energy back to the grid.

This means that the only energy consumed is associated with the losses in the system. In an instance when higher power loading for short periods is required an external resistor bank can be added.

Machine Loading

The separately excited DC machine is used to load the induction machine under test. The torque is controlled by the adjustment of the armature current since the torque is proportional to the armature current. The accuracy of the loading measurements is ensured by calibration of the torque transducer. This is achieved by attaching known weights to the torque arm and altering the amplification factor so that the display gives the expected torque. The torque that is expected is calculated using equation:

$$T = F \times d = m \times g \times d \qquad (5\text{-}1)$$

Where

m is the mass of the weights applied

g is 9.796 m/s^2 is the gravitational force for Cape Town

d is the distance of the torque arm

Machine Alignment

To ensure that the accuracy of the data obtained from the induction machine testing, each of the machines will have to be set up correctly. The machines are coupled to a dynamometer and proper care was taken to ensure that the machine shaft was properly aligned. Proper alignment is required to minimize the effects of vibration and machine eccentricities which negatively impact the temperature by increasing the total losses in the machines. An alignment clock that ensures that the machine and dynamometer shafts are centred was used. The shaft deviation was less than $1mm$.

5.2.1 Power Supply

The 22kW fully programmable power supply from California Instruments was used to simulate the various voltage unbalance conditions. The MX30 can produce both AC and DC output. It uses PWM switching techniques and has a reasonably high bandwidth. The MX30 model provides the facility for varying the magnitude of the voltage supplied to the machine being tested at the desired unbalance, over or under-voltage levels. The fully programmable power supply connected to the main supply was used throughout the duration of this research project.

5.2.2 Quality of Supply Requirements

The IEEE 112-B and IEC 34-2 have requirements regarding the quality of supply when performing tests on induction machines. Accurate data can only be obtained by carefully measuring with appropriate instrumentation and by employing a suitable power source. All the standards define minimal requirements for the quality of voltage and power supply. The different requirements concerning the power of supply and the specifications of the programmable power supply used in this research project are summarised in Table 5-4

Table 5-4: Instrumentation accuracy (%) required by induction machine testing standards

Supply Criteria	IEEE 112	IEC 34-2 (2007)	Compliance
Voltage waveform (THD)	$\leq 0.5\%$	$\leq 0.2\%$	✓
Voltage unbalance	$\leq 0.5\%$	$\leq 0.5\%$	✓
Frequency deviation from rated Frequency	$\leq \pm 0.1\%$	$\leq 0.3\%$	✓
Note concerning convertor supply	N/A	Yes	✓

Total Harmonic Distortion (THD)

The total harmonic distortion coefficient, THD, should not exceed 0.05. It is defined by the equation:

$$THD = \frac{\sqrt{E^2 - E_1^2}}{E_1} \tag{2-4}$$

Where

E is the total root-mean-square value of the voltage wave in volts (V).

E_1 is the root-mean-square value of the fundamental of the voltage wave in volts (V)

Voltage Unbalance

The IEEE 112 standard defines voltage unbalance as the line voltage unbalance rate *(LVUR)* as defined in chapter three.

$$LUVR(\%) = \frac{Max\left[\left|U_{ab} - U_{avg}\right| \cdot \left|U_{bc} - U_{avg}\right| \cdot \left|U_{ca} - U_{avg}\right|\right]}{U_{avg}} \tag{5-2}$$

The IEC 34-2 defines voltage unbalance in terms of the positive and negative sequence components. This voltage unbalance should not be greater than 0.5% under nominal testing conditions. Over a long period of time a voltage unbalance factor of 1% is set as the maximum. In case of short periods (not greater than a few minutes), a voltage unbalance of 1.5% is allowed. The zero-sequence component must not exceed 1% of the positive sequence component.

$$VUF(\%) = \frac{Negative\ Sequence\ Voltage\ Component}{Positive\ Sequence\ Voltage\ Component} \tag{5-3}$$

The recent version of IEC 60034-2 refers to edition 11, section 7 of IEC 60034-1, it uses the harmonic voltage unbalance factor (HVF) as one of the indicators of voltage supply quality. The total HVF should not be greater than 2% for single phase and three phase machines but excluding machines of design N. The HVF should be 3% for design N machines.

The HVF is obtained using

$$HVF = \sqrt{\sum_{n=2}^{k} \frac{U_n^2}{n}} \tag{5-4}$$

Where

U_n is the ratio of the harmonic voltage U_n to the rated voltage U_N

n is the order of harmonic (uneven, not divisible by three in the case of three phase AC motors)

$k = 3$ it is usually sufficient to consider harmonics up to the order 13

Frequency

Whenever testing is done on induction machines, the frequency must be within $\pm 0.5\%$ of the rated value for that test. It is important to avoid rapid variations in frequency when testing takes place, rapid variations in the frequency not only affects the induction machine but also the output measuring devices. The IEC 34-2-1 standard specifies that the frequency must be within $\pm 0.3\%$ of the rated frequency during measurements.

Convertor supply

IEEE Std. 112 B makes no mention of requirements when machines are to be fed from converters. IEC publications indicate that caution is required when induction motors are to be fed from converters. Higher losses are to be expected during a comparable load situation on a sinusoidal system. The extra losses are dependent on the harmonic spectrum of the impressed supply quantity (voltage or current), issues associated with inverter-fed machines are clearly covered in IEC 60034-2 by the publication of amendment 2 in 1996.

5.2.3 Measurement and Instrumentation

The power measuring devices used in this research project are as follows:

Yogokawa WT1800 Power Analyser

The main metering system used is the Yogokawa WT1800 (shown in Figure 5-3) power analyser which has 6 power measuring units as well as torque and speed. The analyser made it possible to take measurements at the various operating conditions. The three-phase power analyser is connected in series with the generator supply to the tested machine.

Figure 5-3: Yogokawa WT1800 Power Analyser

WTViewer

The Yokogawa power analyser uses the WTViewer software package that allows us to interface the power analyser and the computer. Readings can easily be obtained from the WTViewer as well as control of the power analyser. Graphical information of the data measured can also be obtained through this communication interface.

Galvanometer

The Galvanometer was used for measurement of the stator winding resistance of the induction machine. The Galvanometer consists of a Wheatstone-Bridge with four resistance branches, a current source and a meter/detector [51]. The three unknown resistances are matched with the one that is not known for zero current in the detector at balance.

8 Channel Pico Technology Data Logger and HE804 Data Logger Thermometer

Two data loggers were used to measure the temperature of the induction machines. The 8-channel Pico technology data logger uses a program interface to illustrate the recorded temperatures. The HE804 data logger was manually operated and it displayed measured temperatures on its screen.

K-Type Thermocouples

K-type (shown in Figure 5-4) thermocouples were installed on the drive-end side of the stator end windings. This is on the opposite side of the cooling fan. The thermocouples are placed close to parts where the highest temperature measurements of the stator windings were expected. They are placed on the windings above and below the rotor. The other thermocouple is placed on the side of the terminal box. To ensure that the temperatures measured were comparable, the thermocouples were placed at similar positions in all the induction machines.

Figure 5-4: 8-Channel Pico data logger

Magtrol Torque Transducer

The inline TM 312 (high accuracy) torque transducer was used in this research report. The TM 312 has speed sensing and its accuracy is above the rated 0.1%. The transducer is rated 200NM with the ability to go above 100% of rated conditions. The principle of a variable torque proportional transformer coupling is used by the system for measurements. The system is made of two concentric cylinders shrunk on the shaft on each side of the shaft's deformation zone and the two concentric coils attached to the housing. The two concentric cylinders both have a circularly disposed coinciding row of slots and they rotate with the shaft inside the coils [51]. An alternating current at a frequency of 20Hz flows through the primary coil. At zero torque the slots on the two cylinders fail to overlap. An application of torque will result in the deformation zone undergoing an angular deformation and the slots begin to overlap, this means a torque proportional voltage is on the secondary coil [51]. A full-scale analog voltage of $\pm 5V$ is output by

the integrated conditioning electronic module. The system uses a non-contact differential transformer torque measuring technology (none of the electronic components rotate during operation). The speed is obtained from an open collector pin and a $10k\Omega$ pull-up resistor is utilized. There is an active circuit that compensates the zero offset and temperature sensitivity drifts within a tolerance of $0.1\%/10K$.

5.2.4 Instrumentation Accuracy

The experimental setup for this research project is based on the instrumentation requirements stipulated by IEEE 112-B and IEC 60034-2 standards as summarized in Table 5-5.

Table 5-5: Instrumentation accuracy (%) required by induction machine testing standards

Variable Measurement Error	IEC 60034-2-1/IEEE 112	Experimental Setup
Voltage	±0.2%	✓
Current	±0.2%	✓
Power	±0.2%	✓
Resistance	±0.2%	✓
Frequency	±0.1%	✓
Temperature	±1°C	✓
Torque	±0.2%	✓
Speed	±1rpm	✓
Instrument Transformers	±0.3%	✓

5.3 Test Procedures

The induction machines listed in Table 5-1 will be operated under various voltage conditions as shown in Table 5-6 with voltage, current, temperature, torque and speed measurements duly taken. The levels of unbalance to be included in these tests are: 0%, 1%, 2% and 3%. The levels of over- and undervoltage are 90%, 100% and 110% of the nominal voltage. The considered load conditions are 25%, 50%, 75% and 100% of the rated load. The test procedure followed in this research project is summarised in the flow diagram in Figure 5-5. First all the machines are fitted with thermocouples, the thermocouples are fitted at identical locations for the machines to ensure that the measured temperatures are comparable. Tests are then done to obtain the electrical and thermal model parameters of the four machines. The machines are then subjected to the voltage conditions tabulated in Table 5-6 with the relevant measurements duly taken, the

machine temperatures are recorded for post processing and for machine life estimation. The temperatures obtained from the thermal model are compared to the measured values under the specified operating conditions.

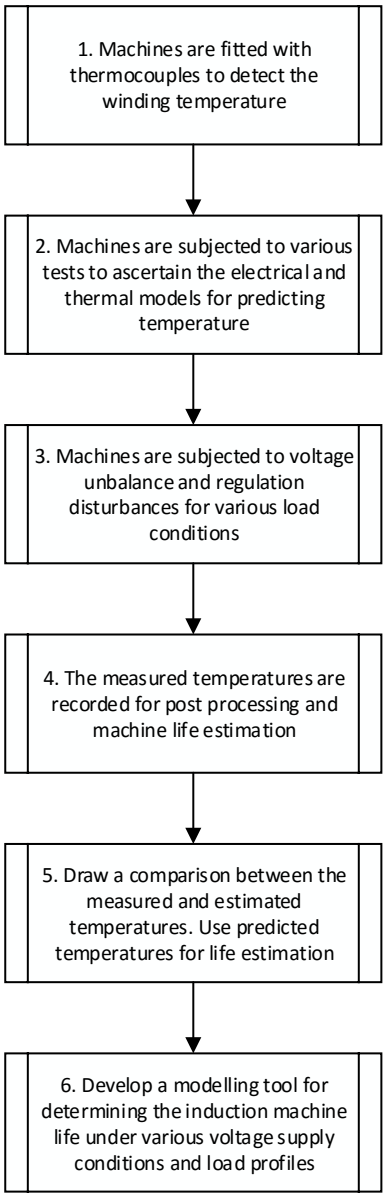

Figure 5-5: Flowchart for the Research Methodology

Table 5-6: Voltage and loading conditions for tests

VUF (%)	VR (%)	LC (%)	VUF (%)	VR (%)	LC (%)	VUF (%)	VR (%)	LC (%)	VUF (%)	VR (%)	LC (%)
0	90	25	1	90	25	2	90	25	3	90	25
		50			50			50			50
		75			75			75			75
		100			100			100			100
	100	25		100	25		100	25		100	25
		50			50			50			50
		75			75			75			75
		100			100			100			100
	110	25		110	25		110	25		110	25
		50			50			50			50
		75			75			75			75
		100			100			100			100

VUF=Voltage Unbalance
VR=Voltage Regulation
LC=Load Condition

The tests performed on the machines include the cold and hot winding temperature tests, no load, blocked rotor and the variable load test for determining induction machine losses and the positive and negative sequence equivalent circuits. The machine will then be subjected to further testing in attaining the thermal conductance and capacitance for the thermal model. Since the heat sources are attributed to the losses within the machine, it will also be tested in accordance with IEEE 112-B to determine the losses and hence validate the thermal model. After validation, the electrical and thermal model are combined to predict the temperature. The predicted and measured temperatures will be compared, after which will serve as inputs to predict the life expectancy of the machine.

5.3.1 Cold Winding Temperature Test

Before any thermal tests are done the ambient temperature and the stator winding temperatures are measured. Since all the induction machines had embedded thermocouples they were used to confirm that the machines were at ambient temperature.

5.3.2 Thermal Tests at Rated Load

The induction machine is coupled to the dynamometer and loaded to its rated torque. The machine was kept running until thermal equilibrium was reached. The thermal equilibrium is reached when the temperature changes by less than 2°C over a period of one hour or 1°C over a period of thirty minutes [51]. The temperature at this thermal equilibrium is recorded and the DC machine is de-energized as well as the supply to the induction machine. The induction machine must come to a complete halt before the galvanometer is used to measure the stator winding resistance. The temperature is also recorded when the resistance is measured. The resistance and the temperature are measured 30 seconds within shutdown to ensure accuracy.

This winding resistance measured after shutdown is used to determine the final temperature of the machine and its temperature rise. If the initial resistance reading is not obtained within 30 seconds for machines with a power rating less than 38kW, additional resistances are to be taken at intervals of 30/60 seconds for a minimum of 10 readings. These readings are plotted as a function of time and extrapolated to a time delay depending on the rating of the induction machine.

5.3.3 No Load Test

The no load test is performed by running the machine at rated voltage and frequency with no load connected. The DC machine is uncoupled from the shaft and the voltage is varied from 500V which is 125% of the rated voltage down to a point where further voltage reduction increases the current. During this test the voltage, current, power, frequency and the machine temperature are recorded.

5.3.4 Blocked Rotor Test

The machine rotor was locked into a stationary position and rated current was applied to the stator windings. This test gave information regarding the leakage impedance of the machine. A G-clamp was used to lock the rotor. To achieve the rated current, the voltage was slowly increased using the programmable power supply. Voltage, current, power and frequency are recorded during this test.

5.3.5 Thermal Conductance Test

One of the induction machine phases (Phase A in this case) is supplied with DC voltage at the rated machine current. The DC voltage is supplied until steady state equilibrium is reached, that is until the temperature doesn't change by more than 2°C over one hour or by 1°C over a thirty-minute interval. The resistances are measured and are used to obtain the induction machine temperature rise. The reduced stator thermal circuit for the first DC test is shown in **Error! Reference source not found.**

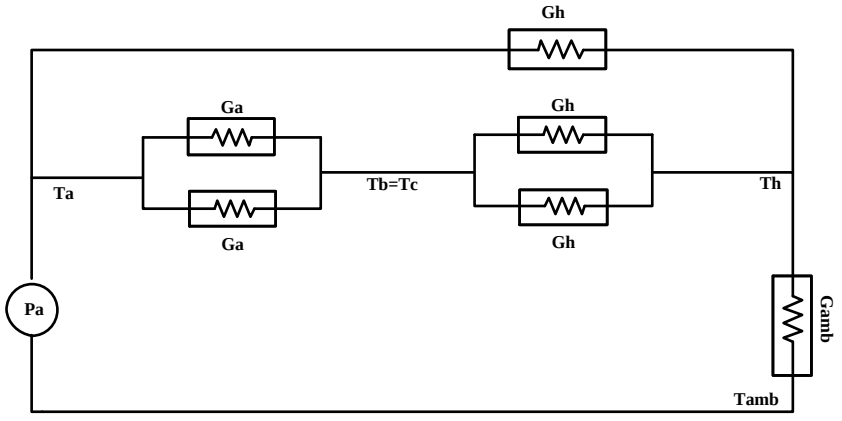

Figure 5-6: Reduced Stator Thermal Circuit During DC Test 1

Phases B and C have roughly the same temperatures due to winding symmetry, since only phase A was excited the heat source P_a, which is the input power is known. The other heat sources, P_b and P_c, are zero. The core loss is also zero because DC voltage was used. By applying KCL at each of the three nodes, three equations can be obtained, however there are four unknowns($G_a, G_h, T_h \; and \; G_{amb}$).

The second part of this test includes connecting all the phases in series and applying DC voltage across them at the rate machine current. This allows us to obtain a fourth equation which is necessary to determine the conductances. The voltage, current, power, resistance and temperature are measured during this test.

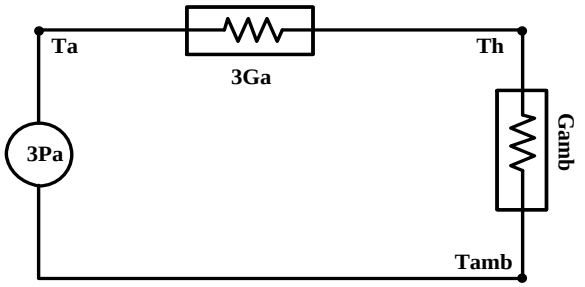

Figure 5-7: Reduced Stator Thermal Circuit during DC Test 2

5.3.6 Thermal Capacities

Similarly, the thermal capacities are obtained by performing DC tests on the induction machine. The windings are connected in series and supplied with a DC voltage at the rated current. The DC voltage is supplied until thermal equilibrium is reached. The voltage, current, temperature and resistance are recorded during this experiment. The temperature is plotted as a function of time and used to obtain the time constant.

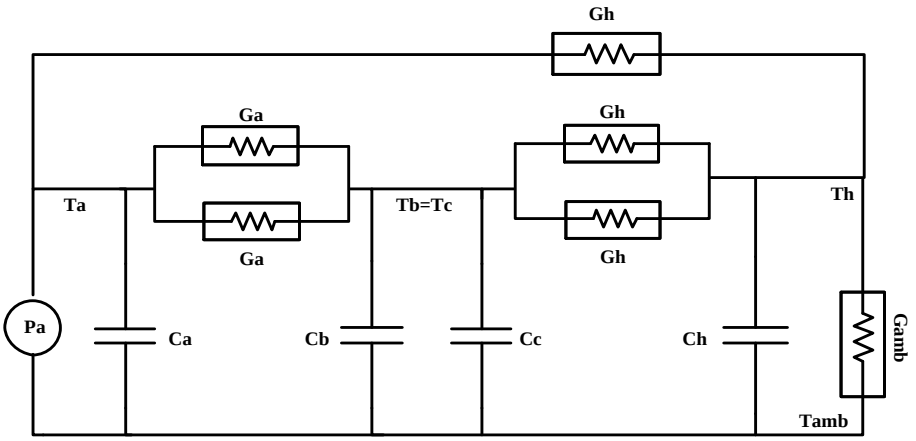

Figure 5-8: Reduced Stator Thermal Circuit During for DC Test 3

In the circuit above only, the thermal capacities (C_a, C_b, C_c, C_h) and the core temperature T_h are the unknowns, the thermal conductances are obtained from the previous two DC tests. The stator winding thermal capacities are all assumed to be equal due to winding symmetry. The circuit was reduced into three equations (three unknowns) with three nodes.

Applying KCL at node A yields

$$P_a = (T_a - T_b) \cdot 2G_a + (T_a - T_h) \cdot G_h + C_a \frac{\partial T_a}{\partial t} \qquad (5\text{-}5)$$

Rearranging the equation gives us

$$C_a = (P_a - (T_a - T_b) \cdot 2G_a - (T_a - T_h) \cdot G_h) \cdot \left(\frac{\Delta t}{\Delta T_a}\right) \quad (5\text{-}6)$$

The other capacities can therefore be obtained using

$$C_b = \left((T_a - T_b) \cdot 2G_a - (T_b - T_h) \cdot 2G_h\right) \cdot \left(\frac{\Delta t}{\Delta T_b}\right) \quad (5\text{-}7)$$

$$C_h = \left((T_a - T_h) \cdot G_h + (T_b - T_h) \cdot G_h - (T_h - T_{amb}) \cdot G_{amb}\right) \cdot \left(\frac{\Delta t}{\Delta T_h}\right) \quad (5\text{-}8)$$

It has been found from the tests that the thermal behavior of the machine can be modeled closely by an exponential equation with one time constant [53]. By applying the assumption that the time constant for an exponential rise curve is the time taken to reach 63% of the final value ΔT and Δt can be easily obtained. These values are extracted from the temperature curve plotted from DC test 3.

5.3.7 Heat Sources

The heat source in the thermal model comprises of the core and stator copper losses which are detailed in Chapter 4. The stator copper losses are attained using the positive and negative per phase equivalent circuits whilst the core losses are attained by performing the no load test under the various voltage conditions (IEEE 112-B).

5.4 Concluding Remarks

Chapter 5 presented the experimental setup and instrumentation required for induction machine loss testing, equivalent circuit parameter testing and thermal parameter testing. A proper description of the instrumentation accuracy required by the IEEE 112 and IEC 60034-2-1 standards is given and the laboratory equipment accuracy is compared against these standards. All the tests (cold winding, no load, load, blocked rotor) are conducted in accordance with recognised standards. The test undertaken to determine the thermal model parameters (DC tests) are conducted in accordance with past literature [53] [31] .

6. RESULTS AND ANALYSIS OF MACHINE LOSSES AND EFFICIENCY UNDER VOLTAGE UNBALANCE AND REGULATION CONDITIONS

This chapter presents the results of the laboratory experiments. The no load test results are given, and the core losses are extracted from them. The core losses are determined for all the considered operating conditions. Similarly, the parameters of the sequence circuits are determined using the no load and blocked rotor test results. These sequence circuits are used to obtain the stator copper losses under the considered operating conditions. Both the stator copper losses and the core losses will serve as inputs in the thermal model discussed in chapter 7. The IEEE 112-A direct method is used to determine the efficiencies of the machines under the proposed operating conditions and these are compared to efficiencies under normal operating conditions.

6.1 Cold Winding Temperature Test Results

The stator winding resistances of the various machines were measured before any thermal test was performed on the machine. The resistance of each machine was recorded and is shown in Table 6-1

Table 6-1: Machine cold winding resistances

Machine *(kW)*	Resistance (Ω)
Manufacturer B *(7.5kW)*	2.149
Manufacturer A *(7.5kW)*	2.3
Manufacturer B *(11kW)*	1.18
Manufacturer A *(11kW)*	1.21

6.2 Rated Torque for Thermal Tests

The machine load conditions are determined from the torque. The rated power and the nameplate speed are used in determining the rated torque of each machine. The torque is obtained using equation (6-1). The rated torque of each machine is given in Table 6-2.

$$T_{rated} = \frac{P_{rated}}{n_{rated}} \times \frac{60}{2\pi} \qquad (6\text{-}1)$$

Table 6-2: Machine torque at rated power and speed

Machine *(kW)*	Torque(Nm)
Manufacturer B *(7.5kW)*	49.39
Manufacturer A *(7.5kW)*	49.05
Manufacturer B *(11kW)*	71.95
Manufacturer A *(11kW)*	71.95

6.3 Steady State Operating Temperature

The four machines were operated at rated load conditions at the nominal voltage conditions. The temperature of each machine was monitored every 30 minutes until it changed by no more than 1°C during that period. The highest tempertature for each of the machines was measured. The steady state temperature of each of the machines is given in **Error! Reference source not found.**.

Table 6-3: Steady state operating temperatures of the four machines

Machine *(kW)*	Temperature (°C)
Manufacturer B *(7.5kW)*	98.83
MANUFACTURER A *(7.5kW)*	103.07
Manufacturer B *(11kW)*	108.95
MANUFACTURER A *(11kW)*	114.12

6.4 No Load Tests

No load tests were conducted to obtain the core losses and the friction and windage losses as per IEEE 112-B. As per IEEE 112-B, the test was carried out at input voltages ranging from 500V (125% of the rated voltage) to 80V(20% of the rated voltage) . The voltage, current, power and temperature were all recorded during this test. The data recorded for all the machines starting with the 7.5kW Manufacturer A machine is given from Table 6-4 to Table 6-11. The no load tests were undertaken at different voltage unbalance levels (0% to 3%) and the core and friction windage losses were extracted respectively.

Table 6-4: Manufacturer A 7.5kW No load test results for VUF=0% and VUF=1%

VUF =0%				VUF=1%			
Temp (°C)	**Voltage (V)**	**Current (A)**	**Pin (W)**	**Temp (°C)**	**Voltage (V)**	**Current (A)**	**Pin (W)**
50.67	499.35	17.082	1750	53.22	496.47	16.75	1694
51.23	439.69	10.813	763	53.24	437.2	10.66	740
51.20	399.86	8.17	468	53.4	400.4	8.206	473
50.21	320.05	5.654	265	53.32	312.12	5.61	258
49.86	240.03	4.124	170	53.30	238.56	4.082	164
49.55	160	2.737	108	53.28	159.05	2.71	103
49.32	79.93	1.494	68	53.2	79.46	1.48	65

Table 6-5: Manufacturer A 7.5kW No load test results for VUF=2% and VUF=3%

VUF =2%				VUF=3%			
Temp (℃)	Voltage (V)	Current (A)	Pin (W)	Temp (℃)	Voltage (V)	Current (A)	Pin (W)
56.45	495.81	16.97	1764	60.54	498.21	17.01	1801
56.55	439.73	11.18	826	60.61	439.35	11.54	903
56.31	399.86	8.42	504	60.21	399.56	8.73	558
56.26	319.95	5.68	272	60.18	319.71	5.82	296
56.18	239.97	4.12	168	60.11	239.75	4.15	175
56.1	160.02	2.72	103	60.01	159.81	2.72	105
56.05	79.85	1.489	65	50.78	79.84	1.49	66.1

Table 6-6: Manufacturer B 7.5kW No load test results for VUF=0% and VUF=1%

VUF =0%				VUF=1%			
Temp (℃)	Voltage (V)	Current (A)	Pin (W)	Temp (℃)	Voltage (V)	Current (A)	Pin (W)
47.99	499.41	15.18	1477	47.95	496.64	14.89	1484
47.05	439.74	9.36	649	49.32	437.43	9.17	645
47.12	399.87	6.91	402	49.21	397.7	6.85	406
47.18	320.09	4.50	224	49.18	318.2	4.50	227
47.25	240.07	3.16	142	49.15	238.36	3.15	145
47.08	160.4	2.06	86	49.10	159.13	2.05	88
47.01	79.97	1.1	51	49.08	79.47	1.10	53

Table 6-7: Manufacturer B 7.5kW No load test results for VUF=2% and VUF=3%

VUF =2%				VUF=3%			
Temp (℃)	Voltage (V)	Current (A)	Pin (W)	Temp (℃)	Voltage (V)	Current (A)	Pin (W)
49.5	495.99	15.33	1569	53.22	496.47	17.73	1959
51.01	439.8	10.01	766	53.24	437.2	10.66	848
51.03	399.9	7.49	480	53.4	400.4	8.08	542
52.2	319.98	4.90	269	53.32	312.12	5.32	296
51.1	240	3.42	167	53.30	238.56	3.72	183
51.01	159.93	2.21	99	53.28	159.05	2.41	105
51.0	79.88	1.17	57	53.2	79.46	1.24	58

Table 6-8: Manufacturer A 11kW No load test results for VUF=0% and VUF=1%

VUF=0%				VUF=1%			
Temp (℃)	**Voltage (V)**	**Current (A)**	**Pin (W)**	**Temp (℃)**	**Voltage (V)**	**Current (A)**	**Pin (W)**
42.61	499.86	19.66	1633	47.89	496.95	14.89	1608
43.55	440	12.41	749	48.44	437.57	9.17	738
43.38	400.05	9.05	498	48.4	398.08	6.85	492
43.12	320.2	6.63	314	48.3	318.26	4.50	310
43.05	240.13	4.84	213	48.24	239	3.15	209
43	160.02	3.23	149	48.15	159.12	2.05	142
42.95	79.87	1.86	106	48.09	79.37	1.10	99

Table 6-9: Manufacturer A 11kW No load test results for VUF=2% and VUF=3%

VUF =2%				VUF=3%			
Temp (℃)	**Voltage (V)**	**Current (A)**	**Pin (W)**	**Temp (℃)**	**Voltage (V)**	**Current (A)**	**Pin (W)**
49.88	440	13.04	846	52.05	439.65	13.90	988
49.97	400.08	9.88	558	52.12	399.79	10.66	657
49.85	320.09	6.75	329	52.08	319.87	7.19	374
49.76	240.06	4.86	211	51.98	239.84	4.99	225
49.5	160.05	3.23	138	51.91	159.88	3.22	137
49.43	79.8	1.85	100	51.88	79.83	1.83	93

Table 6-10: Manufacturer B 11kW No load test results for VUF=0% and VUF=1%

VUF =0%				VUF=1%			
Temp (℃)	**Voltage (V)**	**Current (A)**	**Pin (W)**	**Temp (℃)**	**Voltage (V)**	**Current (A)**	**Pin (W)**
44.31	499.85	21.36	1854	49.91	496.86	21.45	1824
45.42	440.04	13.28	912	49.05	437.59	13.15	919
45.21	400.09	9.98	635	49.35	397.86	9.96	646
45.1	320.24	6.73	411	49.2	318.28	6.76	424
45.01	240.13	4.86	290	49.15	238.69	4.86	299
44.98	159.99	3.24	217	49.05	159.07	3.24	219
44.5	79.92	2.06	168	48.89	79.25	2.01	157

Table 6-11: Manufacturer A 11kW No load test results for VUF=2% and VUF=3%

VUF=2%				VUF=3%			
Temp (℃)	**Voltage (V)**	**Current (A)**	**Pin (W)**	**Temp (℃)**	**Voltage (V)**	**Current (A)**	**Pin (W)**
52.45	496.33	21.50	1957				
52.78	439.99	14.17	1050	54.53	439.67	15.53	1209
52.88	400.04	10.89	736	54.32	399.8	12.02	848
52.71	320.05	7.39	468	54.22	319.87	8.23	522
52.63	240.01	5.29	325	54.18	239.83	5.91	353
52.34	159.98	3.49	224	54.1	159.79	3.9	240
52.2	79.67	2.1	163	54.01	79.66	2.22	169

6.5 Thermal Tests

The thermal tests at various loads was performed on all the machines under consideration. The machine was ran at different load conditions until thermal equilibrium was reached. Four load conditions were considered for each unbalance and over/undervoltage condition. The test data for all the thermal tests are summarised in Table 12-1 to Table 12-47 found in Appendix A.

6.6 Blocked Rotor Tests

As described in the preceding chapter, the locked rotor test involves clamping the machine shaft whilst increasing the voltage until rated current is achieved. The locked rotor test results for each of the machines are given in Table 6-12.

Table 6-12: Blocked Rotor Test Results

Machine (kW)	**Voltage (V)**	**Current (A)**	**$P_{in}(W)$**
Manufacturer A($7.5kW$)	80.55	15.97	1041
Manufacturer B($7.5kW$)	87.82	15.08	988
Manufacturer A($11kW$)	80.36	22.02	1440
Manufacturer B($11kW$)	78.12	22.2	1227

6.7 Per-Phase Equivalent Circuit Parameters

The equivalent circuit parameters of the four machines were determined using the no load and locked rotor results. The method set out by IEEE 112-B was followed. The results are given in Table 6-13.

Table 6-13: Equivalent Circuit Parameters

Machine	**R_s (Ω)**	**X_s (Ω)**	**X_m (Ω)**	**X_{rp} (Ω)**	**X_{rn} (Ω)**	**R_{rp} (Ω)**	**R_{rn} (Ω)**
Manufacturer B(7.5kW)	2.149	4.66	95.920	4.66	4.214	2.413	2.98
Manufacturer A(7.5kW)	2.3	4.01	81.09	4.01	3.872	2.003	2.65

Manufacturer B(11kW)	1.18	2.59	78.21	2.95	2.68	1.97	2.27
Manufacturer A(11kW)	1.21	2.84	73.99	2.84	2.41	1.90	2.01

6.8 Induction Machine Losses

6.8.1 Temperature Dependent Losses

a) I^2R Losses

The winding losses of an induction machines are calculated using equation (6-8), the electrical resistance of metallic materials increases linearly with the temperature. The stator winding resistance of induction machines consist of cooper whilst the rotor mostly consists of aluminium, this leads to different temperature coefficients being used for temperature correction. In [74] it is shown that for windings made from either material and operating at an ambient of 20°C, the winding resistance increases by approximately 4% per 10K of temperature rise.

b) Windage Losses

Induction machine windage losses vary inversely proportional with the temperature. In [74] it is reported that the pressure and ventilating power vary with the air density which in turn depends on air humidity, pressure and temperature. For a relative humidity of 80% and at normal atmospheric pressure the windage losses in the considered temperature range decrease approximately by 4 to 5% for each 10K of temperature rise [74]. In the case of TEFC machines the outer ventilation losses form part of the machine losses, these losses however do not depend on the inner machine temperature. The inner ventilation losses between the rotor and the stator are in most cases negligible at standard machine speeds. Friction and windage losses originate in the bearings of the machine rotor. The friction in the rotor bearings reduces as the temperature increases due to the decrease in lubricants viscosity [75]. In synchronous machines the friction and windage losses are not measurable because they always present in iron losses, in induction machines these losses are separated from the iron losses as per IEEE 112-B and IEC 60034-2.

6.8.2 Load Dependent Losses

6.9.2.1 Core Losses

The no load tests are carried out as quickly as possible with the readings taken in descending order of the machine supply voltage (this is from the maximum voltage to the minimum value for the auto sustenance of the rotation) [75]. For each of the test points, the voltage, current, the temperature and the no load power are captured. To be able to compensate for stator resistance variation with the temperature the stator resistance is measured before and after the completion of the test.

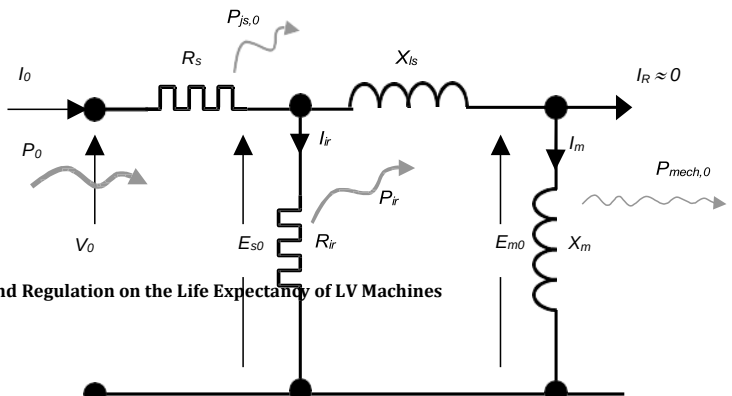

Figure 6-1: Per Phase no load equivalent circuit of induction machines [75]

The per phase equivalent circuit shown in Figure 6-1 is considered when analyzing machine core losses. The circuit above takes into consideration that the core losses depend on the leakage fluxes in the machine too [75]. The no load power equation is given in (6-2), this is the power equation recommended by IEEE 112-B and the IEC 60034-2-1.

$$P_{fe} = P_{NL} - 3R_s I_{NL}^2 - P_{FW} \quad (6\text{-}2)$$

The core losses are drawn as a function of the line to line fundamental stator voltage. IEEE 112-B stipulates that the friction and windage losses can be estimated as the interception with the zero-voltage axis of the linear regression line of the fixed no load losses versus the square of the line to line voltage [75]. The core losses of the four machines under the various voltage unbalance scenarios are given in Figure 6-2 to Figure 6-5.

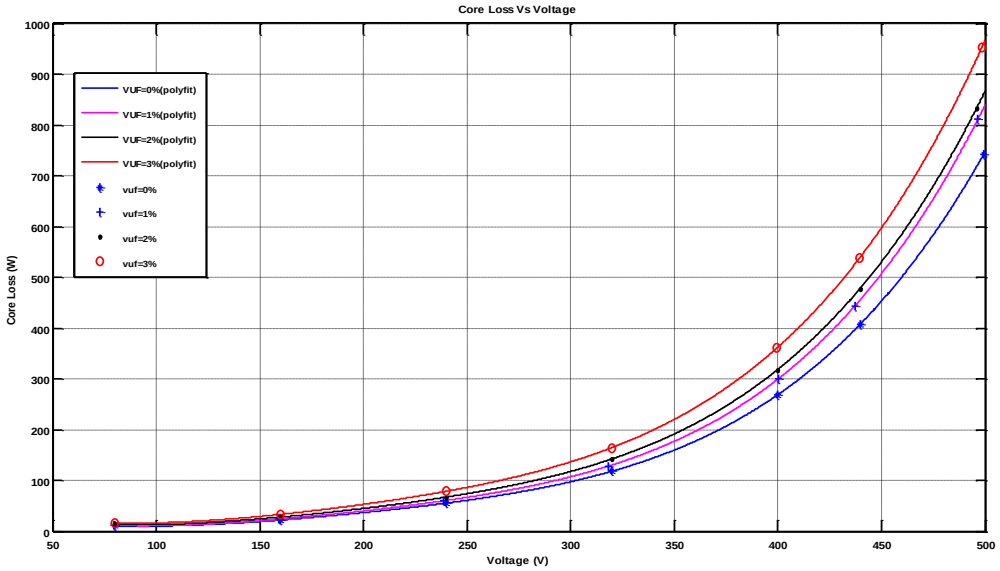

Figure 6-2: 7.5kW Manufacturer A core losses under various voltage unbalance conditions

Table 6-14: 7.5kW Manufacturer A core losses at various voltage unbalance conditions

Voltage Regulation (%)	Voltage Unbalance (%)			
	0	**1**	**2**	**3**
90	179.42	199.03	214.22	245.62
100	269.43	301.74	319.14	361.94

110	404.47	440	475.4	534.54

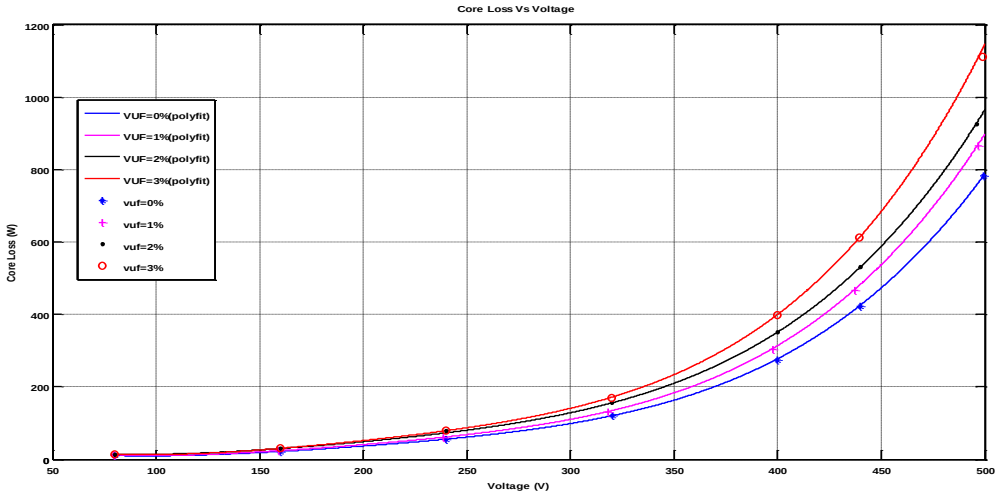

Figure 6-3: 7.5kW Manufacturer B core losses under various voltage unbalance conditions

Table 6-15: 7.5kW Manufacturer B core losses at various voltage unbalance conditions

Voltage Regulation (%)	Voltage Unbalance (%)			
	0	**1**	**2**	**3**
90	183.94	207.02	235.28	263.99
100	278.46	307.56	352.1	400.28
110	421	466.7	526.78	588.99

Under balanced voltage conditions, the 7.5kW Manufacturer A machine has a core loss of 269.43W, the 7.5kW Manufacturer B machine has a core loss of 278.48W under the same operating conditions which is 9.05W more than the Manufacturer A machine. From **Error! Reference source not found.** and **Error! Reference source not found.**, the core losses increase with an increase in voltage unbalance. Under balanced voltage conditions with 90% undervoltage, the core losses are 40% less than at rated voltage conditions. This trend is similar for both the Manufacturer A and Manufacturer B machines. A 50% increase in core losses is observed as the voltage regulation is increased to 110%. As previously discussed, the core losses are obtained by subtracting the no load copper losses and friction and windage losses from the no load input power. The 7.5kW Manufacturer A machine draws more current than the Manufacturer B machine under no load conditions, it also has greater friction and windage losses under all the voltage unbalance conditions hence resulting in lower core losses. The worst case for both machines occurs at 3% voltage unbalance combined with 110% voltage regulation. For this operating condition there is a 98% increase in core losses for the 7.5kW Manufacturer A machine and a 100% increase in core losses for the 7.5kW Manufacturer B machine.

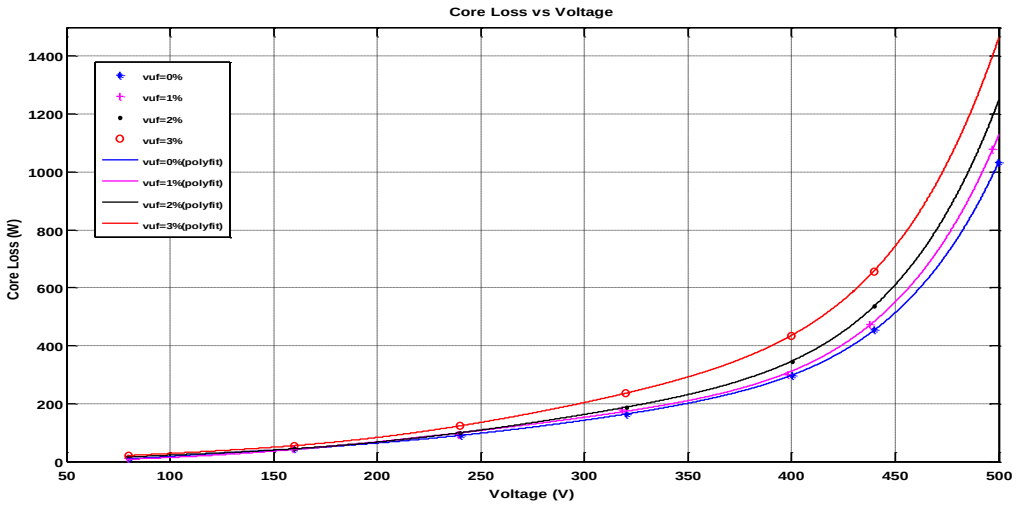

Figure 6-4: 11kW Manufacturer A core losses under various voltage unbalance condition

Table 6-16: 11kW Manufacturer A core losses at various voltage unbalance conditions

Voltage Regulation (%)	Voltage Unbalance (%)			
	0	1	2	3
90	215.01	225.0	249.12	313.11
100	297.88	312.23	347.01	434.01
110	451.23	484.02	534.12	660.01

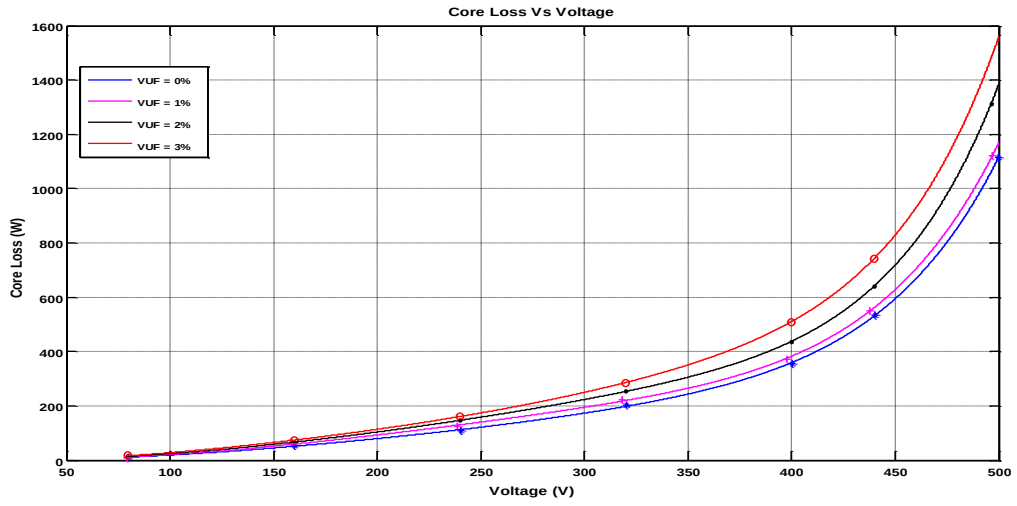

Figure 6-5: 11kW Manufacturer B core losses under various voltage unbalance conditions

Table 6-17: 11kW Manufacturer B core losses at various voltage unbalance conditions

Voltage Regulation (%)	Voltage Unbalance (%)

	0	1	2	3
90	261	283	326	376
100	359	382	437	510
110	531	562	641	743

Under balanced operating conditions, the 11kW Manufacturer A machine has a core loss of 297.88W, this is 61.12W lower than the 11kW Manufacturer B machine under the same voltage conditions. Like the 7.5kW machines, the worst case occurs at 3% voltage unbalance combined with 110% voltage regulation. The 11kW Manufacturer A machine has a core loss of 660.01W while the 11kW Manufacturer B has losses of 743W under the same operating condition. The core losses increase with average voltage. When voltage unbalance is introduced there are additional losses in the rotor due to the reverse airgap field. These additional losses in the rotor form part of the increased core losses. From first principles we know that the core losses in an induction machine are dependent on the induction machine's flux [27]. The machine's flux is proportional to the voltage. The core losses in a SCIM can be categorized as; [24]core losses in the yoke, core losses in the stator teeth and core losses in the rotor. The additional losses in the rotor and the stator teeth results in the core losses being shifted with respect to the supply condition. As expected, the core loss for undervoltage operating conditions are lower than those at nominal operating condition. This is to be expected because the average voltages are different. For operation under overvoltage conditions, the saturation and the quality of electrical steel plays a vital role. The core losses for this operating condition increases as the unbalance increases.
From the basic per-phase equivalent circuit of an induction machine, the iron losses of an induction machine can be expresses according to the voltage unbalance:

$$P_{Fe} = 3 \cdot R_M \cdot \left(\left(\frac{U_p}{Z_m} \right)^2 + \left(\frac{U_n}{Z_m} \right)^2 \right) = 3 \cdot R_M \left(\frac{U_p}{Z_m} \right)^2 (1 + VUF^2) \qquad (6\text{-}3)$$

The core losses depend on the square of the magnitude of the component of positive sequence voltage and the square of the voltage unbalance factor. The voltage unbalance factor is much smaller than unity, this means that the losses are mainly caused by the positive sequence component. The previously mentioned stator copper losses can be divided into hysteresis$\left(P_{L,hyst}\right)$ and eddy current losses$\left(P_{L,hyst}\right)$. Hysteresis losses are a result of Barkhausen jumps and irreversible rotation processes in the magnetic material of induction machines. The losses due to eddy currents can be divided into classic and anomalous eddy current losses. Circular currents caused by the voltages induced by the alternating magnetic field lead to classical eddy current losses. The anomalous eddy current losses are caused by microscopic eddy currents which are caused by the displacement of the Bloch walls [76]. The core losses in the stator iron can be described using [77]:

$$P_{L,iron} = \sigma_{1,5} \cdot m_S \cdot \left(\frac{B}{1.5T} \right)^2 \cdot \left[k_{hyst} \cdot \left(\frac{f}{50Hz} \right) + k_{eddy} \cdot \left(\frac{f}{50Hz} \right)^2 \right] \qquad (6\text{-}4)$$

Where:

f is the electric frequency of the rotating field
B is the magnetic flux density
$\sigma_{1,5}$ is the specific iron losses at $B = 1.5T$
m_S is stator iron mass

k_{hyst} is the hysteresis current loss
k_{eddy} is the eddy curreny loss

This approach to core losses is used when investigating the influence of harmonics or different tooth geometries on induction machines. The core losses obtained from the no load tests are similar to the those obtained using this approach. The temperature dependence of the core losses is explained better using this approach.

Hysteresis Losses
As the temperature increases less polarization energy for the Weiss domains is required due to increased atomic motion [77]. This means that the remanence, B_R and the coercivity H_C decrease in the iron core [77]. This eventually leads to the hysteresis loop contracting, as shown in Figure 6-6. The result will be lower hysteresis losses which are proportional to the area inside the loop.

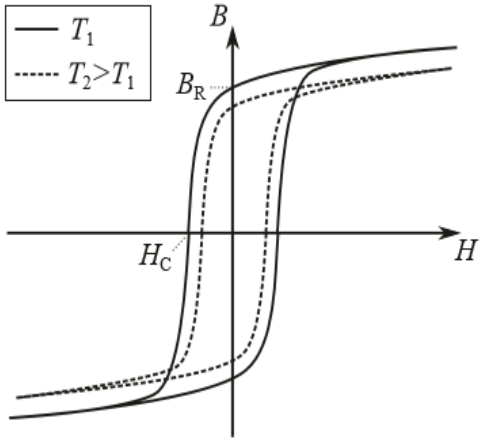

Figure 6-6: Hysteresis loop of a magnetic material at different temperatures

Eddy current losses
The eddy current losses are caused by circular currents caused by the voltages induced by the alternating magnetic field. This means they depend on the electric resistance of the iron sheets and decrease with rising temperatures.

$$P_{L,eddy} \sim \frac{1}{R_{iron}} \sim \frac{1}{1 + \propto_{iron} \cdot \Delta T} \qquad (6\text{-}5)$$

It can be concluded that the induction machine core losses increase with an increase in average voltage and decrease with an increase in machine temperature. This decrease in core losses with an increase in temperature can be explained by decomposing the core losses (into eddy and hysteresis losses) or by using equation (6-2). Since this research report looks to approximate the temperature of induction machines it is evident from these results that the core losses are more likely to have a larger impact on the temperature rise of the machine under overvoltage operating conditions (lower temperatures and higher core losses) then under undervoltage operating conditions (higher temperatures and lower core losses). This is further illustrated in the next

section when explaining the shift in maximum efficiencies of the four machines under the various operating conditions.

6.9 Load Dependent Losses

6.9.1 Stator Copper Losses

Given that the stator winding resistance $R_{s,Tamb}$ and the rotor resistance $R'_{r,Tamb}$ at ambient temperature $T_{ambient}$ are known, and the operating temperature T_{load} of a machine is known, the machine resistances at the operating points can be determined from the following equation [12]:

$$R_{s,load} = \frac{R_{s,Tamb}(T_{load} + k_{Cu})}{T_{ambient} + k_{Cu}} \tag{6-6}$$

$$R'_{r,load} = \frac{R_{r,Tamb}(T_{load} + k_{Al})}{T_{ambient} + k_{Al}} \tag{6-7}$$

Where $k_{Cu} = 234.5$ and $k_{Al} = 225$ are the temperature coefficients for copper and aluminium respectively. The stator copper losses under unbalanced conditions are obtained by combining the positive and negative component losses.

$$P_{cu-total} = \sum_{i=p,n} (I_i)^2 R_{s,load} = 3 \cdot \left(I_p^2 + I_n^2\right) R_{s,load} \tag{6-8}$$

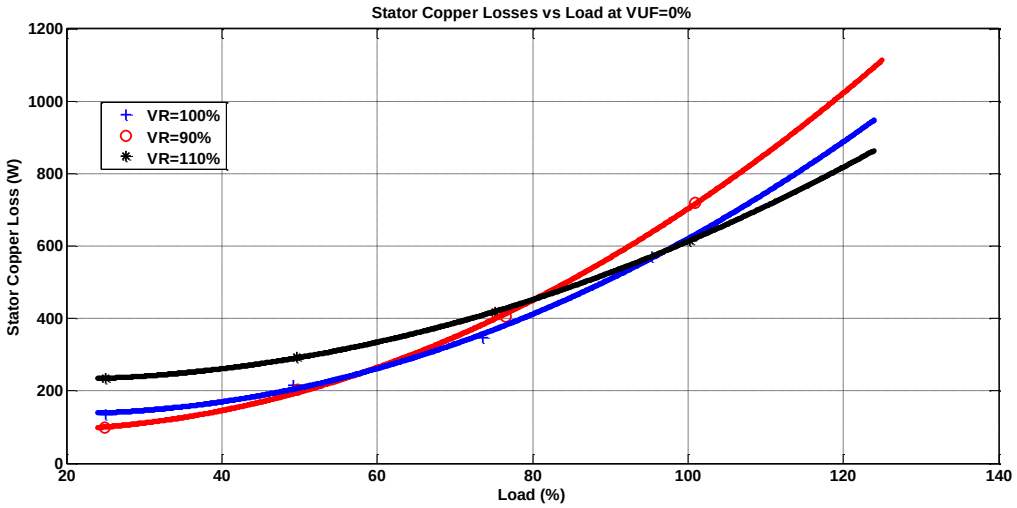

Figure 6-7: 7.5kW Manufacturer B Stator Copper Losses for VUF=0%

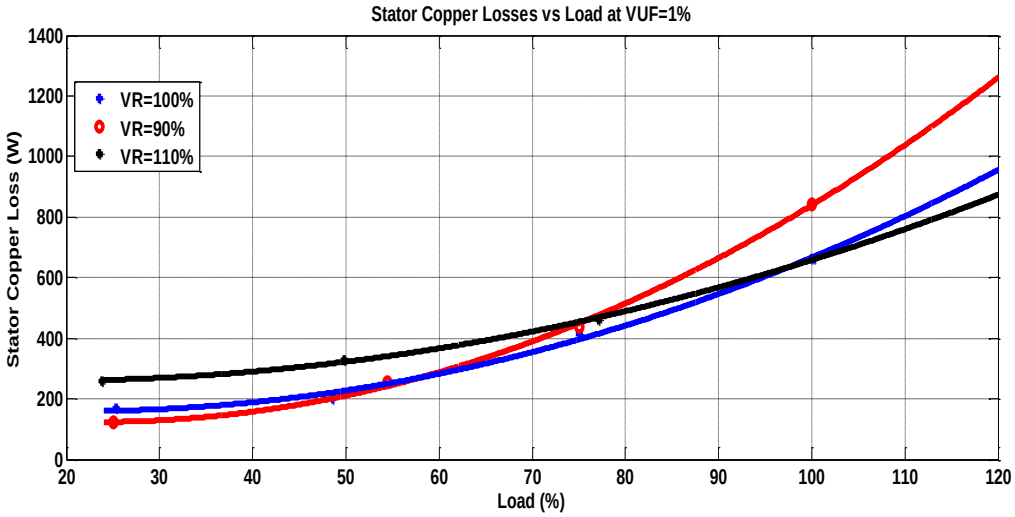

Figure 6-8: 7.5W Manufacturer B Stator Copper Losses for VUF=1%

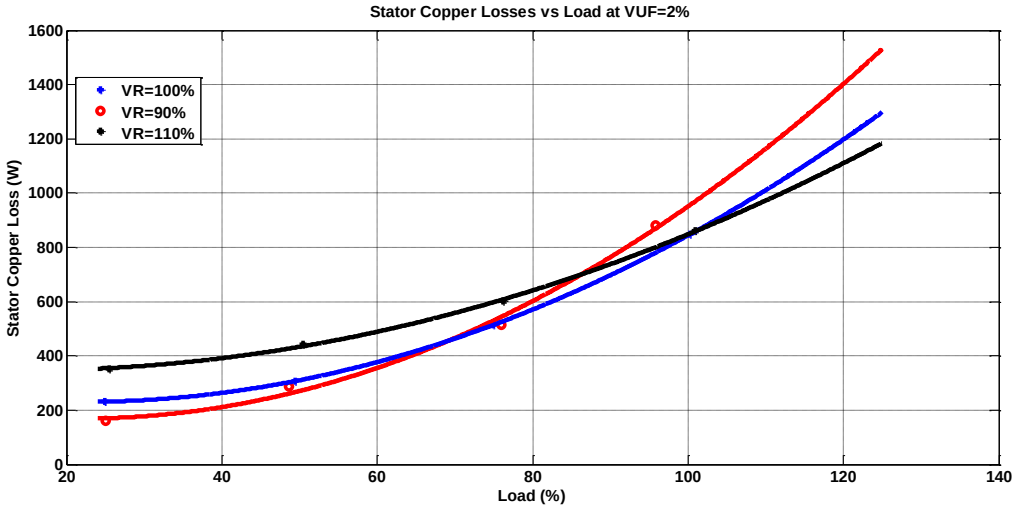

Figure 6-9: 7.5kW Manufacturer B Stator Copper Losses for VUF=2%

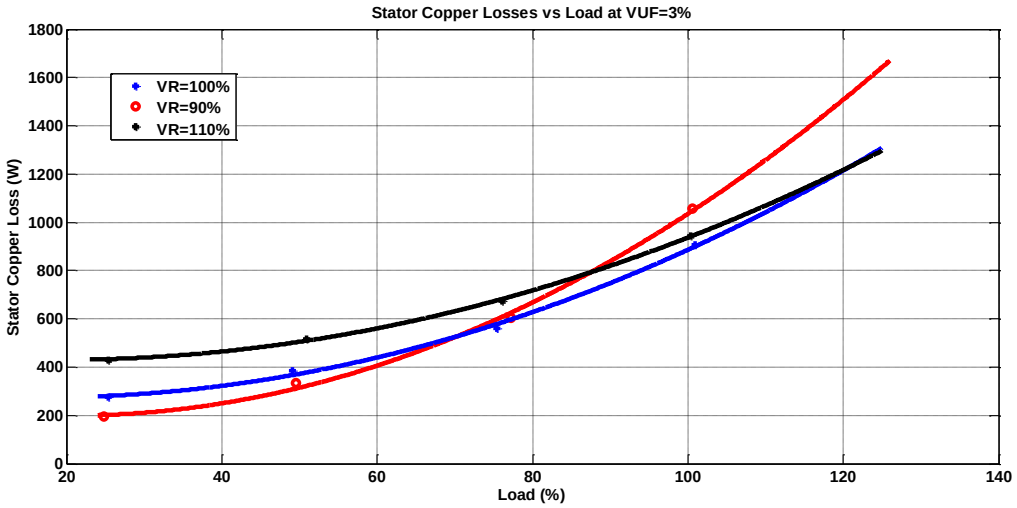

Figure 6-10: 7.5kW Manufacturer B Stator Copper Losses for VUF=3%

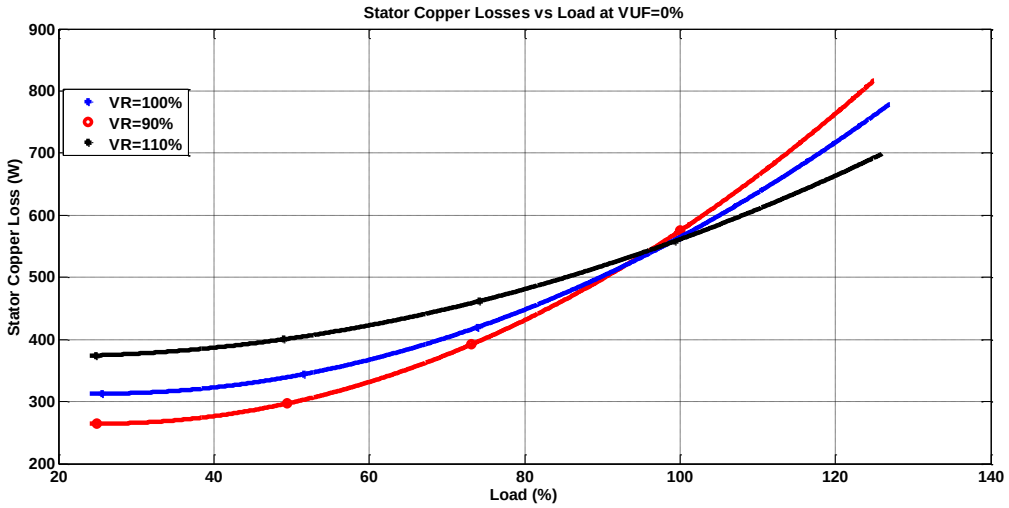

Figure 6-11: 7.5kW Manufacturer A Stator Copper Losses for VUF=0%

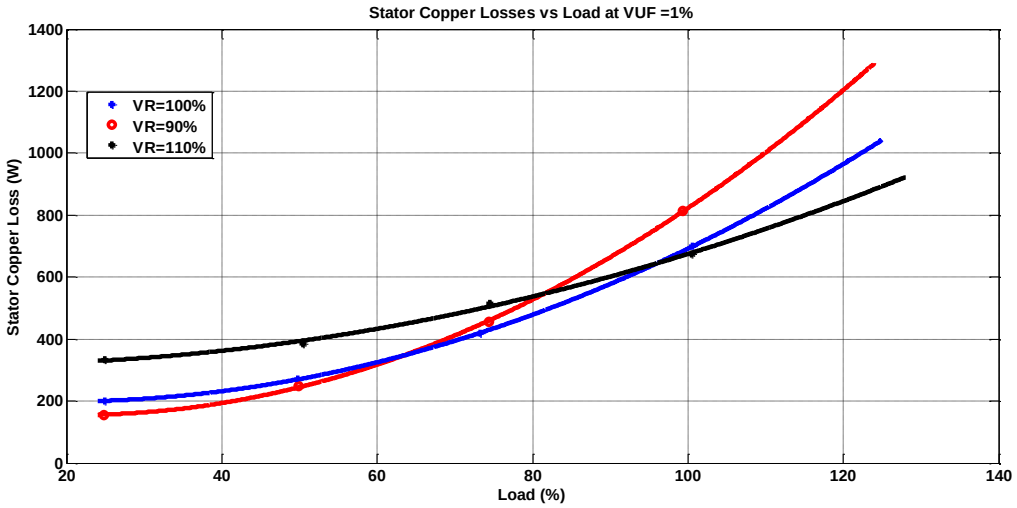

Figure 6-12: 7.5kW Manufacturer A Stator Copper Losses for VUF=1%

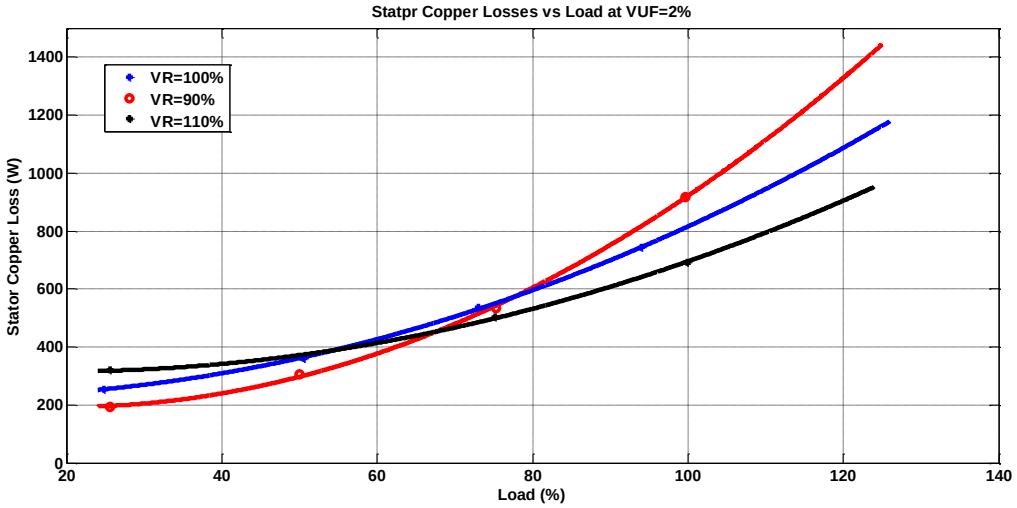

Figure 6-13: 7.5kW Manufacturer A Stator Copper Losses for VUF=2%

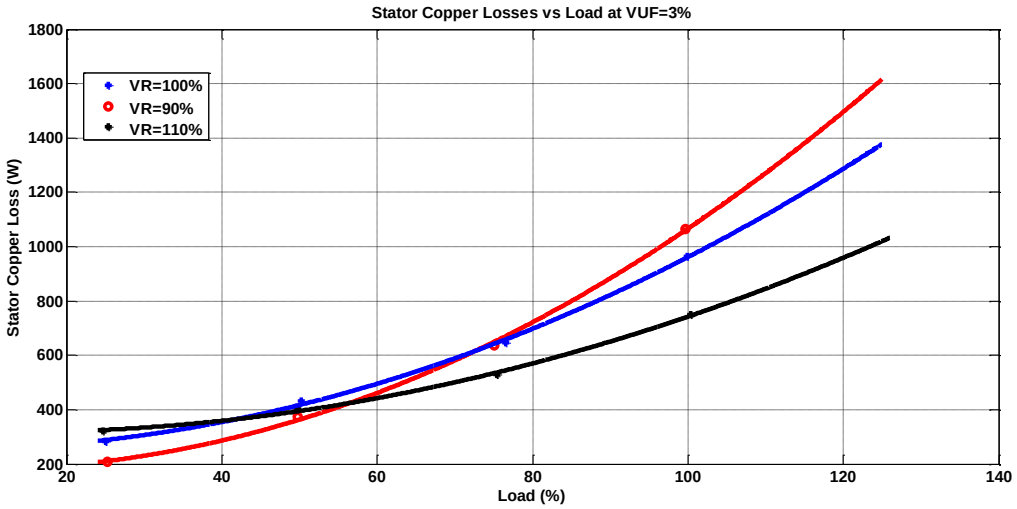

Figure 6-14: 7.5kW Manufacturer A Stator Copper Losses for VUF=3%

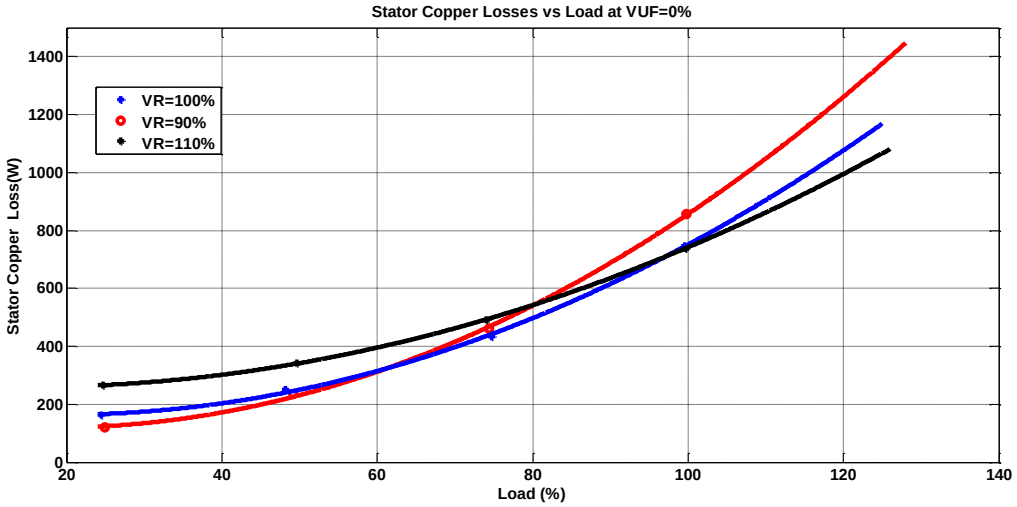

Figure 6-15: 11kW Manufacturer B Stator Copper Losses for VUF=0%

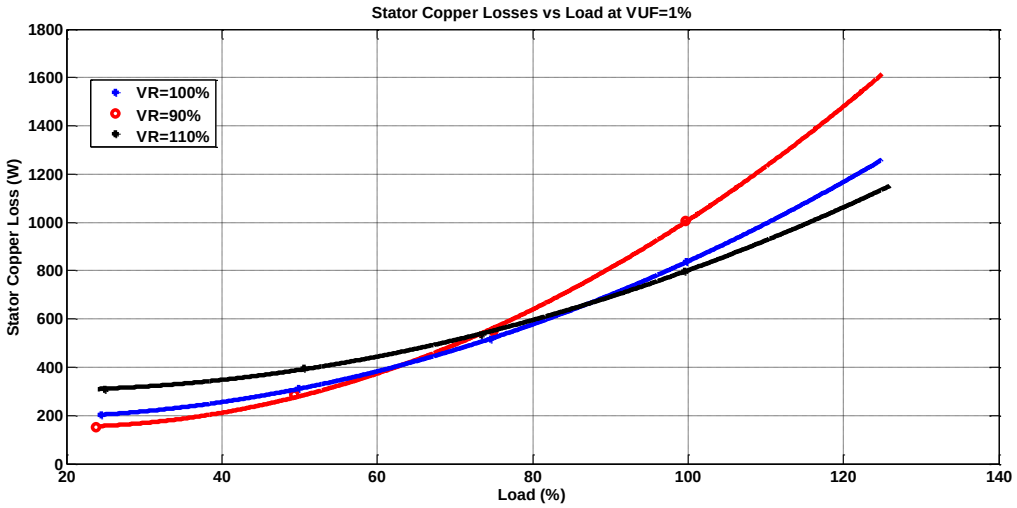

Figure 6-16: 11kW Manufacturer B Stator Copper Losses for VUF=1%

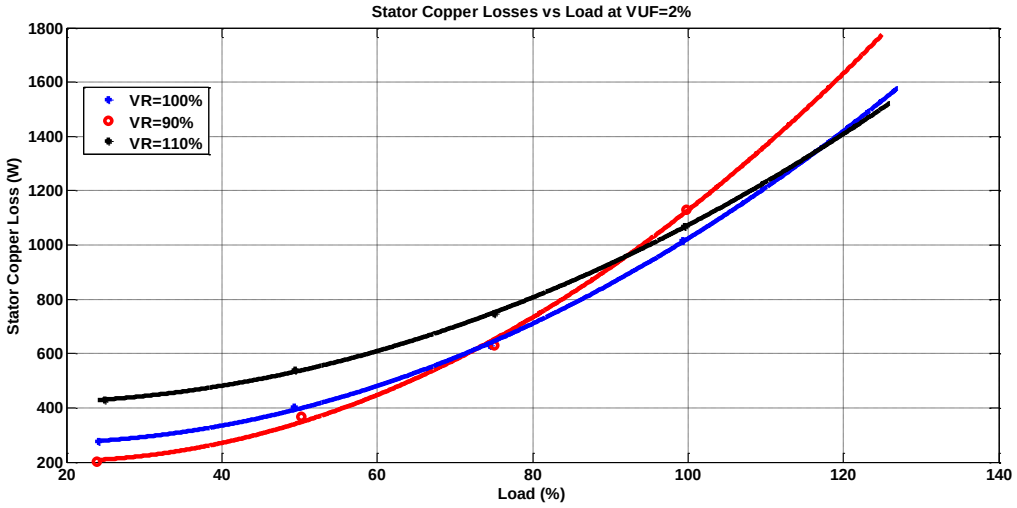

Figure 6-17: 11kW Manufacturer B Stator Copper Losses for VUF=2%

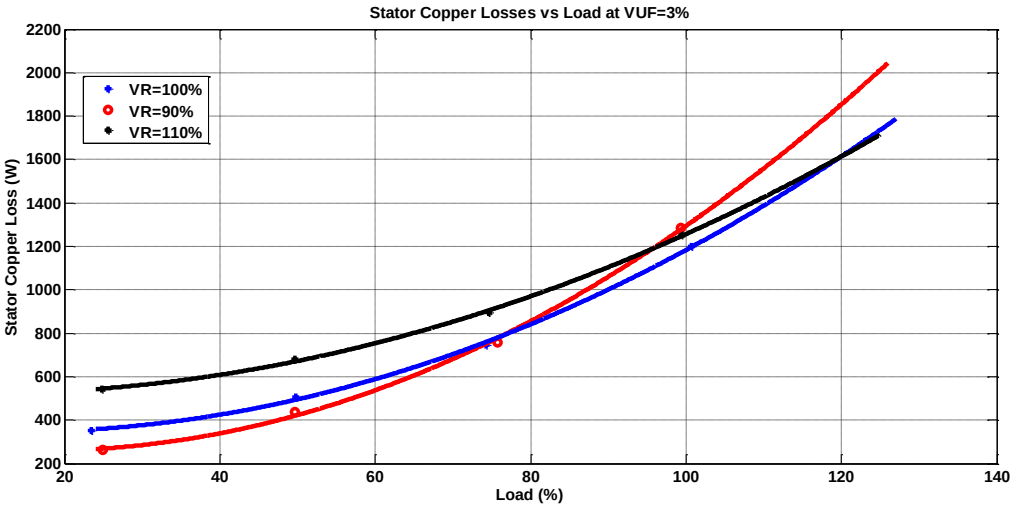

Figure 6-18: 11kW Manufacturer B Stator Copper Losses for VUF=3%

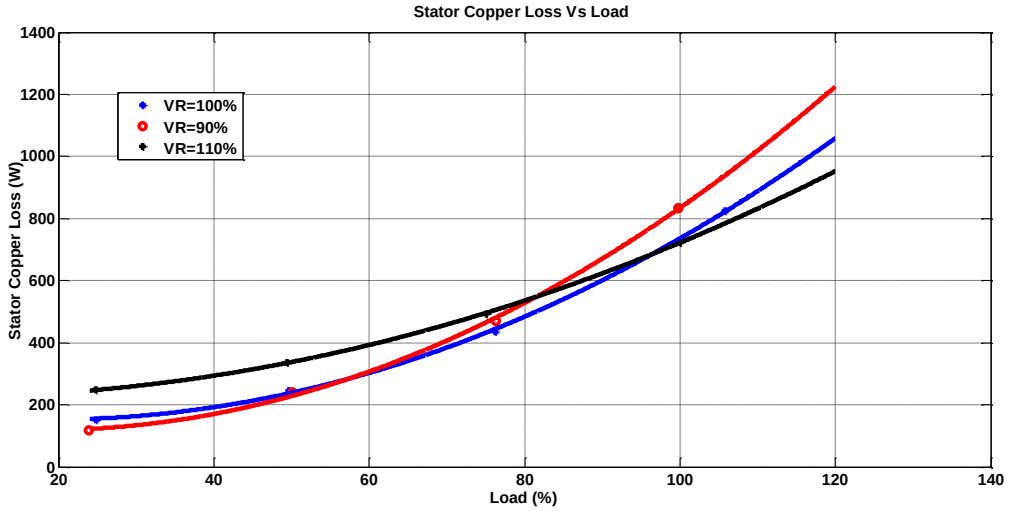

Figure 6-19: 11kW Manufacturer A Stator Copper Losses for VUF=0%

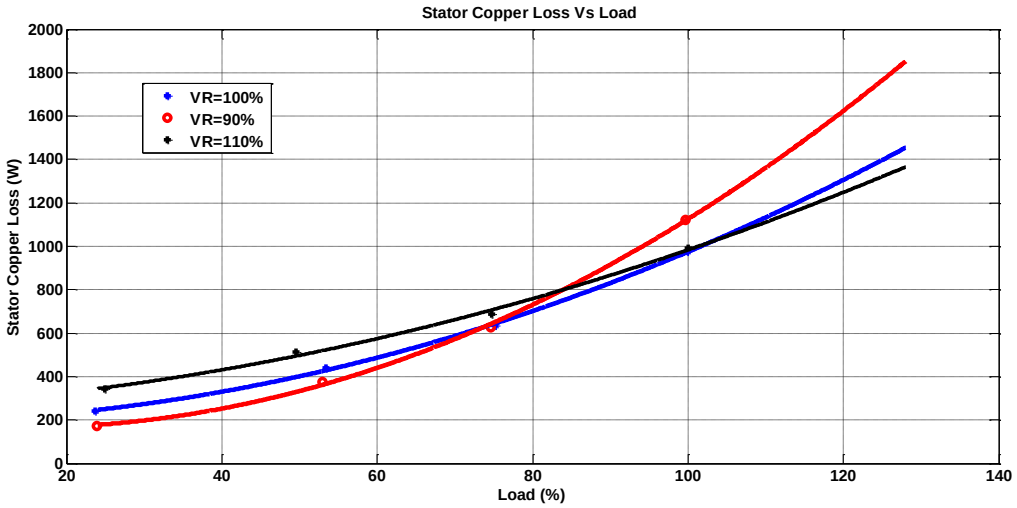

Figure 6-20: 11kW Manufacturer A Stator Copper Losses for VUF=2%

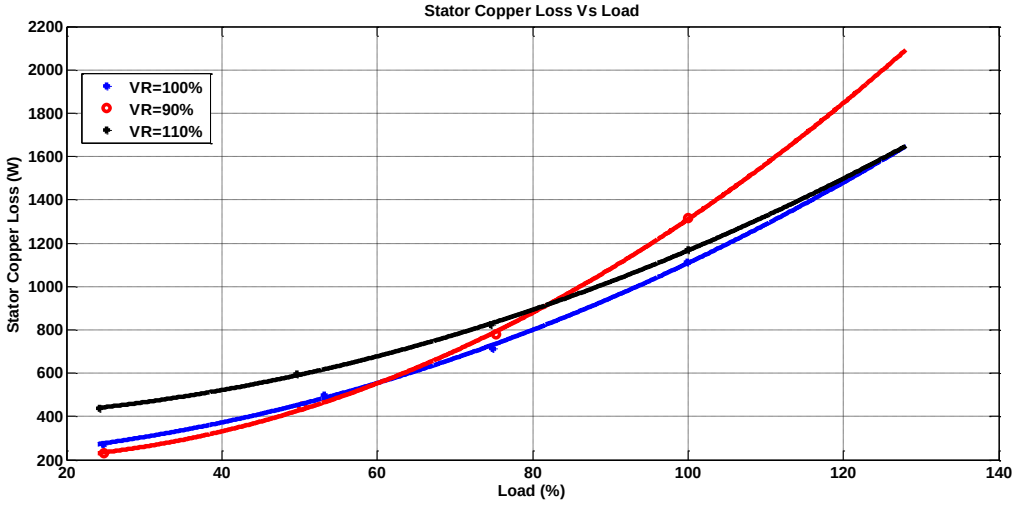

Figure 6-21: 11kW Manufacturer A Stator Copper Losses for VUF=3%

From the stator copper loss figures above, the copper losses are non-zero towards the zero percent load condition. This is because there is always current being drawn by the machine even at no load conditions. The stator copper loss of the 7.5kW Manufacturer B machine is roughly 580W under balanced load conditions at full load, this is 40W less than 7.5kW Manufacturer A machine stator copper loss at the same operating condition. The worst case for both the 7.5kW machines occurs at 3% voltage unbalance at 90% voltage regulation, both machines have stator copper losses greater than 1000W (1056W for Manufacturer B and 1064W for the Manufacturer A machine). This is more than 13% of the machines' rated power. Currents more than 19A are drawn by both machines under this operating condition.

Similar stator copper loss trends can be observed from the 11kW machines. At rated load conditions with no voltage unbalance and regulation of 100% the 11kW Manufacturer B machine has a copper loss of 745 W, this is 105W less than the 11kW Manufacturer A machine under the same operating condition. The 11kW Manufacturer A machine has a stator copper loss of 1990W

when operating under 3% voltage unbalance at 90% undervoltage, under the same operating condition the 11kW Manufacturer B machine has a stator copper loss of 1300W. An increase in voltage unbalance causes an increase in copper losses and these losses are dissipated as heat leading to an increase in motor operating temperature.

From the diagrams given in Figure 6-7 to Figure 6-21, similar trends are observed for the stator copper losses of all the machines under the various voltage conditions. At partial load conditions the stator copper losses for the overvoltage condition is significantly greater than the losses due to rated and undervoltage voltage conditions. Under nominal operating conditions and for conventional induction machines the maximum efficiency lies in the region 60%-80% of the rated power.

Discussion of results for under- and overvoltage conditions with unbalance

As the machine load is increased, the losses for overvoltage, undervoltage and rated voltage unbalance seem to intersect around the rated load condition (80%-100%). The undervoltage condition losses increase at a rapid rate in this region and a temperature increase accompanies the increase in losses. For the undervoltage unbalance case the induction machine draws more current as the load increases, because of the low average stator voltages, more current is required to ensure that the machine produces the required output power. It is important to note that this rapid increase in stator current increases the current unbalance which in turn increases the stator winding temperatures.

For the overvoltage operating condition there is greater magnetization [37]. Operation of induction machines at higher voltages tends to push the magnetic portion of the machine into saturation. This causes the machine to draw excessive current to magnetize the iron core beyond the point to which it can be easily magnetized. An overvoltage supply leads to magnetic materials, such as the iron core to approach saturation, to increase losses, and to increase losses in the copper windings. At this point, the power consumption increases much more rapidly than $(v)^2$.Thus a 5% overvoltage may decrease current flow by in the machine by 4% or less, but the magnetizing current may increase by 8% or more [78]. The power factor also becomes poor due to disproportionate increase in magnetizing current. When an induction machine is operating at an overvoltage condition at loads less than the rated load, the magnetizing currents will increase and if the load reduces further the line current might also increase (as observed in Figure 6-7 to Figure 6-21 and Table 12-1 to Table 12-47). This increase in line currents at partial load conditions helps explain why the stator copper losses are greater for the overvoltage operating condition. If the machine voltage is increased beyond its saturation point additional flux is only possible with a disproportionately large increase in current leading to increased copper losses.

Discussion of unbalanced currents

The introduction of voltage unbalance leads to an associated current unbalance. The voltage unbalance results in a negative sequence component. The current unbalance is proportional to the ratio of the negative sequence slip to the positive sequence slip. For the two 7.5kW machines, at full load Manufacturer B machine operates at lower speeds and has a higher slip than the Manufacturer A machine at the same load. Since the current unbalance is proportional to the ratio of the negative slip to the positive slip (2-s/s), the machine with the lower slip will experience a more severe current unbalance. The 7.5kW Manufacturer A machine has a greater current unbalance than the Manufacturer B machine, this reasoning can be used to explain the large

current unbalance at low loads as compared to the full load conditions. The slip increases with the loading of the machine and this results in a decrease in current unbalance.

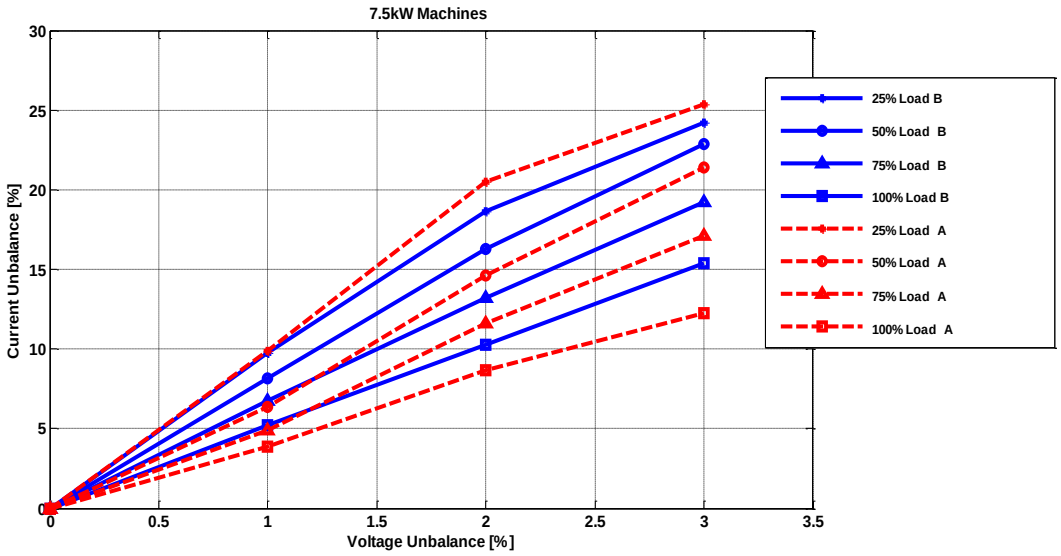

Figure 6-22: 7.5kW Manufacturer A and Manufacturer B machines current unbalance due to undervoltage unbalance

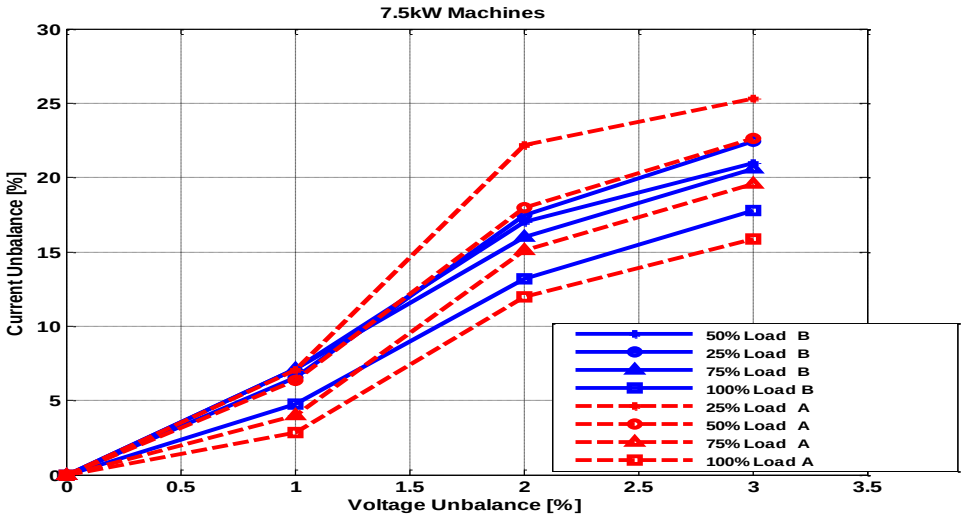

Figure 6-23: 7.5kW Manufacturer A and Manufacturer B machines current unbalance due to rated voltage unbalance

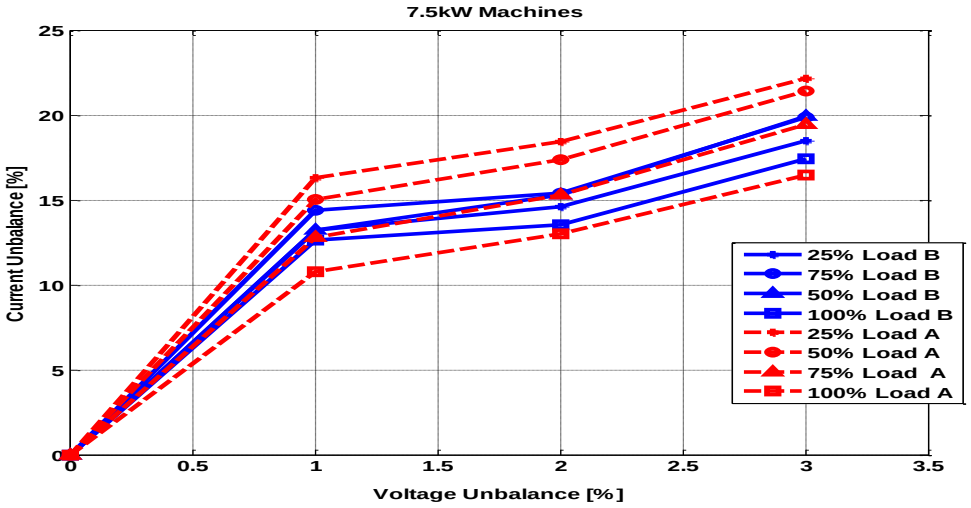

Figure 6-24: 7.5kW Manufacturer A and Manufacturer B machines current unbalance due to over-voltage unbalance

For the voltage unbalance and regulation cases considered in this study (VUF=0%-3%, VR=90%-110%), the resultant current unbalance from these conditions were analyzed. Current unbalance is defined as the ratio of the negative sequence current to the positive sequence current. The current unbalance was measured at the four loading points considered for all four machines, the current unbalance can also be defined as the ratio of the positive sequence impedance to the negative sequence impedance multiplied by the voltage unbalance factor. From the tested machines in Table 12-1 to Table 12-47 the results show that the machine slip increases with a decrease in voltage regulation and decreases with an increase in voltage regulation.

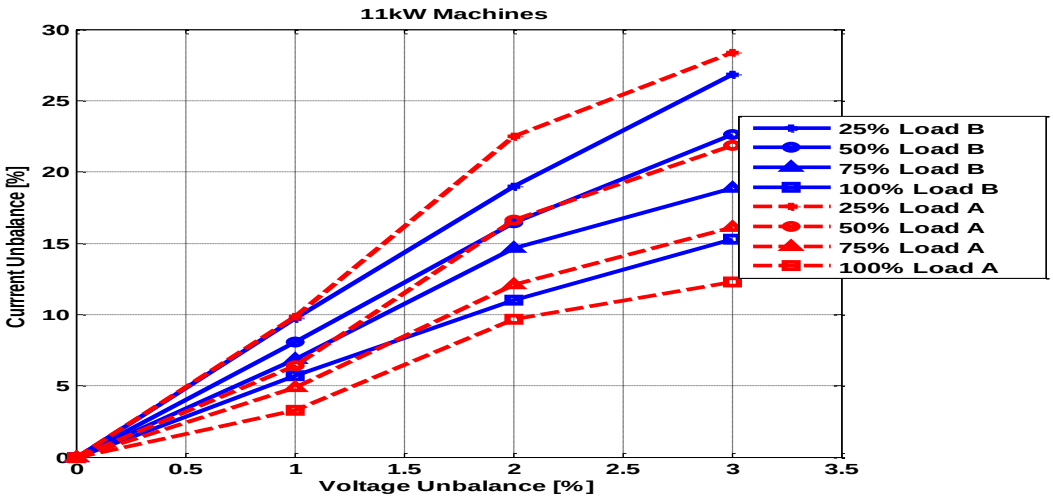

Figure 6-25: :11kW Manufacturer A and Manufacturer B machines current unbalance due to under-voltage unbalance

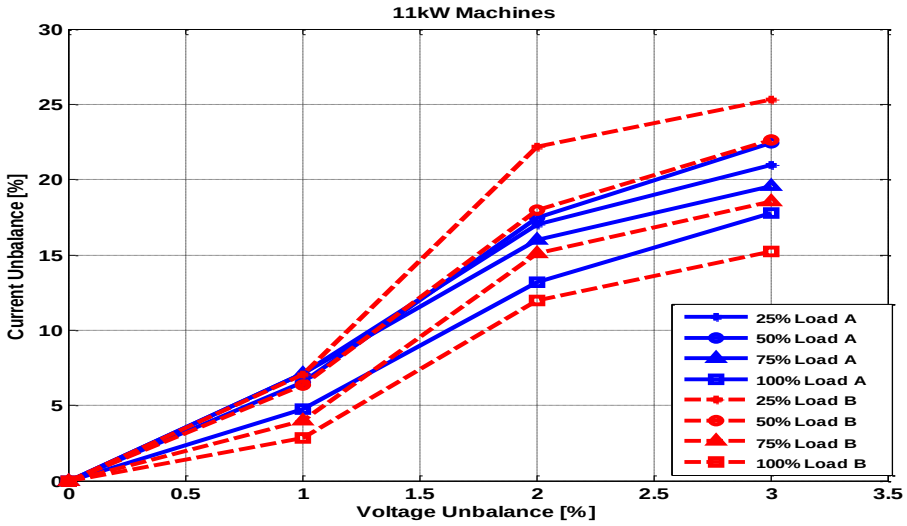

Figure 6-26: 11kW Manufacturer A and Manufacturer B machines current unbalance due to rated-voltage unbalance

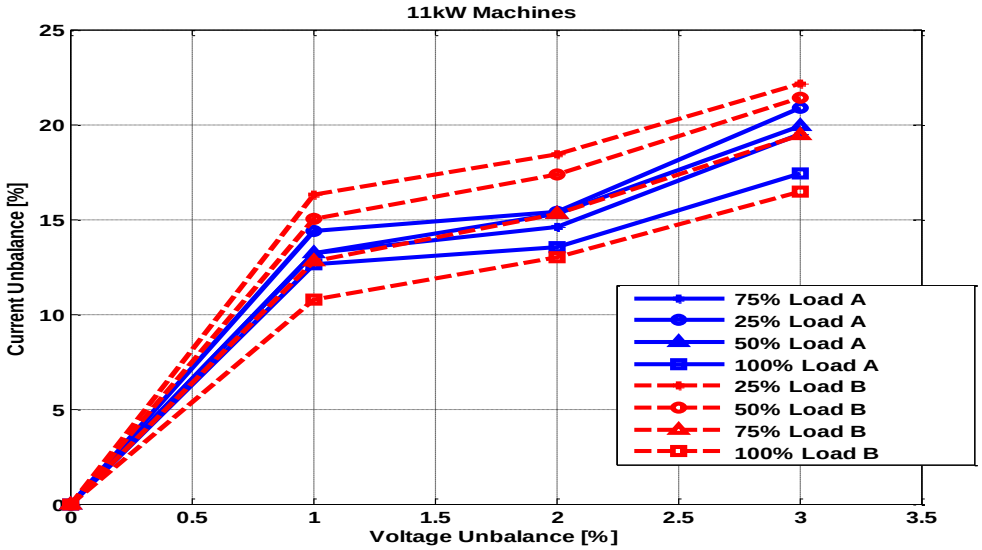

Figure 6-27: 11kW Manufacturer A and Manufacturer B machines current unbalance due to over-voltage unbalance

Lower slip at higher voltages translates to the current unbalance factor increasing with a decrease in voltage regulation. This increase in current unbalance and the high currents drawn by the machine under the undervoltage operating conditions helps explain the higher temperatures in this condition. An introduction of voltage unbalance results in a reverse airgap field caused by the negative sequence currents. From Figure 6-28 the increase in slip with voltage unbalance is illustrated.

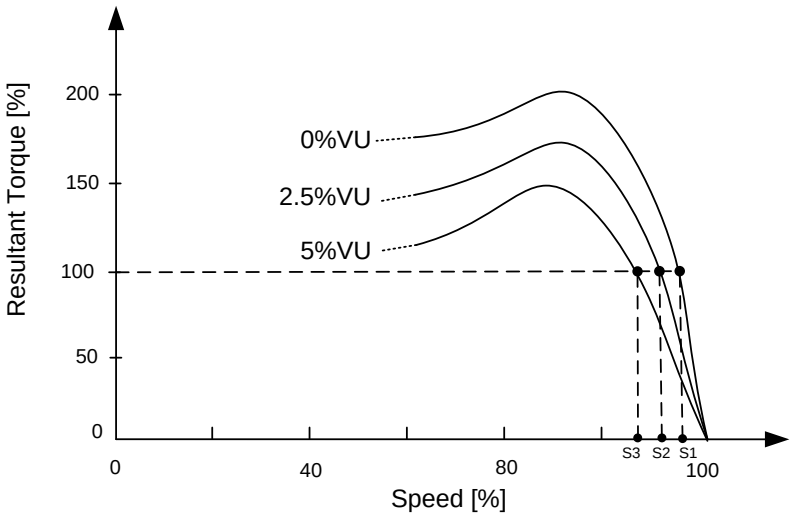

Figure 6-28: Torque vs load speed and change in slip values with variation in voltage unbalance [51]

This increase in slip due to decrease in voltage regulation or the increase in voltage unbalance leads to increased losses in the rotor and stator windings. Varying the applied load changes the machine's speed, a lighter load results in higher speeds and a heavier load in lower speeds. From equation (4-8), it is evident that it is essential to analyse the variation of machine impedance with slip. This allows us to analyse the current unbalance factor as a function machine impedance. From (4-7) it is shown that for a given unbalance scenario, with a fixed positive and negative sequence voltage the values of the negative and positive sequence currents depend on the variation of the impedance with the machine load. These sequence impedances are a function of slip. By plotting the negative sequence impedance from the motor start (s=1) to the no load condition (s ≈ 0.001) it is evident that the value of the positive sequence impedance is dependent on the slip and that the negative sequence impedance varies very little with slip.

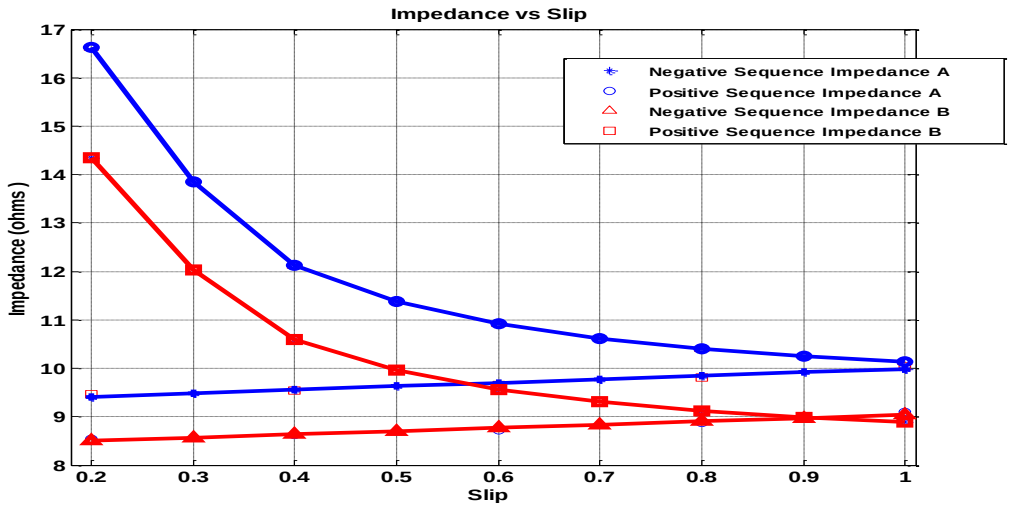

Figure 6-29: Variation of the sequence impedance with the slip. Comparison of the negative sequence impedance in nominal slip with locked rotor impedance for the 7.5kW Machines

From Figure 6-29 the positive sequence impedance is strongly dependent on the slip with the highest value around the no load region and the lowest around the blocked rotor region. The negative sequence impedance varies the most at low slip values (region where the machine mostly operates). The negative sequence impedance is practically independent of the machine slip and can be regarded as a constant. This helps explain why the 7.5kW Manufacturer A machine has a greater current unbalance (due to the lower operational slip hence higher positive sequence impedance) than the Manufacturer B machine. The sequence impedances of the four machines around the operational region is illustrated in the Figure 6-30

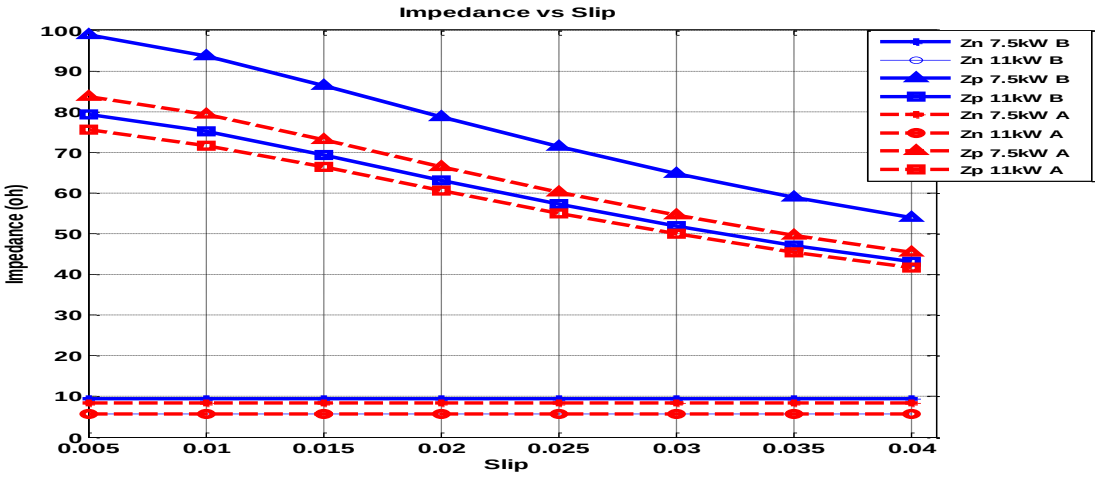

Figure 6-30: Variation of the positive and negative sequence impedances with machine slip in the machine operational zone.

Equation (4-8) states that the current unbalance factor is equal to the voltage unbalance factor multiplied by the ratio of the sequence impedances. From Figure 6-30 above, it is established that the positive sequence impedance increases as the load decreases, this results in the current unbalance factor increasing with a decrease in the machine load.

6.10 Efficiencies under the Various Voltage Conditions

The efficiencies of the four machines were determined under the considered voltage constraints. The efficiencies were considered for unbalanced voltage conditions combined with over- and undervoltage. The aim of this section is to assess the interaction of voltage unbalance and regulation with machine efficiencies. The efficiency results for the different machines are compared relatively, the appropriate approach is considered in the determination of these efficiencies. Both the IEC and the IEEE efficiency standards do not allow unbalanced supply voltages greater than 0.5% when determining the efficiency of induction machines. In this report, the IEEE 112- Direct method was considered in the determination of machine efficiencies, this method is not bounded by the supply conditions. The temperature rise under unbalanced conditions is very fast and results in overload conditions for induction machines. The same measurement routine was used for each machine to ensure repeatability of the results and to reduce the testing time. Efficiencies are determined at the machines rated temperature and it takes several hours before stability is achieved. As described in the preceding chapter, the thermal loading tests are described and, in some instances, heat re-runs have to be done to re-

establish the rated temperature of the machines. As per IEEE 112 recommendations the 10K maximum temperature difference between the hottest and coldest test point was observed.

6.11 Determination of Induction Machine Efficiency

The efficiency of an induction is defined as the ratio of mechanical power delivered at the shaft of the machine divided by the electrical input power to the machine [12]. There are various international standards that define the procedures to be followed in the determination of induction machine efficiency. Table 6-18 below shows the international standards used for induction machine testing [73]

Table 6-18: Efficiency Testing Standards

Standard	Description
SANS 60034 Part 2 (SANS 34-2)	"Methods for determining losses and efficiency of rotating electrical machinery from tests (excluding machines for traction vehicles)" – Published in 1996 by the South African Bureau of Standards
IEC 60034 Part 2 (IEC 34-2) 2007	"Standard Methods for determining losses and efficiency from tests (excluding machines for traction vehicles)" – Published in 2007 by International Electrotechnical Commission
IEEE 112	"Standard Test Procedure for Polyphase Induction Motors and Generators" – Published in 2004 by International Electrical and Electronic Engineers
JEC – 2137	Published in 2000 by the Japanese Electrotechnical Committee
AS/NZ 1359.5	"Three-phase Cage Induction Motors – High Efficiency and minimum energy performance standards requirements" – Published in 2004 by Australia and New Zealand Standards
CSA 390	"Energy Efficiency Test Methods for Three-Phase Induction Motors "– Published in 1999 by the Canadian Standards Association

The IEEE, IEC and SANS are the most commonly used in the industry. Each of these standards are based on three basic efficiency principles. These are the equivalent circuit method, the ratio of output over input and the summation of losses. These basic principles are discussed further below:

6.11.1 Equivalent Circuit Method

The equivalent circuit method is defined by both IEEE 112-F and IEC 34-2-3. The equivalent circuit parameters of the induction machine first must be determined using the locked rotor and no-load test. This method is mostly used in field testing where the machine under consideration cannot be removed and is coupled to a dynamometer [13]. The equivalent circuit method is popular for testing very large machines (up to MW machines) where full rate is not practical. The equivalent circuit method assumes an estimated value of stray load losses (SLL).

6.11.2 Indirect or Separation of Losses Method

The separation of losses method is defined in IEEE 112B, IEC 34-2-2 and SANS 34-2-2, it is also known as the indirect method. The separation of losses is outlined by several procedures/tests done on the machine. The first test is the temperature test (heat –run) to obtain the machine's operating temperature and the ambient temperature (as described in section 5.3.2). The variable

load and no-load tests are performed on the machine to obtain the load dependent and independent losses. The main difference between the IEC and IEEE separation of losses methods is the consideration of the resistive voltage across the stator windings. The IEEE method does not compensate for this voltage drop whilst the IEC reduces the secondary voltage using the following equation;

$$U_r = \sqrt{\left(U_{in} - \frac{\sqrt{3}}{2} \times I \times R_{LL} cos\varphi\right)^2 + \left(\frac{\sqrt{3}}{2} \times I \times R_{LL} sin\varphi\right)^2}$$

Where

U_{in} is the rated line voltage (V)
I is the rated line current (A)
R_{LL} is the line to line resistance (Ω)
φ is the power factor

This results in the IEC method yielding lesser core losses and higher efficiencies.

6.11.3 Direct or Output/Input Method

IEC 34-2-1 and IEEE 112-A are well defined direct methods. The efficiency is simply determined by taking the ratio of the measured output mechanical power to the electrical input power.

$$\eta = \frac{P_{Mechanical}}{P_{Electrical}}$$

There is no defined procedure for determining the efficiency of induction machines under unbalanced supply conditions. There are multiple complications that arise when determining the individual loss components. The direct method was used in determining the efficiencies of the four induction machines. To analyse the impact of voltage unbalance and regulation on each machine, the nominal voltage unbalance (combined with 90%, 100% and 110% voltage regulation) was compared with the largest voltage unbalance (combined with 90%, 100% and 110% voltage regulation). As described in the earlier chapters the IEC (True Definition) of voltage unbalance was considered.

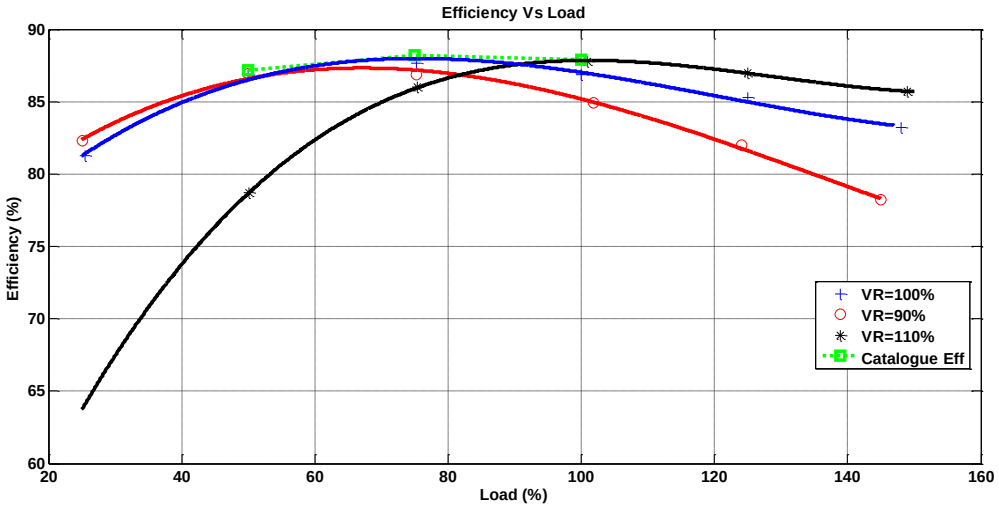

Figure 6-31: 7.5kW Manufacturer B efficiencies for VUF=0%, VR=90%, 100%, 110%

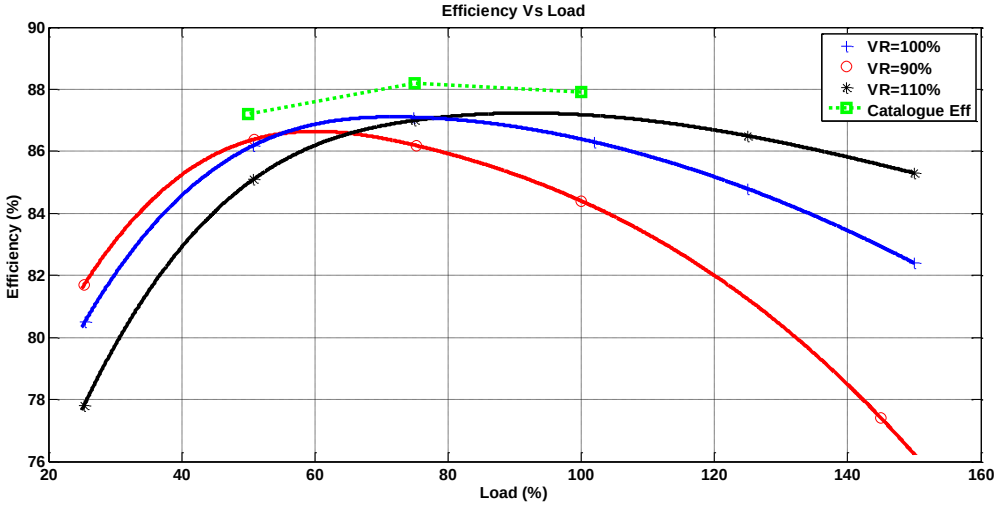

Figure 6-32: 7.5W Manufacturer B efficiencies for VUF=3%, VR=90%, 100%, 110%

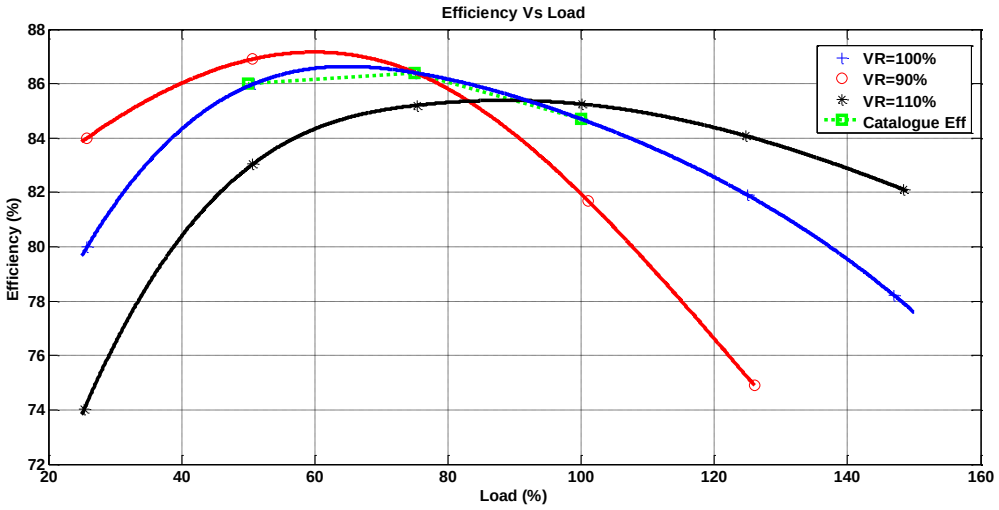

Figure 6-33: 7.5kW Manufacturer A efficiencies for VUF=0%, VR=90%, 100%, 110%

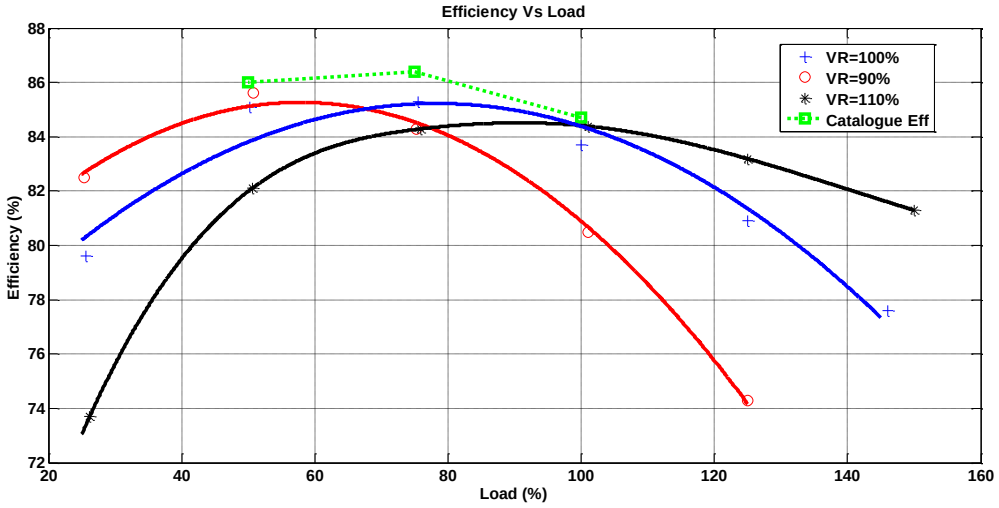

Figure 6-34: 7.5kW Manufacturer A efficiencies for VUF=3%, VR=90%, 100%, 110%

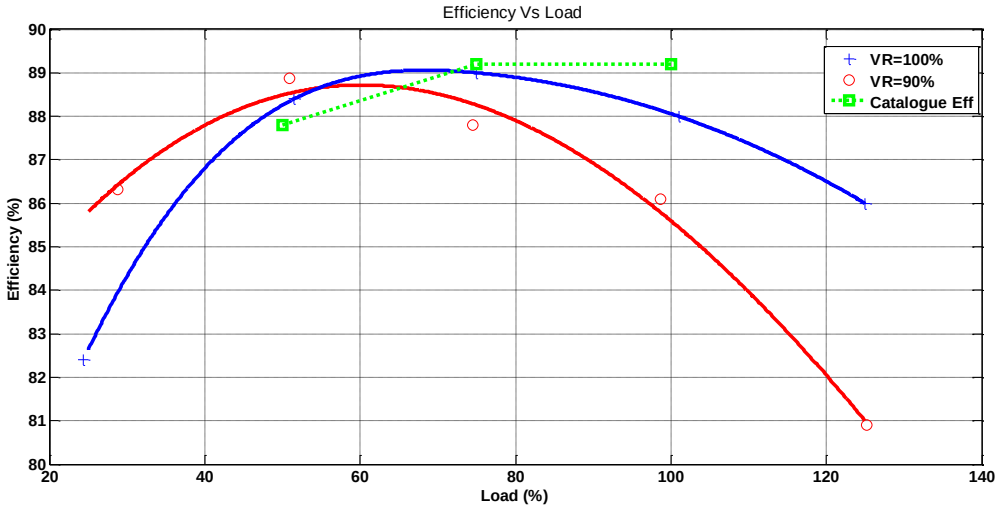

Figure 6-35: 11kW Manufacturer B efficiencies for VUF=0%, VR=90%, 100%, 110%

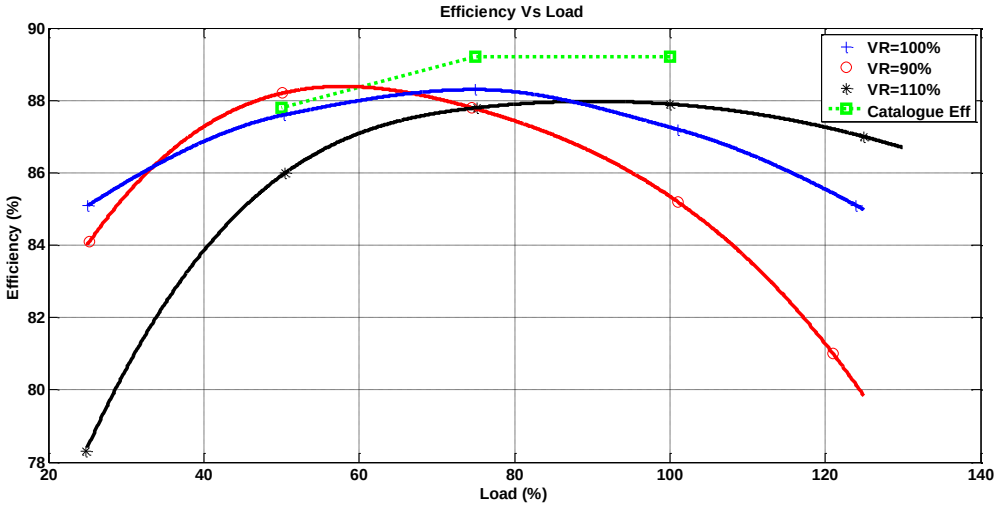

Figure 6-36: 11kW Manufacturer B efficiencies for VUF=3%, VR=90%, 100%, 110%

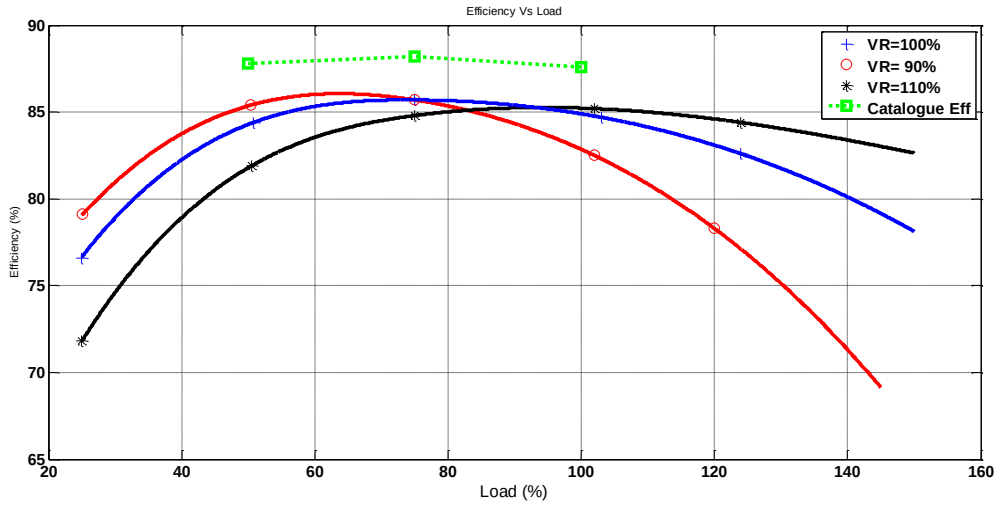

Figure 6-37: 11kW Manufacturer A efficiencies for VUF=0%, VR=90%, 100%, 110%

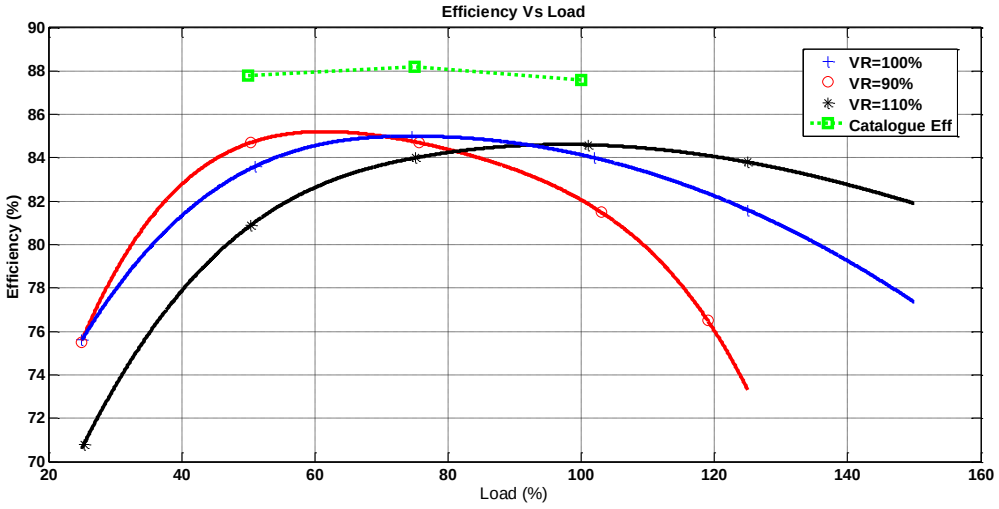

Figure 6-38: 11kW Manufacturer A efficiencies for VUF=3%, VR=90%, 100%, 110%

In motoring mode, the maximum efficiency of a conventional induction machine design lies within the range 60% to 80% of the machine's rated power [37]. This gives a desirable energetic behavior at partial loading. The four induction machines investigated in this report comply with this quality feature. The curves illustrated in Figure 6-31 to Figure 6-38 show the decrease in efficiency depends on the load of the induction machine and the voltage unbalance scenario chosen. The efficiencies of the induction machines under the various voltage unbalances and regulation depends on the losses under those cases.

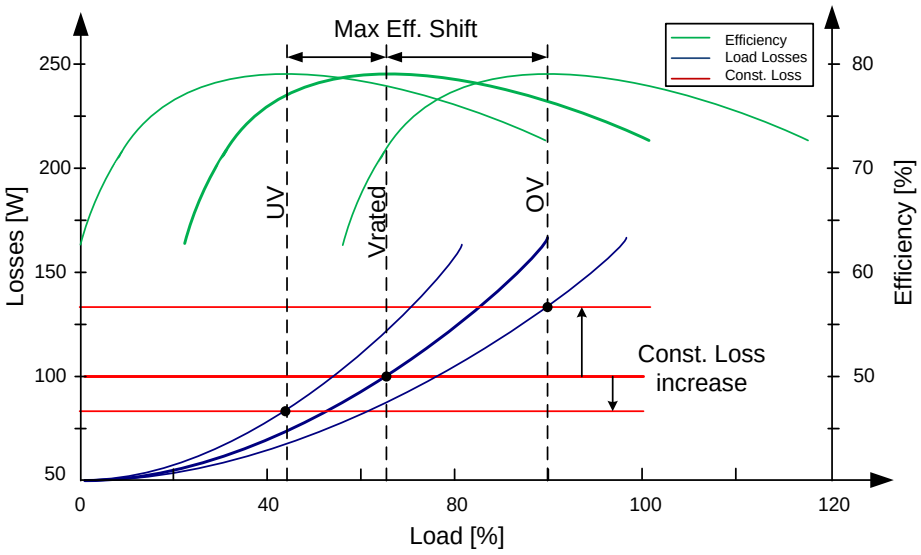

Figure 6-39: Efficiency and loss curves for rated voltage, under voltage and over voltage operating conditions [51]

Figure 6-39 is an illustration of the load dependent losses, constant losses and machine efficiency for rated, over-and undervoltage conditions in the absence of voltage unbalance. As demonstrated with the efficiency curves of the four machines, Figure 6-39 shows how the efficiency peaks shift to a lower load as the supply voltage reduces and towards a higher load as the supply voltage increases.

Discussion of Voltage Unbalance Results

As illustrated in the efficiency curves of the four machines, the efficiencies of the machines decrease with an increase in voltage unbalance. This decrease is because the core, rotor and stator losses are affected by the voltage unbalance. The machine torque vs speed curve is reduced as the supply voltage is increased. The torque is reduced due to the reverse airgap from the negative sequence components, this leads to an increase in the slip even though the shaft torque is kept at full load. An increase in slip will result in additional losses in the machine rotor and stator. The machine slip is proportional to temperature rise and is inversely proportional to efficiency hence a decrease in all machine efficiencies as the unbalance increases. The machine constant losses also increase as the voltage unbalance is increased, it was found that even at constant voltage regulation the core losses increase with an increase in voltage unbalance. From Table 3-2 it can be observed that unbalance was achieved by altering each of the three phases resulting in some phase voltages being greater than others, the addition core losses are from the phases with voltages above the rated voltage.

Discussion of Over and Under Voltage Unbalance Results

When operating the machines at undervoltage conditions the load independent losses are less significant. For the machine to have the same power delivered to load, more current is drawn to compensate for the reduced magnetization of the core. It was observed from the thermal load tests that this increase in drawn current results in an increase in temperature, this relates to the observation from the core loss analysis where it was discovered that the core losses decrease with an increase in temperature. The peak efficiency is shifted towards the lower load region for operation under under-voltage conditions. Operation under overvoltage conditions results in the

peak efficiency shifted towards the higher loading region. The core magnetization is increased at this condition and lower currents are required to develop the desired load torque. The lower currents result in reduced stator and rotor copper losses.

Discussion of Voltage Unbalance and Variation Results

Similarly, when the machine is operated under undervoltage combined with unbalance, the peak efficiency is shifted to lower load regions, this efficiency decreases as the unbalance is increased. When there is a combination of overvoltage with unbalance, the peak efficiency shifts to the higher load region and decreases as unbalance is increased. The torque developed by the machine is proportional to the voltage squared, since the average voltage is 10% lower than the rated voltage, the torque developed by the machine would drop. An introduction of voltage unbalance will lead to further reduction in torque. This can be interpreted as good/bad efficiency depending on the load condition, voltage amplitude and the application. At higher loads the torque vs speed of becomes highly non-linear resulting in a nonlinear increase in slip and hence load losses. This helps explain the sharp decrease in efficiency at higher loads at undervoltage supply conditions. Operation under overvoltage regulation results in the maximum efficiency points shifting towards the rated load operating region. The efficiency curves for the overvoltage operating condition appear to be relatively flatter than the rated and undervoltage conditions. This is because the machine is magnetized more, and the constant losses are more prominent and less current is required to drive the loss. This means there is less variation in load dependent losses resulting in a flatter efficiency curve. The dependence of the machine losses and their temperature dependence is summarized in **Error! Reference source not found.**.

Table 6-19: Characterization of machine losses and their temperature dependence

Machine Loss	Cause of Loss	Temperature dependent parameters	Dependence on Temperature
Electric Losses	Current Heat	Electric winding resistance	Electric resistance increases linearly with temperature
Magnetic Iron Losses	Hysteresis	Hysteresis curve, permanent magnetic flux	Hysteresis losses decrease with an increase in temperature
	Eddy Current	Electric iron sheet resistance, permanent magnet flux	Eddy current losses result from induced voltage, they dependent on electric resistance of the iron sheets and decrease with rising temperature
		Magnetic stator flux	Magnetic flux has a quadratic influence on the iron losses in the stator, in induction machines it depends on electric voltage and frequency and not temperature
Mechanical Losses	Ventilation, Friction	Viscosity of lubricant in bearing	Decrease with rising machine temperature. Windage losses vary inversely proportional with the temperature.

6.12 Concluding Remarks

The experimental results obtained from the tests conducted in accordance with the standards are presented and discussed. An analysis of each of the results was provided following each subsection. The thermal equilibrium temperatures of all four machines are tabulated in Table 12-1 to Table 12-47.

The core losses were determined by performing the no load tests on the machines. Since these core losses are a function of line to line voltage it was expected to obtain the highest losses at the highest voltage regulation combined with the highest voltage unbalance. Careful care was taken to measure the temperature at each load condition and to correct the no load stator winding resistance. The separation of loss method was implemented in the extraction of core losses from the no load tests. It was also implemented in the validation of the per phase equivalent circuits of the induction machines. The stator copper losses were determined (under balanced operating conditions) using the separation of losses method and these were compared with stator copper losses obtained using the per phase equivalent circuit. This was done to validate the parameters of the per phase equivalent circuits of the four machines.

The stator copper losses were obtained using the sequence per phase equivalent circuits. Loading of the machines could only be achieved up to 120% of the rated load conditions. Anything above this load condition resulted in very high temperatures (that continued increasing) and would have resulted in premature failure of the stator windings. Undervoltage results in higher amperage required to produce the needed power. From Ohms' law P=IE where P is power, E is voltage and I is the current. If E is reduced and P is constant I must be increased, the heat produced from stator copper losses varies as the square of the current, this additional heat results in more heat produced by winding resistive losses and higher operating temperatures. The slip of an induction machine is inversely proportional to the voltage applied, the higher the voltage the lower the slip the faster the machine turns. The cooling fan of the machine will move more air at higher speeds hence increasing the power required to turn the fan, this effect could have a large impact on the machine offsetting a portion of the decrease in machine current. The opposite holds, if E is increased, I will have to decrease when P is constant. Higher voltages help the machine run on cooler. One should however be careful when applying this principal. The magnetic flux that is produced in the core iron also increases. For any electrical steel there is a maximum amount of flux per cross sectional area, this amount is known as saturation. If one were to increase the machine voltage beyond this saturation point, additional flux is possible only with a disproportionately large increase in current. This additional current generates heat this is discussed in further detail in section 6.9.2.1.

The stator copper losses trends of the four machines are rigorously discussed in subsection 6.9.1. Similar trends can be observed for the different machines under the different supply conditions. Application of the separation of losses method for the constant losses and validation of the per phase equivalent circuits gave us further insight in the understanding of the efficiency curves. Stator copper losses are dominant in small and medium sized induction machines, under ideal operating conditions they remain constant as the torque is constant. For induction machines with smaller power ratings, a lower temperature is always better for efficiency. Machines with high power ratings are more tolerant to higher temperatures as the load dependent losses are not

dominant. The losses due to the positive sequence voltage dependent on the magnitude of the positive sequence voltage and the machine load. As illustrated in this chapter the negative sequence impedance is practically constant meaning the losses due the negative sequence components are constant with machine load. Losses due to the negative sequence circuits are independent of the machine load, these losses are mainly defined by the magnitude of the negative sequence voltage.

7. THERMAL MODEL TEMPERATURE PREDICTION FOR LOW VOLTAGE INDUCTION MACHINES

7.1 Introduction

The induction machine thermal model described in section 4.3 of this research report is tested in this chapter. The comparison is done between the measured stator winding temperatures and the predicted/calculated temperatures from the thermal model. The temperatures of the four machines were measured using K-type thermocouples installed at the drive end side of the stator end of the windings. This is on the opposite side of the cooling fan. The thermocouples are placed close to parts where the highest temperature measurements of the stator windings were expected. They are placed on the windings above and below the rotor. Two data loggers were used to measure the temperature of the induction machines. The 8 channel Pico technology data logger uses a program interface to illustrate the recorded temperatures. The HE804 data logger was manually operated and it displayed measured temperatures on its screen. The thermal model considered has four inputs, the stator copper losses (per phase for unbalanced operating conditions), the machine core losses and the ambient temperature. There are two outputs to the thermal model namely the three phase winding temperatures and the core temperature value. The temperature and life estimation procedure is summarised in the diagram that follows:

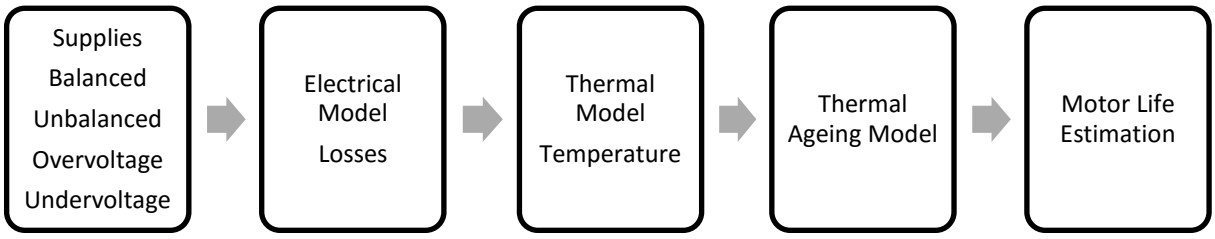

Figure 7-1: Flowchart for predicting motor life using thermal and electrical model [53]

The measured steady state temperatures of the four machines are tabulated in Table 12-1 to Table 12-47. The primary advantage of the using lumped parameter thermal models is that the steady state temperature rise of each machine can be determined at any supply condition in a much shorter time than doing it experimentally.

7.2 Overview of Stator Winding Thermal Protection for Induction Machines

To prevent the machine's stator windings from failing, continuous monitoring is necessary during operation. This monitoring is more important for medium and large machines due to the high costs associated with downtime and unexpected failures. The use of conventional measuring devices such thermocouples, infrared thermal sensors and resistance thermal detectors (RTDs) are more reliable than overcurrent relays but their applications are limited due to economic reasons more specifically for small to medium size machines because the installation of the embedded thermal sensors is difficult and costly. There are many different types of thermal protection devices currently available on the market but most of them are not designed to measure machine temperatures, this are known as active thermal techniques. The most common of these active techniques include the dual-element time-delay fuses and eutectic alloy or bi-metal type overload relays. In most industrial applications the combination of these two devices is used as primary thermal protection. The devices are designed based on thermal limit curves which define the safe operating time for the different magnitudes of input currents under both transient and running overload. These devices have proven to be trustworthy over the years, the thermal limit curves used as thresholds are only a rough and conservative representation of the thermal characteristics of induction machine. The effects of ambient temperature, voltage unbalance, over and undervoltage and the changes of the cooling capabilities of the induction machine are completely neglected. These devices only monitor the input current, they are not capable of monitoring machines when high negative sequence currents are present (voltage unbalance).

The result of using input current as the only parameter for thermal protection is nuisance tripping and under-protection. To solve the shortcomings of conventional fuses and relays microprocessor-based thermal overload protective relays are implemented. These estimate the machine losses and predict the stator winding temperatures based on a predefined thermal model, the machine is immediately tripped when the thermal set limit is reached/exceeded. A first order thermal model is presented in this research project which can be used to predict temperature, this model can be incorporated as an algorithm and used as part of the microprocessor-based thermal protection system. Machine losses and thermal model parameters in this thermal model are determined offline. The only drawback of this thermal model is the negligence of the cooling capability of the ac machines, some of the thermal model parameters are assumed to be constant throughout.

Other than the two mentioned techniques, machine temperatures can be monitored based on the estimation of the stator resistance. In [79] it was proposed to use the dc model of an induction machine to estimate the stator resistance and temperature by creating a dc bias in the machine's input voltage and current. This is because the dc component does not pass through the machine airgap, this allows calculation of the stator resistance using only the dc component of the input current and voltage.

7.3 Thermal Model Parameters

The procedures followed in obtained the thermal model parameters are described in section 5.3.5-5.3.7 of this report. The resultant thermal model parameters from the DC tests performed on the four induction machines are tabulated below.

7.3.1 7.5kW Manufacturer A DC Test Results and Thermal Model Parameters

Table 7-1: 7.5kW Manufacturer A Induction Machine DC Tests Results

DC Test			T_{final}(℃)			
	I_{dc}	V_{dc}	T_{amb}(℃)	T_A(℃)	T_B(℃)	T_C(℃)
Test 1	15.18	36.14	19.09	62.5	49.5	49.75
Test 2	15.22	38.12	19.8	100.6	101.3	102.4
Test 3	15.17	37.22	19.01	101.5	100.8	101.4

Table 7-2: 7.5kW Manufacturer A Induction Machine Thermal Model Parameters

Thermal Parameter	Value
G_{ab}, G_{bc}, G_{ac}	3.20 W/℃
G_{ah}, G_{bh}, G_{ch}	2.37 W/℃
C_a, C_b, C_c	16.31 $W.min$/℃
C_h	86.23 $W.min$/℃
G_{amb}	7.1 W/℃

7.3.2 7.5kW Manufacturer B DC Test Results and Thermal Parameters

Table 7-3: 7.5kW Manufacturer B Induction Machine DC Test Results

DC Test			T_{final}(℃)			
	I_{dc}	V_{dc}	T_{amb}(℃)	T_A(℃)	T_B(℃)	T_C(℃)
Test 1	15.04	35.24	19.18	59.08	40.12	39.62
Test 2	15.06	35.12	20.15	95.33	94.34	95.67
Test 3	15.12	35.22	20.01	96.05	93.44	96.45

Table 7-4: 7.5kW Manufacturer B Induction Machine Thermal Model Parameter

Thermal Parameter	Value
G_{ab}, G_{bc}, G_{ac}	2.98 W/℃
G_{ah}, G_{bh}, G_{ch}	2.59 W/℃
C_a, C_b, C_c	14.54 $W.min$/℃
C_h	89.44 $W.min$/℃
G_{amb}	6.08 W/℃

7.3.3 11kW Manufacturer A DC Test Results and Thermal Parameters

Table 7-5: 11kW Manufacturer A Induction Machine DC Test Results

DC Test			T_{final}(℃)			
	I_{dc}	V_{dc}	T_{amb}(℃)	T_A(℃)	T_B(℃)	T_C(℃)
Test 1	22.5		19.88	67.13	51.22	50.18
Test 2	22.45		21.5	98.56	95.55	91.33
Test 3	22.09		21.5	97.56	94.33	96.55

Table 7-6: 11kW Manufacturer A Induction Machine Thermal Model Parameters

Thermal Parameter	Value
G_{ab}, G_{bc}, G_{ac}	4.512 $W/$℃
G_{ah}, G_{bh}, G_{ch}	3.15 $W/$℃
C_a, C_b, C_c	19.74 $W.min/$℃
C_h	94.32 $W.min/$℃
G_{amb}	9.48 $W/$℃

7.3.4 11kW Manufacturer B DC Test Results and Thermal Parameters

Table 7-7: 11kW Manufacturer B Induction Machine DC Test Results

DC Test			T_{final}(℃)			
	I_{dc}	V_{dc}	T_{amb}(℃)	T_A(℃)	T_B(℃)	T_C(℃)
Test 1	20.88		20.15	64.33	58.18	55.11
Test 2	20.99		19.5	98.55	98.56	101.3
Test 3	21.54		20.11	97.87	101.1	101.4

Table 7-8: 11kW Manufacturer B Induction Machine Thermal Model Parameters

Thermal Parameter	Value
G_{ab}, G_{bc}, G_{ac}	5.18 $W/$℃
G_{ah}, G_{bh}, G_{ch}	3.69 $W/$℃
C_a, C_b, C_c	19.44 $W.min/$℃
C_h	93.2 $W.min/$℃
G_{amb}	8.78 $W/$℃

7.4 Thermal Model Performance Testing

The stator thermal model is treated like an electrical circuit [53]. The thermal model can be analysed by applying Kirchhoff's' current law (KCL) on the respective circuit nodes. Applying KCL at the phase A node in the stator thermal model yields

$$P_a - (T_a - T_b) \cdot G_{ab} + (T_a - T_c) \cdot G_{ac} - (T_a - T_h) \cdot G_{ah} - C_a \frac{\partial T_a}{\partial t} = 0 \quad (7\text{-}1)$$

This can be rearranged into the following

$$\frac{\partial T_a}{\partial t} = \frac{P_a - (T_a - T_b) \cdot G_{ab} + (T_a - T_c) \cdot G_{ac} - (T_a - T_h) \cdot G_{ah}}{C_a} \quad (7\text{-}2)$$

Applying KCL at all the other nodes and rearranging the equations results in the following

$$\frac{\partial T_b}{\partial t} = \frac{P_b - (T_b - T_a) \cdot G_{ab} + (T_b - T_c) \cdot G_{bc} - (T_b - T_h) \cdot G_{bh}}{C_b} \quad (7\text{-}3)$$

(7-4)

$$\frac{\partial T_c}{\partial t} = \frac{P_c - (T_c - T_a) \cdot G_{ac} + (T_c - T_b) \cdot G_{bc} - (T_c - T_h) \cdot G_{ch}}{C_c}$$

$$\frac{\partial T_h}{\partial t} = \frac{(T_a - T_h) \cdot G_{ah} + (T_b - T_h) \cdot G_{bh} - (T_c - T_h) \cdot G_{ch} - (T_h - T_{amb}) \cdot G_{amb}}{C_h} \quad (7\text{-}5)$$

The general mathematical expression that is used to represent the relationship between stator heating and the temperature rise is given by

$$\frac{\partial [T]}{\partial t} = [C]^{-1}([P] - [G][\Delta T]) \quad (7\text{-}6)$$

Where:

C = the thermal capacitance matrix
P = the losses matrix
T = the temperature rise matrix
G = the conductance matrix

Fourth order Runge-Kutta method used to solved coupled differential equations used to determine windings temperatures.

$$y = f(t, y), \; y(t_0) = y_0 \quad (7\text{-}7)$$

A step size is then picked $h > 0$ and define

$$y_{n+1} = y_n + \frac{h}{6}(k_1 + 2k_2 + 2k_3 + k_4)$$
$$t_{n+1} = t_n + h$$

For $n = 0, 1, 2, 3, \ldots$, using

$k_1 = f(t_n, y_n)$,
$k_2 = f\left(t_n + \frac{h}{2}, y_n + \frac{h}{2}k_1\right)$,
$k_3 = f\left(t_n + \frac{h}{2}, y_n + \frac{h}{2}k_2\right)$,
$k_4 = f\left(t_n + \frac{h}{2}, y_n + hk_3\right)$.

In the above defined y_{n+1} is the $RK4$ approximation of $y(t_n + 1)$, and the next value (y_{n+1}) is determined by the present value (y_n) plus the weighted average of four increments, where each increment is the product of the size of the interval, h, and an estimated slope specified by function f on the right-hand side of the differential equation.

- k_1 is the increment based on the slope at the beginning of the interval, using y
- k_2 is the increment based on the slope at the beginning of the interval, using $y + \frac{h}{2}k_1$

- k_1 is the increment based on the slope at the beginning of the interval, using $y + \frac{h}{2}k_2$
- k_1 is the increment based on the slope at the beginning of the interval, using $y + hk_3$

7.4.1 Balanced Voltages

The thermal model was tested under balanced operating conditions. The temperatures recorded during the thermal tests were compared with the temperatures from the thermal model. The measured and predicted temperatures of the four machines are given in **Error! Reference source not found.** to **Error! Reference source not found.**. Four load conditions were considered for this comparison. Since the machines were operating under balanced voltage conditions, the average winding temperatures were compared. The thermal model yielded satisfactory prediction results under balanced operating conditions. The largest difference between measured and predicted temperature values was 4.1°C. This value is much lesser than the 10°C halving interval, the impact of the over/under estimation of machine temperatures on loss of life calculations is evaluated in detail in chapter 8.

Table 7-9: 7.5kW Manufacturer A Induction Machine Thermal Model Test under Balanced Voltage Conditions

LC (%)	Winding Losses	Core Losses	$T_{Measured}$	$T_{Predicted}$
25	175,59449	269.43	71.23	74.33
50	258,43447	269.43	78.22	74.12
75	373,89373	269.43	85.33	82.5
100	617,43669	269.43	103.07	100.55

Table 7-10: 7.5kW Manufacturer B Induction Machine Thermal Model Test under Balanced Voltage Conditions

LC (%)	Winding Losses	Core Losses	$T_{Measured}$	$T_{Predicted}$
25	168,01432	278.46	45.96	43.18
50	201,85438	278.46	57.81	56.15
75	415,1016	278.46	70.79	71.88
100	664,43612	278.46	98.83	101.3

Table 7-11: 11kW Manufacturer A Induction Machine Thermal Model Test under Balanced Voltage Conditions

LC (%)	Winding Losses	Core Losses	$T_{Measured}$	$T_{Predicted}$
25	152,44221	279.88	54.12	51.22
50	248,36128	279.88	67.13	68.58
75	444,90798	279.88	78.89	81.44
100	848,07661	279.88	114.12	117.5

Table 7-12: 11kW Manufacturer B Induction Machine Thermal Model Test under Balanced Voltage Conditions

LC (%)	Winding Losses	Core Losses	$T_{Measured}$	$T_{Predicted}$
25	120,87147	359	48.78	51.00
50	234,61174	359	59.76	61.15
75	459,57689	359	74.12	75.14
100	856,36565	359	110.12	111.58

7.4.2 Unbalanced Voltages

Error! Reference source not found. compares the measured and predicted temperatures for the 7.5kW Manufacturer A machine under various supply conditions. The thermal model predicts the steady state temperature very closely to the measured temperature. The steady state temperature prediction deviates between 3.76°C and -5.58°C, this is for the individual phase windings. For the average stator winding temperature, the maximum deviation ranges between 3.2°C and -0.95°C. The highest winding temperature is used for the life estimation of the machine.

Table 7-13: 7.5kW Manufacturer A Induction Machine Thermal Model Test under unbalanced Voltage Conditions

VU (%)	VR (%)	LC	Winding Losses (W)			Core Losses (W)	$T_{Measured}$			$T_{Predicted}$		
			A	B	C		A	B	C	A	B	C
1	90	24,9	59,4	30,3	41,85	199.03	47.15	40.28	49.63	45.89	39.5	44.3
		49,9	90,48	51,25	73,64		58.64	56.48	63.02	60.47	54.5	60.35
		74,4	160,35	100,14	142,56		82.34	75.71	73.87	80.14	72.44	79.45
		99,3	280,38	197,56	260,35		121.8	109.6	119.5	118.5	107.2	115.9
	100	24,9	74,44	45,61	56,28	301.74	54.15	45.15	49.33	50.35	41.38	47.86
		49,8	98,49	62,533	80,89		64.10	60.45	65.72	65.33	59.33	62.11
		73,2	147,30	98,31	130,18		76.01	73.12	75.43	79.68	70.98	78.73
		100	240,74	175,14	224,38		115.0	96.48	108.4	112.94	98.83	107.58
	110	24,9	163,06	63,64	119,20	440	73.45	72.05	73.23	71.22	68.32	69.58
		50,4	189,52	67,71	143,88		86.89	80.19	85.43	85.23	79.98	83.56
		74,5	246,72	88,56	201,93		92.35	83.7	111.7	91.23	81.22	109.99
		100	301,18	126,77	268,91		117.9	95.6	99.73	115.2	98.47	101.2
2	90	25,5	59,50	69,62	18,28	214.22	47.00	68.89	31.35	46.31	68.30	33.14
		50,1	99,74	103,78	34,30		65.09	76.6	42.72	65.3	74.5	41.39
		75,3	182,12	174,57	75,32		87.26	76.41	82.00	88.53	77.25	81.41
		99,6	315,21	296,68	159,14		136.2	124.5	105.4	138.78	125.44	108.45
	100	24,8	71,150	97,71	28,54	319.14	57.01	65.17	44.18	55.81	64.37	43.21
		50,5	106,23	133,35	37,89		74.15	85.00	44.8	72.15	86.47	44.81
		73,0	166,72	190,02	62,12		88.31	85.64	68.87	86.78	89.57	69.31
		93,9	239,37	255,42	105,17		128.5	96.01	80.57	130.64	93.88	78.32
	110	25,6	109,12	165,81	58,66	475.4	79.45	81.59	54.76	76.31	79.35	52.37
		50,1	130,89	190,62	62,95		88.21	92.47	66.48	85.64	90.51	68.59
		75,1	190,1	253,61	84,59		94.27	101.3	86.87	92.31	99.01	83.11
		99,8	267,62	324,99	125,20		121.0	144.8	79.38	121.4	143.75	79.86

Figure 12-1 to Figure 12-4 illustrates the temperature rise curves of Manufacturer A 7.5kW machine. All the three phases are monitored separately in unbalanced operating conditions. The stator copper losses associated with each phase were fed to the appropriate node in the model. Depending on the type and level of voltage unbalance, the copper losses per phase are different hence the different temperatures.

The predicted temperatures of the 7.5kW Manufacturer A machine are compared with the measured values in **Error! Reference source not found.**. The resulting temperature rise curves for 1% voltage unbalance under the various load and regulation conditions are illustrated in Figure 12-1 to Figure 12-4.

The measured and predicted temperatures for the 7.5kW Manufacturer B machine are tabulated in **Error! Reference source not found.**. For the individual phase windings comparisons, the maximum deviation between the measured and predicted steady state temperatures ranges between 3.35 ℃ and -4.54℃. The difference in the measured and predicted average stator winding temperature ranges between 1.08 ℃ and -1.757℃.

Table 7-14: 7.5kW Manufacturer B Induction Machine Thermal Model Test under unbalanced Voltage Conditions

VU (%)	VR (%)	LC	Winding Losses (W)			Core Losses (W)	$T_{Measured}$			$T_{Predicted}$		
			A	B	C		A	B	C	A	B	C
1	90	25,1	45,55	22,79	33,84	207.02	38.00	37.8	41.28	39.97	34.65	45.05
		54,4	88,93	57,13	80,76		68.3	47.20	63.23	65.14	48.59	61.75
		75,1	149,51	108,42	141,95		87.19	76.09	84.31	86.31	75.33	82.44
		99,9	286,44	230,27	274,89		127.44	121.7	125.61	128.87	119.84	125.48
	100	25,3	61,85	37,84	48,29	307.56	75.09	66.48	70.86	76.99	64.21	68.33
		48,5	85,59	58,38	60,82		88.41	74.01	72.69	87.58	72.45	76.21
		75,0	141,30	108,46	135,17		103.55	88.21	86.92	106.99	84.38	87.01
		100,3	223,73	186,16	219,08		109.47	92.33	105.65	110.4	90.84	108.7
	110	23,8	136,48	42,03	95,36	466.7	87.15	45.13	71.93	89.01	48.37	71.41
		49,7	155,34	54,07	133,48		98.08	47.61	84.05	96.75	49.67	88.59
		77,1	198,03	85,38	194,23		107.29	71.55	99.76	104.21	73.71	101.04
		100	264,74	135,95	275,72		122.00	80.45	143.6	120.93	81.33	142.19
3	90	24,83	76,63	7,98	52	263.99	72.23	21.07	54.14	69.6	19.8	58.38
		49,54	115,69	23,72	106,08		89.54	27.98	81.58	91.58	25.66	83.77
		77,27	199,98	68,65	202,69		110.15	47.69	116.48	108.31	50.89	115.49
		100,58	350,08	158,91	353,90		137.09	126.3	142.51	134.3	129.3	139.9
	100	25,38	115,55	16,74	64,89	400.28	98.33	35.89	65.46	96.14	37.36	65.18
		49,08	145,27	26,57	110,36		105.89	42.15	87.48	107.45	39.41	87.10
		75,46	198,06	53,04	176,05		118.98	46.28	95.23	116.01	47.4	97.34
		100,9	311,78	118,56	291,83		130.0	105.2	122.55	131.48	103.56	124.12
	110	25,3	185,76	37,212	93,80	588.99	107.44	36.06	73.33	108.45	35.65	72.88
		50,95	206,30	41,75	135,64		121.98	45.69	93.8	119.56	43.01	97.25
		76,13	251,2	60,59	196,32		127.36	50.39	114.69	124.01	52.45	117.52
		100,4	337,66	105,48	291,13		137.00	115.2	123.67	135.54	113.78	127.05

The thermal model was also tested on the two 11kW machines, for the 11kW Manufacturer B machine the results are tabulated in **Error! Reference source not found.** Similar to the previous two machines the measured steady state temperatures are compared to the predicted temperatures. The maximum deviation for the individual phases ranges between 5.73 ℃ and -5.34℃. The maximum deviation for the average stator winding steady state temperature ranges between 2.313 ℃ and -1.7℃. The 11kW Manufacturer A machine results are included in Table 12-48 found in the appendix.

Table 7-15: 11kW Manufacturer B Induction Machine Thermal Model Test under unbalanced Voltage Conditions

VU (%)	VR (%)	LC	Winding Losses (W)			Core Losses (W)	$T_{Measured}$			$T_{Predicted}$		
			A	B	C		A	B	C	A	B	C
2	90	23,92	62,57	71,62	11,32	326	57.05	67.8	17.84	58.39	63.14	22.47
		50,28	129,82	115,55	36,09		95.10	77.2	46.06	94.75	74.86	43.84
		75,02	227,43	191,71	87,56		115.23	98.27	54.10	113.12	96.99	57.87
		99,75	405,54	344,46	191,63		137.57	129.4	115.71	141.04	131.45	115.29
	100	24,11	74,66	107,42	18,21	437	62.21	69.18	33.31	60.17	71.0	27.58
		49,33	127,48	140,47	32,48		82.14	90.00	31.47	80.75	93.91	28.53
		74,55	212,40	207,24	69,76		106.25	97.45	56.22	109.36	100.43	53.87
		99,32	349,59	326,54	141,26		135.28	130.6	95.03	137.01	131.44	92.53
	110	24,98	105,74	175,77	38,07	641	70.65	82.14	47.39	69.41	81.67	42.16
		49,47	154,32	203,31	46,39		74.2	101.4	55.67	75.13	99.15	55.78
		75,02	232,72	263,54	75,34		111.71	114.25	62.01	109.45	113.89	64.01
		99,58	348,41	363,90	129,50		137.68	139.52	99.5	136.5	137.8	104.51
3	90	24,88	106,62	8,72	67,80	376	73.16	19.45	54.35	71.63	14.71	58.9
		49,68	155,70	19,798	135,51		86.21	40.0	75.36	83.74	39.01	79.16
		75,69	255,54	60,97	250,75		115.82	45.16	109.44	116.04	43.12	114.78
		99,39	426,44	142,57	430,64		137.24	121.88	135.85	134.3	119.7	139.9
	100	23,49	154,48	19,457	76,75	510	92.55	39.74	63.1	90.18	38.07	65.80
		49,77	196,90	22,89	139,20		99.35	43.67	85.37	97.85	41.09	88.03
		74,29	270,92	47,24	226,7		121.06	48.07	98.89	119.8	46.78	102.27
		100,72	418,85	107,87	381,43		137.98	98.47	134.2	138.2	100.17	130.4
	110	24,77	243,49	42,73	105,85	743	108.91	33.06	81.39	105.73	35.09	82.67
		49,63	281,43	39,86	166,00		121.24	42.67	98.99	119.51	45.19	96.34

The temperature rise curve of Manufacturer B 11kW machine is given in Figure 12-7, this is at full load with 90% voltage regulation and 3 % voltage unbalance. The highest temperature recorded is 140 ℃. Similarly, Manufacturer A 7.5kW machine temperature rise curve for the stated operating condition is given in Figure 12-8.

The shortcomings of currently used thermal protection mechanisms were discussed in the preceding section. The thermal model present in this research project can be incorporated as an algorithm and be implemented in microprocessor devices which enhance the level of accuracy and flexibility. The model can be used in conjunction with microprocessor-based relays and be used to predict the stator winding temperature. Over-current relays only use current and time to thermally protect machines, current limit curves must be set to ensure that the limits are not exceeded. I^2t protection keeps track of the machine temperature by monitoring the machine current and computing the over-temperature. If the machine is operating at currents above the nominal value protection will be triggered. Most microprocessor based thermal protection devices comprise of a thermal model which calculates machine temperature from machine losses and current and time measurements. In most low voltage overload protection relays, protection is done by measuring the current and judging how much more it is than the nominal current, a thermal model calculates the thermal load and checks whether or it not the threshold has been surpassed. Current protection devices are not able to determine safe operating conditions for machines, they cannot detect abnormal operating conditions. With knowledge of the voltage unbalance factor and the input currents the machine losses can be computed and serve as inputs to the thermal model. The thermal model form part of a machine controller which provides machine control and machine protection functions. Machine controllers usually comprise of an overload protection device to protect the electric load especially an induction machine load, in a load circuit comprising of an electric supply line current providing a load current and the electrical load. If the machine controller already comprises of a voltage and current unbalance detection circuit predictive analysis on the machine can be performed.

Discussion of Duty Cycle, Service Factor and Sizing

The induction machine average load factor needs to be known for industrial implementation of this thermal model. The load factor is the average of the machine load during a defined period. Many induction machines in industrial applications are oversized, in the regions where average motor load factor data is collected, the average motor load factor of electric motors in both industry and tertiary sector is estimated to be less than 60% [79].The machine load factor is an average over an operating cycle hence, for any machine it can alternate between values lower and higher than the load factor. In most cases induction machines are operated at lower loads to accommodate voltage unbalance and/or distortion, to accommodate load fluctuations, to have a safety margin to meet the requirements in applications with uncertain mechanical load and to have an allowance for increasing motor load in the future [79]. As mentioned in section 6.11.3, the maximum efficiency of a conventional induction design lies within the range 60% to 80% of the machine's rated power. If a machine has a loading factor greater than 75% it is considered adequate for that application [80]. This value was chosen since the peak efficiency of an induction machine lies in the 60% to 80% region. If the loading factor is lower than the 75% of its rated power, it is deemed oversized. NEMA and the IEC specify the Duty Cycle Ratings of induction machines, NEMA usually specifies continuous, intermittent or special duty, the IEC uses different duty cycle designations (IEC 34-1).

Duty cycle defines the load cycle to which a machine is subjected to, this may include, if applicable, starting, electric braking, no load and rest de-energized periods, and including their durations and sequence in time. In general duty can be classified as continuous, short time or periodic. The thermal model presented in this research report is suited for continuously operated machines (S1). The thermal load tests from the four machines (Table 12-1 to Table 12-47) have shown that for unbalance and regulation conditions considered in this research, loss of life is expected around the rated load condition. Continuously rated machines operate continuously at rated loads and temperature, at these operating conditions an introduction of voltage unbalance or over-and undervoltage leads to operation above the rated temperatures and hence loss of life. The thermal model has not been tested for short time duty (S2) and intermittent period duty (S3 – S4) applications where no thermal equilibrium is ever reached by the machine. The importance of thermal models will potentially increase as the approach to maintenance/repair gradually evolves from reactive (corrective) and preventative (systematic or periodic) to diagnostic and predictive. Machine overloading is one of the common causes of temperature over load in induction machines. In some cases, this overload is intermittent due to load variations in the driven equipment. In some instances, the designer of the machine chooses to operate the machine above the rated load. Ideally, this is only acceptable when the machine has a service factor greater than 1.0. as specified by NEMA [19]. Service Factor as defined by *NEMA MG1-2011* states that a machine is thermally capable of overload to that point within the insulation class at normal service conditions (at rated voltage and frequency). An overload will increase the machine operating temperature, but as observed in section 6.11 most machine efficiencies lie around 75%-85% of the rated load hence the machine will run cooler and consume less power for the same task. Oversizing of line-fed machines can lead to significant efficiency and power factor reduction. If there is no speed control, the lower slip due to the oversizing (low loads and high rated power) results in an increase of the mechanical power required by the load/application, this leads to increased energy consumption.

7.5 Concluding Remarks

The induction thermal model was developed based on [53]. The stator copper losses were determined using the per phase sequence equivalent circuits. The IEEE 112-B method was used to determine the core losses which serve as inputs to the thermal model. From the results it was observed that the thermal model proves to be more accurate in predicting the average stator winding temperatures than the individual phase windings temperatures. As mentioned earlier in this chapter the stator copper losses are well defined and can easily be imposed in at the three nodes representing the three phases of the machine. The difference in the accuracy between the average winding temperatures and the individual windings temperatures could be attributed to the allocation of the core losses. In some lumped parameter thermal models, [25] ad-hoc method was employed by splitting these losses into fixed proportions, 50% to the stator teeth and 50% to the rotor teeth. The maximum deviation between the measured and predicted temperatures for the individual phases is around 5 °C and -5°C, this is well below the 10°C halving rule. There are some extreme cases more specifically for the 11kW Manufacturer B machine where the temperature difference between the phases is more than 30°C. This will have drastic effects on the life expectancy of the induction machine and the operation of the motor. The thermal model presented in this research project can be incorporated as an algorithm and be implemented in

microprocessor devices which enhance the level of accuracy and flexibility. The model can be used in conjunction with microprocessor-based relays and be used to predict the stator winding temperature. The output temperatures of the thermal model will serve as inputs for the loss of life estimation in chapter 8. For operation under balanced voltage conditions the average temperature is used for life estimation since all phases have roughly the same temperatures, for operation under unbalanced combined with under-and overvoltage the highest phase temperature is used for life estimation.

8. LOSS OF LIFE IN LOW VOLTAGE INDUCTION MACHINES DUE TO VOLTAGE UNBALANCE AND REGULATION

This chapter presents the life expectancy of the tested induction machines for operation under unbalanced voltages. As mentioned in the earlier chapters the life of insulation materials can be described by Arrhenius equations. The loss of life is described in detail in section 3.11 of this report.

8.1 Motor Life Estimation

Induction machine life is affected by thermal, mechanical, environmental and electrical stresses. In this instance only, the thermal stresses are considered in the loss of life. The thermal stress is the most dominant of these stresses. This means that the insulation ageing process depends on the magnitude and duration of the temperature the motor is operating at. Induction motor winding insulations have a specific lifetime and it deteriorates with time due to thermal stresses. Insulation materials have been classified in accordance to the temperature they can withstand. Operation of these insulation materials above their rated temperatures will lead to rapid deterioration. **Error! Reference source not found.** shows the insulation class type, thermal limit and the allowable temperature rise at an ambient temperature of 40°C.

Table 8-1: Insulation Class Ratings

Class	Maximum temperature (°C)	Temperature rise (°C)
A	105	65
B	130	90
F	155	115
H	180	140
Ĥ	220	180

The lifespan of any component is defined as the time from when it's manufactured to the time when it can no longer do what it is required to do at the rate it was rated to do it [18].In general, a concept of a 10°C rise above the design level of the winding insulation can lead to a 50% reduction in the motor life expectancy. This concept was introduced by Montsinger in 1930 and became known as the halving interval (HIC) for each type of insulation class [53]. A thermal ageing model that modifies the 10°C rule to a more accurate half interval index is shown in [53]. This model allows us to estimate insulation life for all insulation classes because of its half interval index (HIC).

$$L_x = L_{100} \cdot 2^{\left(\frac{T_C - T_X}{HIC}\right)} \quad (8\text{-}1)$$

Where:

L_x Percent lifetime at temperature T_x (°C)
L_{100} Percent lifetime at rated temperature T_c (°C)
T_c Total allowable temperature for insulation class (°C)
T_x Hotspot temperature for insulation class (°C)
HIC Halving interval (°C); (14, 11, 9.3, 8 and 10 for class A, B, F, H and Ḧ)

There is another form of Arrhenius equation which can be used to estimate insulation life shown in [18] [1]. This second equation takes into consideration the variation of ambient or operating temperature with time. Equation (8-1) assumes the motor is operating continuously at the same temperature throughout its lifespan (Continuous Duty S1 rated machines).

.

$$ln\left(\frac{t_r}{t_i}\right) = \frac{\varphi}{k} \cdot \left(\frac{1}{T_r} - \frac{1}{T_i}\right) \quad (8\text{-}2)$$

Where:

t_r Is the time at temperature T_r
t_i Is the time at temperature T_i
T_r Is the reference temperature
T_i Is the initial temperature
k Is $0.8617*10^{-4}$ eV/K and $\varphi = 1.05$eV

Both equations can be used to estimate motor life. It was shown in previous work that the difference [53] in using the two is marginal therefore equation (8-1) will be used for motor life estimation. The lifespan of induction motor winding insulation is based on 20 000-hour continuous operation. This is equivalent to continuous operation at rated conditions for 2.3 years (24hours × 365 × 2.3 =20 148 hours) or it can be equated to a 10-year duty cycle assuming a 2000-hour duty cycle per year. Similarly, there are other standardized reference lifespans for motors operating at certain load conditions. An approximation table in Brancato's paper [18] illustrates the expected life of different insulation classes operating continuously at various load conditions throughout their lives.

If we assume that the 7.5kW Manufacturer A induction machine will operate continuously at 100% of its rated voltage at its rated load condition without experiencing any voltage unbalance, its estimated life obtained using equation (8-3):

$$L_x = L_{100} \cdot 2^{\frac{T_c - T_X}{HIC}} = 100 \times 2^{\frac{155 - 122.57}{9.3}} = 1121.29 \quad (8\text{-}3)$$

This means that the insulation life of the 7.5kW Manufacturer A induction machine operating at a temperature rise of 82.57 °C at an ambient temperature of 40 °C will be 11.21 times the class F insulation at the same ambient temperature of 40 °C. If the class F insulation life is 2.3 years when operating at rated load conditions the 7.5kW Manufacturer A induction machine will last for 2.3 × 11.2 = 25.78 years.

As will be observed with some of the machines tested in this research report, the 7.5kW Manufacturer A induction machine has a class B temperature rise with class F insulation. Manufacturers are using this criterion to prolong machine life. For operation above rated load conditions the equation below is used in the calculation of insulation life.

$$Loss\ of\ Life = \frac{1}{L_{x^i}} \cdot L_{x_{rated}} \times t_i \qquad (8\text{-}4)$$

Where

L_{xi} The expected lifespan at a temperature T_{xi} (in years)

$L_{x_{rated}}$ The expected lifespan at rated conditions (in years)

t_i The time in years the motor will be operating at temperature T_{xi}.

Both equations ((8-1) and (8-4)) can be used to estimate motor life.

8.1.1 Motor Life Estimation Under Constant Operating Conditions

The life expectancies of the four machines under the considered test conditions were calculated and tabulated below. In **Error! Reference source not found.** to **Error! Reference source not found.** only the expected life for 100% loading at the considered unbalance combined with over- and undervoltage conditions is tabulated.

Table 8-2: Manufacturer A 7.5kW Life Estimation under Constant Operating Conditions

VUF (%)	VR (%)	EL (Years)	VUF (%)	VR (%)	EL (Years)	VUF (%)	VR (%)	EL (Years)	VUF (%)	VR (%)	EL (Years)
0	90	9.39	1	90	8.76	2	90	6.21	3	90	3.31
	100	24.85		100	19.31		100	17.54		100	8.09
	110	31.52		110	22.99		110	10.17		110	4.45

VUF=Voltage Unbalance
VR=Voltage Regulation
EL=Expected Life

The expected life values for the 7.5kW Manufacturer A induction machine is tabulated in **Error! Reference source not found.**. The expected life for the three voltage regulation and unbalance conditions are included. The life expectancy at zero voltage unbalance, 100% voltage regulation is used as the reference/nominal value. As explained earlier in the chapter, this machine has a temperature rise of a class B machine with a class F insulation. Under nominal operating conditions this machine will have an approximated life expectancy of 24.85 years. This is close to the mentioned average life of 25 years for an induction machine. At zero voltage unbalance combined with 110% voltage regulation the machine will have a longer lifespan due to the lower operating temperature, inversely at zero voltage unbalance with 90% voltage regulation over 60% loss of life is expected. These expected life values are based on a 2.3-year continuous operation (24hours × 365 × 2.3 =20 148 hours), depending on the operating schedule of the machine the expected life can be increased.

Table 8-3: Manufacturer B 7.5kW Life Estimation under Constant Operating Conditions

VUF (%)	VR (%)	EL (Years)	VUF (%)	VR (%)	EL (Years)	VUF (%)	VR (%)	EL (Years)	VUF (%)	VR (%)	EL (Years)
0	90	15.86	1	90	4.93	2	90	4.54	3	90	2.27
	100	34.08		100	27.82		100	7.23		100	7.44
	110	25.08		110	9.96		110	7.40		110	4.74

VUF=Voltage Unbalance
VR=Voltage Regulation
LC=Load Condition

Like the 7.5kW Manufacturer A machine the expected life of the Manufacturer B can be increased through operation under overvoltage conditions (with zero voltage unbalance), there would however be a trade-off between life expectancy and operational efficiency. The Manufacturer B 7.5kW machine has an expected life of 34.08 years corresponding to a thermal equilibrium temperature of 98.83℃. The combination of 3% voltage unbalance with 90% voltage regulation yields the worst loss of life (2.27 years= 19885 continuous operational hours). At first glance 2.27 years seems too little of a life expectancy, for machines utilized 12 hours a day, 5 days a week this corresponds to 6.5 years of expected life under the worst condition.

Table 8-4:Manufacturer B 11kW Life Estimation under Constant Operating Conditions

VUF (%)	VR (%)	EL (Years)	VUF (%)	VR (%)	EL (Years)	VUF (%)	VR (%)	EL (Years)	VUF (%)	VR (%)	EL (Years)
0	90	16.03	1	90	5.17	2	90	4.00	3	90	3.34
	100	26.7		100	12.64		100	7.03		100	5.46
	110	17.912		110	8.51		110	5.03		110	4.40

VUF=Voltage Unbalance
VR=Voltage Regulation
LC=Load Condition

The 11kW Manufacturer B machine has a life expectancy of 26.7 years. The 10℃ rule discussed earlier in this chapter is observed between the 0% voltage unbalance and 1% voltage unbalance conditions at 100% voltage regulation. An increase of (112.13 ℃ - 102.12℃ = 10.01 ℃) 10.01℃ results in over 10 years loss of life. The worst operating condition for the 11kW Manufacturer B is 3% voltage unbalance combined with 90% voltage regulation.

Table 8-5:Manufacturer A 11kW Life Estimation under Constant Operating Conditions

VUF (%)	VR (%)	EL (Years)	VUF (%)	VR (%)	EL (Years)	VUF (%)	VR (%)	EL (Years)	VUF (%)	VR (%)	EL (Years)
0	90	19.17	1	90	7.05	2	90	6.96	3	90	4.14
	100	22.98		100	20.15		100	17.05		100	7.36
	110	26.12		110	14.96		110	8.87		110	5.87

VUF=Voltage Unbalance

VR=Voltage Regulation
LC=Load Condition

The 11kW induction machine has a higher thermal equilibrium than the Manufacturer B hence the lower expected life under nominal operating conditions. A similar trend is observed in terms of the life expectancy at zero voltage unbalance with 110% voltage regulation (extended life).

8.2 Conclusions

The expected life of the four machines was determined for continuous operation at constant temperatures. It was observed that operation at high temperatures reduces the life expectancy. The primary solution to prevent the loss of useful machine life is to ensure that the windings temperatures are kept at rated or below rated temperature rise conditions. Derating of machines is highly recommended by NEMA for operation under voltage unbalances that are greater than 1%. Class F insulated machines are designed to handle a temperature rise of 115°C at an ambient of 40°C, at this temperature conditions the machine will have a life expectancy of 2.3 years. Results from the thermal tests of the four machines show that all the machines have a temperature rise lower than the recommended class F temperature rise (class B temperature rise), this results in the machines having greater life expectancies. Depending on the application of the machine the expected operational hours the life expectancy can be multiple years if continuous operation is not applied.

From the thermal test results, both machines from Manufacturer B operate at lower temperatures than Manufacturer A machines under balanced operating conditions. The two Manufacturer B machines have greater impedances than the Manufacturer A machines, this results in reduced currents and hence reduced copper losses under this operating condition. Manufacturer B machines also yielded greater core losses than Manufacturer A machines for all the operating conditions, more specifically the overvoltage condition. Under overvoltage operating conditions the core losses are more significant and contribute more to the temperature rise of the machines. This why Manufacturer A machines have greater life expectancies when operating in the overvoltage conditions. When voltage unbalance is introduced, Manufacturer A machines are more tolerant to operation under unbalanced voltage conditions. For both machine sizes the Manufacturer A machines have greater life expectancies (under voltage unbalance combined with over- and undervoltage conditions) when compared to Manufacturer B machines. The 7.5kW Manufacturer A machine has a higher rated speed than its Manufacturer B counterpart. As mentioned in section 6.12 the slip of an induction machine is inversely proportional to the voltage applied, the higher the voltage the lower the slip and the faster the machine turns. Since the Manufacturer A machine is already operating at a lower slip (higher speed) and with a further decrease in slip due to overvoltage, the 7.5kW Manufacturer A machine runs cooler and displays a considerably higher life expectancy at for operation under- overvoltage conditions.

It is evident from the life expectancy calculations that the operation of Manufacturer A machines under overvoltage conditions without any voltage unbalance results in a higher life expectancy this means that these machines run cooler at this operating condition. Both Manufacturer A machines have higher life expectancies under the overvoltage condition when compared to Manufacturer B machines of the same size. The voltage conditions considered in this report include mixed undervoltage unbalance (MUVU) for rated voltage regulation, undervoltage

unbalance (UVU) for 90% voltage regulation and overvoltage unbalance (OVU) for 110% voltage regulation. All the four machines tested in this research report are standard efficiency class (IE1). It is well documented [6] [51] that higher efficiency machines (Premium/IE3 and Super-Premium/IE4) machines have lower temperature rise because of their lower losses and their improved heat dissipation. This results in extended winding insulation lifetime or a higher service factor. The higher the efficiency class of the machine the lower the internal temperature rise will be, this advantage is however attenuated at lower loads. When voltage unbalance is introduced it is assumed that the losses for all efficiency classes increase in the same percentage. Higher efficiency machines have lower rotor impedance and starting torque and are more sensitive to voltage unbalance conditions from a starting performance point of view. Operation at lower slip results in lower negative sequence currents. This results in lower copper losses and hence lower operating temperatures. All the four machines tested are standard efficiency machines (IE1). For induction machines with smaller power ratings, a lower temperature is always better for efficiency. Machines with high power ratings are more tolerant to higher temperatures as the load dependent losses are not dominant.

9. CONCLUSIONS AND RECOMMENDATIONS

This research report investigated the impact of voltage unbalance and regulation on induction machine losses, efficiency, temperature and life expectancy. Four machines were considered for this study, two of them were from Manufacturer A while the other two were from Manufacturer B. The IEEE 112-B Standard Test Procedure for Polyphase Induction Motors and Generators was used in the determination of the core losses, the stator copper losses were determined using the positive and negative sequence equivalent circuits. The thermal model parameters were obtained through a series of DC tests.

The adopted thermal model [52], was refined to improve the temperature prediction accuracy. The model in [52] was tested on one machine (3kW), the iron losses were determined the same way as the referenced model. The stator copper losses in the refined thermal model were corrected to the operating temperatures of the various machines. In the original thermal model, it was assumed that the thermal conductance was constant. In the refined model applied in this report, the thermal conductance is dependent on the speed of the machine [30].

Efficiencies of the four induction machines were determined following the direct method mentioned in IEEE 112-B Standard Test Procedure for Polyphase Induction Motors and Generators. The thermal model test was in the estimation of the average stator winding temperatures and the life expectancy under the considered operating conditions was analysed.

Based on the experimental results and analysis presented in this report the following conclusions can be made:

- The induction machine core losses increase with average voltage but most when saturation occurs. As voltage unbalanced is increased so are the additional losses in the rotor due to the reverse airgap field. The additional losses form part of the increased machine core losses. As observed in Figure 6-2 to Figure 6-5 the additional core losses result in the total core loss curves being shifted with respect to the nominal operating condition. Since the core losses are dependent on the average voltage, the core losses for under voltage condition is lower than those at nominal voltage regulation. For operation under overvoltage conditions the saturation and quality of the electrical steel plays a vital role. The induction machine core losses increase with an increase in average voltage and decrease with an increase in machine temperature.

- At partial load conditions it was observed that the stator copper losses for the overvoltage unbalance condition is significantly greater than the other two conditions (nominal regulation with unbalance and undervoltage unbalance). As the load condition is increased, the copper losses for the overvoltage unbalance, undervoltage unbalance and rated voltage unbalance intersect around the rated load condition (80-100%). The rate of increase for these losses is greater for the undervoltage unbalance, this alarming rate of increase is accompanied by an increase in temperature. For this operating condition, the

induction machine draws more current as the load is increased but since the machine is operating at low average stator voltages more current is required to ensure that the required output power is produced.

Operation of induction machines at higher voltages tends to push the magnetic portion of the machine into saturation. This causes the machine to draw excessive current to magnetize the iron core beyond the point to which it can be easily magnetized. An overvoltage supply leads the magnetic materials, such as the iron core to approach saturation, to increase losses and to increase the losses in the copper windings. The power factor also becomes poor due to disproportionate increase in magnetizing current. When an induction machine is operating at an overvoltage condition at loads less than the rated load, the magnetizing currents will increase and if the load reduces further the line current might also increase (as observed in Figure 6-7 to Figure 6-21 and Table 12-1 to Table 12-47). If the machine voltage is increased beyond its saturation point additional flux is only possible with a disproportionately large increase in current leading to increased copper losses.

- The positive sequence impedance is strongly dependent on the slip with the highest value around the no load region and the lowest around the blocked rotor region. The negative sequence impedance varies the most at low slip values (region where the machine mostly operates). The negative sequence impedance is virtually independent of the machine slip and can be regarded as a constant. This means that the losses due to negative sequence components are independent of the machine load.

- From the design of most induction machines the maximum efficiency lies within the range 60% to 80% of the machine's rated power. In Figure 6-31 to Figure 6-38 the efficiencies of the four machines are illustrated, determined using the direct method. At partial load conditions the impact of the core losses is more significant (due to the lower currents and temperatures). Around the rated load condition, the stator and rotor copper losses are more significant, the efficiency results show that the for the undervoltage unbalance condition the maximum efficiency position is shifted towards the partial load region. The overvoltage unbalance results in the maximum efficiency shifting towards the rated load operating region.

- The stator copper losses and core losses discussed above served as inputs to the thermal model of the induction machine. The thermal model which predicted the temperature rise of the stator windings proved to be more accurate in predicting the average stator winding temperature than the individual phase temperatures. The maximum deviation between the measured and predicted temperatures for the individual phases is around 5 °C and -5°C, this is well below the 10°C-halving rule.

- The temperature predicted by the thermal model was used to calculate the life expectancy of the induction machines. The lifespan of induction motor winding insulation is based on 20 000-hour continuous operation. This is equivalent to continuous operation at rated conditions for 2.3 years (24hours × 365 × 2.3 =20 148 hours) or it can be equated to a 10-year duty cycle assuming a 2000-hour duty cycle per year. For all the machines tested

in this research report the worst loss of life came from the undervoltage unbalance operating condition.

Based on the conclusions discussed above the following recommendations can be made

- There is currently no defined standardized procedure for determining the core losses under unbalanced operating conditions hence quantification of these losses can be hard. Recent methods using non-intrusive techniques can be applied to obtain the core losses which are fed into the thermal model. A comparison of results obtained from new techniques and the IEEE method can prove vital in improving the accuracy of the thermal model.

- This study only included two machine sizes, 7.5kW and 11kW. In future projects larger machines can be tested to get a more representative sample of the application in the industry. The validity of the thermal model could then be extended to larger machines.

- There are currently online thermal monitoring models [81], lumped parameter thermal models and finite element methods being applied in the industry. The model applied in this research report can be extended to include the effect of harmonics on the life expectancy of induction machines. Thermal stresses are main cause of loss of life for induction machine insulation systems, there are other stresses contributing to the loss of life. Literature shows that harmonics have a remarkable effect on the thermal ageing and loss of life in induction machines. .

- The voltage unbalance cases used in this research report are only theoretical, factual data can be obtained from the power utility (ESKOM) for time intervals. This data/voltage conditions can then be implemented in the machines lab. By using the power utility's actual data, a more direct conclusion can be drawn. A case study may be chosen and studied individually. A better comparison on the loss of life/expected life of induction machines can be done if the operational schedule is known. It is true that total expected total number of operational hours can be determined but this can further be broken into years if the scheduling is known.

10. EBE Faculty: Assessment of ethics in research projects

Any person planning to undertake research in the Faculty of Engineering and the Built Environment at the University of Cape Town is required to complete this form before collecting or analysing data. When completed it should be submitted to the supervisor (where applicable) and from there to the Head of Department. If any of the questions below have been answered YES, and the applicant is NOT a final year student, the Head should forward this form for approval by the Faculty EIR committee: submit to Ms Zulpha Geyer (Zulpha.Geyer@uct.ac.za; Chem Eng Building, Ph (021 650 4791). Students must include a copy of the completed form with the final year project when it is submitted for examination.

Name of Principal Researcher/Student:	Samuel Mponwana	**Department:**	ELECTRICAL ENGINEERING
If a Student: YES	**Degree:** MSc in Electrical Engineering	**Supervisor:**	Prof Paul Barendse
If a Research Contract indicate source of funding/sponsorship:			
Research Project Title:	The Impact of Voltage Unbalance and Regulation on the Life Expectancy of Induction Machines		

Overview of ethics issues in your research project:

Question 1: Is there a possibility that your research could cause harm to a third party (i.e. a person not involved in your project)?	YES	NO ✓
Question 2: Is your research making use of human subjects as sources of data? If your answer is YES, please complete Addendum 2.	YES	NO ✓
Question 3: Does your research involve the participation of or provision of services to communities? If your answer is YES, please complete Addendum 3.	YES	NO ✓
Question 4: If your research is sponsored, is there any potential for conflicts of interest? If your answer is YES, please complete Addendum 4.	YES	NO ✓

If you have answered YES to any of the above questions, please append a copy of your research proposal, as well as any interview schedules or questionnaires (Addendum 1) and please complete further addenda as appropriate.

I hereby undertake to carry out my research in such a way that

- there is no apparent legal objection to the nature or the method of research; and

- the research will not compromise staff or students or the other responsibilities of the University;
- the stated objective will be achieved, and the findings will have a high degree of validity;
- limitations and alternative interpretations will be considered;
- the findings could be subject to peer review and publicly available; and
- I will comply with the conventions of copyright and avoid any practice that would constitute plagiarism.

Signed by:

	Full name and signature	**Date**
Principal Researcher/Student:	**Samuel Mponwana**	

This application is approved by:

Supervisor (if applicable):	**A. Prof Paul Barendse**	
HOD (or delegated nominee): Final authority for all assessments with	**Janine Buxey**	
Chair: Faculty EIR Committee For applicants other than undergraduate		

11. REFERENCES

[1] P. Pillay and M. Manyage, "Loss of Life in Induction Machines Operating with Unbalanced Supplies," *IEEE Transactions On Energy Conversion ,* vol. 21, no. 4, pp. 813-822, December 2006.

[2] B. Herndler, "Non-Intrusive Efficiency Estimation of Induction Machines," University of Cape Town, Cape Town, October 2010.

[3] P. Walder and C. Brunner, "Energy efficiency policy opportunities for electric motor driven systems," Internaional Energy Agency , 2001.

[4] F. J. Ferreira, G. Boaming and A. de Almeida, "Reliability and Operation of High Efficiency Induction Motors," *PSEC-0008,* pp. 1-13, 2015.

[5] G. M. R. Work, "Report of Large Motor Reliability Survey of Industrial and Commercial Installations, Part II," *IEEE transaction of Industry Applications Society,* pp. 865-872, 1985.

[6] F. J. Ferreira, G. Baoming and A. T. de Almeida, "Reliability and Operation of High Efficiency Induction Motors," *51st Industrial & Commercial Power Systems Technical Conference (I&CPS),* pp. 5-13, 2015.

[7] F. Ferreira, "Strategies to Improve the Performance of Three Phase Induction Motor Driven Systems Ph.D Thesis," University of Coimbra, 2008.

[8] A. H. Bonnet, "Root Causes of AC motor Failures Analysis with a Focus on Shaft Failures," *IEEE Trans. on Ind. Appl,* vol. 36, pp. 1435-1448, Sept/Oct 2000.

[9] C. Bussmann, "Motor Protection Voltage Unbalance," Duke Energy Progress, Novemember 2014. [Online]. Available: www.bussman.com . [Accessed June 2016].

[10] I. Standard, *Electrical Insulation - Thermal Classification,* IEC60085, 2004.

[11] N. R. S. N. 0. -. 2. E. 1.3, "Minimum Standards Part 2," 13-16, 2001.

[12] C. Gajjar, "Non-Intrusive Efficiency Estimation of Induction Machines under Various Power Suplies," Univrsity of Cape Town , Cape Town, October 2013.

[13] H. Mzungu, S. A.B and M. Khan, "Comparison of Standard for Determining Losses and Efficiency of Three-Phase Induction Motors," *IEEE PES Power Africa,* July 2007.

[14] P. Sen, Principles of Electric Machines and Power Electronic, Kingston: John Wiley and Sons, 1997.

[15] G. C. Stone, I. Culbert, E. A. Boutler and H. Dhirani, Electrical Insulation For Rotating Machines Design, Evaluation, Aging, Testing and Repair Second Edition, New Jersey: John Wiley & Sons, 2014.

[16] S. Grubic, J. Aller, B. Lu and T. Habetler, "A Survey on Testing and Monitoring Methods for Stator Insulation Systems of Low-Voltage Induction Machines Focusing on Turn Insulation Problems," *IEEE Transaction on Industrial Electronics,* vol. 55, no. 12, pp. 4127- 4136, December 2008.

[17] T. Dakin, "Electrical Insulation Deterioration Treated as a Chemical Rate Phenomenon," *AIEE Tra s,* vol. 1, no. 67, pp. 113-122, 1948.

[18] E. Brancato, "Estimation of Life Expectancies of Motors," *IEEE Insulation Magazine,* vol. 49, no. 2, pp. 5-13, May/June 1992.

[19] J. Bryan, "Keeping it cool: A look at causes of motor overheating," Electrical Apparatus Service Association, March 2015.

[20] V. K. Kumar, S. S. Kumar and B. Praveena, "Soft Computing Based Diagnosis," *International journal of Computer and Electrical Engineering ,* vol. 2, no. 4, pp. 1793-8163, August 2010.

[21] A. Siddique, "A Review of Stator Fault Monitoring Techniques of Induction Motors," *IEEE TRANSACTIONS ON ENERGY CONVERSION, VOL. 20, NO. 1,* pp. 106-114, 2005.

[22] D. Sonje and R. Munje, "Rotor Cage Fault Detection in Induction motors by Motor Current Signature Analysis," *International Conference in Computational Intelligence ,* pp. 22-25, 2011.

[23] O. I. Okoro, B. Weidemann and O. Ojo, "An Efficient Thermal Model for Induction Machines," *Industry Applications Conference,* pp. 2477-2484, 2004.

[24] P. Mellor, "Lumped parameter thermal model for electrical machines of TEFC design," in *IEE Proceedings-B*, September 1991.

[25] N. Benamrouch, M. Bouheraoua and S. Haddad, "A Thermal Model for a TEFC Induction Motor Development and Sensitivity Analysis," *Electrical Power Components and Systems,* vol. 34, pp. 249-269, 2006.

[26] O. I. Okoro, "Steady and Transient States Thermal Analysis of a 7.5-kW Squirrel-Cage Induction Machine at Rated-Load Operation," *IEEE Transaction On Energy Conversion,* pp. VOL. 20, NO. 4, 2005.

[27] M. Miles and B. J, "Empirical Thermal Model for Invertor Driven Squirrel Cage Induction Machines," *IEEE Proc. Electrical Power Application,* vol. 141, no. 6, pp. 360-372, November 1994.

[28] J. Griffith, D. Sharma and R. McCoy, "Induction Motor Squirrel Cage Rotor Winding Thermal Analysis," *IEEE Transactions on Energy Conversion,* Vols. EC-1, no. 3, pp. 22-25, September 1986.

[29] C. Chan, L. Yan and K. Chau, "Analysis of Electromagnetic and Thermal Fields for Induction Motors During Starting," *IEEE Transactions on Energy Conversion,* vol. 9, no. 1, pp. 55-58, March 1994.

[30] J. Morena, F. Hildago and M. Martinez, "Realisation of tests to determine the parameters of thermal model of an induction machine," *IEEE Proc. Electr. Power App,* vol. 148, no. 5, pp. 393-397, September 2001.

[31] A. Siddique, G. Yadava and B. Singh, "Effect of Voltage Unbalance on Induction Motors," *International Symposium on Electrical Insulation,* pp. 26-29, 19-22 September 2004.

[32] J. De Abreu and E. A, "Induction Motor Loss of Life Due to Voltage Imbalance and Harmonics: A Preliminary Study," *EFEI,* vol. 4, no. 1, pp. 75-80, 2000.

[33] R. Sedaghati, M. Afroozi, Y. Nemati, A. Rohani, A. R. Toorani, N. Javidtash, A. Heydarzadegan and H. Sedaghati, "A Survey of Voltage Sags and Voltage swells Phenomena in Power Quality Problems," *International Journal of Scientific Research and Management ,* vol. 1, no. 9, pp. 458-462, 2013.

[34] I. 1159, "IEEE Standards: Recommended Practice for Monitoring Electric Power Quality," IEEE, 2009.

[35] NERSA, “Electricity Supply - Quality of Supply Part 2: Voltage Characterisitics, Compatability Levels, Limits and Assessment Methods,” NERSA, 2003.

[36] A. Dexters, W. Deprez and R. Belmans, “The Effect of Practical Operating Conditions on the Performance of Induction Machines,” in *19th International Conference on Electricity Distribution*, 21-24 May 2007.

[37] V.J.A and B.B, “Assessment of Voltage Unbalance,” *IEEE Trans on Power Delivery,* vol. 16, no. 4, pp. 782-788, 2001.

[38] D. Caetano Garcia, “DISSERTAÇÃO DE MESTRADO EM ENGENHARIA ELÉTRICA :Avaliação e Minimização Numérica do Desequilíbrio de Tensão: Estimativa por Análise de Sensibilidade Incremental e Soluções Analíticas,” Universidade De Brasilia , December 2007.

[39] J.-G. Kim, E.-W. Lee, D.-J. Lee and J.-H. Lee, “Comparison of Voltage Unbalance Factor by Line and Phase Voltage,” Electrical Machines and Systems , Nanjing, China, September 2005.

[40] J. Kim, L. Eun-Woong, L. Dong-Ju and L. Jong-Han, *Comparison of Voltage Unbalance Factor by Line and Phase Voltage,* Daejeon South Korea: Separtment of Electrical Enngineering: Chung-Nam National University , 1998-2001.

[41] C. Lee, “Effects of Voltage Unbalance on the Operation and Performance of a Three Phase Induction Motor,” *IEEE Transactions on Energy Conversion,* vol. 14, no. 2, pp. 202-203, 1999.

[42] A. Von Jouanne and B. Banerjee, “Assessment of voltage unbalance,” *IEEE Transactions on Power Delivery,* vol. 16, no. 4, pp. 782, 790, October 2001.

[43] Y.-J. Wang, “Analysis of Effects of Three Phase Voltage Unbalance on Induction Motors with Emphasis on the Angle of the Complex Voltage Unbalance Factor,” *IEEE Transactions on Energy Conversion,* vol. 16, no. 3, p. 271, September 2001.

[44] C.-Y. Lee, B.-K. Chen and W.-J. Lee, “Effects of various unbalanced voltages on the operation performance of an induction motor under the same voltage unbalance factor condition,” *Industrial and Commercial Power Systems Technical Conference,* pp. 51,59, 11-16 May 1997.

[45] V. Chaudhary and K. Sandhu, “Steady State Modelling of Induction Motor Operating with Unbalanced Supply System,” *WSEAS Transactions on Circuits and Systems* , vol. 5, no. 2, pp. 197-205, February 2009.

[46] G. P. Kini, R. C. Bansal and R. S. Aithal, “A Novel Approach Toward Interpretation and Application of Voltage Unbalance Factor,” *IEEE Transactions on Industrial Electronics* , vol. 54, no. 4, pp. 2315-2321, August 2007.

[47] P. G. Kini, R. C. Bansal and R. S. Aithal, “Performance analysis of centrifugal pump subjected to voltage variation and unbalance,” *IEEE Transactions on Industrial Electronics.*

[48] G. P. Kini, R. C. Bansal and R. S. Aithal, “Impact of voltage variation on three-phase induction motor performance,” *S.PAc.J.Nat.Sci,* vol. 24, pp. 45-50, 2006.

[49] Z. Kun, P. Ciufo and S. Perera, "Induction motors subject to regular voltage fluctuations: Stator and rotor current analysis from a heating perspective," *IEEE 15th International Conference oon Harmonics and Quality of Supply (ICHQP),* pp. 642,648, 17-20 June 2012.

[50] A. L. Van Wyk, "Effects of Voltage Unbalanced Supplies on Energy Efficient Motors," University of Cape Town , Cape Town , November 2010.

[51] E. C. Quispe, X. M. Lopez-Fernandez, M. A. M, A. Cardoso and J. A. Palacios, "Influence of Positive Sequence Voltage on the derating of Three Phase Induction Motors under Voltage Unbalance," *Electric Machines & Drives Conference,* 2013.

[52] M. Manyage, *Operation of Induction Machines in the Presence of Unbalnced Supplies,* Cape Town: University of Cape Town, 2001.

[53] W. Kersting and H. Phillips, "Phase Frame Analysis of Effects of Voltage Unbalance on Induction Machines," *IEEE Transactions on Industry Applications,* vol. 33, no. 2, pp. 415-420, 1997.

[54] P. Cummings, J. Dunki-Jacobs and R. Kerr, "Protection of Induction Motors Against Unbalanced Voltage Operation," *IEEE Transactions on Industry Applications,* Vols. IA-21, no. 4, May/June 1985.

[55] J. Williams, "Operation of 3-Phase Induction Motors on Unbalanced Voltages," *AIEE Transactions Power Apparatus and Systems,* vol. 73 pt III, pp. 125-133, April 1954.

[56] D. C. Garcia, A. L. Filho and M. A. Oliviera, "Voltage unbalance Numerical Evaluation and Minimization," *Electrical Power Research ,* vol. 79, no. 10, pp. 1441-1445, October 2009.

[57] "AEGIS Website," [Online]. Available: www.est-aegis.com/index.php. [Accessed 14 June 2016].

[58] I.-2. T. Specification, "Rotating electrical machines-Part 25: Guidance for the design and performance of a.c motors specifically designed for convertor supply 2nd Edition," 2007.

[59] A. Jacob, V. Jose and D. Sebastian, "Stator Fault Detection in Induction Motor Under Unbalanced Supply Voltage," *International Conference on Magnetics, Machines & Drives ,* 2014.

[60] Y.-J. Wang, "An analytical study on steady-state performance of an induction motor connected to unbalanced three-phase voltage," *Power Engineering Society ,* 2000.

[61] B. Amar, *An Investigation into the thermal modelling of induction motors,* Sheffield: University of Sheffield , June 1993.

[62] R. T.J, "The solution of heat equations in large electrical machines," *Poc. IME,* vol. 184, pp. 70-83, 1969-70.

[63] L. Popova, "Combined Electromagnetic and Thermal Design Platform for Totally Enclosed Induction Machines," Lappeenranta University of Technology, Lappennranta, 2010.

[64] A. Bousbaine, "An Investigation into The Thermal Modelling of Induction Motors," University of Sheffield , Sheffield , June 1993.

[65] K. Schwarz, "Survey of basic stray load losses in squirrel cage induction motors," *Proc. IEE,* vol. 111, pp. 1565-1573, 1964.

[66] E. Csanyi, “Cooling and Ventilation of Electric Motors (IC),” Electrical Engineering Portal , 8 August 2011 .

[67] M. Broussely, Y. Bertin and P. Lagonette, “Reduction and Optimisation of Thermal Models using Kirchoff Network Theory,” *International Journal of Thermal Sciences ,* vol. 42, no. 8, pp. 795-804, August 2003.

[68] S. E. Zocholl, E. O. Scheitzer and A. Aliaga-Zegarra, “Thermal Protection of Induction Motors Enhanced by Interactive Electrical and Thermal Models,” *IEEE Transaction on Power Apparatus and Systems,* Vols. PAS-103, no. 7, pp. 1749-1755, 7 July 1984.

[69] O. Souto, D. O. J and N. L, “Induction Motors Thermal Behaviour and Life Expectancy Under Non-Ideal Supply Conditions,” *Seminario Brasileiro Sobre Qualidade de Energia Electrica ,* pp. 899-904, 1999.

[70] C. Swarz, A. B. Sebitosi and L. Mthombeni, “Energy efficiency measurement methods for motors in industry in South Africa,” University of Cape Town, 2006.

[71] M. Yusuf, “Testing of impact of voltage unbalance and undervoltage on rural motors: literature and planning,” Eskom, 2009.

[72] H. Mzungu, “Impact of Armature Rewinding on Induction Motor Efficiency in South Africa, MSc Thesis,” University of Cape Town, Cape Town , Dec 2009.

[73] H. Auinger, “Determination and Designation of Efficiency of Electrical Machines,” *Power Engineerng Journal ,* pp. 20-23, February 1999.

[74] J. Schutzhold and W. Hoffmann, “Analysis of Temperature Dependence of Losses in Electrical Machines,” *Energy Conversion Congress and Exposition ,* pp. 3159-3165, 2013.

[75] A. Boglietti, R. Bojoi, A. Cavagnino and M. Lazarri, “Core Loss Estimation Method for PWM Invertor fed Induction Motors,” *IECON,* pp. 811-816, 23 December 2010.

[76] J. Schutzhold and W. Hoffman, “Analysis of the Temperature Dependence of Losses in Electrical Machines”.

[77] G. Muller, K. Vogt and B. Ponick, Berechnung elektrischer Maschinen, Wiley - VCH, 2008.

[78] P. Dimitriadis, “Effects of Overvoltage on Power Consumption,” Brunel University London , London , Septemper 2015.

[79] D. Paice, “Motor Thermal Protection by Continuous Monitoring of Winding Resistance,” *Industrial Electronics and Control Instrumentation ,* Vols. IEC-27, pp. 137-141, 1980.

[80] F. J. d. A. A. T. Ferreira, “Induction Motor Downsizing as Low-Cost Strategy to Save Energy,” *Journal of Cleaner Production,* pp. 117-131, 20 November 2011.

[81] E. da Casta Bortoni, “Motor Oversizing Outlook,” *Proceeding of International Conference on Electrical Machines and Systems (ICEMS),* pp. 1385-1396, October 2007.

[82] H. Zhang, “Online Thermal Monitoring Models for Induction Machines,” *IEEE TRANSACTIONS ON ENERGY CONVERSION,* vol. 30, no. 4, pp. 1279-1287, December 2015.

[83] N. Mohan, Power electronics coonverters, applications and design, John Wiley and Sons, 2003.

[84] H. Toliyat, Electric Machines modeling, condition monitoring and fault diagnosis, New York: Crc Press taylor and Francis Group, 2012.

[85] P. Zhang, "A Survey of Condition Monitoring and Protection Methods for Medium-Voltage Induction Motors," *IEEE TRANSACTIONS ON INDUSTRY APPLICATIONS, VOL. 47, NO. 1,,* pp. 34-46, 2011.

[86] N. B. Shaikh, "Online Off-Site Condition Monitoring Of Three Phase Induction Motor by Using GSM Technology," *International Journal of Emerging Technology and Advanced Engineering,* pp. 693-696, 2013.

[87] N. Mehala, "Condition monitoring and fault diagnosis on induction motors using motor current signature analysis," Kurukshetra, October 2010.

[88] T. A. Kawady, "Modeling and Experimental Investigation of Stator Winding Faults in Induction Motors," *Electric Power Components and Systems,,* pp. 599-611, 2009.

[89] Q. Yu, "Improved Lumped Parameter Thermal Model and Sensitivity Analysis for SR Drives," in *Electrical Machines (ICEM), 2010 XIX International Conference on*, 6-8 Sept. 2010.

[90] T. G. Habetler, "Online Adaptive Stator winding temperature estimator based on a hybrid thermal model for induction machines," in *2005 IEEE International Conference on Electric Machines and Drives*, 15-15 May 2005.

[91] "Frequency to voltage converter using LM331," 12 January 2010. [Online]. Available: www.circuitstoday.com/frequency-to-voltage-converter-using-lm331. [Accessed 5 August 2013].

[92] T. instruments, "Precision voltage to frequency converters," 2013.

[93] R. Obaid, T. Habetler and J. Stack , "Stator current analysis for bearing damage detection in induction motors," in *IEEE 4th International Symposium on Diagnostics for Electric Machines, Power Electronics and Drives (SDEMPED)* , Atlanta, 2003.

[94] B. Herndler, "Developing Methods for Implementing Faults on Induction Machines," Univeristy of Cape Town, Cape Town, 2008.

[95] P. Sen, Principles of Electric Machines and Power Electronics, John Wiley & Sons , 1997.

[96] W. Tong, Mechanical Design of Electric Motors, CRC Press, 2014.

12. Appendix A: Thermal Tests Results

12.1 Manufacturer A 7.5kW Thermal Tests Results

VUF= 0%

VR= 90%

Torque (Nm)	Load (%)	Pin (W)	Voltage (V)	Current (A)	Speed (rpm)	Temp (℃)
12.30	24.90	2237	359.2	7.66	1492.5	45.6
24.43	49.47	4213	358.41	9.50	1478.8	56.82
36.12	73.14	6211	357.61	12.58	1474.1	74.73
49.40	100.02	8659	356.47	16.40	1456.2	116.12

Table 12-1:Manufacturer A 7.5kW Thermal Tests at VUF=0% VR=90%

VUF= 0%

VR = 100%

Torque (Nm)	Load (%)	Pin (W)	Voltage (V)	Current (A)	Speed (rpm)	Temp (℃)
12.66	25.64	2402	398.43	8.873	1493.61	71.23
25.48	51.59	4494	397.69	10.533	1485.2	78.22
36.52	73.94	6328	397.02	12.455	1477.3	85.33
49.36	99.95	8598	396.09	15.348	1465	103.07

Table 12-2:Manufacturer A 7.5kW Thermal Tests at VUF=0% VR=100%

VUF= 0%

VR= 110%

Torque (Nm)	Load (%)	Pin (W)	Voltage (V)	Current (A)	Speed (rpm)	Temp (℃)
12.25	24.81	2619	439.03	11.308	1495	67.21
24.20	49.00	4534	438.5	12.182	1488.2	75.25
36.62	74.14	6557	437.82	13.695	1481.3	85.14
49.05	99.31	8675	437.08	15.621	1473.1	99.88

Table 12-3:Manufacturer A 7.5kW Thermal Tests at VUF=0% VR=110%

VUF= 1%
VR= 90%

Torque (Nm)	Load (%)	Pin (W)	Voltage (V)	Current (A)	Speed (rpm)	Temp (°C)
12.285	24.87	2242	358.05	7.689	1492.3	46.08
24.653	49.91	4273	357.18	9.642	1478.3	59.38
36.752	74.41	6340	356.39	12.832	1473.3	77.18
49.06	99.33	8621	355.35	16.386	1456.1	117.05

Table 12-4:Manufacturer A 7.5kW Thermal Tests at VUF=1% VR=90%

VUF= 1%
VR= 100%

Torque (Nm)	Load (%)	Pin (W)	Voltage (V)	Current (A)	Speed (rpm)	Temp (°C)
12.34	24.97	2358	396.89	8.87	1493.8	51.6
24.61	49.83	4354	396.16	10.17	1483.3	64.11
36.17	73.23	6277	395.48	12.47	1478.2	74.52
49.66	100.55	8638	394.55	15.52	1466.7	106.45

Table 12-5:Manufacturer A 7.5kW Thermal Tests at VUF=1% VR=100%

VUF= 1%
VR= 110%

Torque (Nm)	Load (%)	Pin (W)	Voltage (V)	Current (A)	Speed (rpm)	Temp (°C)
12.33	24.97	2724	443.12	11.83	1494.8	72.91
24.91	50.43	4775	442.49	12.48	1485.9	84.11
36.81	74.531	6735	441.88	14.18	1481.6	95.81
49.64	100.50	8953	441.06	16.03	1470.3	104.11

Table 12-6:Manufacturer A 7.5kW Thermal Tests at VUF=1% VR=110%

VUF= 2%
VR= 90%

Torque (Nm)	Load (%)	Pin (W)	Voltage (V)	Current (A)	Speed (rpm)	Temp (°C)
12.64	25.60	2324	360.25	7.904	1491.9	49.08
24.72	50.06	4372	359.3	9.91	1477.9	61.44
37.18	75.28	6489	358.46	13.02	1470	81.92
49.23	99.68	8705	357.46	16.51	1455.8	121.68

Table 12-7:Manufacturer A 7.5kW Thermal Tests at VUF=2% VR=90%

VUF= 2%
VR= 100%

Torque (Nm)	Load (%)	Pin (W)	Voltage (V)	Current (A)	Speed (rpm)	Temp (℃)
12.27	24.83	2391	399.17	9.11	1493.5	55.45
24.99	50.59	4507	398.34	10.55	1482.9	67.91
36.07	73.03	6352	397.7	12.76	1478.2	80.94
46.42	93.99	8200	396.91	14.90	1466	101.69

Table 12-8:Manufacturer A 7.5kW Thermal Tests at VUF=2% VR=100%

VUF= 2%
VR= 110%

Torque (Nm)	Load (%)	Pin (W)	Voltage (V)	Current (A)	Speed (rpm)	Temp (℃)
12.67	25.64	2753	438.3	11.587	1494.7	72.45
24.77	50.15	4740	437.65	12.216	1485.7	82.23
37.14	75.20	6762	437.02	14.059	1481	94.38
49.33	99.87	8854	436.27	15.972	1471.7	115.06

Table 12-9:Manufacturer A 7.5kW Thermal Tests at VUF=2% VR=110%

VUF= 3%
VR= 90%

Torque (Nm)	Load (%)	Pin (W)	Voltage (V)	Current (A)	Speed (rpm)	Temp (℃)
12.51	25.32	2333	359.9	7.827	1490	52.11
24.58	49.77	4384	359.01	10.264	1479.2	67.23
37.05	75.019	6579	358.08	13.238	1467.1	94.16
49.21	99.63	8833	357.09	16.786	1453.1	130.1

Table 12-10:Manufacturer A 7.5kW Thermal Tests at VUF=3% VR=90%

VUF= 3%
VR= 100%

Torque (Nm)	Load (%)	Pin (W)	Voltage (V)	Current (A)	Speed (rpm)	Temp (℃)
12.35	24.99	2444	398.92	9.103	1492.1	67.56
24.79	50.19	4540	398.17	10.896	1483.5	77.16
37.82	76.58	6773	397.33	13.321	1473.6	88.13
49.36	99.95	8823	396.53	15.948	1464.1	118.13

Table 12-11:Manufacturer A 7.5kW Thermal Tests at VUF=3% VR=100%

VUF= 3%
VR= 110%

Torque (Nm)	Load (%)	Pin (W)	Voltage (V)	Current (A)	Speed (rpm)	Temp (℃)
12.23	24.75	2757	439.19	11.57	1493.3	76.33
24.59	49.79	4771	438.53	12.657	1486.1	88.13
37.25	75.42	6913	437.82	14.3	1478.5	99.22
49.59	100.40	9049	437.06	16.352	1470.3	126.14

Table 12-12:Manufacturer A 7.5kW Thermal Tests at VUF=3% VR=100%

12.2 Manufacturer B 7.5kW Thermal Tests Results

VUF= 0%
VR= 90%

Torque (Nm)	Load (%)	Pin (W)	Voltage (V)	Current (A)	Speed (rpm)	Temp (℃)
12.332	24.97	2171	359.59	6.473	1489.2	41.09
24.607	49.82	4206.6	358.75	9.109	1477	56.82
37.8	76.53	6464.6	357.88	12.38	1459.2	78.31
49.82	100.87	8710	356.38	16.193	1434.2	89.99

Table 12-13:Manufacturer B 7.5kW Thermal Tests at VUF=0% VR=90%

VUF= 0%
VR= 100%

Torque (Nm)	Load (%)	Pin (W)	Voltage (V)	Current (A)	Speed (rpm)	Temp (℃)
12.39	25.08	2287.9	399.71	7.593	1491.6	45.96
24.32	49.24	4227.9	399.13	9.354	1481.2	57.81
36.35	73.59	5589.72	398.52	11.601	1468.5	70.79
47.08	95.32	8087	397.75	14.251	1462.3	98.83

Table 12-14:Manufacturer B 7.5kW Thermal Tests at VUF=0% VR=100%

VUF= 0%
VR= 110%

Torque (Nm)	Load (%)	Pin (W)	Voltage (V)	Current (A)	Speed (rpm)	Temp (℃)
12.358	25.02	2497.9	439.73	9.697	1493	61.24
24.538	49.68	4444.6	439.22	10.744	1484	65.95
37.14	75.20	6510	438.5	12.502	1474.5	83.26
49.516	100.26	8646	437.97	14.718	1460	102.72

Table 12-15:Manufacturer B 7.5kW Thermal Tests at VUF=0% VR=110%

VUF= 1%
VR= 90%

Torque (Nm)	Load (%)	Pin (W)	Voltage (V)	Current (A)	Speed (rpm)	Temp (℃)
12.396	25.10	2180.5	358.39	6.55	1489.7	42.75
26.882	54.43	4558.3	357.51	9.528	1474	59.51
37.071	75.06	6335.1	356.81	12.205	1459.8	82.53
49.384	99.99	8721.1	355.74	16.152	1427.8	124.77

Table 12-16:Manufacturer B 7.5kW Thermal Tests at VUF=1% VR=90%

VUF= 1%
VR= 100%

Torque (Nm)	Load (%)	Pin (W)	Voltage (V)	Current (A)	Speed (rpm)	Temp (℃)
12.525	25.36	2282	397.42	7.547	491.4	70.78
24.003	48.60	4133	396.78	9.122	1481.3	77.7
37.062	75.04	6325	395.98	11.797	1469.2	92.64
49.552	100.33	8557	395.17	14.891	1452.2	101.55

Table 12-17:Manufacturer B 7.5kW Thermal Tests at VUF=1% VR=100%

VUF= 1%
VR= 110%

Torque (Nm)	Load (%)	Pin (W)	Voltage (V)	Current (A)	Speed (rpm)	Temp (℃)
11.788	23.87	2497.9	443.97	10.1	1492.2	68.02
24.595	49.80	4444.6	443.3	11.19	1483.4	76.35
38.1	77.14	6510	442.57	12.967	1472.5	91.92
49.4	100.02	8646	441.9	14.974	1461.1	115.34

Table 12-18:Manufacturer B 7.5kW Thermal Tests at VUF=1% VR=110%

VUF= 2%
VR= 90%

Torque (Nm)	Load (%)	Pin (W)	Voltage (V)	Current (A)	Speed (rpm)	Temp (℃)
12.378	25.06	2218	360.49	6.754	1489.2	45.25
24.04	48.67	4151	359.78	9.069	1477.2	69.33
37.496	75.92	6485	358.82	12.433	1455.6	80.61
47.325	95.82	8390	357.96	15.528	1430.2	125.88

Table 12-19:Manufacturer B 7.5kW Thermal Tests at VUF=2% VR=90%

VUF= 2%
VR= 100%

Torque (Nm)	Load (%)	Pin (W)	Voltage (V)	Current (A)	Speed (rpm)	Temp (℃)
12.337	24.98	2327	399.63	7.964	1491.6	53.41
24.423	49.45	4336	398.98	9.335	1475.3	66.71
37.023	74.96	6400	398.23	12.036	1469.5	83.04
49.49	100.20	8651	397.37	15.049	1450.9	119.63

Table 12-20:Manufacturer B 7.5kW Thermal Tests at VUF=2% VR=100%

VUF= 2%
VR= 110%

Torque (Nm)	Load (%)	Pin (W)	Voltage (V)	Current (A)	Speed (rpm)	Temp (℃)
12.575	25.46	2605	439.09	9.925	1491.6	68.51
24.922	50.46	4580	438.44	11.052	1482.7	77.64
37.66	76.25	6692	437.72	12.788	1471.8	93.79
49.82	100.87	8810	437	15.034	1459.1	119.33

Table 12-21:Manufacturer B 7.5kW Thermal Tests at VUF=2% VR=110%

VUF= 3%
VR= 90%

Torque (Nm)	Load (%)	Pin (W)	Voltage (V)	Current (A)	Speed (rpm)	Temp (℃)
12.266	24.83	2232	360.29	7.026	1489.1	48.38
24.47	49.54	4249	359.55	9.409	1475.7	65.86
38.167	77.28	6625	358.56	12.77	1456.7	91.39
49.68	100.59	8819	357.63	16.395	1432.9	135.2

Table 12-22:Manufacturer B 7.5kW Thermal Tests at VUF=3% VR=90%

VUF= 3%
VR= 100%

Torque (Nm)	Load (%)	Pin (W)	Voltage (V)	Current (A)	Speed (rpm)	Temp (℃)
12.537	25.38	2398	399.36	8.302	1490.9	66.56
24.242	49.08	4315	398.73	9.857	1480.3	78.21
37.27	75.46	6507	397.92	12.169	1465	85.66
49.852	100.94	8825	397.01	15.258	1442.9	119.25

Table 12-23: Manufacturer B 7.5kW Thermal Tests at VUF=3% VR=100%

VUF= 3%
VR= 110%

Torque (Nm)	Load (%)	Pin (W)	Voltage (V)	Current (A)	Speed (rpm)	Temp (℃)
12.511	25.33	2657	439.9	10.51	1492.2	75.31
25.168	50.96	4701	439.27	11.399	1481.7	86.49
37.605	76.14	6751	438.63	12.997	1471.1	97.36
49.588	100.40	8849	437.92	15.16	1458.2	125.29

Table 12-24:Manufacturer B 7.5kW Thermal Tests at VUF=3% VR=110%

12.3 Manufacturer A 11kW Thermal Tests Results

VUF= 0%
VR= 90%

Torque (Nm)	Load (%)	Pin (W)	Voltage (V)	Current (A)	Speed (rpm)	Temp (℃)
17.20	23.86	2812	359.99	9.46	1494.9	44.13
35.84	50.13	6100	359.33	13.14	1484.9	57.55
54.58	76.34	9237	355.45	17.83	1470.1	76.66
71.33	99.76	12204	357.63	22.68	1458.4	106.55

Table 12-25:Manufacturer A 11kW Thermal Tests at VUF=0% VR=90%

VUF= 0%
VR= 100%

Torque (Nm)	Load (%)	Pin (W)	Voltage (V)	Current (A)	Speed (rpm)	Temp (℃)
17.87	24.84	3212	399.53	10.54	1493.2	54.12
35.70	9.62	6113	398.23	13.16	1485.2	67.13
54.81	76.18	9289	396.81	17.28	1476.8	78.89
76.14	105.83	13022	393.42	22.62	1460.3	114.12

Table 12-26:Manufacturer A 11kW Thermal Tests at VUF=0% VR=100%

VUF= 0%
VR= 110%

Torque (Nm)	Load (%)	Pin (W)	Voltage (V)	Current (A)	Speed (rpm)	Temp (℃)
17.85	24.82	3226	439.78	13.126	1495.4	67.14
35.53	49.38	6312	437.99	15.04	1489.8	79.12
53.97	75.01	9365	443.42	17.88	1481.7	90.12
71.98	100.05	12406	441.9	21.00	1472.3	110.67

Table 12-27:Manufacturer A 11kW Thermal Tests at VUF=0% VR=100%

VUF= 1%
VR= 90%

Torque (Nm)	Load (%)	Pin (W)	Voltage (V)	Current (A)	Speed (rpm)	Temp (℃)
17.77	24.70	3146	358.42	9.157	1489.6	48.13
37.89	52.67	6457	356	13.721	1482.7	61.34
53.64	74.55	9099	354.64	17.718	1471.8	80.14
71.75	99.73	12416	353.24	23.203	1450.7	119.98

Table 12-28:Manufacturer A 11kW Thermal Tests at VUF=1% VR=90%

VUF= 1%
VR= 100%

Torque (Nm)	Load (%)	Pin (W)	Voltage (V)	Current (A)	Speed (rpm)	Temp (℃)
17.939	24.93	3262	399.04	10.596	1493	54.13
35.94	49.95	6170	397.56	13.064	1483.4	67.45
54.575	75.85	9281	393.91	17.309	1479.7	76.13
72.764	101.13	12439	394.42	21.478	1463.1	109.88

Table 12-29:Manufacturer A 11kW Thermal Tests at VUF=1% VR=100%

VUF= 1%
VR= 110%

Torque (Nm)	Load (%)	Pin (W)	Voltage (V)	Current (A)	Speed (rpm)	Temp (℃)
17.77	24.70	3555	443.03	13.783	1494.5	69.34
35.55	49.41	6435	441.84	15.524	1488.8	81.78
53.25	74.02	9334	440.63	18.099	1482.7	99.67
71.60	99.52	12400	439.27	21.397	1475.9	109.88

Table 12-30:Manufacturer A 11kW Thermal Tests at VUF=1% VR=110%

VUF= 2%
VR= 90%

Torque (Nm)	Load (%)	Pin (W)	Voltage (V)	Current (A)	Speed (rpm)	Temp (℃)
17.22	23.93	3087	359.73	9.296	1490.3	54.12
38.05	52.89	6540	358	13.846	1480.6	64.12
53.64	74.56	9198	356.56	17.901	1470.6	82.12
71.68	99.63	12434	354.64	23.308	1455	120.14

Table 12-31:Manufacturer A 11kW Thermal Tests at VUF=2% VR=90%

VUF= 2%
VR= 100%

Torque (Nm)	Load (%)	Pin (W)	Voltage (V)	Current (A)	Speed (rpm)	Temp (℃)
17.06	23.71	3208	398.88	11.082	1494.1	54.14
38.39	53.37	6735	396.04	14.4	1486	68.18
54.08	75.17	9332	394.77	17.422	1476.3	83.12
71.90	99.94	12397	394.42	21.636	1465.5	108.12

Table 12-32:Manufacturer A 11kW Thermal Tests at VUF=2% VR=100%

VUF= 2%
VR= 110%

Torque (Nm)	Load (%)	Pin (W)	Voltage (V)	Current (A)	Speed (rpm)	Temp (℃)
17.94	24.94	3577	438.22	13.046	1492.9	73.13
35.61	49.50	6467	436.99	15.527	1489.8	82.12
53.79	74.76	9433	435.75	17.955	1480.5	94.15
71.93	99.98	12502	434.28	21.291	1471.4	116.89

Table 12-33:Manufacturer A 11kW Thermal Tests at VUF=2% VR=110%

VUF= 3%
VR= 90%

Torque (Nm)	Load (%)	Pin (W)	Voltage (V)	Current (A)	Speed (rpm)	Temp (℃)
17.88	24.85	3270	359.46	10.263	1490	49.89
36.25	50.38	6340	357.86	14.067	1480	66.98
54.14	75.26	9380	356.3	18.613	1480	91.33
71.98	100.04	12500	354.67	23.83	1470	127.1

Table 12-34:Manufacturer A 11kW Thermal Tests at VUF=3% VR=90%

VUF= 3%
VR= 100%

Torque (Nm)	Load (%)	Pin (W)	Voltage (V)	Current (A)	Speed (rpm)	Temp (℃)
17.77	24.70	3360	398.46	11.056	1491.1	69.67
38.25	53.16	6779	396.93	14.696	1484.8	78.31
53.85	74.85	9391	395.83	17.733	1476.3	89.3
71.90	99.94	12518	394.15	21.946	1464.2	119.4

Table 12-35:Manufacturer A 11kW Thermal Tests at VUF=3% VR=100%

VUF= 3%
VR= 110%

Torque (Nm)	Load (%)	Pin (W)	Voltage (V)	Current (A)	Speed (rpm)	Temp (℃)
17.45	24.26	3624	439.05	14.278	1494.7	71.1
35.71	49.63	6566	437.84	15.98	1489	89.34
53.67	74.60	9540	43655	18.632	1482.8	101.23
71.95	100.01	12618	435.2	21.954	1476	122.44

Table 12-36:Manufacturer A 11kW Thermal Tests at VUF=3% VR=110%

12.4 Manufacturer B 11 kW Thermal Tests Results

VUF= 0%
VR= 90%

Torque (Nm)	Load (%)	Pin (W)	Voltage (V)	Current (A)	Speed (rpm)	Temp (℃)
17.9	24.88	3252	358.83	9.69	1490.6	43.14
35.41	49.21	6072	357.39	13.15	1481	58.12
53.56	74.44	9102	355.82	17.81	1469.9	77.99
71.81	99.81	12245	354.08	23.19	1457.4	108.95

Table 12-37:Manufacturer B 11kW Thermal Tests at VUF=0% VR=90%

VUF= 0%
VR= 100%

Torque (Nm)	Load (%)	Pin (W)	Voltage (V)	Current (A)	Speed (rpm)	Temp (℃)
17.61	24.48	3334	398.88	11.12	1492.7	48.78
34.71	48.24	6058	397.65	13.56	1485.6	59.76
53.80	74.78	9185	396.21	17.39	1477.1	74.12
71.64	99.56	12188	394.74	21.64	1468.1	110.12

Table 12-38:Manufacturer B 11kW Thermal Tests at VUF=0% VR=100%

VUF= 0%
VR= 110%

Torque (Nm)	Load (%)	Pin (W)	Voltage (V)	Current (A)	Speed (rpm)	Temp (℃)
17.74	24.66	3585	439.26	13.96	1493.7	59
35.70	49.62	6416	438.08	15.63	1487.5	67.8
53.32	74.10	9272	436.87	18.21	1480.9	85.13
71.71	99.67	12324	435.54	21.59	1473.6	107.46

Table 12-39:Manufacturer B 11kW Thermal Tests at VUF=0% VR=100%

VUF= 1%
VR= 90%

Torque (Nm)	Load (%)	Pin (W)	Voltage (V)	Current (A)	Speed (rpm)	Temp (℃)
17.14	23.82	3136	357.55	9.64	1490.6	45.67
35.50	49.33	6101	355.93	13.23	1480.1	63.12
53.92	74.94	9186	354.25	18.00	1468.4	84.44
71.69	99.64	12266	352.55	23.30	1455.7	124.12

Table 12-40:Manufacturer B 11kW Thermal Tests at VUF=1% VR=90%

VUF= 1%
VR= 100%

Torque (Nm)	Load (%)	Pin (W)	Voltage (V)	Current (A)	Speed (rpm)	Temp (℃)
17.63	24.50	3322	396.66	11.00	1492	68.13
35.85	49.83	6238	395.27	13.69	1483.8	75.12
53.68	74.60	9172	393.87	17.34	1474.9	93.13
71.79	99.77	12229	392.4	21.70	1465.2	112.13

Table 12-41:Manufacturer B 11kW Thermal Tests at VUF=1% VR=100%

VUF= 1%
VR= 110%

Torque (Nm)	Load (%)	Pin (W)	Voltage (V)	Current (A)	Speed (rpm)	Temp (℃)
17.92	24.90	3773	443.02	14.96	1493.2	64.54
36.41	50.60	6709	441.76	16.53	1486.4	77.12
52.76	73.33	9363	440.63	18.79	1480.1	93.13
71.61	99.53	12482	439.26	22.10	1472.3	117.45

Table 12-42:Manufacturer B 11kW Thermal Tests at VUF=1% VR=110%

VUF= 2%
VR= 90%

Torque (Nm)	Load (%)	Pin (W)	Voltage (V)	Current (A)	Speed (rpm)	Temp (℃)
17.21	23.92	3205	359.65	9.97	1490.1	47.23
36.18	50.28	6270	358.03	13.61	1479	73.12
53.98	75.02	9263	356.42	18.19	1467.2	84.124
71.77	99.75	12349	354.74	23.41	1454	127.56

Table 12-43:Manufacturer B 11kW Thermal Tests at VUF=2% VR=90%

VUF= 2%
VR= 100%

Torque (Nm)	Load (%)	Pin (W)	Voltage (V)	Current (A)	Speed (rpm)	Temp (°C)
17.35	24.11	3374	399.26	11.6	1491.8	54.9
35.50	49.33	6283	397.84	14.06	1483.5	67.87
53.64	74.55	9261	396.42	17.66	1474.3	86.74
71.46	99.32	12301	394.96	21.91	1464.5	120.01

Table 12-44:Manufacturer B 11kW Thermal Tests at VUF=2% VR=100%

VUF= 2%
VR= 110%

Torque (Nm)	Load (%)	Pin (W)	Voltage (V)	Current (A)	Speed (rpm)	Temp (°C)
17.97	24.98	3753	438.12	14.54	1492.9	67.13
35.60	49.47	6555	436.92	16.09	1486.2	76.89
53.98	75.02	9535	435.61	18.74	1478.8	95.67
71.65	99.58	12472	434.32	21.99	1471.2	124.5

VUF= 3%
VR= 90%

Torque (Nm)	Load (%)	Pin (W)	Voltage (V)	Current (A)	Speed (rpm)	Temp (°C)
17.90	24.88	3408	359.31	10.85	1489.4	48.45
35.75	49.68	6304	357.75	13.96	1478.7	67.12
54.46	75.69	9443	356.06	18.68	1466.1	89.14
71.51	99.39	12423	354.42	23.69	1453.1	129.99

Table 12-45:Manufacturer B 11kW Thermal Tests at VUF=3% VR=90%

VUF= 3%
VR= 100%

Torque (Nm)	Load (%)	Pin (W)	Voltage (V)	Current (A)	Speed (rpm)	Temp (°C)
16.90	23.49	3419	398.51	12.54	1491.7	65.13
35.81	49.77	6452	397.06	14.73	1482.6	76.13
53.45	74.29	9370	395.63	18.12	1473.4	88.34
72.47	100.72	12603	394.05	22.58	1462.5	123.4

Table 12-46:Manufacturer B 11kW Thermal Tests at VUF=3% VR=110%

VUF= 3%
VR= 110%

Torque (Nm)	Load (%)	Pin (W)	Voltage (V)	Current (A)	Speed (rpm)	Temp (℃)
17.82	24.77	3902	438.82	15.70	1492.6	74.13
35.71	49.63	6741	437.58	17.00	1485.5	87.33
53.69	74.62	9667	436.28	19.37	1477.9	99.67
71.55	99.44	12635	434.97	22.52	1470	126.3

Table 12-47:Manufacturer B 11kW Thermal Tests at VUF=3% VR=110%

12.5 Thermal Model Results

VU (%)	VR (%)	LC	Core Losses (W)	$T_{Measured}$			$T_{Predicted}$		
				A	B	C	A	B	C
2	90	23.93	249,12	58.31	47.92	45.20	59.60	49.05	42.64
		52.89		69.44	68.15	46.06	72.33	67.88	48.88
		74.56		109.79	83.68	54.10	108.75	86.23	56.01
		99.63		133.15	122.00	107.2	130.58	123.17	104.13
	110	24.94	534,12	77.56	78.55	65.03	79.09	76.59	63.08
		49.50		95.08	83.55	78.23	93.83	81.57	79.00
		74.76		101.36	89.06	81.47	103.08	92.27	83.05
		99.98		127.89	111.08	108.44	101.02	109.82	105.98
3	90	24.85	313,11	67.25	54.31	40.01	71.63	51.09	43.01
		50.38		75.32	62.18	53.66	77.05	68.79	54.61
		75.26		109.55	85.29	71.18	105.00	82.15	70.89
		100.04		138.22	125.22	119.99	134..66	123.00	121.5
	100	24.70	434,01	79.85	64.77	58.00	82.05	63.01	56.87
		53.16		89.34	75.55	63.08	91.79	74.66	64.08
		74.85		99.50	85.01	80.11	102.40	84.78	81.08
		99.94		127.00	118.05	109.00	125.05	120.16	106.89

Table 12-48: 11kW Manufacturer A Induction Machine Thermal Model Test under unbalanced Voltage Conditions

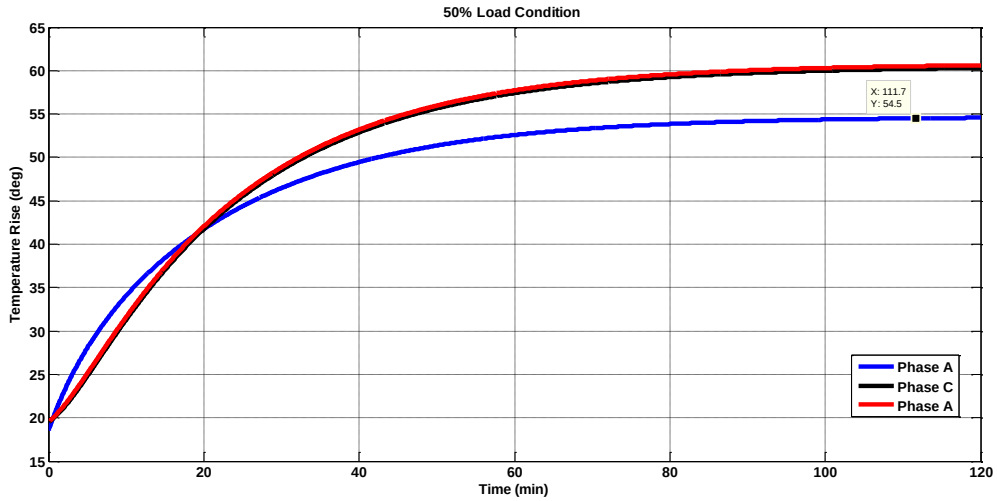

Figure 12-1: Manufacturer A 7.5kW Temperature Rise Curves for VUF=1% LC=50% VR=90%

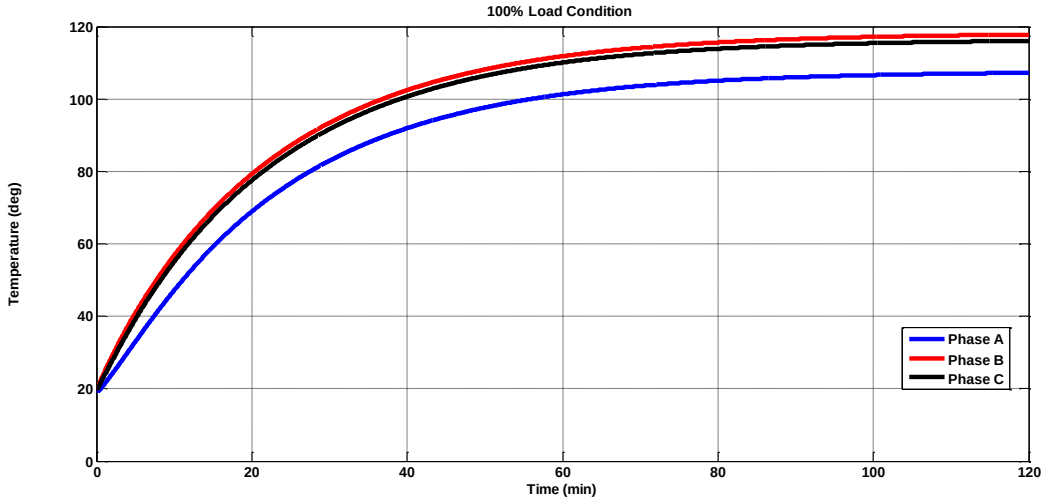

Figure 12-2: Manufacturer A 7.5kW Temperature Rise Curves for VUF=1% LC=100% VR=90%

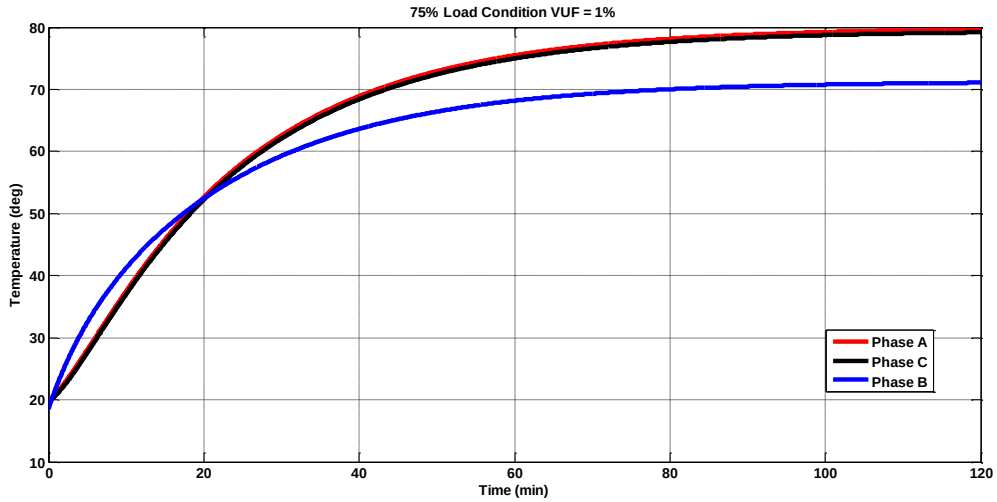

Figure 12-3: Manufacturer A 7.5kW Temperature Rise Curves for VUF=1% LC=100% VR=100%

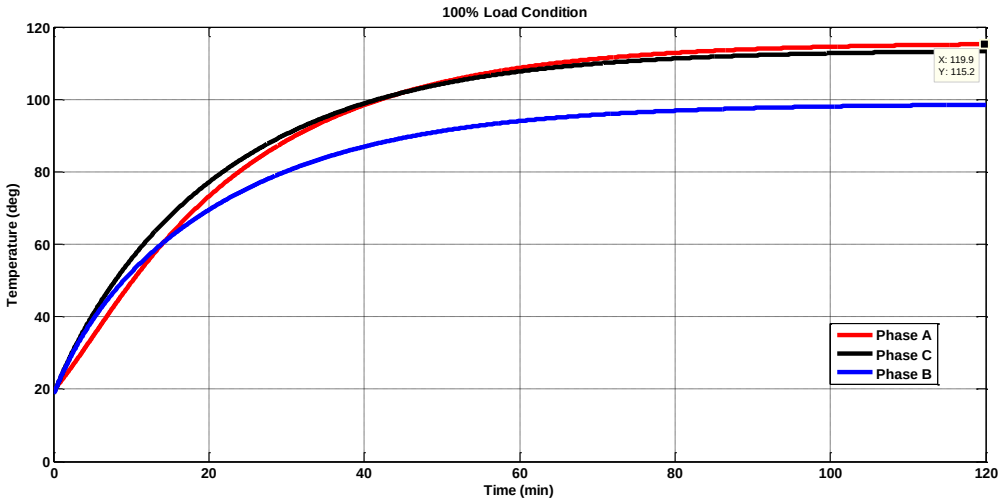

Figure 12-4: Manufacturer A 7.5kW Temperature Rise Curves for VUF=1% LC=100% VR=110%

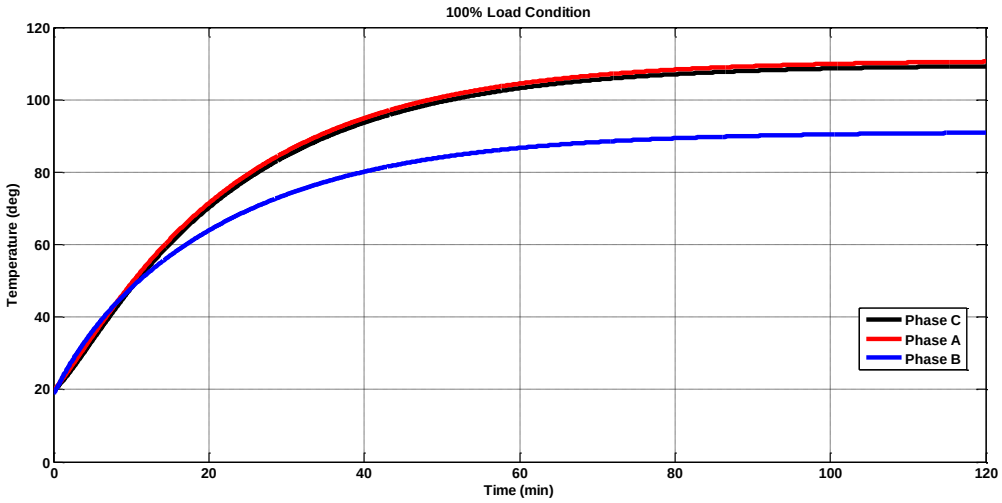

Figure 12-5: Manufacturer B 7.5kW Temperature Rise Curves for VUF=1% LC=100% VR=100%

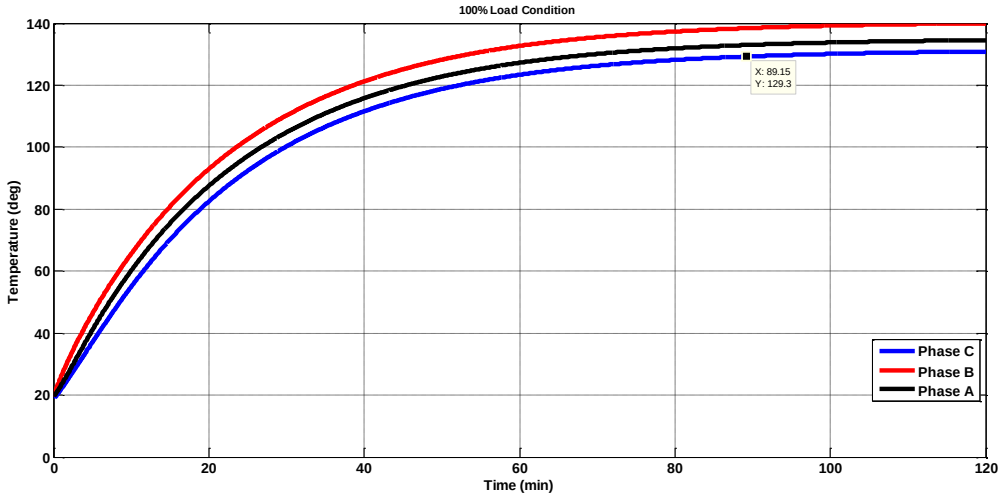

Figure 12-6: Manufacturer B 7.5kW Temperature Rise Curves for VUF=3% LC=100% VR=90%

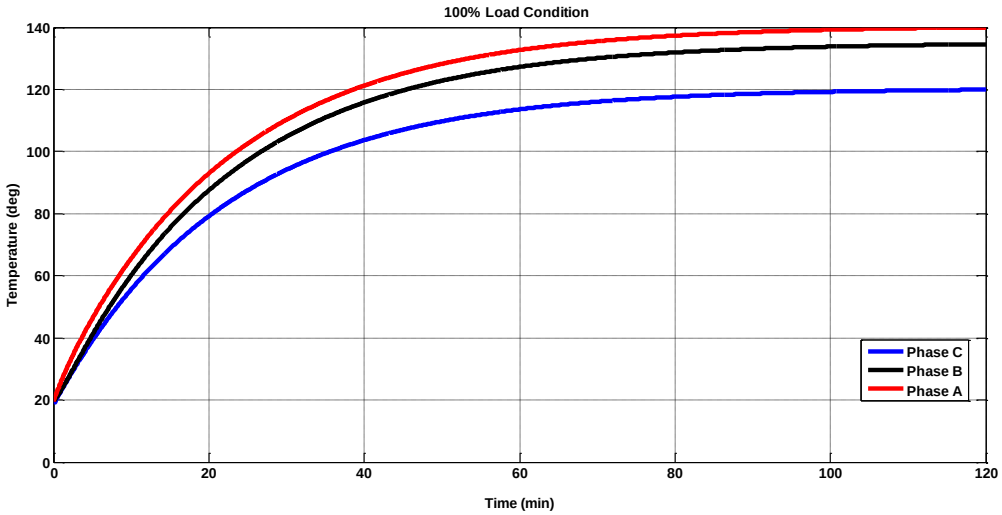

Figure 12-7: Manufacturer B 11kW Temperature Rise Curves for VUF=3% LC=100% VR=90%

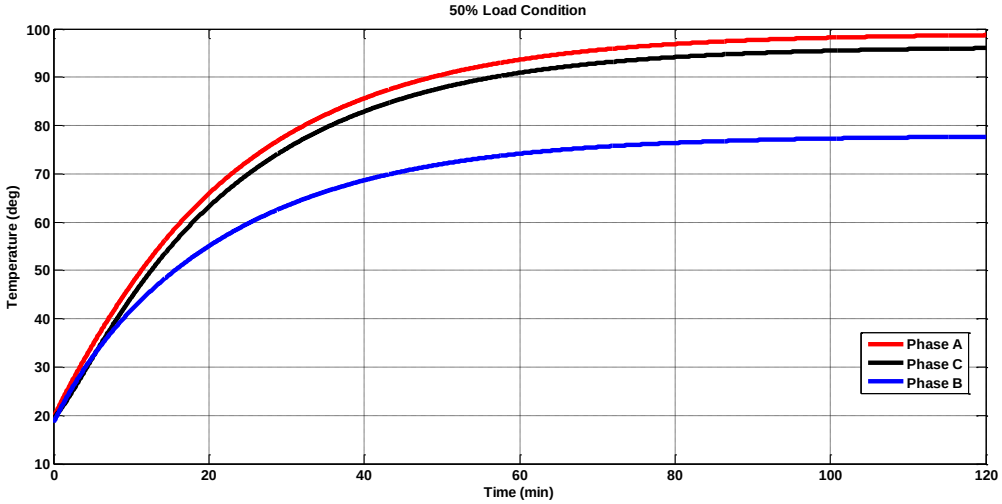

Figure 12-8: Manufacturer A 7.5kW Temperature Rise Curves for VUF=3% LC=50% VR=90%

13. Appendix B: Source Code

A1 Runge-Kutta Octave/Matlab Implementation

```
--------------------------------------------------------------------------
%Runge kutta for Temperature Prediction
%clear
%clc
%close all
%--------------------------------------------------------------------------
%Step-size  and length of analysis
timestep=0.1;
time=0:timestep:120
theta_vec=zeros(4,length(time));
%--------------------------------------------------------------------------
%Initial values of the motor temperature
theta1=18.6;
theta2=19.5;
theta3=18.5;
theta4=18.5;
theta_vec(:,1)=[theta1,theta2,theta3,theta4];
%--------------------------------------------------------------------------
%Runge Kutta for loop
for idx=1:length(time)-1
    idx/length(time)*100
    k1=Derivative_Function(theta_vec(:,idx));
    k2=Derivative_Function(theta_vec(:,idx)+k1*timestep/2);
    k3=Derivative_Function(theta_vec(:,idx)+k2*timestep/2);
    k4=Derivative_Function(theta_vec(:,idx)+k3*timestep);
    kRK4=(1/6)*(k1+2*k2+2*k3+k4);
    theta_vec(:,idx+1)=theta_vec(:,idx)+kRK4*timestep;


end
%--------------------------------------------------------------------------
%Temperature plot of all the locations
for jdx=1:4
figure()
plot(time,theta_vec(jdx,:),'-','linewidth',1)
ylabel(['Temperature',num2str(jdx),'(C)'])
xlabel('Time')
set(gca,'fontsize',8)
set(gcf,'paperunits','centimeters')
set(gcf,'papersize',[5 5])
set(gcf,'paperposition',[0 0 5 5 ])
end
```

Table A 1 Fourth Order Runge Kutta Matlab Code

```
function dthetadt_vec = Derivative_Function(theta_vec)
%--------------------------------------------------------------------------
%input parameters
%Input Power/Heat Sources
P1=59.4;
P2=30.3;
P3=41.85;
P4=199.03;
```

```
%-------------------------------------------------------------------------
%Thermal Capacitance
C1=16.2;
C2=16.2;
C3=16.2;
C4=99.4;
%-------------------------------------------------------------------------
%Thermal Conductance
G14=2.38;G41=2.38;
G24=2.38;G42=2.38;
G34=2.38;G43=2.38;
G4A=7.275;
G12=2.01;G21=2.01;
G13=2.01;G31=2.01;
G23=2.01;G32=2.01;
Cmat=diag([C1,C2,C3,C4]);
thetaA=21.5;
%-------------------------------------------------------------------------
%Conductance matrix
G11=G12+G13+G14;
G22=G21+G23+G24;
G33=G31+G32+G34;
G44=G41+G42+G43+G4A;
Gmat=[G11,-G12,-G13,-G14; -G21,G22,-G23,-G24;-G31,-G32,G33,-G34;-G41,-G42,-G43,G44;]
%-------------------------------------------------------------------------
%Initial Temperature Values
theta1=18.6;
theta2=19.5;
theta3=18.5;
theta4=18.5;
theta_vec(:,1)=[theta1,theta2,theta3,theta4];
%-------------------------------------------------------------------------
%Derivative Function of Time
dthetadt_vec=inv(Cmat)*[P1;P2;P3;P4+thetaA*G4A]-inv(Cmat)*Gmat*theta_vec;
```

Table A 2 Temperature Approximation ODES functions Matlab Code

A2 Voltage Unbalance Octave/Matlab Implementation

```
function k = modK(par)
% modK() takes 3 phasors as input, and calculates their
% K factor (symmetrical components factor).
% INPUT:
%    par: 5x1 vector indicating the phasors' configuration.
%         Phase A is considered the angle reference for all phasors.
%         par(1) = magnitude of phase A
%         par(2) = magnitude of phase B
%         par(3) = magnitude of phase C
%         par(4) = angle of phase B in radians, having phase A as reference
%         par(5) = angle of phase C in radians, having phase A as reference
% OUTPUT:
%    Sols: voltage unbalance measurement, based on the symmetrical components method.
par = [458.94;  416.74; 438.06;-120*pi/180; 120*pi/180];
Va = par(1);
Vb = par(2);
Vc = par(3);
Tab = - par(4);
Tbc = par(4) - par(5);
Tac = - par(5);
mV1 = Va*Va + Vb*Vb + Vc*Vc + 2*Va*Vb*cos(Tab - 2*pi/3) + 2*Va*Vc*cos(Tac + 2*pi/3) +
2*Vb*Vc*cos(Tbc - 2*pi/3);  %% |3V1|^2
mV2 = Va*Va + Vb*Vb + Vc*Vc + 2*Va*Vb*cos(Tab + 2*pi/3) + 2*Va*Vc*cos(Tac - 2*pi/3) +
2*Vb*Vc*cos(Tbc + 2*pi/3);  %|3V2|^2
k = real(sqrt(mV2/mV1));
```

Table A 3 Voltage Unbalance Factor Matlab Code

```
function T = angK(par)
% angK() takes 3 phasors as input, and calculates the angle
% between the negative- and positive-sequence components (which would correspond to the
angle of the K factor, or symmetrical components factor).
% INPUT:
%    par: 5x1 vector indicating the phasors' configuration.
%         Phase A is considered the angle reference for all phasors.
%         par(1) = magnitude of phase A
%         par(2) = magnitude of phase B
%         par(3) = magnitude of phase C
%         par(4) = angle of phase B in radians, having phase A as reference
%         par(5) = angle of phase C in radians, having phase A as reference
% OUTPUT:T: angle between the negative- and positive-sequence components, in radians
a = exp(i*2*pi/3);
TV1 = par(1) + par(2)*a*exp(i*par(4)) + par(3)*a*a*exp(i*par(5));
TV2 = par(1) + par(2)*a*a*exp(i*par(4)) + par(3)*a*exp(i*par(5));
% angTV1 = angle(TV1)*180/pi
% angTV2 = angle(TV2)*180/pi
T = angle(TV2/TV1);
```

Table A 4 Angle Between the Negative and Positive Sequence Components

```
function mV1 = modV1(par)
% modV1() takes 3 phasors as input, and calculates the
% magnitude of the corresponding positive-sequence component
% (symmetrical components method).
% INPUT:
%    par: 5x1 vector indicating the phasors' configuration.
%         Phase A is considered the angle reference for all phasors.
%         par(1) = magnitude of phase A
%         par(2) = magnitude of phase B
%         par(3) = magnitude of phase C
%         par(4) = angle of phase B in radians, having phase A as reference
%         par(5) = angle of phase C in radians, having phase A as reference
% OUTPUT:
%    mV1: magnitude of the corresponding positive-sequence component (symmetrical
components method).
par = [27.677;  13.58;  24.604;-120*pi/180; 120*pi/180]
ReV1 = par(1) + par(2)*cos(par(4) + 2*pi/3) + par(3)*cos(par(5) - 2*pi/3);
ReV1 = ReV1/3;
ImV1 = par(2)*sin(par(4) + 2*pi/3) + par(3)*sin(par(5) - 2*pi/3);
ImV1 = ImV1/3;
mV1 = sqrt(ReV1*ReV1 + ImV1*ImV1);
```

Table A 5 Positive Sequence Component Magnitude

```
function tV1 = angV1(par)
% function tV1 = angV1(par)
% angV1() takes 3 phasors as input, and calculates the angle
% of the positive-sequence component (symmetrical components method).
% INPUT:
%    par: 5x1 vector indicating the phasors' configuration.
%         Phase A is considered the angle reference for all phasors.
%         par(1) = magnitude of phase A
%         par(2) = magnitude of phase B
%         par(3) = magnitude of phase C
%         par(4) = angle of phase B in radians, having phase A as reference
```

```
%         par(5) = angle of phase C in radians, having phase A as reference
% OUTPUT:
%tV1: angle of the positive-sequence component, in radians
ReV1 = par(1) + par(2)*cos(par(4) + 2*pi/3) + par(3)*cos(par(5) - 2*pi/3);
ReV1 = ReV1/3;
ImV1 = par(2)*sin(par(4) + 2*pi/3) + par(3)*sin(par(5) - 2*pi/3);
ImV1 = ImV1/3;
tV1 = atan2(ImV1,ReV1);
```

Table A 6 Angle of the Positive Sequence Component

```
function mV2 = modV2(par)
% modV2() takes 3 phasors as input, and calculates the
% magnitude of the corresponding negative-sequence component
% (symmetrical components method).
% INPUT:
%    par: 5x1 vector indicating the phasors' configuration.
%         Phase A is considered the angle reference for all phasors.
%         par(1) = magnitude of phase A
%         par(2) = magnitude of phase B
%         par(3) = magnitude of phase C
%         par(4) = angle of phase B in radians, having phase A as reference
%         par(5) = angle of phase C in radians, having phase A as reference
% OUTPUT:
%    mV2: magnitude of the corresponding negative-sequence component (symmetrical
components method).
par = [27.677;  13.58;  24.604;-120*pi/180; 120*pi/180]
ReV2 = par(1) + par(2)*cos(par(4) - 2*pi/3) + par(3)*cos(par(5) + 2*pi/3);
ReV2 = ReV2/3;
ImV2 = par(2)*sin(par(4) - 2*pi/3) + par(3)*sin(par(5) + 2*pi/3);
ImV2 = ImV2/3;
mV2 = sqrt(ReV2*ReV2 + ImV2*ImV2);
```

Table A 7 Negative Sequence Component Magnitude

```
function tV2 = angV2(par)
% angV2() takes 3 phasors as input, and calculates the angle
% of the negative-sequence component (symmetrical components method).
% INPUT:
%    par: 5x1 vector indicating the phasors' configuration.
%         Phase A is considered the angle reference for all phasors.
%         par(1) = magnitude of phase A
%         par(2) = magnitude of phase B
%         par(3) = magnitude of phase C
%         par(4) = angle of phase B in radians, having phase A as reference
%         par(5) = angle of phase C in radians, having phase A as reference
% OUTPUT: tV2: angle of the negative-sequence component, in radians
ReV2 = par(1) + par(2)*cos(par(4) - 2*pi/3) + par(3)*cos(par(5) + 2*pi/3);
ReV2 = ReV2/3;
ImV2 = par(2)*sin(par(4) - 2*pi/3) + par(3)*sin(par(5) + 2*pi/3);
ImV2 = ImV2/3;
tV2 = atan2(ImV2,ReV2);
```

Table A 8 Angle of the Negative Sequence Component

A3 Positive and Negative Sequence Components Sensitivity Matlab/Octave Implementation

```
function S = SensAngK(par)
% SensAngK() takes 3 phasors as input, and calculates the relative sensitivity of the angle
of the corresponding K factor
% (symmetrical components factor) to the phasors' magnitudes and angles.
% INPUT:
%    par: 5x1 vector indicating the phasors' configuration.
%         Phase A is considered the angle reference for all phasors.
%         par(1) = magnitude of phase A
%         par(2) = magnitude of phase B
%         par(3) = magnitude of phase C
%         par(4) = angle of phase B in radians, having phase A as reference
%         par(5) = angle of phase C in radians, having phase A as reference
% OUTPUT:
% S: relative sensitivity of the angle of the K factor (symmetrical components method)to
phasors' magnitudes and angles
Va = par(1);
Vb = par(2);
Vc = par(3);
Tb = par(4);
Tc = par(5);
ReV1 = (Va + Vb*cos(Tb + 2*pi/3) + Vc*cos(Tc - 2*pi/3))/3;
ImV1 = (Vb*sin(Tb + 2*pi/3) + Vc*sin(Tc - 2*pi/3))/3;
mV1 = ReV1^2 + ImV1^2;  %|V1|^2
ReV2 = (Va + Vb*cos(Tb - 2*pi/3) + Vc*cos(Tc + 2*pi/3))/3;
ImV2 = (Vb*sin(Tb - 2*pi/3) + Vc*sin(Tc + 2*pi/3))/3;
mV2 = ReV2^2 + ImV2^2;  %|V2|^2
dV1 = zeros(5,1);
dV1(1) = -ImV1/mV1;
dV1(2) = (ReV1*sin(Tb + 2*pi/3)-ImV1*cos(Tb + 2*pi/3))/mV1;
dV1(3) = (ReV1*sin(Tc - 2*pi/3)-ImV1*cos(Tc - 2*pi/3))/mV1;
dV1(4) = (ReV1*cos(Tb + 2*pi/3)+ImV1*sin(Tb + 2*pi/3))*Vb/mV1;
dV1(5) = (ReV1*cos(Tc - 2*pi/3)+ImV1*sin(Tc - 2*pi/3))*Vc/mV1;
dV2 = zeros(5,1);
dV2(1) = -ImV2/mV2;
dV2(2) = (ReV2*sin(Tb - 2*pi/3)-ImV2*cos(Tb - 2*pi/3))/mV2;
dV2(3) = (ReV2*sin(Tc + 2*pi/3)-ImV2*cos(Tc + 2*pi/3))/mV2;
dV2(4) = (ReV2*cos(Tb - 2*pi/3)+ImV2*sin(Tb - 2*pi/3))*Vb/mV2;
dV2(5) = (ReV2*cos(Tc + 2*pi/3)+ImV2*sin(Tc + 2*pi/3))*Vc/mV2;
S = zeros(5,1);
Theta = angK(par);
if Theta ~= 0
    for j = 1:5
        S(j) = (dV2(j)-dV1(j))*par(j)/Theta;
    end
end
```

Table A 9 Sensitivity of the angle of the VUF to the phasors magnitudes and angles

```
function SK = SensModK(par)
% SensModK() takes 3 phasors as input, and calculates the
% relative sensitivity of the corresponding K factor
% (symmetrical components factor) to the phasors' magnitudes and angles
% INPUT:
%    par: 5x1 vector indicating the phasors' configuration.
%         Phase A is considered the angle reference for all phasors.
%         par(1) = magnitude of phase A
%         par(2) = magnitude of phase B
%         par(3) = magnitude of phase C
%         par(4) = angle of phase B in radians, having phase A as reference
%         par(5) = angle of phase C in radians, having phase A as reference
```

```
% OUTPUT:  Sk: relative sensitivity of the K factor (symmetrical components method) to
phasors' magnitudes and angles
par = [440; 418; 462; -120*pi/180; 120*pi/180];
Va = par(1);
Vb = par(2);
Vc = par(3);
Tb = par(4);
Tc = par(5);
Tab = - Tb;
Tbc = Tb - Tc;
Tca = Tc;
ang120 = 2*pi/3;
Tab_p120 = Tab+ang120;
Tab_m120 = Tab-ang120;
Tbc_p120 = Tbc+ang120;
Tbc_m120 = Tbc-ang120;
Tca_p120 = Tca+ang120;
Tca_m120 = Tca-ang120;
mV1 = Va*Va + Vb*Vb + Vc*Vc + 2*Va*Vb*cos(Tab_m120) + ...
    2*Va*Vc*cos(Tca_m120) + 2*Vb*Vc*cos(Tbc_m120);  %|3V1|^2
dV1 = zeros(5,1);
dV1(1) = 2*(Va + Vb*cos(Tab_m120) + Vc*cos(Tca_m120));  %d|3V1|^2/dVa
dV1(2) = 2*(Vb + Vc*cos(Tbc_m120) + Va*cos(Tab_m120));  %d|3V1|^2/dVb
dV1(3) = 2*(Vc + Va*cos(Tca_m120) + Vb*cos(Tbc_m120));  %d|3V1|^2/dVc
dV1(4) = 2*Vb*(  Va*sin(Tab_m120) - Vc*sin(Tbc_m120));  %d|3V1|^2/dTb
dV1(5) = 2*Vc*(  Vb*sin(Tbc_m120) - Va*sin(Tca_m120));  %d|3V1|^2/dTc
mV2 = Va*Va + Vb*Vb + Vc*Vc + 2*Va*Vb*cos(Tab_p120) + ...
    2*Va*Vc*cos(Tca_p120) + 2*Vb*Vc*cos(Tbc_p120);  %|3V2|^2
dV2 = zeros(5,1);
dV2(1) = 2*(Va + Vb*cos(Tab_p120) + Vc*cos(Tca_p120));  %d|3V2|^2/dVa
dV2(2) = 2*(Vb + Vc*cos(Tbc_p120) + Va*cos(Tab_p120));  %d|3V2|^2/dVb
dV2(3) = 2*(Vc + Va*cos(Tca_p120) + Vb*cos(Tbc_p120));  %d|3V2|^2/dVc
dV2(4) = 2*Vb*(  Va*sin(Tab_p120) - Vc*sin(Tbc_p120));  %d|3V2|^2/dTb
dV2(5) = 2*Vc*(  Vb*sin(Tbc_p120) - Va*sin(Tca_p120));  %d|3V2|^2/dTc
SV1 = dV1.*par/mV1;
SV2 = dV2.*par/mV2;
SK = (SV2 - SV1)/2;
```

Table A 10 Sensitivity of the VUF magnitude to the phasors magnitudes and angles

```
function S = SensAngV1(par)
% SensAngV0() takes 3 phasors as input, and calculates the
% relative sensitivity of the angle of the corresponding positive-sequence component to the
phasors' magnitudes and angles.
% INPUT:
%    par: 5x1 vector indicating the phasors' configuration.
%         Phase A is considered the angle reference for all phasors.
%         par(1) = magnitude of phase A
%         par(2) = magnitude of phase B
%         par(3) = magnitude of phase C
%         par(4) = angle of phase B in radians, having phase A as reference
%         par(5) = angle of phase C in radians, having phase A as reference
% OUTPUT:
%    S: relative sensitivity of the angle of the positive-sequence component to phasors'
magnitudes and angles
Va = par(1);
Vb = par(2);
Vc = par(3);
Tb = par(4);
Tc = par(5);
ReV1 = (Va + Vb*cos(Tb + 2*pi/3) + Vc*cos(Tc - 2*pi/3))/3;
ImV1 = (Vb*sin(Tb + 2*pi/3) + Vc*sin(Tc - 2*pi/3))/3;
```

```
mV1 = ReV1^2 + ImV1^2;  %|V1|^2
dV1 = zeros(5,1);
dV1(1) = -ImV1/mV1;
dV1(2) = (ReV1*sin(Tb + 2*pi/3)-ImV1*cos(Tb + 2*pi/3))/mV1;
dV1(3) = (ReV1*sin(Tc - 2*pi/3)-ImV1*cos(Tc - 2*pi/3))/mV1;
dV1(4) = (ReV1*cos(Tb + 2*pi/3)+ImV1*sin(Tb + 2*pi/3))*Vb/mV1;
dV1(5) = (ReV1*cos(Tc - 2*pi/3)+ImV1*sin(Tc - 2*pi/3))*Vc/mV1;
S = zeros(5,1);
Theta = angV1(par);
if Theta ~= 0
    for j = 1:5
        S(j) = dV1(j)*par(j)/Theta;
    end
end
```

Table A 11 Sensitivity of the angle of the positive sequence component to the phasors magnitudes and angles

```
function SmV1 = SensModV1(par)
% SensModV1() takes 3 phasors as input, and calculates the
% relative sensitivity of the corresponding magnitude of the
% positive-sequence component to the phasors' magnitudes and angles.
% INPUT:
%    par: 5x1 vector indicating the phasors' configuration.
%         Phase A is considered the angle reference for all phasors.
%         par(1) = magnitude of phase A
%         par(2) = magnitude of phase B
%         par(3) = magnitude of phase C
%         par(4) = angle of phase B in radians, having phase A as reference
%         par(5) = angle of phase C in radians, having phase A as reference
% OUTPUT:
%    SmV1: relative sensitivity of the magnitude of the positive-sequence component to
phasors' magnitudes and angles
par = [201; 220; 220; -120*pi/180; 120*pi/180]
Va = par(1);
Vb = par(2);
Vc = par(3);
Tb = par(4);
Tc = par(5);
Tab = - Tb;
Tbc = Tb - Tc;
Tac = - Tc;
mV1 = modV1(par);
dV1 = zeros(5,1);
dV1(1) = 2*Va + 2*Vb*cos(Tab - 2*pi/3) + 2*Vc*cos(Tac + 2*pi/3);  %d|3V1|^2/dVa
dV1(2) = 2*Vb + 2*Va*cos(Tab - 2*pi/3) + 2*Vc*cos(Tbc - 2*pi/3);  %d|3V1|^2/dVb
dV1(3) = 2*Vc + 2*Va*cos(Tac + 2*pi/3) + 2*Vb*cos(Tbc - 2*pi/3);  %d|3V1|^2/dVc
dV1(4) = 2*Va*Vb*sin(Tab - 2*pi/3) - 2*Vb*Vc*sin(Tbc - 2*pi/3);   %d|3V1|^2/dTb
dV1(5) = 2*Va*Vc*sin(Tac + 2*pi/3) + 2*Vb*Vc*sin(Tbc - 2*pi/3);   %d|3V1|^2/dTc
dV1 = dV1/9;
SmV1 = zeros(5,1);
for j = 1:5
    SmV1(j) = dV1(j)*par(j)/(mV1*mV1*2);
end
```

Table A 12 Sensitivity of the magnitude of the positive sequence component to the phasors magnitudes and angles

```
function S = SensAngV2(par)
% SensAngV2() takes 3 phasors as input, and calculates the
```

```
% relative sensitivity of the angle of the corresponding negative-sequence component to the
phasors' magnitudes and angles.
% INPUT:
%    par: 5x1 vector indicating the phasors' configuration.
%         Phase A is considered the angle reference for all phasors.
%         par(1) = magnitude of phase A
%         par(2) = magnitude of phase B
%         par(3) = magnitude of phase C
%         par(4) = angle of phase B in radians, having phase A as reference
%         par(5) = angle of phase C in radians, having phase A as reference
% OUTPUT:
%    S: relative sensitivity of the angle of the negative-sequence component to phasors'
magnitudes and angles
Va = par(1);
Vb = par(2);
Vc = par(3);
Tb = par(4);
Tc = par(5);
ReV2 = (Va + Vb*cos(Tb - 2*pi/3) + Vc*cos(Tc + 2*pi/3))/3;
ImV2 = (Vb*sin(Tb - 2*pi/3) + Vc*sin(Tc + 2*pi/3))/3;
mV2 = ReV2^2 + ImV2^2;  %|V2|^2
dV2 = zeros(5,1);
dV2(1) = -ImV2/mV2;
dV2(2) = (ReV2*sin(Tb - 2*pi/3)-ImV2*cos(Tb - 2*pi/3))/mV2;
dV2(3) = (ReV2*sin(Tc + 2*pi/3)-ImV2*cos(Tc + 2*pi/3))/mV2;
dV2(4) = (ReV2*cos(Tb - 2*pi/3)+ImV2*sin(Tb - 2*pi/3))*Vb/mV2;
dV2(5) = (ReV2*cos(Tc + 2*pi/3)+ImV2*sin(Tc + 2*pi/3))*Vc/mV2;
S = zeros(5,1);
Theta = angV2(par);
if Theta ~= 0
    for j = 1:5
        S(j) = dV2(j)*par(j)/Theta;
    end
end
```

Table A 13 Sensitivity of the angle of the negative sequence componentn to the phasors magnitudes and angles

```
function SmV2 = SensModV2(par)
% function SmV2 = SensModV2(par)
% SensModV2() takes 3 phasors as input, and calculates the
% relative sensitivity of the magnitude of the corresponding negative-sequence component to
the phasors' magnitudes and angles.
% INPUT:
%    par: 5x1 vector indicating the phasors' configuration.
%         Phase A is considered the angle reference for all phasors.
%         par(1) = magnitude of phase A
%         par(2) = magnitude of phase B
%         par(3) = magnitude of phase C
%         par(4) = angle of phase B in radians, having phase A as reference
%         par(5) = angle of phase C in radians, having phase A as reference
% OUTPUT:
%    SmV2: relative sensitivity of the magnitude of the negative-sequence component
%          to phasors' magnitudes and angles
par = [201; 220; 220; -120*pi/180; 120*pi/180]
Va = par(1);
Vb = par(2);
Vc = par(3);
Tb = par(4);
Tc = par(5);
Tab = - Tb;
Tbc = Tb - Tc;
```

```
Tac = - Tc;
mV2 = modV2(par);
dV2 = zeros(5,1);
dV2(1) = 2*Va + 2*Vb*cos(Tab + 2*pi/3) + 2*Vc*cos(Tac - 2*pi/3);  %d|3V2|^2/dVa
dV2(2) = 2*Vb + 2*Va*cos(Tab + 2*pi/3) + 2*Vc*cos(Tbc + 2*pi/3);  %d|3V2|^2/dVb
dV2(3) = 2*Vc + 2*Va*cos(Tac - 2*pi/3) + 2*Vb*cos(Tbc + 2*pi/3);  %d|3V2|^2/dVc
dV2(4) = 2*Va*Vb*sin(Tab + 2*pi/3) - 2*Vb*Vc*sin(Tbc + 2*pi/3);   %d|3V2|^2/dTb
dV2(5) = 2*Va*Vc*sin(Tac - 2*pi/3) + 2*Vb*Vc*sin(Tbc + 2*pi/3);   %d|3V2|^2/dTc
dV2 = dV2/9;
SmV2 = zeros(5,1);
for j = 1:5
    SmV2(j) = dV2(j)*par(j)/(mV2*mV2*2);
end
```

Table A 14 Sensitivity of the magnitude of the negative sequence component to the phasors magnitudes and angles

A4 Voltage Unbalance Optimization Matlab/Octave Implementation

```
function Sols = Analit1(par,Kdes)
% ANALIT1() takes 3 phasors as input, and calculates the phasors'individual parameter
changes in order to achieve a desired K factor.
% INPUTS:
%    par: 5x1 vector indicating the phasors' configuration.
%         Phase A is considered the angle reference for all phasors.
%         par(1) = magnitude of phase A
%         par(2) = magnitude of phase B
%         par(3) = magnitude of phase C
%         par(4) = angle of phase B in radians, having phase A as reference
%         par(5) = angle of phase C in radians, having phase A as reference
%    Kdes: desired value for the K factor (symmetrical components factor)
% OUTPUT:
%    Sols: 5x2 vector indicating the solutions for the desired K factor,
%          by changing only one of par's values (not all simultaneously).
%          If a solution is not feasible, a null value is returned.
par = [440; 418; 462; -120*pi/180; 120*pi/180];
Kdes =0.0289;
Va = par(1);
Vb = par(2);
Vc = par(3);
Tb = par(4);
Tc = par(5);
Sols = zeros(5,2);
A = (1-Kdes^2);
B = 2*Vb*(cos(-Tb+2*pi/3)-Kdes^2*cos(-Tb-2*pi/3))+2*Vc*(cos(Tc+2*pi/3)-Kdes^2*cos(Tc-
2*pi/3));
C = A*(Vb^2+Vc^2)+2*Vb*Vc*(cos(Tb-Tc+2*pi/3)-Kdes^2*cos(Tb-Tc-2*pi/3));
delta = B^2-4*A*C;
if delta >= 0
  Sols(1,1) = (-B-sqrt(delta))/(2*A);
  Sols(1,2) = (-B+sqrt(delta))/(2*A);
end
B = 2*Va*(cos(-Tb+2*pi/3)-Kdes^2*cos(-Tb-2*pi/3))+2*Vc*(cos(Tb-Tc+2*pi/3)-Kdes^2*cos(Tb-Tc-
2*pi/3));
C = A*(Va^2+Vc^2)+2*Va*Vc*(cos(Tc+2*pi/3)-Kdes^2*cos(Tc-2*pi/3));
delta = B^2-4*A*C;
if delta >= 0
  Sols(2,1) = (-B-sqrt(delta))/(2*A);
  Sols(2,2) = (-B+sqrt(delta))/(2*A);
end
B = 2*Va*(cos(Tc+2*pi/3)-Kdes^2*cos(Tc-2*pi/3))+2*Vb*(cos(Tb-Tc+2*pi/3)-Kdes^2*cos(Tb-Tc-
2*pi/3));
C = (1-Kdes^2)*(Va^2+Vb^2)+2*Va*Vb*(cos(-Tb+2*pi/3)-Kdes^2*cos(-Tb-2*pi/3));
delta = B^2-4*A*C;
```

```
if delta >= 0
  Sols(3,1) = (-B-sqrt(delta))/(2*A);
  Sols(3,2) = (-B+sqrt(delta))/(2*A);
end
A = 2*Va*Vb*(cos(2*pi/3)-Kdes^2*cos(-2*pi/3))+2*Vb*Vc*(cos(Tc-2*pi/3)-
Kdes^2*cos(Tc+2*pi/3));
B = 2*Va*Vb*(sin(2*pi/3)-Kdes^2*sin(-2*pi/3))+2*Vb*Vc*(sin(Tc-2*pi/3)-
Kdes^2*sin(Tc+2*pi/3));
C = (1-Kdes^2)*(Va^2+Vb^2+Vc^2)+2*Va*Vc*(cos(Tc+2*pi/3)-Kdes^2*cos(Tc-2*pi/3));
beta = atan2(B,A);
gama = acos(-C/sqrt(A^2+B^2));
if isreal(beta)&&isreal(gama)
  Sols(4,1) = beta+gama-2*pi;
  Sols(4,2) = beta-gama;
end
A = 2*Va*Vc*(cos(-2*pi/3)-Kdes^2*cos(2*pi/3))+2*Vb*Vc*(cos(Tb+2*pi/3)-Kdes^2*cos(Tb-
2*pi/3));
B = 2*Va*Vc*(sin(-2*pi/3)-Kdes^2*sin(2*pi/3))+2*Vb*Vc*(sin(Tb+2*pi/3)-Kdes^2*sin(Tb-
2*pi/3));
C = (1-Kdes^2)*(Va^2+Vb^2+Vc^2)+2*Va*Vb*(cos(-Tb+2*pi/3)-Kdes^2*cos(-Tb-2*pi/3));
beta = atan2(B,A);
gama = acos(-C/sqrt(A^2+B^2));
if isreal(beta)&&isreal(gama)
  Sols(5,1) = beta+gama;
  Sols(5,2) = beta-gama+2*pi;
end
```

Table A 15 Attaining desired VUF by variation of one parameter: phase magnitude/angle

```
function Sol = Analit3(par,Kdes)
% ANALIT3() takes 3 phasors as input, and calculates the phasors' simultaneous magnitude
parameter changes in order to achieve a desired K factor.
% INPUTS:
%    par: 5x1 vector indicating the phasors' configuration.
%         Phase A is considered the angle reference for all phasors.
%         par(1) = magnitude of phase A
%         par(2) = magnitude of phase B
%         par(3) = magnitude of phase C
%         par(4) = angle of phase B in radians, having phase A as reference
%         par(5) = angle of phase C in radians, having phase A as reference
%    Kdes: desired value for the K factor (symmetrical components factor)
% OUTPUT:
% Sols: 5x1 vector indicating the solutions for the desired K factor,
%by changing all 3 magnitudes simultaneously.If a solution is not feasible, the same input
phasors are returned.
par = [201; 220; 220; -120*pi/180; 120*pi/180];
Kdes= 0.000
A = 2/(1-Kdes^2)*(cos(-par(4)+2*pi/3)-Kdes^2*cos(-par(4)-2*pi/3));
B = 2/(1-Kdes^2)*(cos(par(4)-par(5)+2*pi/3)-Kdes^2*cos(par(4)-par(5)-2*pi/3));
C = 2/(1-Kdes^2)*(cos(par(5)+2*pi/3)-Kdes^2*cos(par(5)-2*pi/3));
Van = par(1);
Vbn = par(2);
Vcn = par(3);
A2 = (-
16*C*Vcn*Van+Vbn^2*A^2*C^2+4*Vcn*B^3*Vbn+Vcn^2*A^2*C^2+Van^2*A^2*B^2+4*Van*C^3*Vcn+Vcn^2*A^
2*B^2+...
    Vbn^2*C^2*B^2+4*Vbn*A^3*Van+Van^2*C^2*B^2+2*B*Vbn*C^2*Vcn*A^2+2*C*Van*A^2*B^2*Vcn-
6*A*Vbn*C*B^2*Vcn-...
    6*A*Vcn*C^2*Van*B-6*Vbn*A^2*Van*C*B-4*Vcn^2*C^2+16*Van^2+16*Vbn^2+16*Vcn^2-
16*A*Van*Vbn-16*B*Vbn*Vcn+...
    2*A*Van*B^2*Vbn*C^2-A*Van^2*B^3*C+4*A*Vbn^2*C*B-
A*Vbn^2*C^3*B+4*A*Vcn^2*C*B+4*Van*C*B^2*Vcn-...
    2*Vbn*C^3*Vcn*A-
2*Van*C^3*B*Vbn+8*B*Vbn*Van*C+4*B*Vbn*C^2*Vcn+4*A*Van*Vbn*C^2+8*A*Van*Vcn*B+...
```

```
    8*A*Vcn*C*Vbn+4*A*Van*B^2*Vbn+4*Van*Vcn*A^2*C+4*Vbn*A^2*Vcn*B-Vcn^2*A^3*B*C-
2*Vbn*A^3*C*Vcn-...
    2*Van*B^3*Vbn*C-2*Van*B^3*Vcn*A+4*A*Van^2*C*B-8*Vcn^2*A^2+Vcn^2*A^4-4*Van^2*C^2-
4*Vbn^2*B^2-...
    4*Vcn^2*B^2-4*Vbn^2*A^2-4*Van^2*A^2-8*Van^2*B^2+Van^2*B^4-8*Vbn^2*C^2+Vbn^2*C^4-
2*Van*A^3*B*Vcn);
B2 = (-32*C*Vcn*Van+8*Vcn*B^3*Vbn+8*Van*C^3*Vcn+8*Vbn*A^3*Van-8*A*Vbn*C*B^2*Vcn-
8*A*Vcn*C^2*Van*B-...
    8*Vbn*A^2*Van*C*B-16*Vcn^2*C^2+64*Van^2+64*Vbn^2+64*Vcn^2-32*A*Van*Vbn-
32*B*Vbn*Vcn+16*A*Vbn^2*C*B+...

16*A*Vcn^2*C*B+8*Van*C*B^2*Vcn+8*B*Vbn*C^2*Vcn+8*A*Van*Vbn*C^2+8*A*Van*B^2*Vbn+8*Van*Vcn*A^
2*C+...
    8*Vbn*A^2*Vcn*B+16*A*Van^2*C*B-16*Vcn^2*A^2-16*Van^2*C^2-16*Vbn^2*B^2-16*Vcn^2*B^2-
16*Vbn^2*A^2-...
    16*Van^2*A^2-16*Van^2*B^2-16*Vbn^2*C^2);
C2 = (4*Vcn*B^3*Vbn+4*Van*C^3*Vcn+4*Vbn*A^3*Van-
20*Vcn^2*C^2+96*Van^2+96*Vbn^2+96*Vcn^2+12*A*Vbn^2*C*B+...
    12*A*Vcn^2*C*B+4*Van*C*B^2*Vcn-24*B*Vbn*Van*C+4*B*Vbn*C^2*Vcn+4*A*Van*Vbn*C^2-
24*A*Van*Vcn*B-...
    24*A*Vcn*C*Vbn+4*A*Van*B^2*Vbn+4*Van*Vcn*A^2*C+4*Vbn*A^2*Vcn*B+12*A*Van^2*C*B-
8*Vcn^2*A^2-20*Van^2*C^2-...
    20*Vbn^2*B^2-20*Vcn^2*B^2-20*Vbn^2*A^2-20*Van^2*A^2-8*Van^2*B^2-8*Vbn^2*C^2);
D2 = (32*C*Vcn*Van+64*Vbn^2+32*A*Van*Vbn+64*Vcn^2-16*A*Van*Vcn*B-8*Vcn^2*C^2-
16*B*Vbn*Van*C+32*B*Vbn*Vcn+64*Van^2-...
    8*Van^2*C^2-8*Vbn^2*B^2-8*Vcn^2*B^2-16*A*Vcn*C*Vbn-8*Van^2*A^2-8*Vbn^2*A^2);
E2 = 16*Van^2+16*A*Van*Vbn+16*C*Vcn*Van+16*Vbn^2+16*B*Vbn*Vcn+16*Vcn^2;
lambdas = roots([A2 B2 C2 D2 E2]);
pars = zeros(3,4);
dists = 10*ones(4,1);
for j = 1:4
  lambda = lambdas(j);
  if isreal(lambda)
    pars(1,j) = (-4-8*lambda-4*lambda^2+B^2*lambda^2)/(-4-12*lambda-
12*lambda^2+B^2*lambda^2-4*lambda^3+...
        B^2*lambda^3+A^2*lambda^2+A^2*lambda^3-
A*lambda^3*C*B+C^2*lambda^2+C^2*lambda^3)*Van+lambda*(2*A+...
        2*A*lambda-C*lambda*B)/(-4-12*lambda-12*lambda^2+B^2*lambda^2-
4*lambda^3+B^2*lambda^3+A^2*lambda^2+...
        A^2*lambda^3-A*lambda^3*C*B+C^2*lambda^2+C^2*lambda^3)*Vbn-lambda*(A*lambda*B-2*C-
2*C*lambda)/(-4-...
        12*lambda-12*lambda^2+B^2*lambda^2-
4*lambda^3+B^2*lambda^3+A^2*lambda^2+A^2*lambda^3-
A*lambda^3*C*B+C^2*lambda^2+C^2*lambda^3)*Vcn;
    pars(2,j) = lambda*(2*A+2*A*lambda-C*lambda*B)/(-4-12*lambda-12*lambda^2+B^2*lambda^2-
4*lambda^3+...
        B^2*lambda^3+A^2*lambda^2+A^2*lambda^3-
A*lambda^3*C*B+C^2*lambda^2+C^2*lambda^3)*Van+(-4-8*lambda-...
        4*lambda^2+C^2*lambda^2)/(-4-12*lambda-12*lambda^2+B^2*lambda^2-
4*lambda^3+B^2*lambda^3+A^2*lambda^2+...
        A^2*lambda^3-A*lambda^3*C*B+C^2*lambda^2+C^2*lambda^3)*Vbn-lambda*(-2*B-
2*B*lambda+A*lambda*C)/(-4-...
        12*lambda-12*lambda^2+B^2*lambda^2-
4*lambda^3+B^2*lambda^3+A^2*lambda^2+A^2*lambda^3-
A*lambda^3*C*B+C^2*lambda^2+C^2*lambda^3)*Vcn;
    pars(3,j) = -lambda*(A*lambda*B-2*C-2*C*lambda)/(-4-12*lambda-12*lambda^2+B^2*lambda^2-
4*lambda^3+...
        B^2*lambda^3+A^2*lambda^2+A^2*lambda^3-
A*lambda^3*C*B+C^2*lambda^2+C^2*lambda^3)*Van-lambda*(-2*B-2*B*lambda+A*lambda*C)/(-...
        4-12*lambda-12*lambda^2+B^2*lambda^2-
4*lambda^3+B^2*lambda^3+A^2*lambda^2+A^2*lambda^3-A*lambda^3*C*B+C^2*lambda^2+...
        C^2*lambda^3)*Vbn+(-4-8*lambda-4*lambda^2+A^2*lambda^2)/(-4-12*lambda-
12*lambda^2+B^2*lambda^2-4*lambda^3+B^2*lambda^3+...
        A^2*lambda^2+A^2*lambda^3-A*lambda^3*C*B+C^2*lambda^2+C^2*lambda^3)*Vcn;
    dists(j) = sum((pars(1:3,j)-par(1:3)).^2);
  end
```

```
end
Sol = par;
for j = 1:4
  if dists(j) == min(dists)
    Sol(1:3) = pars(:,j);
  end
end
```

Table A 16 Attaining new VUF by varying three parameters simultaneously